Constraints on mantle processes and late accretion from chalcogen and highly siderophile element abundances in rocks from the Earth's mantle

Zaicong Wang

Dissertation submitted to obtain the academic degree

Doktor der Naturwissenschaften
(Dr. rer. nat.)

Institut für Geologische Wissenschaften
Fachbereich Geowissenschaften
Freie Universität Berlin

Freie Universität Berlin

Berlin, November 2013

Supervisor: Prof. Dr. Harry Becker

Date of defence: 2014-02-14

Reviewers:

1. Erster Gutachter: Prof. Dr. Harry Becker

   Institut für Geologische Wissenschaften

   Freie Universität Berlin

   Malteserstrasse 74-100, Haus B

   D-12249 Berlin, Germany

2. Zweiter Gutachter: Prof. Dr. Andreas Stracke

   Institut für Mineralogie

   Westfälische Wilhelms Universität Münster

   Corrensstrasse 24, Room 208

   D-48149 Münster, Germany

Erklärung

Hiermit versichere ich, dass ich die vorliegende Arbeit selbstständig gefertigt habe und die angegebenen Quellen und Hilfsmittel in einem vollständigen Verzeichnis enthalten sind. Alle Stellen der Arbeit, die aus anderen Werken dem Wortlaut oder dem Sinne nach entnommen sind, gegebenenfalls auch aus elektronischen Medien, wurden eindeutig unter Angabe der Quellen als Entlehnung gekennzeichnet.

Diese Arbeit hat in gleicher oder ähnlicher Form noch keiner Prüfungsbehörde vorgelegen.

Berlin, Date: Signature:

Table of Contents

Summary

Abundances and ratios of chalcogen elements (S, Se and Te) and highly siderophile (iron-loving) elements (HSE) and Os isotopes in the upper mantle and mantle-derived melts are essential to constrain late accretion history of the Earth and a spectrum of mantle processes such as melt extraction, transport, refertilization and crustal recycling. The excess of HSE and the chondritic ratios of most HSE in primitive mantle (PM) have been interpreted to reflect the accretion of a chondritic 'late veneer' of about 0.5 % of Earth's mass after core formation. The moderately volatile chalcogens S, Se and Te are moderately to highly siderophile at high pressure-temperature (P-T) conditions, thus, if depleted by core formation, their mantle abundances would reflect the volatile composition of the late veneer. Mantle peridotites with different extent of depletion by partial melting and re-enrichment by melt infiltration have been analyzed for abundances of S, Se and Te, in comparison to HSE, to constrain their abundances and ratios in the PM. Comparative studies of the Baldissero and Balmuccia peridotite bodies (Ivrea-Verbano Zone, Italian Alps) and of mantle pyroxenites from Balmuccia indicate details of the influence of partial melting and melt infiltration on abundances of HSE, S, Se and Te and $^{187}Os/^{188}Os$ in the mantle and fractionation of these elements during melt transport and redistribution in the mantle.

At Balmuccia, Re depletion ages (T_{RD}) of lherzolites and replacive dunites display a uniform distribution with a peak at 300-500 Ma. Baldissero peridotites also display a Paleozoic distribution peak but a significant number of samples yielded Proterozoic T_{RD}. The different extents of preservation of ancient $^{187}Os/^{188}Os$ in Balmuccia and Baldissero peridotites reflect different degrees of isotopic homogenization and chemical re-equilibration with infiltrating incompatible element-depleted melt during the Paleozoic. The differences between the two bodies are also reflected by homogeneity of HSE and chalcogen abundances at Balmuccia. The lithophile element, HSE and chalcogen variations of different suites of lherzolites likely reflect different extents of reactive melt infiltration in mantle peridotites with partial re-equilibration and melt extraction in open system environments. The compositions and contact relations of the replacive Balmuccia dunites with the host lherzolites indicate that focused flow of sulfur-undersaturated melt occurred after the melting episode in the lherzolites. The compositional record of the Balmuccia massif thus reflects the composition of different types of melts and their interaction with the peridotites at different P-T conditions.

Magmatic fractionation of chalcogens, the HSE and Os isotopes in websterites and spinel clinopyroxenites in the Balmuccia peridotite massif sheds significant

insight on the connection between the reactive infiltration of mantle peridotites and pyroxenite formation and on the role of pyroxenites during melting of heterogeneous mantle. Both websterites and clinopyroxenites are consistent with crystal accumulation from S saturated melts but have different contents and fractionations of the HSE and chalcogens. Notably, in websterite parent melts, Re/Os, Pd/Ir, S/Re, S/Se, Se/Te, high HSE contents and initial Os isotopes are similar to values for secondary interstitial sulfides of refertilized peridotites reported in the literature, but different from unequilibrated sulfide inclusions in peridotite minerals. These observations suggest a common origin of sulfides precipitated from silicate melts during refertilization of peridotites and melts that have precipitated websterites. The similarities imply that open system melting of peridotites occurred by preferential removal of interstitial sulfides with silicate melts during melt extraction and melt-peridotite reaction. Clinopyroxenites have MORB-like HSE and chalcogen compositions and high S, Se and Re contents similar to websterites, but display lower abundances and stronger fractionations of other HSE and Te compared to websterites. Subparallel HSE patterns with several orders of magnitude variation and S/Se and Se/Te ratios suggest that clinopyroxenites formed from evolved melts that have undergone sulfide segregation in the mantle. Incomplete equilibration of infiltrating melts with peridotites and selective remelting of pyroxenites or veined peridotites can explain Os isotopic disequilibrium and heterogeneity in the mantle and in basalts.

Results for mantle peridotites and pyroxenites are consistent with sulfide-silicate melt partitioning and mixing during reactive infiltration as the dominant control on abundances of the HSE, S, Se and Te in magmas and mantle rocks. Apparent partition coefficients during low to moderate degrees of melt extraction and subsequent fractional crystallization are: $D_{Pt} > D_{Pd} > D_{Te} > D_{Au}$ (?) $> D_{Se} \geq D_S \approx D_{Re}$. Variable degrees of refertilization of lherzolites apparently does not produce significant differences in HSE and chalcogen ratios such as Os/Ir, Ru/Ir, Rh/Ir, Pd/Pt, S/Se and Se/Te. A linear decrease of S abundances with decreasing Al_2O_3 contents, both for the whole data set of mantle peridotites, and for individual suites of peridotites, reflects sulfide removal controlled by sulfur solubility in silicate melt, or co-precipitation with pyroxenes and spinel. Similarly, Se and Te also display positive trends with Al_2O_3 and S contents, although with larger scatter. S/Se and Se/Te in the lherzolites change little with decreasing Al_2O_3, with a mean S/Se of 2690±700 (1σ, n=53) and Se/Te of 7.9±1.6 (1σ, n=63). Regression of abundances of S, Se, Te, Pd and Al_2O_3 contents in the peridotites yield minimum estimates on abundances of S, Se and Te in the PM (S=211±40 μg/g, Se=80±17 ng/g, Te =11.0±1.7 ng/g, 1σ; or 0.0040±0.0008×CI chondrites).

The mean S/Se and Se/Te of mantle lherzolites overlap with CI chondrite values, and Se/Te in these samples are significantly different from ordinary and enstatite chondrites. The chalcogen/HSE ratio of the PM is similar to CM group carbonaceous chondrites, consistent with the view that the HSE signature of the PM reflects a predominance of slightly volatile depleted carbonaceous chondrite like material, possibly with a minor proportion of non-chondritic material. The chondritic composition indicates that the proportion of chalcogens in the mantle that are leftover from core formation must be negligible. A volatile-rich late veneer after formation of Earth's core may have provided from 20 % to 100 % of the budget of water and carbon in the silicate Earth.

Geological reference materials with variable composition and NIST SRM 612 have been analyzed to evaluate the utility of the analytical methods newly developed in this work. The results show that the method may minimize loss of volatile chalcogens during the closed-system digestion of a high pressure asher and indicates different extent of heterogeneity of chalcogens and HSE at low test portion size and importance of obtaining HSE and chalcogen contents in the same sample aliquot.

Zusammenfassung

Häufigkeiten und Verhältnisse chalkogener (S, Se und Te) und hoch siderophiler Elemente (HSE) sowie Osmium Isotopenverhältnisse im oberen Mantel und in Mantelschmelzen sind entscheidend, um die späte Akkretionsgeschichte der Erde sowie ein Spektrum von Mantelprozessen wie Schmelzextraktion, Schmeltransport, Refertilisation und Krusten- Recycling zu belegen. Der Überschuss der HSE und die chondritischen Verhältnisse der meisten HSE im primitiven Mantel (PM) werden als Akkretion eines chondritischen „late veneer", mit ungefähr 0,5 % der Erdmasse, nach der Kernbildung interpretiert. Die moderat volatilen Chalkogene S, Se und Te sind unter Hochdruckbedingungen (P-T) moderat bis hoch siderophil und ihre Mantelvorkommen reflektieren die volatile Zusammensetzung des „late veneer" wenn sie bei der Kernbildung verarmt wurden. Mantelperidotite, die in unterschiedlichen Ausmaßen durch partielles Aufschmelzen verarmt und durch Schmelz Infiltrationwieder- angereichert wurden, sind auf ihre S, Se und Te Konzentrationen und Verhältnisse, im Vergleich zu HSE, analysiert worden um Konzentrationen und Verhältnisse dieser Elemente im primitiven Mantel zu belegen. Vergleichende Studien der Baldissero und Balmuccia Peridotitkörper (Ivrea-Verbano Zone, italienische Alpen) und an Mantelpyroxeniten aus Balmuccia zeigen Details des Einflusses partieller Aufschmelzung und Schmelzinfiltration auf die Häufigkeiten der HSE, S, Se und Te sowie $^{187}Os/^{188}Os$ im Mantel und die Fraktionierung dieser Elemente während des Schmelztransports und der Umverteilung im Mantel an.

Re Verarmungsalter (T_{RD}) von Lherzolithen und Lherzolith ersetzenden Duniten in Balmuccia zeigen eine gleichförmige Verteilung mit einem Maximum um 300-500 Ma. Peridotite aus Baldissero zeigen ebenfalls ein paläozoisches Verteilungs Maximum, wobei aber eine signifikante Anzahl von Probenauch proterozoische T_{RD} ergeben. Das unterschiedliche Ausmaß der Konservierung alter $^{187}Os/^{188}Os$ Verhältnisse in Peridotiten aus Balmuccia und Baldissero spiegelt verschiedene Grade der isotopischen Homogenisierung und chemischen Re-equillibrierung mit infiltrierenden, an inkompatiblen Elementen verarmten, Schmelzen im Paläozoikum wieder. Die Unterschiede beider Körper spiegeln sich ebenso in der Homogenität der HSE und chalkogener Elemente in Balmuccia wieder. Die lithophilen, HSE und chalkogenen Elementvariationen verschiedener Lherzolith- Folgen spiegeln wahrscheinlich verschiedene Grade reaktiver Schmelzinfiltration in Mantelperidotiten mit partieller Re-equillibrierung und Schmelzextaktion unter „open system"-Bedingungen wieder. Die Zusammensetzungen und Kontaktbeziehungen der Lherzolith ersetzenden Dunite in Balmuccia mit den umgebenden Lherzolithen deuten auf das Auftreten räumlich fokussierter, Schwefel-untersättigter Schmelzen nach

Schmelzepisoden in den Lherzolithen hin. Die Zusammensetzung des Balmuccia-Massivs spiegelt die verschiedenen Zusammensetzungen verschiedener Arten von Schmelzen und ihre Interaktion mit den Peridotiten unter verschiedenen P-T Bedingungen wieder.

Die Magmatische Fraktionierung der Chalkogene, HSE und Os-Isotope in Websteriten und Spinell-Klinopyroxeniten im Balmuccia Peridotitmassiv gibt signifikante Einblicke über die Beziehung zwischen der reaktiven Infiltration von Mantelperidotiten und der Pyroxenit Genese sowie der Rolle von Pyroxeniten während dem Aufschmelzen des heterogenen Mantels. Websterite und Klinopyroxenite sind beide konsistent mit einer kristallinen Akkumulation aus Schwefel gesättigten Schmelzen, haben aber verschiedene Gehalte und Fraktionierungen der HSE und chalkogenen Elemente. Bemerkenswert ist, dass die Re/Os, Pd/Ir, S/Re, S/Se, Se/Te, hohe HSE-Gehalte und initiale Os Isotopenverhältnisse in den Ausgangsschmelzen der Websterite Literaturwerten sekundärer interstitieller Sulfiden von refertilisierten Peridotiten ähneln, sich aber von unequilibrierten Sulfid-Inklusionen in Peridotitmineralen unterscheiden. Diese Beobachtungen deuten auf einen gemeinsamen Ursprung der Sulfide, die während der Refertilisierung der Peridotite aus den Silikatschmelzen ausgefallen sind, und der Schmelzen, aus denen die Websterite präzipitiert sind, hin. Die Ähnlichkeiten implizieren, dass sich das Aufschmelzen der Peridotite im offenen System, während der bevorzugten Entfernung interstitieller Sulfide durch die Silikatschmelzen während Schmelzextraktion und Schmelz-Peridotit Reaktion, ereignet hat. Klinopyroxenite haben MORB-ähnliche HSE und chalkogene Zusammensetzungen und hohe S, Se und Re Gehalte, die Websteriten ähneln, zeigen aber geringere Häufigkeiten und stärkere Fraktionierungen der anderen HSE und Te verglichen mit Websteriten. Subparallele HSE-Muster mit Variationen in verschiedenen Größenordnungen und S/Se- und Se/Te-Verhältnisse zeigen an, dass sich die Klinopyroxenite aus entwickelten Schmelzen gebildet haben, welchen Sulfidsegregation im Mantel vorangegangen ist. Unvollständige Equilibrierung der infiltrierten Schmelzen mit Peridotiten und selektives Wiederaufschmelzen der Pyroxenite oder von durch Adern durchzogenen Peridotiten können Os Isotopenungleichgewichte und –heterogenitäten im Mantel und in Basalten erklären.

Die Ergebnisse für Mantelperidotite und Pyroxenite sind konsistent mit Sulfid-Silikat Schmelzverteilungen und –Mischung währendreaktiver Schmelzinfiltration als dominantem Prozess für die Häufigkeiten der HSE, S, Se und Te in den Magmen und Mantelgesteinen. Die offensichtlichen Verteilungskoeffizienten während geringer bis moderater Grade der Schmelzextraktion und nachfolgender fraktionierter Kristallisation sind: $D_{Pt} > D_{Pd} > D_{Te} > D_{Au}$ (?) $> D_{SE} \geq D_S \approx D_{RE}$. Verschiedene Grade

der Refertilisierung der Lherzolithe produzieren anscheinend keine signifikanten Unterschiede in den HSE und chalkogenen Elementverhältnissen wie Os/Ir, Ru/Ir, Rh/Ir, Pd/Pt, S/Se und Se/Te. Eine lineare Abnahme der S Häufigkeiten mit abnehmenden Al_2O_3 Gehalten, sowohl im gesamten Datensatz der Mantelperidotite, als auch für einzelne Anzahlen von Peridotiten, spiegeln eine Entfernung von Sulfiden, welche entweder durch die Schwefellöslichkeit in Silikatschmelzen oder durch die Co-Präzipitation mit Pyroxenen und Spinellen kontrolliert wird, wieder. In ähnlicher Weise zeigen Se und Te ebenfalls positive Trends mit Al_2O_3 und S Gehalten, wenn auch mit größerer Streuung. S/Se und Se/Te in den Lherzolithen ändern sich geringfügig mit abnehmenden Al_2O_3-Gehalten, mit durchschnittlichen S/Se-Verhältnissen von 2690±700 (1σ, n=53) und Se/Te-Verhältnissen von 7,9±1,6 (1σ, n=63). Regressionen der Häufigkeiten von S-, Se-, Te-, Pd- und Al_2O_3-Gehalten in den Peridotiten ergeben Minimumabschätzungen für S-, Se- und Te-Häufigkeiten im PM (S=211±40 µg/g, Se=80±17 ng/g, Te =11,0±1,7 ng/g, 1σ; oder 0.0040±0.0008×CI chondritisch).

Die durchschnittlichen S/Se und Se/Te der Mantellherzolithe überschneiden sich mit den CI-chondritischen Werten und die Se/Te-Verhältnisse dieser Proben unterscheiden sich signifikant von gewöhnlichen- und Enstatit- Chondriten. Die chalkogen/HSE-Verhältnisse des PM sind den Verhältnissen der kohligen Chondrite der CM-Gruppe ähnlich, übereinstimmend mit der Ansicht, dass die HSE-Signatur des PM ein Übergewicht eines kohligen chondrit-ähnlichem Material wiederspiegelt, das leicht an volatilen Elementen verarmt ist, welches wahrscheinlich einen kleinen Anteil nicht-chondritischen Materials enthält. Die chondritische Zusammensetzung zeigt, dass die Anteile der Chalkogene im Mantel, die von der Kernbildung übrig geblieben sind, zu vernachlässigen ist. Eine volatil-reiches „late veneer“ nach der Bildung des Erdkerns lieferte 20% bis 100% des Gesamtanteils an Wasser und Kohlenstoff in der Silikaterde.

Geologische Referenzmaterialien mit variierenden Zusammensetzungen und NIST SRM 612 wurden analysiert, um die Brauchbarkeit der in dieser Arbeit neu entwickelten Methoden zu evaluieren. Die Ergebnisse zeigen, dass die Methode den Verlust an volatilen Chalkogenen während dem Aufschluss im geschlossenen System in einem Hochdruckverascher minimieren kann und zeigt verschiedene Ausmaße von Heterogenitäten der Chalkogene und HSE in kleinen Probenfraktionen und die Bedeutung für HSE- und Chalkogengehalte aus den selben Probenaliquoten.

Chapter 1

Introduction

1.1 Chalcogen and HSE compositions of the silicate Earth

Last three decades' research results show that the absolute abundances of highly siderophile elements (HSE, Os, Ir, Ru, Rh, Pt, Pd, Au and Re) in the bulk silicate Earth (here the term is used synonymously for primitive mantle, PM) exceed expected abundances after core formation by more than two orders of magnitude (e.g., Chou, 1978; Morgan, 1986; O'Neill, 1991; Becker et al., 2006; Day et al., 2007; Fischer-Gödde et al., 2011; Mann et al., 2012). Diverse hypotheses have been proposed to account for the observations, such as incomplete core formation, lower metal-silicate partition coefficients at elevated temperatures (T) and pressures (P), and especially the 'late veneer' model (see review in Walker, 2009). The late veneer model postulates that chondritic materials with about 0.5 wt.% of the Earth' mass had been added the early Earth after its core formed, and that the influx failed to segregate into the core and thoroughly mixed with the mantle until the late Archean (e.g., Chou, 1978; Day et al., 2007; Righter et al., 2008; Brenan and McDonough, 2009; Maier et al., 2009; Walker, 2009). This model has received strong support from chondritic relative abundances of most HSE and Os isotopes in the PM, based on data for mantle peridotites, picrites and komatiites (e.g., Meisel et al., 2001b; Puchtel et al., 2004a, 2004b, 2009; Becker et al., 2006; Ireland et al., 2009; Walker, 2009; Fischer-Gödde et al., 2011). Recent high P-T experiments indeed have indicated significantly lower partition coefficients than previously thought for the HSE during terrestrial core formation, but a late veneer is still required (Righter et al., 2008; Brenan and McDonough, 2009; Mann et al., 2012).

The chalcogen elements S, Se and Te (In the present context, the term chalcogens is exclusively used for S, Se and Te. Oxygen, which is a member of the same group in the periodic table, has very different geochemical properties) have similar and rather low 50 % condensation temperatures near 700 K in a canonical solar nebula composition (Lodders, 2003). The chalcogens become more siderophile

with increasing pressure and are moderately to highly siderophile during metal-silicate segregation at high P-T conditions (Rose-Weston et al., 2009). As for the HSE, during metal-silicate partitioning at high P-T conditions, $D_{Se}^{metal\text{-}silicate}$ ($>10^4$) and $D_{Te}^{metal\text{-}silicate}$ ($>10^5$) will be high enough so that the mantle after core formation should be strongly depleted in Se and Te if core-mantle equilibration was achieved (Rose-Weston et al., 2009). The observed abundances and ratios of S, Se and Te in the PM are notably different from abundances and ratios expected from high P-T experimental results, thus also requiring a late veneer (Morgan, 1986; McDonough and Sun, 1995; Yi et al., 2000; Rose-Weston et al., 2009). However, several key questions and processes remain incompletely understood.

1.2 The late veneer and the Earth's volatiles

The possible origins of the volatiles such as water and carbon that are essential for life on the Earth have been mysterious and whether the late veneer has delivered these volatiles has been hotly debated. Understanding the history of delivery of volatile elements, particularly water and carbon, is of fundamental importance for understanding planetary evolution and origins of materials for life on the Earth (e.g., Abe et al., 2000; Albarède, 2009). The detailed origin and history of moderately volatile and atmophile elements in the Earth remains uncertain, mostly due to considerable element redistribution during core formation and silicate differentiation (Halliday, 2004; Wood et al., 2006; Albarède, 2009; Rubie et al., 2011; Marty, 2012; Ballhaus et al., 2013). It is likely that a fraction of the atmophile element budget of the Earth was delivered after core formation, but little agreement exists on sources and mass fractions of volatiles delivered late (Albarède, 2009; Wood and Halliday, 2010; Ballhaus et al., 2013). Traditionally, the composition of the late veneer was thought to be mostly comprised of water and carbon depleted ordinary or enstatite chondrites, because the $^{187}Os/^{188}Os$ and $^{186}Os/^{188}Os$ of the PM (which reflect time-integrated Re/Os and Pt/Os, respectively) are similar to these classes of chondrites, but different from volatile rich carbonaceous chondrites (e.g., Meisel et al., 2001b; Drake and Righter, 2002; Walker et al., 2002; Horan et al., 2003; Brandon et al., 2006; Fischer-Gödde et al., 2010). For a while, these data were the strongest evidence for anhydrous ordinary or enstatite chondrites as dominant composition of the late veneer, implying difficulties for late veneer to explain the water and carbon budget of the Earth (O'Neill, 1991; Drake and Righter, 2002; Palme and O'Neill, 2003). However, recently, combined isotopic and compositional data have indicated that carbonaceous chondrite like material was the most likely source of a large fraction of the Earth's noble gases, H, N, and presumably also C (Alexander et al., 2012; Marty, 2012).

Because different classes of chondrites display variable fractionation behavior of moderately volatile elements, the chalcogens S, Se and Te can distinguish contributions from carbonaceous, ordinary or enstatite chondrite like materials in the late veneer. Notably, different carbonaceous chondrite groups all display Se/Te similar to the chemically most primitive chondrites (CI chondrites, Se/Te = 8.5±0.7) (Lodders, 2003), irrespectively of the extent of depletion of the chalcogens; whereas ordinary and enstatite chondrites are characterized by significantly higher Se/Te (11-30) than carbonaceous chondrites. In addition, the abundance of the chalcogens relative to the refractory HSE in the PM may constrain the depletion of the chalcogens in the late veneer, the type of primitive material, and its likely contribution to highly volatile elements such as water and carbon.

Abundances of the chalcogens in the PM have been estimated previously on the basis of a limited number of mantle peridotites, however, owing to analytical difficulties, abundance estimates of Se and Te in the PM were based on very little data, and thus reliable data for S/Se and Se/Te have been scarce (Morgan, 1986; McDonough and Sun, 1995; Palme and O'Neill, 2003; Lorand and Alard, 2010). Thus, obtaining better constraints on abundances and ratios of S, Se and Te in the silicate Earth and understanding their significance in terms of the late veneer model and the origin of the volatile elements in the Earth is one of the main objectives of the present study (chapter 4).

1.3 Representative compositions of chalcogens and the HSE in the PM

Whether or not the HSE composition of the PM derived from mantle peridotites really represents the signature of the PM has been challenged in recent years (e.g., Alard et al., 2000, 2002; Luguet et al., 2003, 2008, 2010, 2013; Le Roux et al., 2007). Many studies over the last decade have concluded that the major and trace element composition of many peridotites can be affected by silicate melt migration in various ways (e.g., Bodinier and Godard, 2003; Zhang et al., 2004; Le Roux et al., 2007; Piccardo et al., 2007b; Dick et al., 2010; Batanova et al., 2011; Riches and Rogers, 2011). These processes also affect the distribution of the HSE in mantle peridotites.

It has been shown that secondary interstitial sulfides in refertilized peridotites commonly display enrichment of Pt, Pd, Re and Au (here termed incompatible HSE), as well as Te and Se relative to compatible Os, Ir and Ru (e.g., Alard et al., 2000, 2002, 2005; Luguet et al., 2001, 2004; Harvey et al., 2010, 2011). Textural evidence

indicates co-precipitation of such grain boundary sulfides with pyroxenes and spinels from melts, which would replenish depleted peridotites in basaltic components, Pd, Re, Au and S by such melt infiltration. The process is often referred to as refertilization that is defined as the addition of phases that are mineralogically indistinguishable from common mantle peridotite phases (e.g., Dawson, 1984; Le Roux et al., 2007; O'Reilly and Griffin, 2013). Suites of variably depleted peridotites yield evidence for these processes, both from HSE abundances and Os isotopic data of different sulfide generations in such samples and from bulk rock systematics of elements such as Pd (e.g., Burton et al., 1999; Alard et al., 2000, 2002; Pearson et al., 2004; van Acken et al., 2008; Lorand et al., 2010; Fischer-Gödde et al., 2011, Harvey, et al., 2011). The variations of Pd abundances and Pd/Ir with lithophile incompatible elements indicate mixing of depleted peridotite with infiltrating melt, and was been argured for suprachondritic Pd/Ir (or Pd/Pt) and Ru/Ir in fertile mantle peridotites (e.g., Alard et al., 2000, 2005; Luguet et al., 2003; Pearson et al., 2004; Lorand et al., 2008a, 2013; Lorand and Alard, 2010). These results have prompted critique of estimates of the HSE composition of the Earth's primitive mantle.

Alternatively, a different viewpoint has been indicated by komatiites which formed by high degree of melting of the mantle (Keays, 1995). It has been shown that, likewise peridotites, mantle sources of komatiites display Pd/Pt ratios also mostly suprachondritic (0.9 to 1.1) and initial γOs consistent with chondrites (e.g., Puchtel 2004a, 2004b, 2007, 2009; Puchtel and Humayun, 2005). The HSE composition of komatiite sources are within or slightly below the range of estimates for the PM.

Ratios of chalcogen elements S, Se and Te in lherzolites from the Lherz ultramafic massif are similar or only slightly different from CI chondrites. The lherzolites at Lherz have been interpreted to have formed by refertilization of harzburgites (Le Roux et al., 2007), and accordingly, the sulfides and their compositions have been interpreted to have precipitated mostly from the infiltrating melt (Lorand and Alard, 2010). An obvious question that follows from these data is why infiltration of silicate melt into depleted peridotite should produce chalcogen element ratios close to CI chondrites. This question also bears on the related issue of chondritic Re/Os and $^{187}Os/^{188}Os$ of refertilized lherzolites, given the strongly divergent partitioning of Re and Os during crust-mantle fractionation (e.g., Becker et al., 2001a, 2004, 2006; Meisel et al., 2001b; Fischer-Gödde et al., 2011). In a large scale, recycling of oceanic crust back the mantle, and remelting and mixing of these rocks may reflect deconstruction of heterogeneity of the chalcogen and the HSE.

Addressing these related issues will also yield insights into the efficiency of crustal recycling and mixing processes in the mantle, and on the relevance of primitive mantle model compositions for chalcogens and the HSE. Therefore,

comparative studies on peridotite bodies with different extent of melt infiltration will shed important insight on the processes of redistribution and re-equilibration of HSE and more incompatible S, Se and Te in the mantle.

1.4 Magmatic fractionation of chalcogens and the HSE in the mantle

The chalcogen, HSE and Os isotopic compositions of infiltrating melts, and the fractionation of these elements during migration in the mantle have not been well constrained. This question will also illuminate the effects of refertilization on abundances and Os isotopic compositions in mantle peridotites.

Mantle pyroxenites are cumulates of migrating melts in the mantle. Their compositional variability indicates that their parent melts have been affected by reactive infiltration, fractional crystallization and mixing (e.g., Sinigoi et al., 1983; Suen and Frey, 1987; Becker et al., 2001a, 2004; Pearson and Nowell, 2004; Downes, 2007; van Acken et al., 2008, 2010b). Because of their lower solidus temperatures compared to peridotite (Kogiso and Hirschmann, 2001; Pertermann and Hirschmann, 2003; Lambart et al., 2009), pyroxenites are also possible sources of mantle melts (Hirschmann and Stolper, 1996; Sobolev et al., 2005, 2007). Mantle pyroxenites as cumulates and possible melt source can constrain the composition of mantle derived melts and fractionation processes.

Refertilized peridotites are commonly associated with sharp or diffuse pyroxenite banding (e.g., Garrido and Bodinier, 1999; Mukasa and Shervais, 1999; Müntener et al., 2004; Le Roux et al., 2007; Piccardo et al., 2007a, 2008; Bodinier et al., 2008; Gysi et al., 2011). Infiltration and trapping of melts produce refertilized peridotites with ratios of chalcogen elements close to CI chondrites and apparently have very similar effects on abundances of incompatible chalcophile Pd, Te, Se, S and Re as equilibrium partitioning during open system melting (Lorand and Alard, 2010; Fischer-Gödde et al., 2011; Wang and Becker, 2013; Wang et al., 2013). This implies a common origin of melts infiltrating peridotites and parent melts of pyroxenites, and transport by diffusive porous flow and channelized flow, respectively.

Secondary interstitial or metasomatic sulfides in refertilized peridotites commonly have suprachondritic $^{187}Os/^{188}Os$ (e.g., Burton et al., 1999; Alard et al., 2002, 2005; Harvey et al. 2011) and reflect the composition of infiltrating melts whose precursors must have had high Re/Os and may be derived from recycling of oceanic crust (e.g., Becker et al., 2001a, 2004; Pearson and Nowell, 2004; van Acken et al., 2008, 2010b). Sulfide segregation during fractional crystallization of oceanic

crust (Rehkämper et al., 1999b; Yi et al., 2000; Bézos et al., 2005) would deplete the HSE and chalcogens and enhance their fractionation compared to primitive partial melts. Thus, it is likely that primitive partial melts and infiltrating melts that have reacted with mantle peridotites have abundances and ratios of HSE and chalcogens different from most MORB. Recycling of oceanic crust may produce melts with different composition of chalcogens and the HSE from those for pyroxenite formation and refertilization.

Melting of veined pyroxenite-peridotites can produce local elemental and isotopic heterogeneity in basalts and in the mantle (e.g., Reisberg et al., 1991; Becker et al., 2001a, 2004; Pearson and Nowell, 2004; Luguet et al., 2008; van Acken et al., 2008, 2010b; Borghini et al., 2013), but it may also lead to homogenization on larger scales. Consequently, the composition and fractionation of chalcophile trace elements in pyroxenites will constrain the nature of different types of mantle derived melts and reveal information about the creation and destruction of the chemical and isotopic signatures of mantle heterogeneity.

The present contribution, and in particular chapters 2 and 3 will address many of these processes that concern the distribution of the chalcogens and HSE in the mantle: 1) to display their compositions and fractionations in the melt products in the mantle; 2) to compare fractionation of element ratios in the mantle with those observed in the oceanic crust; and 3) to evaluate the effects of infiltrating melts on compositions of mantle peridotites and on primitive mantle model compositions for chalcogens and the HSE.

Because sulfides, the HSE and chalcogens are prone to effects of secondary processes such as shallow assimilation and infiltration by melts or fluids and supergene weathering (e.g., Lorand, 1990; Handler et al., 1999; Lorand et al., 2003; Pearson et al., 2004; Reisberg et al., 2005; Ackerman et al., 2009; Lorand and Alard, 2010; Fischer-Gödde et al., 2011), choosing the right samples with minimum influence from these processes has been essential.

1.5 Development of analytical methods for chalcogen element abundances

Because of the predominant control of chalcogen and HSE abundances in mantle derived rocks by accessory micro-phases such as sulfides, alloys and sulfosalts (e.g., Lorand, 1989; Alard et al., 2000, 2005; Meisel et al., 2003b; Luguet et al., 2004, 2007; Meisel and Moser, 2004a; Lorand et al., 2008b, 2010; Wang et al., 2009; Lorand and Alard, 2010; van Acken et al., 2010b; Harvey et al., 2011), the ‘nugget

effect' or sample and powder heterogeneity is a major concern, especially for the HSE (Meisel and Moser, 2004a; Savard et al., 2010; Wang and Becker, In press). Therefore, the precise and accurate analysis of concentrations of all HSE, $^{187}Os/^{188}Os$, and the chalcogens S, Se, Te in the same digestion aliquots is advantageous to limit scatter in the comparison of HSE and chalcogen concentrations, and $^{187}Os/^{188}Os$ in whole rock samples.

Most of these elements have been difficult to analyze at the low abundance levels of the ng/g to pg/g range in crustal and mantle rocks (e.g., Yi et al. 1998, Meisel and Moser 2004b, Bédard et al. 2008, Savard et al. 2009). The analytical methods for the HSE and Os isotopes in mantle peridotites have been mature (e.g., Meisel et al., 2003b; Meisel and Moser, 2004b; Fischer-Gödde et al., 2011).

Problems have existed for precise measurements of S, Se and Te abundances at low concentration levels. For instance, S abundances in geological reference materials (RMs) have been reported in many studies (e.g., Okai et al. 2001, Bédard et al. 2008, Andrade et al. 2009, Ackerman et al. 2012). However, different methods have yielded systematically different results for some samples (e.g., Okai et al. 2001, Ackerman et al. 2012). This may be due to different oxidation states of S in some RMs (presence of sulfates and sulfides), which can lead to incomplete decomposition or partial loss of S as H_2S or SO_2 during acid digestion (Okai et al. 2001, Ackerman et al. 2012). Another explanation of variable results may be heterogeneous distribution of S-rich phases. Therefore, complete digestion of a large amount of sample portion size in a closed system is essential for volatile chalcogen elements, especially for mantle peridotites and pyroxenites where accessory sulfides control the budgets of these elements.

In the Method sections of chapters 2-5 of this study, isotope dilution-ICP-MS methods and closed-system digestion in a high pressure asher for S, Se and Te are described in detail. These methods were newly developed to achieve improved precision and accuracy of concentration data. Chapter 5 reports abundances of the HSE and the chalcogens in geological reference materials with variable compositions which were determined to evaluate precision and accuracy of the newly developed methods.

1.6 Scope of the dissertation

In this dissertation, mantle peridotites from different geological settings, pyroxenites from the Balmuccia peridotite body, geological reference materials and some chondrites have been analyzed for abundances of chalcogen and highly

siderophile elements and Os isotopes, with the objective to constrain some of the open questions discussed in chapters 1.1 to 1.5. The core of the dissertation consist of four chapters (chapters 2 to 5) and mainly address: 1) the behavior of S, Se, Te and HSE during partial melting, melt transport and infiltration in the mantle and effect on their abundances in mantle peridotites; 2) the composition of S, Se and Te in the silicate Earth and the late veneer, its volatile element composition; and 3) the utility of the analytical methods for geological samples.

Chapter 2 introduces new methods for precise abundances of S, Se, Te, the HSE, and $^{187}Os/^{188}Os$ from the same bulk rock digestion aliquots and the application to a comparative case study on the Baldissero and Balmuccia peridotite massifs (Ivrea Zone, Italian Alps). There, the influence of partial melting and melt infiltration on abundances of chalcogens, HSE, and $^{187}Os/^{188}Os$ have been studied.

Chapter 3 reports the abundances and fractionations of the HSE, S, Se and Te and $^{187}Os/^{188}Os$ on different generations of websterites and spinel clinopyroxenites from Balmuccia peridotite body. The data shed significant insight on fractionation of these elements during melt transport in the mantle and possible common nature and origins of migrating silicate melts for mantle refertilization and formation of pyroxenites. It also shows that, besides recycling of oceanic crusts and sediments, fractionation of magmas in the mantle can lead to changes in ratios of these elements, and heterogeneity of the HSE and Os isotopes.

In chapter 4, mantle peridotites from different geological settings and with different extent of partial melting and melt infiltration have been analyzed on abundances of S, Se and Te to constrain abundances and ratios of these elements in the PM. The results offer a strong argument for accretion of a volatile-rich late veneer after Earth's core formation which was predominantly comprised of slightly volatile depleted carbonaceous group chondrites.

In chapter 5, geological RMs with variable compositions and the NIST SRM 612 were analyzed by isotope dilution for bulk rock concentrations of S, Se, Te, HSE (except monoisotopic Ru and Au), including their $^{187}Os/^{188}Os$ composition. The results show the utility of the HPA-S digestion method for these elements, including volatile chalcogens, and the contrasting abundance variations for different HSE, in comparison to S, Se and Te. Concentrations of the HSE in most RMs are highly variable at the <1 gram level. In contrast, S, Se and Te display good precision (RSD < 5 %) in most RMs in the same aliquot.

Chapters 2 to 5 are based on three journal publications and an unpublished manuscript:

Chapter 2:

Wang Z., Becker H. and Gawronski T. (2013) Partial re-equilibration of highly siderophile elements and the chalcogens in the mantle: A case study on the Baldissero and Balmuccia peridotite massifs (Ivrea Zone, Italian Alps). *Geochimica et Cosmochimica Acta* 108, 21-44. Doi: 10.1016/j.gca.2013.01.021.

Zaicong Wang and Harry Becker collected samples and wrote the paper. Harry Becker designed the project. Timo Gawronski initiated to develop analytical methods for Se and Te abundances and provided assistance in measurements of ICP-MS and TIMS. Zaicong Wang completed the development of analytical methods for S, Se and Te abundances and carried out the analyses.

Chapter 3:

Wang Z. and Becker H. Magmatic fractionation of highly siderophile and chalcogen elements in the mantle: constraints from pyroxenites in the Balmuccia peridotite massif. In preparation for submission to *Earth and Planetary Science Letters.*

Zaicong Wang and Harry Becker collected samples and wrote the manuscript. Zaicong Wang performed sample preparation, the analyses and data reduction.

Chapter 4:

Wang Z. and Becker H. (2013) Ratios of S, Se and Te in the silicate Earth require a volatile-rich late veneer. *Nature* 499, 328-331. Doi: 10.1038/nature12285.

Zaicong Wang and Harry Becker wrote the paper. Harry Becker designed the project. Zaicong Wang developed the analytical methods and performed the analyses.

Chapter 5:

Wang Z. and Becker H. (In press) Abundances of sulphur, selenium, tellurium, rhenium and platinum group elements in eighteen reference materials by isotope dilution sector-field ICP-MS and negative TIMS. *Geostandards and Geoanalytical Research.* Doi: 10.1111/j.1751-1908X.2013.00258.x.

Zaicong Wang and Harry Becker wrote the paper. Zaicong Wang performed the analyses and data reduction.

Chapter 2

Partial re-equilibration of highly siderophile elements and the chalcogens in the mantle: A case study on the Baldissero and Balmuccia peridotite massifs (Ivrea Zone, Italian Alps)

Zaicong Wang, Harry Becker and Timo Gawronski

Freie Universität Berlin, Institut für Geologische Wissenschaften,
Malteserstrasse 74-100, 12249 Berlin, Germany

This chapter has been published as:

Wang Z., Becker H. and Gawronski T. (2013) Partial re-equilibration of highly siderophile elements and the chalcogens in the mantle: A case study on the Baldissero and Balmuccia peridotite massifs (Ivrea Zone, Italian Alps). *Geochimica et Cosmochimica Acta* 108, 21-44. Doi: 10.1016/j.gca.2013.01.021.

2.1 Abstract

The conditions at which melt percolation and reactive infiltration of depleted mantle peridotites fractionate highly siderophile elements (HSE) and cause re-equilibration of $^{187}Os/^{188}Os$ in mantle rocks are still poorly constrained. In a comparative study of the Paleozoic Balmuccia (BM) and Baldissero (BD) peridotite tectonites (Ivrea-Verbano Zone, Northern Italy), the influence of partial melting and melt infiltration on abundances of HSE, chalcogens (S, Se and Te) and $^{187}Os/^{188}Os$ have been studied.

At BM, Re depletion ages (T_{RD}) of lherzolites and replacive dunites display a uniform distribution with a maximum near 400-500 Ma. BD peridotites also display a Paleozoic distribution peak but a significant number of samples yielded Proterozoic T_{RD}. The predominance of Paleozoic Re depletion ages in both bodies is consistent with Sm-Nd ages and the late Paleozoic magmatic and geodynamic evolution of the Ivrea-Verbano Zone. The different extents of preservation of ancient $^{187}Os/^{188}Os$ in BM and BD peridotites are interpreted to reflect different degrees of isotopic homogenization and chemical re-equilibration with incompatible element-depleted infiltrating melt during the Paleozoic. The differences between the two bodies are also reflected by differences in HSE and chalcogen abundances, with BD displaying large scatter among HSE patterns, slight re-enrichment of Re relative to Au, and linear trends of Pd, Se and Te with Al_2O_3. The differences in distributions of model ages and heterogeneity in HSE abundances support the view that the lithophile element, HSE and chalcogen variations of different suites of lherzolites likely reflect different extents of reactive melt infiltration in mantle peridotites, with partial re-equilibration and melt extraction in open system environments. However, the variable re-equilibration of BM and BD lherzolites apparently did not produce significant differences in HSE ratios such as Os/Ir, Ru/Ir, Rh/Ir, and Pd/Pt, which are in the range of primitive mantle values, whereas Au, Re and S are somewhat depleted.

The good linear correlation of S with Al_2O_3 in both suites reflects sulfide removal controlled by sulfur solubility in silicate melt, or co-precipitation with pyroxenes and spinel, and indicates very similar bulk partition coefficients for S and Al. S/Se and Se/Te in the lherzolites change little with decreasing Al_2O_3. Results for BM lherzolites are consistent with sulfide-silicate melt partitioning as the dominant control on abundances of the HSE, S, Se and Te during low to moderate degrees of melt extraction ($D_{Pt} > D_{Pd} > D_{Te} \geq D_{Se} \geq D_S \approx D_{Re}$).

Replacive dunites at Balmuccia have low abundances of Re, Au, Pd and chalcogens, but variable and higher abundances of Os, Ir and Ru, high S/Se and Se/Te, yet $^{187}Os/^{188}Os$ similar to BM lherzolites. The residual HSE and chalcogen compositions differ from those in dunites of subduction-related ophiolites. The composition and contact relations of the BM dunites with the host rocks likely reflect focused flow of sulfur-undersaturated melt after open system melting and re-equilibration of the lherzolites. The compositional record of the Balmuccia massif thus reflects the composition of different types of melts and their interaction with the peridotites at different P-T conditions.

2.2 Introduction

The abundances of highly siderophile elements (HSE) and radiogenic Os isotopes in mantle peridotites have been used to constrain the accretion history of the Earth and a spectrum of mantle processes such as melt extraction, melt percolation and crustal recycling (see reviews by Lorand et al., 2008a and Walker, 2009). In spite of many studies that report HSE abundances and $^{187}Os/^{188}Os$ data on mantle peridotites, distinguishing the influence of processes such as closed system partial melting, silicate melt percolation, metasomatism by sulfide melts, or effects by hydrothermal or surface processes on the abundances of HSE and $^{187}Os/^{188}Os$ in mantle rocks has remained difficult (e.g., Lorand et al., 2008a; Rudnick and Walker, 2009; Fischer-Gödde et al., 2011). Abundance variations of the HSE and the chalcogens S, Se and Te in the upper mantle and their fractionation in mantle-derived melts are strongly influenced by the behavior of the sulfide phases and alloys of platinum-group elements (e.g., Garuti et al., 1984; Morgan, 1986; Peach et al., 1990; Lorand et al., 1999, 2010; Rehkämper et al., 1999a; Alard et al., 2000). Thus, a clearer distinction of some of the processes mentioned before should become possible if HSE and chalcogen abundances can be obtained on the same sample aliquot.

Many studies over the last decade have concluded that the major and trace element composition of many peridotites can be affected by silicate melt migration in various ways (e.g., Bodinier and Godard, 2003; Zhang et al., 2004; Le Roux et al., 2007; Piccardo et al., 2007b; Dick et al., 2010; Batanova et al., 2011; Riches and Rogers, 2011). These processes also affect the distribution of the HSE in mantle peridotites in different ways. It has been noted that secondary sulfides on grain boundaries in peridotites are often enriched in Pd, Re, Au and radiogenic Os (e.g., Alard et al., 2000, 2002, 2005; Luguet et al., 2001; Pearson et al., 2004; Harvey et al., 2011). Textural evidence indicates co-precipitation of such grain boundary sulfides with pyroxenes and spinels from melts, which would replenish depleted peridotites in

basaltic components, Pd, Re, Au and sulfur by such melt infiltration and even more extremely by refertilization that is defined as the addition of phases that are mineralogically indistinguishable from common mantle peridotite phases (e.g., Dawson, 1984; Le Roux et al., 2007; Lorand and Alard, 2010). Suites of variably depleted peridotites yield evidence for these processes, both from HSE abundances and Os isotopic data of different sulfide generations in such samples and from bulk rock systematics of elements such as Pd (e.g., Burton et al., 1999; Alard et al., 2000, 2002; Pearson et al., 2004; van Acken et al., 2008; Lorand et al., 2010; Fischer-Gödde et al., 2011). In contrast, because of higher melt/rock ratios, melt percolation that leads to the formation of replacive dunites involves dissolution of pyroxenes, Al phases and sulfides, and precipitation of olivine (Kelemen et al., 1995, 1997). Because of sulfide dissolution and reprecipitation, and higher melt/rock ratios compared to melt infiltration processes, some replacive dunites display melt like HSE abundance patterns, with depletion in compatible HSE such as Os, Ir and Ru and enrichments in Pt, Pd, Re and radiogenic Os (e.g., Büchl et al., 2002).

In recent work on peridotites that display evidence for refertilization, it appears that only harzburgites can be identified as melting residues with a simple history, and this begs the question: where are the lherzolitic melting residues that have been postulated to exist in the upper mantle as a consequence of low to moderate degrees of partial melting (e.g., Walter, 2003). Experimental sulfide-silicate partitioning studies indicate that in melting residues that reflect sulfide-silicate equilibrium, Re should become gradually depleted during moderate degree of partial melting (Mallmann and O'Neill, 2007; Brenan, 2008), whereas abundances and ratios of compatible HSE (Os, Ir, Ru and Rh, possibly also Pt and Pd) should remain nearly constant until sulfides are exhausted (Fleet et al., 1999). On the basis of the behavior of specific ratios (e.g., Pd/Pt), some lherzolite compositions may indeed reflect sulfide-silicate equilibrium (e.g., Fischer-Gödde et al., 2011), but many lherzolites for which high-quality Pt, Pd and Re data on whole rocks are available reflect melt-peridotite mixing and disequilibrium (e.g., Pearson et al., 2004; Becker et al., 2006; Lorand et al., 2010; Fischer-Gödde et al., 2011). As an alternative process, fractionation of the HSE during melting has been ascribed to preferential removal of Cu-Pt-Pd-Au rich sulfide liquids that would leave behind a refractory monosulfide solid solution (MSS), and at higher degrees of melting, Os-Ir-Ru alloys that sequester compatible HSE (Alard et al., 2000; Bockrath et al., 2004; Ballhaus et al., 2006; Luguet et al., 2007). Because Re should be retained in residual MSS, according to partition coefficients between MSS and sulfide melt (Brenan, 2002), the latter process is inconsistent with the enrichment of Re in mantle-derived melts, the depletion of Re in many lherzolites and detailed Pt-Pd-Au variations in mantle peridotites (e.g.,

Gannoun et al., 2007; Fischer-Gödde et al., 2011). If sulfide-silicate equilibration controls the HSE distribution during moderate degrees of partial melting, residues of such processes should exist. On the other hand, if peridotites with such compositions do not occur, melt extraction viewed from an HSE and Os isotopic standpoint would be mostly a disequilibrium process that preferably removes radiogenic and fertile components from grain boundaries of peridotites.

Because of the major control of HSE abundances in peridotites by sulfides, a better understanding of the systematics of the chalcogens is a key for understanding and distinguishing the effects of partial melting and melt infiltration, and their influence on equilibration and partitioning behavior of the HSE in mantle rocks. This may be achieved by obtaining precise and accurate abundances of the HSE, S, Se and Te, and $^{187}Os/^{188}Os$ data on the same sample aliquot. At present, only very limited abundance data for the chalcogens in mantle rocks are available (Morgan, 1986; Lorand and Alard, 2001, 2010; Lorand et al., 2003; Luguet et al., 2003; König et al., 2012), and both HSE and chalcogen data sets are incomplete. Remarkably, S/Se and Se/Te in lherzolites from the Lherz ultramafic massif are similar or only slightly different from CI chondrites. The lherzolites at Lherz have been interpreted to have formed by refertilization of harzburgites (Le Roux et al., 2007), and accordingly, the sulfides and their compositions have been interpreted to have precipitated mostly from the infiltrating melt (Lorand and Alard, 2010). An obvious question that follows from these data is why infiltration of silicate melt into depleted peridotite should produce chalcogen element ratios close to CI chondrites? This question also bears on the related issue of chondritic Re/Os and $^{187}Os/^{188}Os$ of refertilized lherzolites, given the strongly divergent partitioning of Re and Os during crust-mantle fractionation (e.g., Meisel et al., 2001b; Becker et al., 2006; Fischer-Gödde et al., 2011). Addressing these related issues will also yield insights into the efficiency of crustal recycling and mixing processes in the mantle, and on the relevance of primitive mantle model compositions for these elements.

In the present study, we present a new method for the precise and accurate analysis of concentrations of all HSE and $^{187}Os/^{188}Os$ (following Fischer-Gödde et al., 2011), and the chalcogens S, Se, Te in the same digestion aliquots. This method limits scatter in the comparison of HSE and chalcogen concentrations, and $^{187}Os/^{188}Os$ in whole rock samples, that result from trace phase heterogeneity in sample powder. The method is applied to peridotites of variable fertility from the Balmuccia and Baldissero bodies in the Ivrea-Verbano Zone (Northern Italy). These peridotite bodies are from a well-constrained geologic setting and permit sampling of the least weathered and least serpentinized peridotite tectonites worldwide. Such samples are prime targets for the analysis of mobile elements such as the chalcogens in mantle

rocks. Goals of this work have been: 1) to constrain the coupling of HSE and chalcogen abundances in variably depleted mantle rocks and the details of the relevant partitioning processes; 2) to evaluate the different effects of percolation of sulfur saturated and sulfur undersaturated melt on HSE and chalcogen abundance variations in mantle peridotites and the role of partial melting; 3) to study the different extent of re-equilibration of the HSE and Os isotopes in mantle peridotites, exemplified by the Balmuccia and Baldissero sample suites; and 4) to explain the differences in HSE abundance and Os isotopic compositions of Balmuccia dunites compared to tabular dunites from subduction-related settings (Becker et al., 2001a; Büchl et al., 2002, 2004; Zhou et al., 2005).

2.3 Geological setting

The Ivrea-Verbano Zone (IVZ), in the western Italian Alps represents one of the best studied cross-sections of lower-to-middle continental crust. The section forms part of the Adriatic plate and was exposed in the course of its collision with Europe during the Alpine orogeny (e.g., Fountain, 1976; Handy et al., 1999; Quick et al., 2009). The IVZ consists of two main units: the high-grade paragneiss Kinzigite Formation and the voluminous Mafic Complex which intruded into the Kinzigite Formation over a protracted time interval between 290 Ma and 210 Ma (Peressini et al., 2007). The peridotites massifs near Baldissero (BD) and Balmuccia (BM) were emplaced into lower crustal granulite facies metabasites of the IVZ, presumably in the Carboniferous or Permian (e.g., Shervais and Mukasa, 1991; Quick et al., 1995; Peressini et al., 2007; Mazzucchelli et al., 2010; please also see geological maps therein). They are comprised of fresh, unserpentinized spinel facies peridotites and by a wide range of gabbroic and pyroxenitic dikes and veins. The presence of gabbroic dikes indicates shallow crustal exhumation of the peridotite bodies during Mesozoic extension (Mukasa and Shervais, 1999; Mazzucchelli et al., 2010).

The Balmuccia massif, a 4.5 km long, 0.8 km wide lens, is the main occurrence of mantle rock near the base of the IVZ. It has an igneous contact with the Ivrea-Verbano mafic-ultramafic complex at its eastern margin, which indicates that peridotite emplacement predated the main mafic intrusions. Its western contact is along the mylonitic Insubric line (Shervais, 1979). The BM massif predominantly consists of spinel lherzolite (>85 % volume), with subordinate dunite (～10 %) and rare harzburgite gradating into lherzolite (Shervais and Mukasa, 1991; Mukasa and Shervais, 1999). Spinel lherzolite typically contains 60-70 % olivine, 20-25 % orthopyroxene (opx), and 12 % clinopyroxene (cpx) by volume with granular texture. The composition has been interpreted to reflect low to moderate degrees of melt

extraction (e.g., Shervais and Mukasa, 1991). Peridotites are discordantly cut by several generations of abundant websterite dikes (Cr-diopside and later Al-augite suites), which are parallel to and sometimes at low angle with lherzolite foliations, representing multistage melt intrusion before crustal emplacement (Sinigoi et al., 1983; Rivalenti et al., 1995; Mukasa and Shervais, 1999). Crustal emplacement of the body during extension is indicated by late gabbro dikes and rare hornblendite veins. Dunite dikes of limited thickness (<40 cm wide) are thought to originate by pyroxene-dissolving reactions caused by melt infiltration into the host lherzolite from dike conduits (Rivalenti et al., 1995). Spinel-rich tabular dunite bodies (50 m thick and 150 m long) display sharp or gradational contacts with lherzolites. These dunites were interpreted to have formed by focused melt percolation (Mazzucchelli et al., 2009). Because Cr-diopside websterite dikes and clinopyroxene from dunite bodies display similar Sr and Nd isotopic composition, it has been argued that the melt that produced the dunites may have been derived from Cr-diopside pyroxenite veins (Mazzucchelli et al., 2009).

The Baldissero massif occurs in the southern-western part of the IVZ and consists of a 3 km long and 0.5-2 km wide peridotite lens. It is in contact with gabbroic rocks of the Mafic Complex in the east, whereas it was sheared by the faults of the Insubric system in the west, where it is in tectonic contact with the Canavese terrains of the Austroalpine domain. The Baldissero peridotite, like Balmuccia, also consists of spinel-facies lherzolites, with average modal composition of 53 % olivine, 25 % opx, 15 % cpx and 2 % spinel (Ernst, 1978; Sinigoi et al., 1980), but it appears relatively homogenous and does not display a strong foliation. It is also cut by different generations of pyroxenite dikes (Cr-diopside and Al-Augite suites) that are much less abundant than in the Balmuccia massif. Late diorite dikes, which occur as NE trending swarms cutting sharply and discordantly across the peridotite foliations and all the pyroxenite dikes, intruded during the Mesozoic (Sm-Nd age from 204±31 Ma to 198±29 Ma, Mazzucchelli et al., 2010). The magma that produced the diorite dikes induced local reaction with ambient host lherzolite. Abundances of lithophile incompatible elements of whole rocks and clinopyroxenes from Baldissero peridotites are consistent with low-degree (～4-5 %) near-fractional melting of depleted mantle, possibly under garnet-facies conditions (Mazzucchelli et al., 2010). A Paleozoic Re depletion model (T_{RD}) and a Sm-Nd errorchron age (378±48 Ma) of clinopyroxene separates from the Baldissero spinel peridotite were interpreted to reflect Paleozoic partial melting, presumably during the Variscan orogeny (Obermiller, 1994; Mazzucchelli et al., 2010). It has been noted that even some lherzolites far from dikes may have been slightly affected by melt percolation, as evidenced by the

crystallization of accessory titanian pargasite and the slight enrichment of highly incompatible elements (Mazzucchelli et al., 2010).

2.4 Sample description

In this contribution 27 peridotites of variable fertility from BD and BM and four samples from tabular dunite bodies from BM were analyzed. Eleven peridotites have been analyzed previously for major elements, trace elements and Sr-Nd-O isotopes of clinopyroxene separates (Obermiller, 1994; Rivalenti et al., 1995). These 11 samples were collected distant to mafic dikes (Obermiller, 1994). The other samples were collected in 2011 (some by using a rock coring device), and are also macroscopically unweathered and unaltered and were collected far from dikes (generally >0.3 m), to limit any influence of melt percolation. Four Balmuccia dunites analyzed in this study were from tabular dunite bodies in Balmuccia (Mazzucchelli et al., 2009). In some areas, dunite bodies display hornblendite domains or spinel Cr-diopside veinlets. With the exception of BM11-07A, all dunites were sampled far from dikes (>0.3 m). These dunite samples display a homogenous distribution of olivine and minor tiny spinel grains (0.5-2 %). BM11-07A is cut by later sulfide-rich orthopyroxene veins, and was collected 15 cm away from the vein. Harzburgite BM11-03B grades into dunite BM11-03A with decreasing orthopyroxene abundance, probably reflecting increasing dissolution of pyroxenes by percolating melt. Both samples were collected some distance from their gradational boundary (around 20 cm).

Peridotites collected in 2011 were split into two portions. One portion was used for thin sections and the other for whole-rock powder. Rocks that were ground to powder had visibly altered surfaces removed by cutting with a rock saw. Cut surfaces were abraded with silica emery paper and washed with 18.2Ω Milli-Q (Nanopure) water, and subsequently dried overnight. Pieces of 0.5-1.5 kg (two drill cores, 100-200 g) were crushed into small chips under paper to ensure protection from contamination by the hammer, and were processed to fine powder (～200-300 g, 10 μm) using an agate disc mill.

Most samples are exceptionally fresh, as indicated by the absence of serpentine minerals and low loss on ignition (LOI, typically <1 %). Accordingly, sulfides often display mineral assemblages unaffected by alteration processes. Two samples (BD11-12 and BD11-13) from drill cores are weakly serpentinized, the alteration degree is still low (max. LOI of these samples is 4.7 wt.%). Most sulfides in Baldissero and Balmuccia peridotites are interstitial and anhedral intergrowths 20-500 μm across and abundant sulfide grains occur adjacent to olivine, spinel and pyroxene.

Pentlandite and subordinate chalcopyrite are the major base metal sulfides (>95 % by volume). They are often intergrown in different proportions, reflecting exsolution from high-temperature solid solutions upon cooling during ascent (e.g., Lorand, 1989). A few tiny (<30 μm) sulfide inclusions occur in silicate minerals, mostly in olivine in both locales. Sulfide inclusions appear to be more abundant in BD samples. Sulfides in dunites are sparse and also tiny (10-20 μm), but most are interstitial and occur with spinel. Brief petrological and microscopic descriptions of samples collected in 2011 are given in the Supplement.

2.5 Analytical methods

2.5.1 Major elements

Major and some trace elements of new samples and old ones without data were determined at the GFZ Potsdam using XRF method (Panalytical Axios Advanced) as in Fischer-Gödde et al (2011). The precision of measurement typically ranges from 2-3 % relative standard deviation (RSD) for SiO_2, MgO and FeO, 5–8 % RSD for Al_2O_3 and CaO, and 10–20 % RSD for Na_2O, TiO_2 and MnO. The typical detection limits are 0.01 %. LOI was determined gravimetrically after combustion at 1100ºC.

2.5.2 Sample digestion and chemical separation

Digestion in concentrated HCl and HNO_3 in a high-pressure asher (HPAS, Anton Paar ^{TM}) employed in this study is now a standard method for the digestion of HSE in ultramafic materials (Meisel and Moser, 2004b). Sulfur, Se and Te in peridotites are hosted by sulfides or tellurides which are easily digested using the HPSA method (Lorand and Alard, 2010). About 3 g of sample powder were weighted into 90 ml quartz glass digestion tubes and mixed with ^{185}Re-^{190}Os, ^{191}Ir-^{99}Ru-^{194}Pt-^{105}Pd, ^{77}Se-^{125}Te and ^{34}S spike solutions, followed by 2.5 ml 9 M HCl and 5 ml 14 M HNO_3. The vessels were sealed immediately with Teflon-tape after adding reverse aqua regia and placed into a high-pressure asher for 16 h digestion at 320 °C and 100 bar. After digestion, osmium was extracted by solvent extraction from the reverse aqua regia into CCl_4, back extracted into HBr (Cohen and Waters, 1996), and further purified by microdistillation from a H_2SO_4-dichromate solution into 15 μl of HBr (Birck et al., 1997). One third of the aqua regia solution was used for HSE separation and another third for S-Se-Te separation.

2.5.3 HSE separation

Chemical separation of the HSE aliquot followed techniques described previously (Fischer-Gödde et al., 2010, 2011). Rhenium, Ir, Ru, Pt, Rh, Pd and Au were separated from the matrix by cation exchange chromatography using 10 ml of pre-cleaned Eichrom 50W-X8 (100-200 mesh) resins. After collection of 14 ml 0.5 M HCl-40 % (v/v) acetone eluent which contains HSE, the eluted HSE fraction was split: one half for the analysis of Au, Re, Ir, and Pt (Au fraction), and the other half for analysis of Rh, Ir, Ru, Pt and Pd (Pd fraction). Iridium and Pt were analyzed in both splits. A second clean-up procedure was further performed on the Pd fraction using 2 ml Eichrom 50W-X8 (100-200 mesh) resin and 0.2 M HCl. The Pd fraction was evaporated to near dryness and the residue was taken up in 0.28 M HNO_3 for ICP-MS analysis. The recovery yield was >95 % for all HSE.

2.5.4 S-Se-Te separation

For the chemical separation of S, Se and Te, a two-step ion exchange chromatography method was used, followed by hydride generation (HG) ICP-MS. About 2 ml of the aqua regia sample solution were evaporated to dryness at 85 °C, and further dried twice with 2 ml 9 M HCl to ensure complete reduction of Se and Te to quadrivalence and conversion of the solution to chloride form. After dissolution of the residue in 4 ml 6 M HCl, the solution was loaded on 3 ml pre-cleaned Eichrom AG1-X8 (100-200 mesh) anion resin (Fehr et al., 2004). The anion resin was pre-treated with 3 ml 1 M HNO_3 twice and 3 ml Nanopure water and conditioned with 3 ml 6 M HCl twice. S and Se are not absorbed on the anion resin and collected in 8 ml 6 M HCl with matrix. 4 ml 9 M HCl and 5 ml 10 % HF were further eluted to remove remaining matrix from the column. Finally, tellurium was eluted by 8 ml 1 M HNO_3.

The S-Se fraction in 6 M HCl was dried at 85 °C, Se completely converted to Se (IV), and then dissolved in 4 ml 0.06 M HNO_3. To remove remaining matrix in the fraction, a second purification step was employed using 3 ml Eichrom 50W-X8 (100-200 mesh) resin. The S-Se solution was loaded on to resin which was cleaned in 6 M HCl and Nanopure water and conditioned with 0.06 M HNO_3. The S-Se cut was collected in 8 ml 0.06 M HNO_3 and 1 ml 7 M HNO_3 was added to facilitate the hydride generation reaction. Because the sulfonic acid groups of the cation exchange resin can be easily decomposed by oxidizers, and thus may produce high S blanks, significant Fe^{3+} in the solution must be removed on the anion resin which has been done before loading on the cation resin.

Recovery of S and Se in this procedure is high (>95 %), but Te yields are highly variable, ranging from 10 % to >95 %, depending on the composition of the matrix. Of note, procedural blanks without matrix always achieved high yield of Te (>95 %), whereas Te yields from lherzolites were typically around 10-30 % (see also Yi et al., 1998; Fehr et al., 2004). Precise and accurate Te data can nevertheless be obtained due to application of the isotope dilution method and hydride generation.

2.5.5 Mass spectrometry

Osmium isotopic ratios were determined using negative thermal ionization mass-spectrometry and a Thermo-Finnigan^{TM} Triton at Freie Universität Berlin. The measured Os isotopes were corrected for mass fractionation using the $^{192}Os/^{188}Os$ ratio of 3.0827 after isobaric OsO_3^- interferences and oxygen correction and subsequent subtraction of the spike contribution. Faraday cups were used for all samples and the in-run precisions were typically better than 0.005 % relative standard error (RSE) at 0.5-2 voltage for intensities of ^{190}Os. Analysis of 30 ng aliquots of the UMD Os standard during the duration of the project resulted in $^{187}Os/^{188}Os$ values of 0.11380±3 (2SD, n=14). Os concentrations were determined using the isotope dilution method.

All other HSE were measured by sector-field inductively coupled plasma mass spectrometry (SF-ICPMS) using the ThermoElectron Element XR at Freie Universität Berlin, following the methods outlined in Fischer-Gödde et al (2011). The Au fraction was analyzed using a Scott type glass spray chamber after reducing the volume of the solution to 2 ml. The Pd fraction was analyzed by Aridus membrane desolvator. Rhodium and Au concentrations were calculated by standardization to the ^{101}Ru and ^{193}Ir signal intensities and concentrations of other elements by the isotope dilution method (Fischer-Gödde et al., 2011). The standard errors of the mean of measured isotopic ratios for HSE were better than 0.3 % (2 RSE, n=750 scans) using a peak dwell time of 45 ms.

Sulfur measurements were performed on the S-Se fraction using a Scott type glass spray chamber. In order to resolve molecular interferences, masses ^{32}S, ^{33}S and ^{34}S were detected at medium mass resolution mode ($m/\Delta m$=4000) on the Element XR by analog mode (Craddock et al., 2008). After two-step purification, the double charged ions of Ni^{2+} and Zn^{2+} interferences are insignificant. Molecular interferences, especially O_2 and HS^- can be easily resolved at $m/\Delta m$=4000. Acid blank solutions were measured before and after each sample to control background intensities and memory effects. Subtraction of acid blank was always carried out, although background intensities were <0.5 % of samples signals. Mass fractionation was determined and corrected by the comparison of the isotope ratios of a S standard

solution, which was prepared using K_2SO_4 powder (Merck company, >99 %), a reference material with well-determined $\delta^{34}S$=10.70±0.15 by gas source mass spectrometry. $^{32}S/^{34}S$ ratios were used to calculate S concentrations by isotope dilution. The standard error of $^{32}S/^{34}S$ were better than ±0.1 % (2 RSE) using n = 800 scans and a peak dwell time of 5 ms.

Se and Te were measured using low mass solution mode on the Element XR combined with a hydride generation sample introduction system by reacting the sample solution with 1 % m/m $NaBH_4$ in 0.05 M NaOH (Rouxel et al., 2002; Elwaer and Hintelmann, 2008b). The HG technique significantly reduces memory effects and facilitates the efficiency of Se and Te transfer to the plasma and the ionization yield. Because of the formation of volatile hydrides, the effective separation of the gaseous hydrides of Se and Te from potential interferences can be easily achieved. In order to avoid potential bias from fluctuations of the Ar background (Elwaer and Hintelmann, 2008a), we have chosen $^{77}Se/^{82}Se$ and $^{125}Te/^{126}Te$ to calculate Se and Te concentrations by isotope dilution. For Ar-based polyatomic interferences, subtraction of gas blank followed by mass discrimination correction is sufficient for accurate Se and Te data reduction. Other possible inferences derived from the formation of $^{76}SeH^+$ and $^{125}TeH^+$ also can be neglected. Details of Se and Te measurements by HG have been given in the Supplement. Due to variations in the gas flow during HG, the Se and Te intensities were not as stable as for the HSE and S, typically yielding 3-8 % RSD for samples. Standard errors of the mean of $^{77}Se/^{82}Se$ and $^{125}Te/^{126}Te$ were better than 0.1 % (2 RSE) using peak dwell times of 5 ms and sample gas flow of 1.195 L/min and n = 6000 and 9000 scans, respectively.

2.5.6 Analytical blanks

The total procedural Os blank was 1-2 pg with $^{187}Os/^{188}Os$ ratio of 0.11-0.15, which was negligible for all samples in this study. Other HSE procedural blanks were 6±3 pg for Re, 1±0.5 pg for Ir, 1±1 pg for Ru, 8±3 pg for Pt, 8±4 pg for Pd, 2±2 pg for Au and 10±3 pg for Rh (n=8). Blank corrections were negligible (<1 %) for Ir, Ru, Pt, Pd and Rh in all samples, and for Au and Re in most samples, but up to 15 % for the latter elements in harzburgites and dunites. The S blank was typically 2-3 μg (mainly from the cation resin), whereas Se blanks ranged from 0.5 to 1.5 ng and Te blanks from 5 to 15 pg. Procedural blank corrections for the chalcogens were always applied and in most cases insignificant (<1 %). For depleted harzburgites and dunites, procedural blanks may comprise up to 5 % for S, Se and Te using 3 g sample powder.

2.6 Results

2.6.1 Data quality

The accuracy and reproducibility of HSE abundance measurements and Os isotopes of the techniques used at Freie Universität Berlin have been discussed by Fischer-Gödde et al. (2010, 2011) using chondrites, the reference material UB-N (a serpentinized lherzolite), and duplicate analyses of samples. For the HSE, several duplicates analyzed in the course of the present study show similar reproducibility as in previous studies (Table 2.1). The accuracy of S, Se and Te concentration data is more difficult to evaluate, because concentration determinations of these elements in geological reference materials tend to vary significantly (Table 2.2). This is in part because of analytical problems in previous studies, but also because of the possible heterogeneity of sulfides in sample powder in mafic and ultramafic rocks. For the present study, we used the reference material UB-N and the CI chondrite Orgueil (Table 2.2). For the latter, various types of data for these elements are available; however, no analyses where all three elements have been determined on the same sample aliquot. Our Orgueil data can be used as a reference for normalization, and thus permits a precise assessment of the relative fractionation of the chalcogens between the analyzed peridotites and a CI chondrite. The Se content of UB-N agrees within 1 % with values determined by isotope dilution method by König et al. (2012), and the abundance of Se in Orgueil determined in the present study is within 2.5 % of the results determined by INAA by Dreibus (et al., 1995). There is no available reference value for Te in UB-N. Our value is about 10 % higher compared with the limited published data (Table 2.2). The Te concentration determined for our Orgueil aliquot is within 2.2 % of most radiochemical neutron activation data from the literature as compiled by various authors (e.g., Anders and Grevesse, 1989), suggesting excellent accuracy. The Te (2.31 μg/g) and Pd concentrations (569 ng/g) of our Orgueil aliquot are very similar to data on Orgueil obtained by the isotope dilution method by Loss et al. (1984), with Te/Pd of both studies overlapping within 2 %. Duplicates of peridotite samples and repeated analysis of Se and Te concentrations from different aliquots of the same digestion indicate very good reproducibility (<5 %), even for dunites and harzburgites with low concentrations of these elements (Table 2.1). A few samples display larger variations (5-10 %) between different measurements. These results reflect the developmental process of our analytical methods for initial samples and unstable gas flow with 0.1-2 % variation (RSD) of isotope ratios. The S content of the UB-N aliquot is broadly consistent with published data that give large ranges (Okai et al., 2001; Lorand et al., 2008b; Ackerman et al., 2012). Duplicate analyses of the depleted lherzolite BM11-08 and

dunite BM11-05 display larger variations for S (20-40 %), but BM11-02 which has the highest S concentration (349 ppm) matches its duplicate well (Table 2.1). The variation of S contents in these duplicates of depleted samples likely reflects heterogeneous distribution of sulfides in the sample powder. For samples with multiple analyses, we use average results in the following discussion. Errors of concentrations are within the size of the symbols in all figures.

2.6.2 Main results

The BM lherzolites are depleted to moderately fertile, and Al_2O_3 contents of samples from the present study range from 2.0 % to 3.4 % with Mg# (atomic ratio of Mg/(Mg+Fe) * 100) from 89.4 to 90.4 (except harzburgite BM11-03B, Table 2.1, Figure 2.1, and the Supplement). Good correlations of Al_2O_3 and CaO with MgO for BM and BD peridotites are consistent with previous data (e.g., Obermiller, 1994; Rivalenti et al., 1995; Mazzucchelli et al., 2010). All samples have very low Na_2O (0.01-0.15 %) and low TiO_2 (0.02-0.10 %), which display scattered negative trends with MgO. The slopes of the trends for Balmuccia and Baldissero are different (Figure 2.1).

The BM lherzolites have unfractionated Os, Ir, Ru, Rh and Pt abundances and show variable depletion of Pd, Au and Re (Figures 2.2-2.4). Sample BM11-11 has a higher Pt content than other BM samples (Figure 2.4a). In contrast, BD lherzolites display, although similar in major element composition, much more variable HSE patterns, especially for incompatible HSE (Figure 2.4b). The patterns are flat from Os to Rh and variably depleted from Pt to Re. Abundances of Os, Ir, Ru and Rh in the lherzolites from Balmuccia and Baldissero remain relatively constant with lithophile melt extraction indicators (e.g., Al_2O_3, Figure 2.2a) and S contents (not shown). Notably, the scatter of abundances of compatible HSE for BM lherzolites (e.g., Os_n = 3.99±0.32, 2SD) is considerably less than for BD lherzolites (Os_n = 3.93±0.87, 2SD). Os/Ir, Ru/Ir, Rh/Ir and Pt/Ir in the lherzolites overlap with the primitive mantle value (Becker et al., 2006, Fischer-Gödde et al. 2011). Pd/Pt of the lherzolites is constant but mostly suprachondritic, whereas Pt/Ir and Pt/Os are mostly in the range of chondrites (Figure 2.3). As observed for peridotites elsewhere (e.g., Pearson et al., 2004; Becker et al., 2006), depleted samples tend to display more scatter in these ratios. For example, harzburgites have variable and fractionated HSE, e.g., variable Os contents and Os/Ir ratios (Figures 2.2 and 2.3). The mean Os/Ir and Ru/Ir of lherzolites from Baldissero tend to be slightly higher than those from Balmuccia (Figure 2.3). And unlike BM, BD has more variable Pt/Ir and Pd/Ir ratios. For a given Al_2O_3 content, Re/Ir ratios in BM and BD are lower (Figure 2.3f) than in peridotites elsewhere (e.g., Becker et al., 2006).

Initial $^{187}Os/^{188}Os$ at emplacement age 280 Ma are subchondritic to chondritic (0.11774-0.13054), corresponding to $\gamma Os_{(280Ma)}$ from -5.7 to +4.3 (Table 2.1). BM peridotites display a positive trend of Re/Os with Al_2O_3, consistent with variations of initial $^{187}Os/^{188}Os$ with $^{187}Re/^{188}Os$ (Figure 2.5). In contrast, BD peridotites display substantially more scatter in these diagrams.

For 11 samples, no S data are available, because the S spike was prepared later during this project. Sulfur, Se and Te concentrations display large, but mostly systematic variations (Figures 2.6 and 2.7). The exceptions are two BM samples (BM11-02A and BM90-15) with notably high S, Se and Te abundances compared with samples of similar Al_2O_3 content. Sulfur displays excellent linear correlation with Al_2O_3 for both BM and BD suites (Figure 2.6a), in spite of the fact that these elements were analyzed in different sample aliquots and are hosted by different phases. Selenium and Te also display positive correlations with Al_2O_3, but with larger scatter and a systematic offset of the two sample suites (Figures 2.6 and 2.7). Similar correlations and systematic differences for the two suites are found for correlations with Re and Pd (Figure 2.7). No systematic difference between lherzolites of the two suites is notable in the Se-Te diagram, whereas a systematic difference appears in the S-Se diagram (Figure 2.8).

The dunites from Balmuccia analyzed in the present study have major element composition and Mg# of 90.7 to 91.1 (Figure 2.1 and the Supplement), similar to data in Mazzucchelli et al. (2009). With the exception of sample BM11-05, all HSE and the chalcogens display low and variable concentrations in the dunites, consistent with the rare occurrence of sulfide grains in thin sections. Platinum, Pd, Au and Re are mostly depleted compared to Os, Ir, and Ru (Figure 2.4a). Sample BM11-05 is quite high in Ir, Rh and Ru, even higher than in fertile lherzolites, but Pt, Pd, Re, Au and the chalcogens display low concentrations (Figure 2.4). HSE ratios in the dunites are more strongly fractionated than in other peridotites (Figure 2.3). Se/Te and S/Se are variable but tend to be significantly higher than in lherzolites (Figure 2.9). $^{187}Os/^{188}Os$ in Balmuccia dunites are similar to other peridotites from Balmuccia, but show a considerable range, given their very similar Al_2O_3 content (Figure 2.5, Table 2.1).

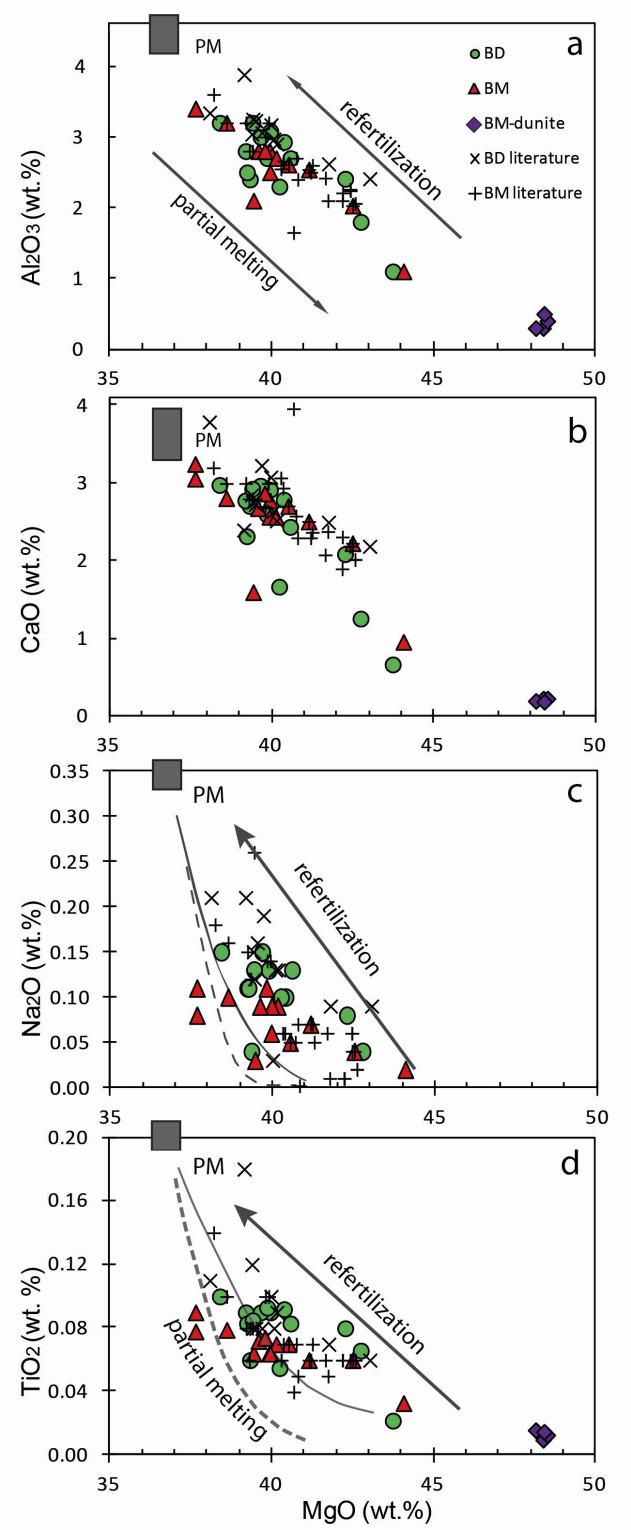

Figure 2.1 Correlations of bulk rock MgO with Al_2O_3 (a), CaO (b), Na_2O (c) and TiO_2 (d) in Balmuccia and Baldissero peridotites. Trends show roughly linear decrease in Al_2O_3 and CaO with decreasing MgO, whereas Na_2O and TiO_2 contents do not fit curved trends of batch (solid line) or fractional (dashed line) melting for most samples (Niu, 1997). The data in (c) and (d) suggest that some samples record melt infiltration processes. Literature data are from (Hartmann and Wedepohl, 1993; Obermiller, 1994; Rivalenti et al., 1995; Mazzucchelli et al., 2010). Na_2O contents of dunites are below detection limits. PM data is from Palme and O'Neill (2003).

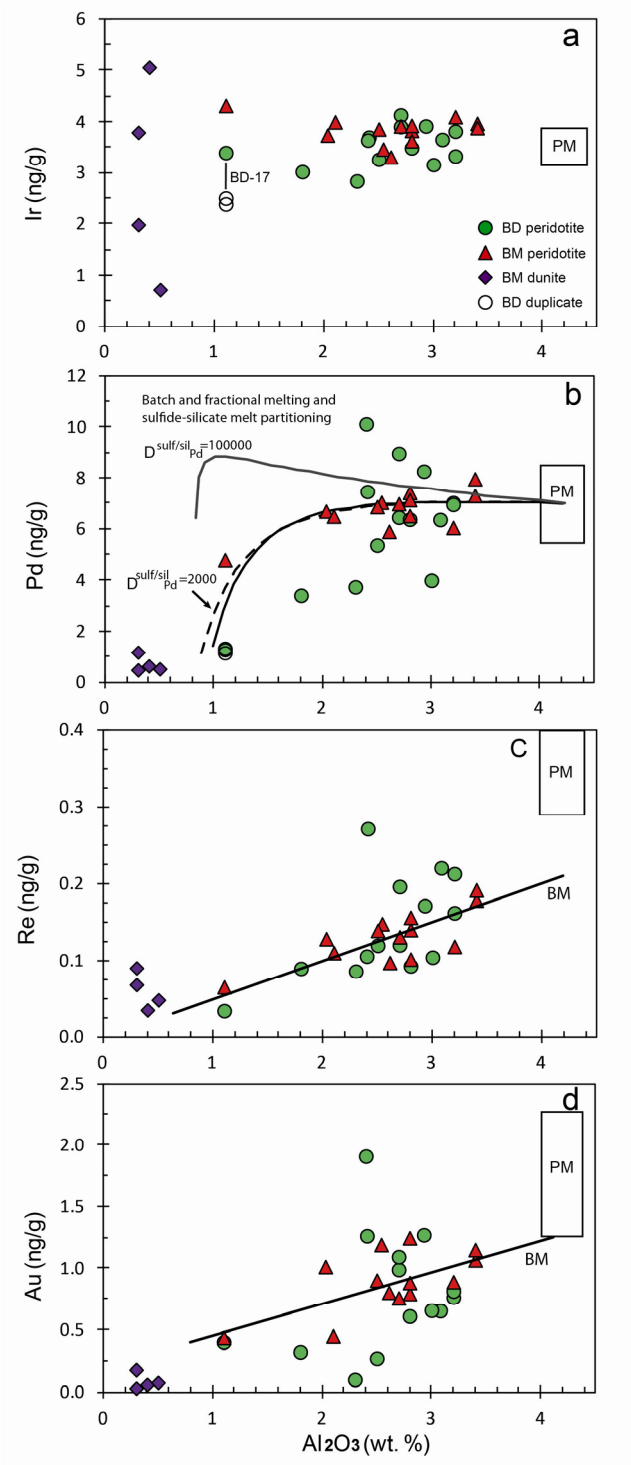

Figure 2.2 Diagrams of Al_2O_3 contents with Ir (a), Pd (b), Re (c) and Au (d). Fertile samples have roughly constant compatible HSE abundances, but decreasing Pd, Re and Au contents with decreasing Al_2O_3. Modeling of batch (solid line) or fractional (dashed line) melting assuming sulfide-silicate partitioning and $D_{Pd}^{sulf/sil}$ =2000 is roughly consistent with the Balmuccia samples; whereas high $D_{Pd}^{sulf/sil}$ of 100000 may be too high (see discussion). Three duplicates of harzburgite BD-17 have considerably different Os and Ir contents, implying heterogeneous distribution of HSE or incomplete digestion. Dunites display variable Ir contents and very low Pd, Re and Au. Replicates are not shown due to limited variation, except BD-17. PM data is from (Becker et al., 2006; Fischer-Gödde et al., 2011). Error is within symbol size in figures, including following ones.

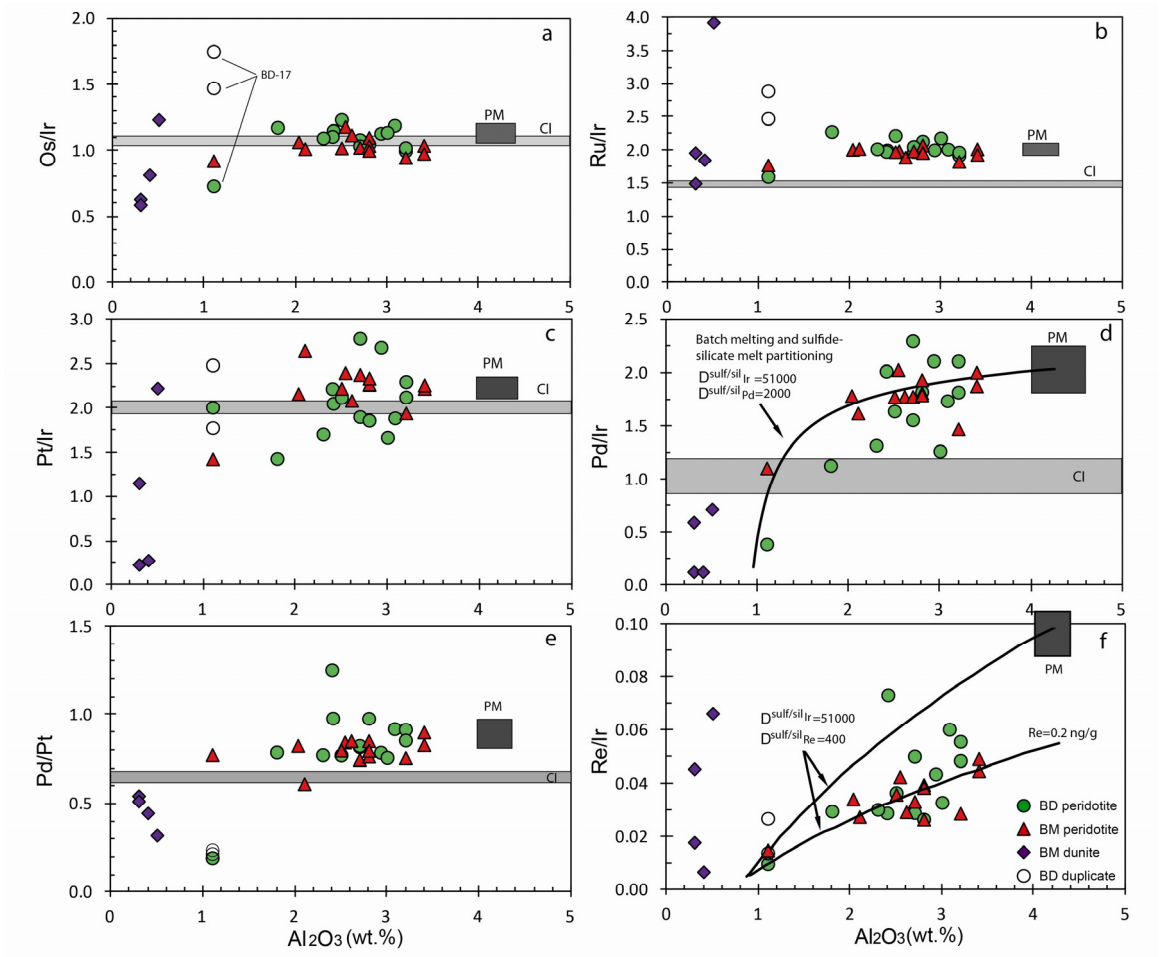

Figure 2.3 Diagrams of Al_2O_3 with HSE ratios. Os/Ir (a), Ru/Ir (b) and Pd/Pt (e) ratios are constant over a wide range of Al_2O_3. Deviations occur in highly depleted harzburgites and dunites, indicating fractionation during high degrees of melting or melt percolation. Os/Ir and Pt/Ir (c) overlap carbonaceous chondrites (CI) (Horan et al., 2003; Fischer-Gödde et al., 2010) and PM inferred from orogenic peridotites and mantle xenoliths (Becker et al., 2006). Ru/Ir and Pd/Pt in BM and BD are suprachondritic and similar to PM. Pd/Ir (d) and Re/Ir (f) generally decrease with decreasing Al_2O_3. Modeling of batch melting by sulfide-silicate partitioning using $D_{Ir}^{sulf/sil}$ =51000 (Fleet et al., 1999) and $D_{Pd}^{sulf/sil}$ =2000 is consistent with the Balmuccia samples, but BD samples tend to display a linear Pd/Ir-Al_2O_3 correlation that may be explained by infiltration of depleted peridotite with melt and disequilibrium. Re/Ir ratios in BM and BD are relatively lower than what would be expected from a depletion trend starting at a PM like composition and using $D_{Re}^{sulf/sil}$=400 (Brenan, 2008). This may indicate that both BM and BD compositions reflect recycling of Re via melts and variable re-equilibration.

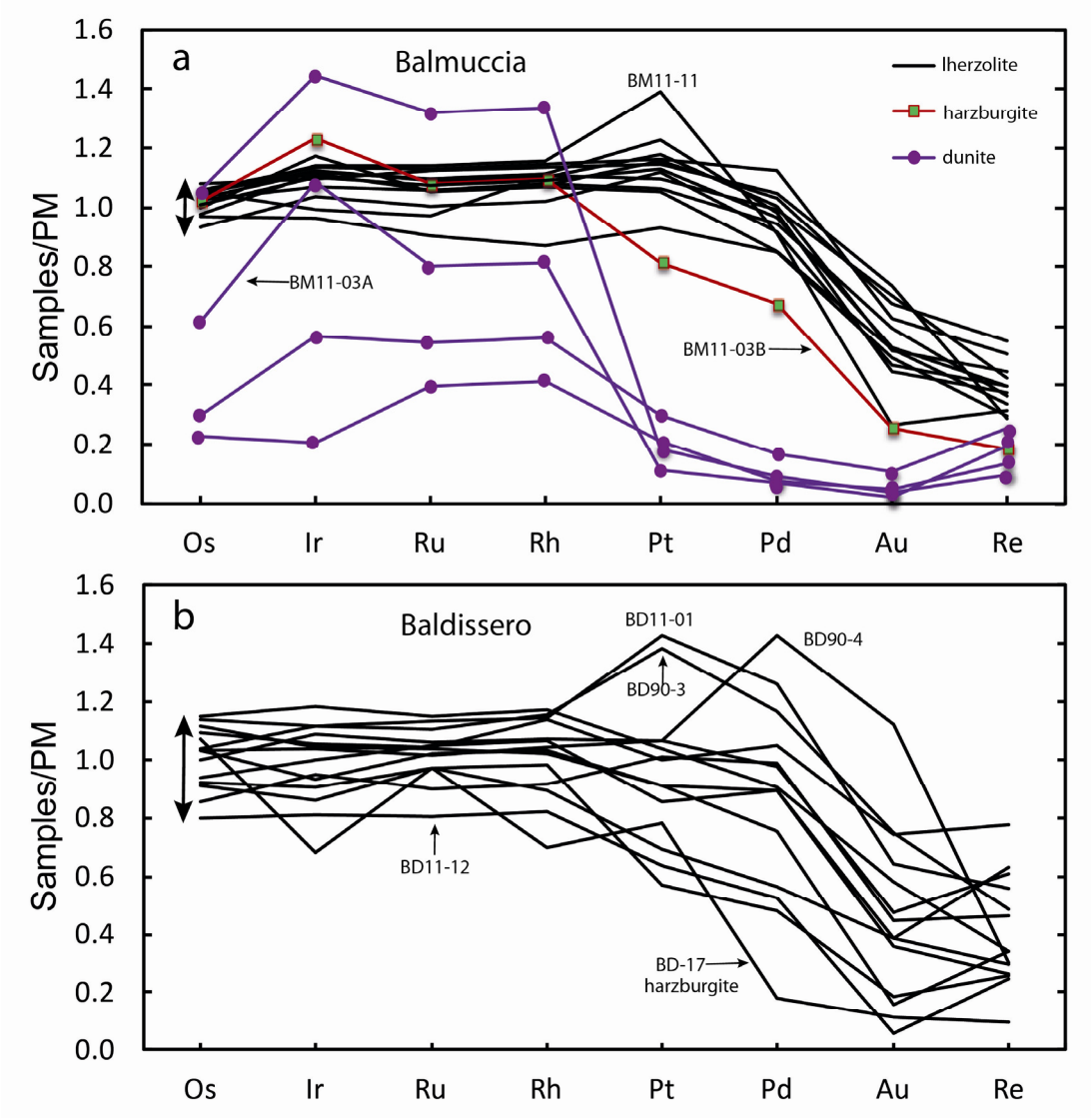

Figure 2.4 HSE patterns of whole rock peridotites normalized to PM (Becker et al., 2006, Fischer-Gödde et al., 2011). Balmuccia lherzolites (a) have relatively homogenous HSE contents with strong depletion of Au and Re. BM dunites have low incompatible HSE, slight Re enrichment relative to Au and variable compatible HSE contents with low ratios of incompatible HSE to compatible HSE. Baldissero peridotites (b) display similar behavior, but abundances show a larger range and Re in some samples is enriched relative to more compatible Au.

2.7 Discussion

2.7.1 Effects of weathering and serpentinization

Low temperature alteration processes, such as serpentinization and weathering have the potential to affect the concentrations of some HSE, and in particular S, Se and Te abundances in altered rocks (Lorand et al., 2003; Liu et al., 2009). The Balmuccia and Baldissero peridotite bodies are renowned for their exposures of fresh rocks which are neither weathered nor serpentinized. With the exception of two drill

core samples, which are somewhat serpentinized, rocks collected for the present study display no petrographic evidence for weathering or serpentinization. Accordingly, the LOI values for most samples are very low (<1 %) and only 4.7 % and 3.0 % for the serpentinized samples BD11-12 and BD11-13, respectively. Sulfide petrography also shows no obvious alteration in these samples (see Supplement). The most conclusive argument for the negligible influence of low temperature alteration is provided by the systematic variation of the alteration sensitive elements S, Se and Te with each other (Figure 2.8) and with lithophile fertility indices (e.g., Al_2O_3, Figure 2.6) and incompatible HSE (e.g., Pd and Re, Figure 2.7). This is further supported by the "typical" mantle like values of HSE ratios (Figure 2.3). We conclude that no substantial effects of weathering and hydrothermal processes on samples in this study can be observed.

2.7.2 Evidence for Phanerozoic re-equilibration

Re-Os model ages (T_{Ma}) and Re depletion model ages may provide estimates for the minimum age of melt extraction in ancient peridotites (Walker et al., 1989; Shirey and Walker, 1998; Rudnick and Walker, 2009). Here, we use Re depletion model ages because of evidence for late Re addition in some samples (Figures 2.3 and 2.4). Most Balmuccia samples have very similar Re depletion ages, mostly around 0.3-0.5 Ga (Figure 2.10). Only one sample yielded a mid-Proterozoic age (1.4 Ga). Even the dunites from Balmuccia record similar young depletion ages as lherzolites. Two samples that display evidence for late sulfide metasomatism and high S, Se and Te contents have future model ages. The distribution of the BM data in the $^{187}Os/^{188}Os$-$^{187}Re/^{188}Os$ diagram is also indicative of a major Phanerozoic re-equilibration event (Figure 2.5). In contrast, Re depletion ages of Baldissero peridotites display larger variations, ranging from 0 to 1.6 Ga, including a Paleozoic distribution peak as for Balmuccia (Mazzucchelli et al., 2010, Table 2.1, Figure 2.10). Baldissero has better preserved a record of ancient depletion, but at the same time displays evidence for late enrichment (Paleozoic?) of Re (Figures 2.2, 2.4 and 2.5). The Paleozoic Re depletion ages are consistent with Sm-Nd clinopyroxene errorchrons of lherzolites from Baldissero and Balmuccia (378 Ma±48 Ma and 435±35 Ma, respectively, Obermiller, 1994). The Paleozoic ages also match the regional geological evolution of Northern Italy with major events of mantle-derived magmatism and lithospheric extension beginning in the late Carboniferous (e.g., Mukasa and Shervais, 1999; Peressini et al., 2007 and references therein). The distribution maximum of T_{RD} near 400-500 Ma indicates that one or several major igneous events affected both bodies during the Paleozoic. The Sm-Nd dates were obtained on LREE depleted clinopyroxenes from different lherzolite samples. Some

pyroxenites also lie on these errorchron trends and thus these trends seem to record the last major melt migration and melting events (Obermiller, 1994; Rivalenti et al., 1995; Mazzuchelli et al., 2009, 2010). The precise timing of the magmatic processes remains somewhat uncertain because both Nd and Os isotopic compositions may not have been completely homogenized over sampling distances. The magmatic processes in the mantle may have taken place either between 200 and 300 Ma, the time of the intrusion of the Mafic Complex in the lower crust of the Ivrea Zone, or somewhat earlier (Peressini et al., 2007). Similar Sm-Nd errorchron ages at Balmuccia and Baldissero and differences in the distribution of Re depletion model ages indicate the different response of Nd and Os to re-equilibration and isotopic homogenization during melt infiltration. The difference likely reflects easy diffusional modification of Nd in clinopyroxene in the presence of melt (e.g., Hofmann and Hart, 1978; Ionov et al., 2006), whereas Os in sulfide and HSE alloy inclusions in silicates and spinel may be shielded in cases of restricted melt flux and permeability, as was presumably the case in Baldissero. In Balmuccia, the rock that displays the oldest Re depletion age is a harzburgite, indicating that the body may have had a similar history as Baldissero, but was affected by a higher flux of melt that has erased the memory of Proterozoic Re depletion.

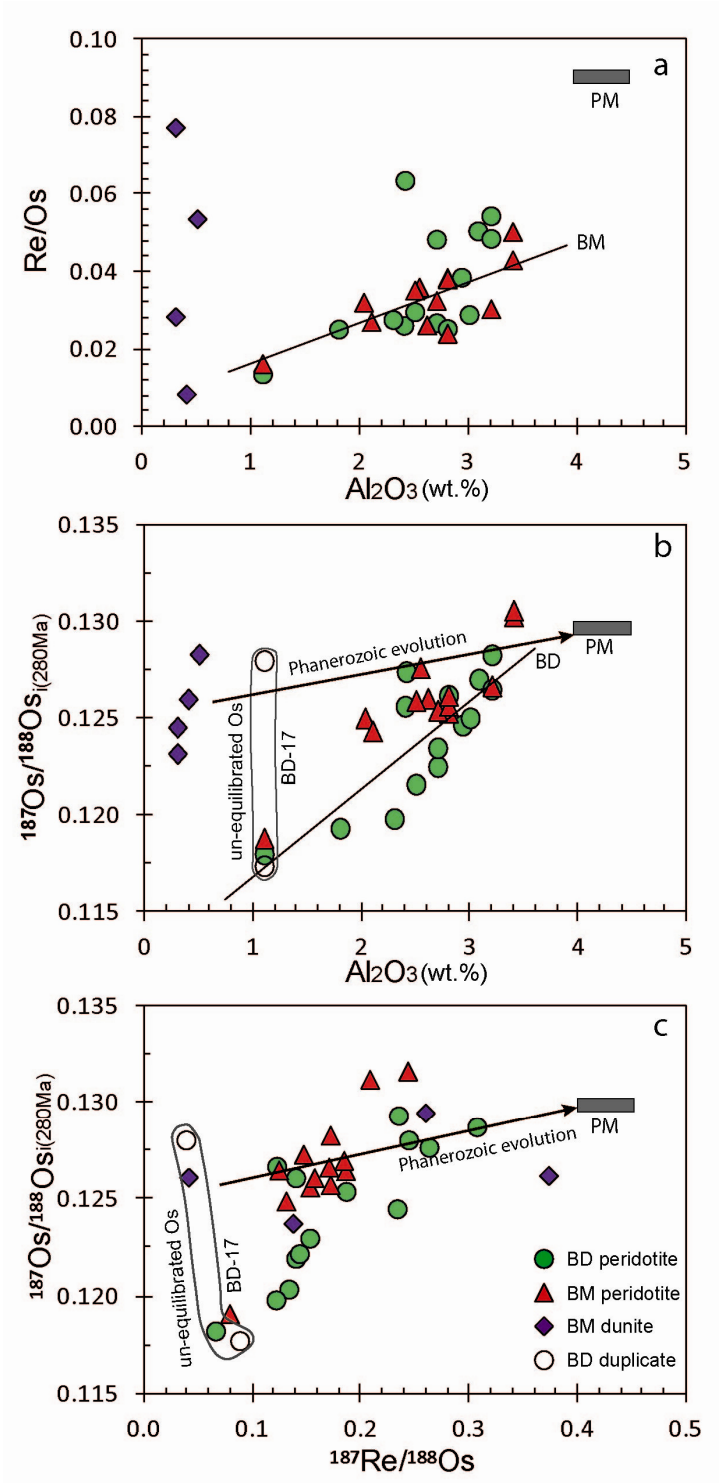

Figure 2.5 Variation of Re/Os and $^{187}Os/^{188}Os$ with Al_2O_3. BM peridotites show a broadly positive trend of Re/Os with Al_2O_3 (a), whereas BD samples display more scatter, which likely reflects Paleozoic re-enrichment of Re (see Figure 2.4 and text). Most BM lherzolites display slightly subchondritic $^{187}Os/^{188}Os$ with variable Al_2O_3, consistent with Phanerozoic re-equilibration; whereas BD peridotites show linear correlation of $^{187}Os/^{188}Os$ with Al_2O_3 and $^{187}Re/^{188}Os$ (b and c). Some BD samples have noticeably low $^{187}Os/^{188}Os$, implying preservation of ancient Re depleted compositions. Duplicates of harzburgites BD-17 have significantly different $^{187}Os/^{188}Os$. BM dunites have similar $^{187}Os/^{188}Os$ to lherzolites in the same body. PM data is from (Meisel et al., 2001b; Becker et al., 2006).

2.7.3 HSE systematics in BM and BD peridotites

The lherzolites from Balmuccia and Baldissero are variably depleted in Re, Au, Pd and, much less, in Pt. Like in other suites of peridotites, ratios such as Re/Ir, Au/Ir and to a lesser extent Pd/Ir correlate with whole rock Al_2O_3. As for some lithophile incompatible elements such as Na and Ti (Figure 2.1c, d), there are some notable differences in HSE systematics between the two sample suites. With few exceptions, compatible and incompatible HSE of BM lherzolites display homogeneous (e.g., Os_n = 3.99±0.32, 2SD, Figure 2.4) and similar PM normalized patterns over a range of Al_2O_3 of 2.0 to 3.4 wt. %. The patterns show strong depletions of Re and Au, and only minor depletions in Pd, consistent with a limited range of degrees of melt extraction, as derived from lithophile elements (Shervais and Mukasa, 1991; Mazzucchelli et al., 2010). Compatible HSE in BM lherzolites have relatively constant concentrations and ratios (e.g., Os/Ir and Ru/Ir). The uniform Pd/Pt ratios for a wide range of Al_2O_3 contents suggest no significant fractionation of Pd from Pt. The constant Pd/Pt and variations of Pd/Ir with Al_2O_3 of most lherzolites from Balmuccia are consistent with model compositions of residues after 5-15 % degrees of melt extraction (Figure 2.3d), using sulfide-silicate melt partition coefficients for Pd and Ir of 2000 and 51000, respectively (see also Luguet et al., 2007; Liu et al., 2009). The sulfide-silicate partition coefficient for Pd that best fits the BM data is much lower than data from experimental studies (Peach et al., 1994; Fleet et al., 1999), however, the value could be higher, if the harzburgite, which also has the lowest $^{187}Os/^{188}Os$, is excluded from the data. Balmuccia peridotites exhibit a positive correlation of whole rock Re/Ir and Re/Os with Al_2O_3 (Figures 2.3 and 2.5), similar to the trend for the Baldissero samples. Two samples (BM11-02A and BM90-15) from Balmuccia display convincing evidence for sulfide addition in that they show enhanced S, Se and Te concentrations, yet their HSE patterns are depleted in the incompatible HSE (Figure 2.4).

In contrast, lherzolites from Baldissero have more variable HSE patterns and display a larger range in abundances of compatible and incompatible HSE (e.g., Os_n = 3.93±0.87, 2SD, Figure 2.4). Rhenium is slightly enriched relative to Au in PM normalized patterns of BD lherzolites (Figure 2.4b), and Re, Pt and Pd tend to scatter more than in BM lherzolites (Figure 2.2 and 2.4b). Most Baldissero samples do not follow the sulfide-silicate equilibrium partitioning model for Pd. Instead, the samples display a scattered positive correlation of Pd/Ir with Al_2O_3 (Figure 2.3d), with some samples scattering towards higher Pd/Ir. Such trends have been interpreted to reflect addition of sulfide-bearing basaltic magma to residual peridotites (Rehkämper et al., 1999a; Pearson et al., 2004; Lorand et al., 2008a). Three samples from Baldissero have somewhat higher Pt and Pd contents than other lherzolites (Figure 2.4b), but

their subchondritic $^{187}Os/^{188}Os$ and the lack of an enrichment of S and Se do not support sulfide addition from migrating fluid or sulfide melt as a cause of the Pt and Pd enrichment. From the perspective of HSE compositions, the BM lherzolites are clearly more homogeneous than the BD lherzolites (Figure 2.4). This is in contrast to the lithological heterogeneity, which is more pronounced in Balmuccia with more abundant dunites, websterite and Al augite pyroxenites than in Baldissero.

The general picture of more homogeneous HSE abundances of the Balmuccia body is supported by differences in the distributions of Re depletion model ages at both locales (homogeneous at BM, dispersion towards Proterozoic model ages at BD, Figure 2.10), and their interpretation in the context of Sm-Nd ages on clinopyroxenes and the geological history of the area (see previous section). The implications for the HSE abundance systematics and the behavior of the Re-Os system are as follows: BD peridotites have been less overprinted by melt transport and re-equilibration and thus record ancient depletion processes with some overprint from migrating melt (enrichment of Na and Ti for a given Mg content compared to BM samples, Re over Au, Figure 2.1 c, d, 2.4b). We note that the re-enrichment of Re in BD samples is minor, and overall, these samples still show strong depletions of Au and Re, and no or only slight depletion of Pd and Pt, relative to primitive mantle values. The more homogenous HSE abundances in lherzolites from Balmuccia and their young model ages indicate that these peridotites have been re-equilibrated more efficiently. Most likely, this has been accomplished by porous flow of larger volumes of incompatible element depleted melt, which is also indicated by the presence of tabular dunite bodies and abundant websteritic dikes in some parts of the ultramafic body. In this context, the different curved trends for BM and BD samples in the Re-Os isochron diagram (Figure 2.5c) reflect partial resetting of the Re-Os system. Because likely precursor lithologies, such as the harzburgites and some depleted lherzolites at Baldissero had unradiogenic $^{187}Os/^{188}Os$ during the Paleozoic, fertile samples and the dunites likely gained radiogenic Os from externally derived mafic melt. The importance of the introduction of radiogenic Os as a means of resetting of the Re-Os clock is supported by the variable $^{187}Os/^{188}Os$ obtained for duplicates of harzburgite BD17, which indicates heterogeneity of the sample powder, but also the presence of radiogenic and Proterozoic components in this rock (see Burton et al., 1999; Chesley et al., 1999; Becker et al., 2001a, 2006; Büchl et al. 2002; Alard et al. 2002, 2005 for additional examples).

The BM lherzolite bulk rocks of the present study are on average more depleted in the lithophile incompatible elements Na and Ti than those at BD (Figure 2.1c, d). This may reflect stronger depletion of incompatible elements in the melts that re-equilibrated BM, or may represent open-system fractional melt extraction

(Obermiller, 1994; Rivalenti et al., 1995; Mazzuchelli et al., 2009). We suggest that equilibration of lherzolites with large volumes of pyroxene saturated mafic melt drives HSE abundances and ratios towards compositions, consistent with sulfide-silicate equilibrium (e.g., Figure 2.3). Such equilibrated compositions mimic results of closed-system partial melting models of incompatible element abundances of clinopyroxenes from these rocks (as for BM lherzolites, Obermiller, 1994; Rivalenti et al., 1995). The homogeneity of compatible HSE, uniform distribution of Paleozoic Re-Os model ages, and the difficulties for re-equilibrating MSS in ancient mantle residues (e.g., Harvey et al., 2006; Liu et al., 2008; Lorand et al., 2010) provide the main evidence for an open-system equilibration model of the BM lherzolites.

Three harzburgites (BD-17, BD92-2 and BM11-03B) have undepleted Os, Ir Ru and Rh contents and highly depleted and fractionated incompatible HSE (Figures 2.3 and2.4). These features are consistent with high degrees of partial melting. Like harzburgites from other locales (Pearson et al, 2004; Becker et al., 2006; Luguet et al., 2007; Liu et al., 2009), we also observe some fractionation among compatible HSE, in particular Os, Ir and Ru (Figure 2.3). Residual MSS cannot explain these fractionations, because most harzburgites are BMS-poor or -free, as indicated by low abundances of sulfides and low sulfur contents (this study and Luguet et al., 2007), whereas they still have high abundances of compatible HSE. Luguet et al. (2007) have shown that harzburgites that experienced up to 24 % partial melting have retained Ru-Os±Ir bearing sulfides and Pt-Ir±Os alloys possibly due to decrease in f_{S2} induced by sulfur extraction (Fonseca et al., 2012) and the high melting points of these phases (Brenan and Andrews, 2001). Under these conditions, the fractionation of the compatible HSE in melting residues is controlled by the different solubilities of these elements in silicate melt (Brenan and Andrews, 2001).

2.7.4 Suprachondritic Pd/Ir and Ru/Ir in the mantle

Suprachondritic Pd/Ir (or Pd/Pt) and Ru/Ir in fertile mantle peridotites have been widely reported from different tectonic settings (e.g., Pattou et al., 1996; Rehkämper et al., 1999a; Schmidt et al., 2000; Becker et al., 2006; Liu et al., 2009), and contrast with chondritic ratios of other HSE in such rocks. Study of the HSE patterns of grain boundary sulfides and sulfide inclusions in silicates of peridotites and the variations of Pd abundances and Pd/Ir with lithophile incompatible elements indicate that mixing of depleted peridotite with infiltrating melt is an important process that replenishes depleted mantle in basaltic components, but also in Pd, Au and Re (e.g., Alard et al., 2000; Luguet et al., 2003; Pearson et al., 2004; Lorand and Alard, 2010). These results have prompted some critique of estimates of the HSE composition of the Earth's primitive mantle (Becker et al., 2006), in that Pd (and by

implication Re and Au) abundances from rocks have seen secondary addition of these elements (e.g., Lorand et al. 2008a). As noted in the previous section, the present results shed some light on the processes of redistribution and re-equilibration of Pd in the mantle. We note that in spite of the different distribution of Pd in fertile samples in the Pd-Al_2O_3 diagram (Figures 2.2b and 2.3d), the Pd/Pt are uniform and agree with the primitive mantle value (Figures 2.2 and 2.3). Since Pd contents in most BM lherzolites are consistent with control by partial melting or equilibration with melt, these samples seem to resemble some lherzolites from oceanic environments (Liu et al. 2009). Compatible HSE in BM and BD have relatively constant concentrations and ratios with melt extraction (Figures 2.2 and 2.3). Ru/Ir ratios in lherzolites from both bodies are similar and consistent with PM. These results provide further support that the Earth's mantle has suprachondritic ratios of Ru and Pd, relative to other HSE.

2.7.5 Behavior of S, Se and Te in mantle processes

As discussed above, some harzburgites and lherzolites from Balmuccia and Baldissero record low to moderate degree of partial melting and/or sulfide-silicate re-equilibration, whereas other samples are residues of Proterozoic depletion events, and were affected by later addition of melt, including some Re, Au and radiogenic Os. Sulfur, Se and Te contents in these samples constrain the behavior of these elements during these processes. S and Se contents in BM and BD have been analyzed three decades ago by high temperature combustion (50 ppm detection limits) and AAS analyses, respectively (Garuti et al., 1984). Selenium contents in Garuti et al. (1984) are typically higher than data on other mantle peridotites (Morgan, 1986; Lorand and Alard, 2010) and results of the present study, and thus lead to lower S/Se ratios (mostly <1500). Thus we will not use Se data in Garuti et al. (1984) for the following discussion.

2.7.5.1 Origin of S-Se-Te abundance variations in BM and BD peridotites

Sulfur displays excellent linear correlations with Al_2O_3 for both BM and BD sample suites (Figure 2.6a) although these elements are controlled by different phases. The correlations of S with Al_2O_3 indicate that sulfide melt in these rocks did not migrate significant distances, and that the main transport agent must have been silicate magma (see also discussion in Becker et al., 2006; Fischer-Gödde et al., 2011). The new data, and previous, less precise S data on peridotites (e.g., Becker et al., 2006; Lorand and Alard 2010) suggest that precipitation of secondary sulfides in S depleted residual peridotites (e.g., BD samples) is typically associated with precipitation of pyroxenes and spinel. More equilibrated rocks that show differences in their HSE behavior such as the BM samples, nevertheless display comparable correlations of S

with Al_2O_3. The correlation in Figure 2.6a is consistent with a modeling curve using sulfide-silicate liquid partition coefficients for sulfur of 393, and assuming melt extraction of S saturated basaltic melt with a sulfur content on saturation of 1000 ppm and 35 wt.% S in the sulfide phases (Lorand et al., 1999).

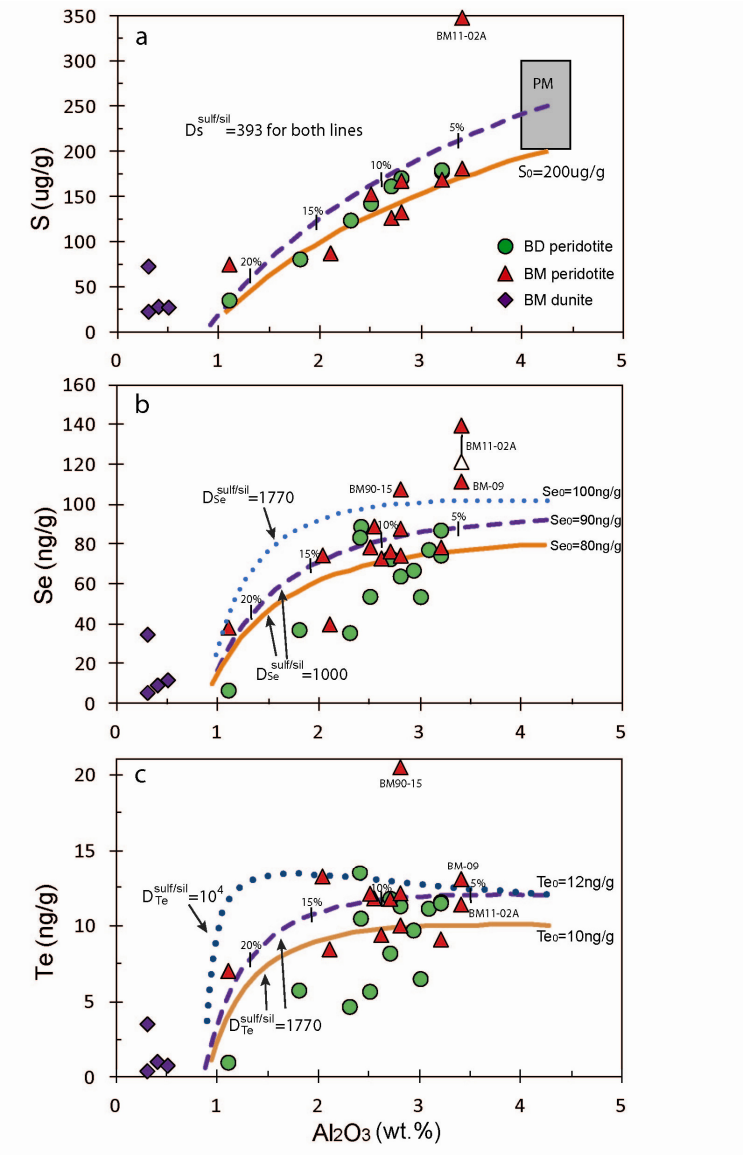

Figure 2.6 Sulfur, Se and Te contents as a function of Al_2O_3. BM11-02A and BM90-15 have anomalously high S, Se or Te contents, reflecting secondary, presumably local, sulfide metasomatism. Lines are results of batch melting calculations, assuming sulfur concentrations at saturation of partial melts of 1000 ppm (Lorand et al., 1999), and model parameters for Al_2O_3 from (Niu, 1997). Curves for residue compositions were calculated using sulfide-silicate liquid partition coefficients of D_S=393, D_{Se}=1770, and D_{Te}=10000 (estimated from MORB, Peach et al., 1990; Yi et al., 2000) or D_{Se}=1000 (solid line in b) and D_{Te}=1770 and different initial element abundances. Labels on lines indicate melting percentage. Sulfur contents of BM and BD samples, except dunites and BM11-02A, display excellent linear correlations with Al_2O_3 (a), which is consistent with the modeling curve and passes through estimated S contents of PM, although at the low S concentration side (McDonough and Sun, 1995; Becker et al., 2006; Lorand and Alard, 2010). However, Se and Te show rather poor correlations with Al_2O_3. The equilibrium partial melting curves roughly fit the BM data, if Te has a much lower

sulfide-silicate partition coefficient than previously inferred from MORB (c). The BD data may reflect mixing of a chalcogen enriched melt component with a depleted component (see discussion).

Selenium and Te also display positive trends with Al_2O_3 contents (Figure 2.6), indicating their moderate incompatibility, however, these trends are much more scattered, similar to Re and Pd (Figure 2.7). These data are not as straightforward to explain as S. Selenium and particularly Te contents do not decrease much with depletion for lherzolites in Balmuccia. Lorand and Alard (2010) explained such trends in the Pyrenean peridotites by difficulties in the removal of disseminated sulfide melts during low degree melting due to non-wetting properties of sulfide melt. However, if this were so, abundances of incompatible HSE should not decrease, and S would also be not removed and thus should display similar scatter as Se and Te at low degrees of melting. Evidently, this is not the case (Figure 2.6). An alternative explanation is that Se and Te are more compatible than sulfur, as suggested by previous studies. Estimates from MORB and magmatic sulfide deposits yielded sulfide-silicate melt partition coefficients for S and Se of 393 and 1770, respectively (Peach et al., 1990) or 1200 for Se (Barnes et al., 2009), and values for Te $\geq 10^4$ (Yi et al., 2000). Selenium and Te data of most samples from Balmuccia are consistent with modeling of equilibrium sulfide-silicate partitioning using similar $D^{sulf/sil}_{Se}$ and $D^{sulf/sil}_{Te}$ (e.g., 1770, Figure 2.6). In Baldissero peridotites, Se and Te display similar trends as observed for Pd and Pd/Ir *vs.* Al_2O_3 (Figures 2.2b, 2.3d and 2.6). These data, especially the good correlation between Pd and Te, are consistent with the notion that the BD data predominantly reflect mixing of Pd, Au, Re and chalcogen depleted peridotites with sulfides precipitated from silicate melt enriched in these elements. Recent studies of depleted harzburgites (König et al., 2012), in situ analyses of sulfides from peridotites (Lorand and Alard, 2010) were interpreted to reflect preferential partitioning of Se and Te into Cu-Ni sulfide melt, or into exsolved Te-rich phases during cooling. Accordingly, S/Se and S/Te in Cu-rich sulfides should be lower than in refractory MSS (Helmy et al., 2010). Thus if MSS-Cu rich sulfide partitioning is relevant during partial melting, Se and Te in residual peridotites should decrease much faster than S with melt extraction, which is opposite to observed results (Figure 2.6). Selenides and tellurides may exsolve from base metal sulfides during cooling (Dare et al., 2011; Piña et al., 2012), but at high temperatures >900ºC Cu-rich sulfide melts should remain homogeneous as long as the Te concentration does not exceed its solubility in sulfide melt (<0.2 wt. % Te, Helmy et al., 2007). The positive relationships of Re with incompatible Pd, Au, S, Se and Te in BM peridotites strongly support that Re is dominantly controlled by sulfide-silicate partitioning rather than by MSS-sulfide melt partitioning during partial melting (Mallmann and O'Neill, 2007; Brenan, 2008; Fischer-Gödde et al. 2011). Consequently, the data indicates that during partial

melting, Se and Te, like Re, are moderately incompatible and controlled by sulfide-silicate melt partitioning.

2.7.5.2 Fractionation of S, Se and Te during partial melting

Good linear positive correlations of S with Se and Se with Te exist for BD and BM peridotites (Figures 2.8 and 2.10). Although S/Se ratios display a systematic difference between the two sample suites, S/Se and Se/Te of each sample suite remain relatively constant or change only slightly with depletion (Figure 2.9). The high S/Se in some harzburgites and dunites hints that in these rocks, S may have become more compatible than Se (see discussion below). Sulfide-silicate partition coefficients used in modeling of sulfide silicate equilibrium (Ds=393, D_{Se}=1770, Peach et al., 1990) barely fit the data for BM lherzolites and hint that at low to moderate degree of partial melting or melt infiltration, Se is only slightly more compatible than S (Figure 2.9a). As for S/Se, Se/Te displays a weak correlation with Al_2O_3 in BM lherzolites, but not in BD lherzolites (Figure 2.9b). Thus, Te may be similar or only slightly more compatible than Se during partial melting. The BM lherzolite data are difficult to reconcile with the very high D_{Te} (>10^4) as inferred from MORB (Yi et al., 2000). Overall, Se/Te in lherzolites scatters non-systematically, and is on average only 20-30 % lower than the ratio in CI chondrites (～9, this study and Lodders, 2003). In previous work, lower S/Se and Se/Te in mantle peridotites and their sulfides compared to MORB, have been used to propose a relative compatibility sequence of Te > Se > S (e.g, Hertogen et al., 1980; Morgan, 1986; Hattori et al., 2002). It should be noted that much of the differences between MORB and peridotites may reflect additional fractionation processes during melt transport in the mantle and in the oceanic crust. Some mantle sulfides from peridotites from a subduction zone setting are characterized by low Se/Te (2 to 4, Hattori et al., 2002). These data have been interpreted to indicate higher compatibility of Te than Se (Hattori et al., 2002). This interpretation has been challenged by LA-ICPMS data on sulfides from Ligurian peridotites and from the Lherz peridotite massif, which have much higher Se/Te than the CI ratio (e.g., >10-50, Luguet, et al., 2004; Lorand and Alard, 2010). High Se/Te in bulk rocks of harzburgites from Lherz have been interpreted to indicate that Te behaves more incompatible than Se in such rocks (König et al., 2012). Harzburgites in the present data set tend to have similar or lower Se/Te than lherzolites (Figure 2.9b). The variable and high S/Se and Se/Te ratios in harzburgites from Lherz are similar to data for the dunites from Balmuccia, which will be discussed below (Figure 2.9). Given the hints for trends for S/Se and Se/Te of the lherzolites and the general sulfide-silicate partitioning relations of S, Se and Te, we consider it plausible, that truly residual harzburgites have lower S/Se and Se/Te than lherzolites. Suprachondritic S/Se and Se/Te and low abundances of the chalcogens in refractory mantle rocks may

simply reflect precipitation of small quantities of sulfide from basic melt, which commonly shows such high values (Hertogen et al., 1980).

2.7.5.3 Relationships of the HSE with S-Se-Te

As shown above, S, Se and Te display moderately incompatible properties during igneous processes in the mantle, and this is also reflected in positive correlations with Pd and Re (Figure 2.7). For instance, Pd displays excellent positive correlations with S, Se and Te (Figure 2.7d), with the exception of a few samples that may have been affected by melt percolation. We note that Te/Pd only slightly decreases with depletion indices, indicating somewhat lower bulk partition coefficients of Te than Pd. Both elements tend to be enriched in Cu-rich sulfides, which may exsolve Pd tellurides during post magmatic cooling (Helmy et al., 2007; Helmy et al., 2010; Piña et al., 2012). Because Te correlates with Se and several HSE, the present data do not yield indications that tellurides play a significant role in controlling chalcogen and Pd or Pt abundances in peridotite-silicate melt systems. Diagrams of S/Pt, S/Pd, Se/Pt, Se/Pd, Te/Pt and Te/Pd with Al_2O_3 contents suggest that Pt is more compatible than S, Se and Te (not shown), whereas Pd is slightly more compatible than S, Se and Te (Figure 2.11). An empirical compatibility sequence derived from these data and the data in Figure 2.7 for little to moderately depleted peridotites would be: Pt > Pd > Te ≥ Se ≥ S ≈ Re. Figure 2.9 shows that there is no resolvable difference in Se/Te between fertile lherzolites from equilibrated (BM) and unequilibrated (BD) environments, which, as for the S-Al_2O_3 trends, suggests that the net results of equilibrium partitioning of these elements vs. melt infiltration are indistinguishable for fertile lherzolites from the IVZ (Figures 2.8 and 2. 9).

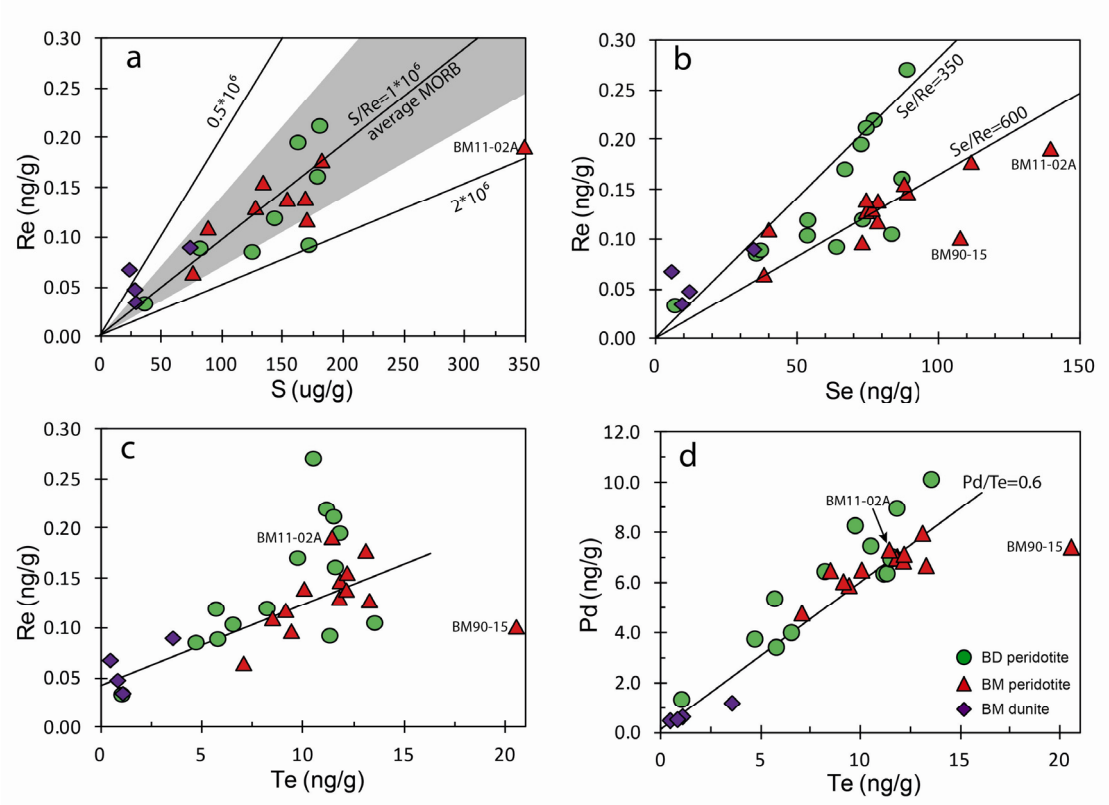

Figure 2.7 Variation of S, Se, and Te abundances in BM and BD peridotites with Re and Pd. As expected (Morgan, 1986), Re displays positive trends with S, Se and Te in BM samples. For BD samples, the trends are more scattered. S/Re ratios in mantle peridotites overlap average values of MORB worldwide (shaded area in a, Gannoun et al., 2007), indicating their similar bulk partition coefficients. Pd displays a good linear correlation with Te contents for both localities. The regression lines (c, d) are based on Balmuccia samples, including dunites but except BM11-02A and BM90-15, both of which are not included in the following figures unless it is indicated.

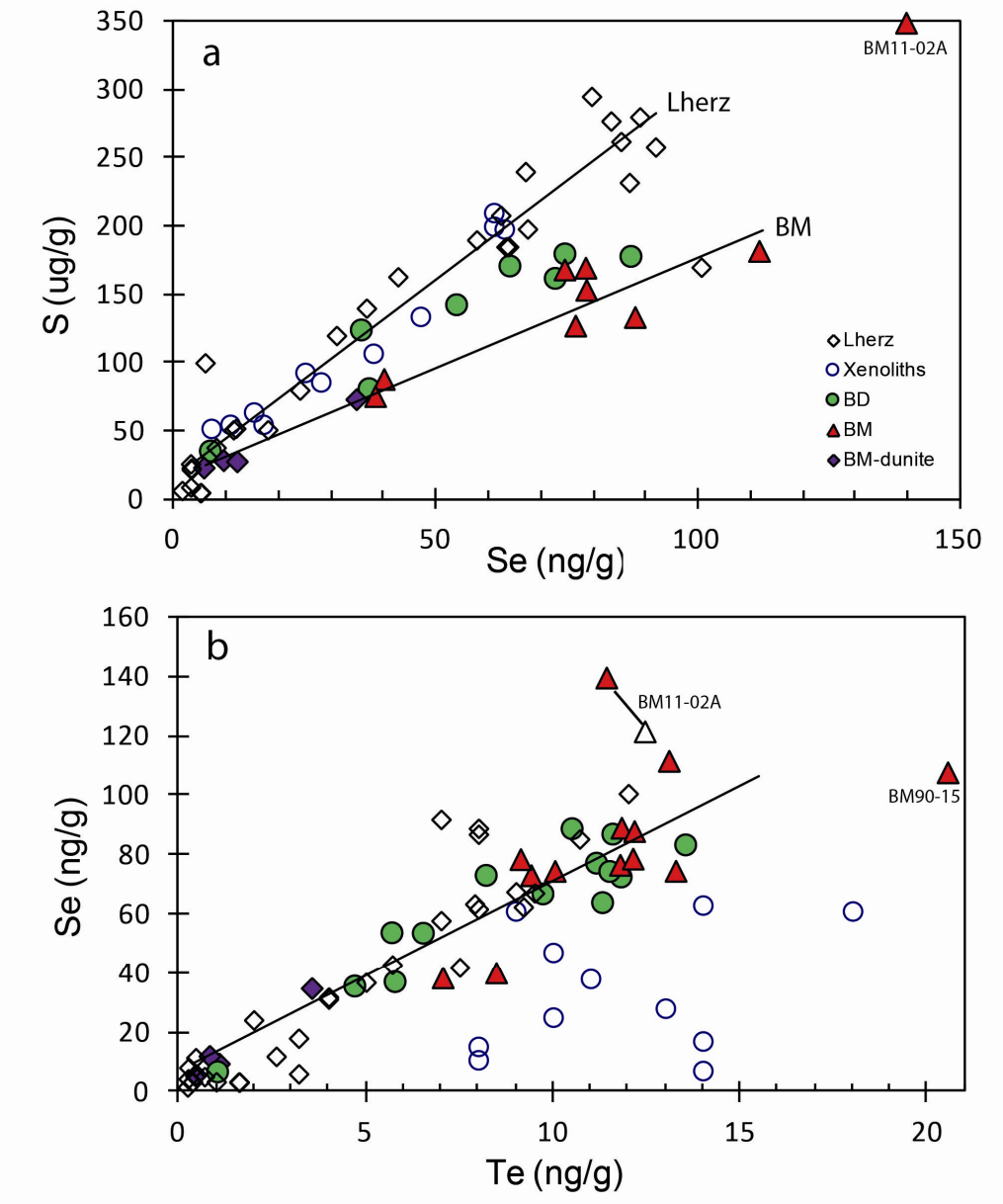

Figure 2.8 S vs. Se (a) and Se vs. Te (b). S shows excellent positive correlations with Se contents in Balmuccia peridotites (except BM11-02A), Baldissero peridotites and peridotites from Lherz (Lorand and Alard, 2010; König et al., 2012), but the different suites are characterized by different slopes. Selenium has similar good correlation with Te contents in this study. Note that Lherz peridotites were interpreted to be products of refertilization (Lorand and Alard, 2010), but still display the same Se/Te as BD and BM samples, implying no strong fractionation of Se from Te in bulk rocks of lherzolites, regardless of extent of re-equilibration. Mantle xenoliths studied by Morgan (1986) have similar S/Se compared to Lherz, but the Se-Te systematics of these samples is different compared to more recent analyses of mantle peridotites.

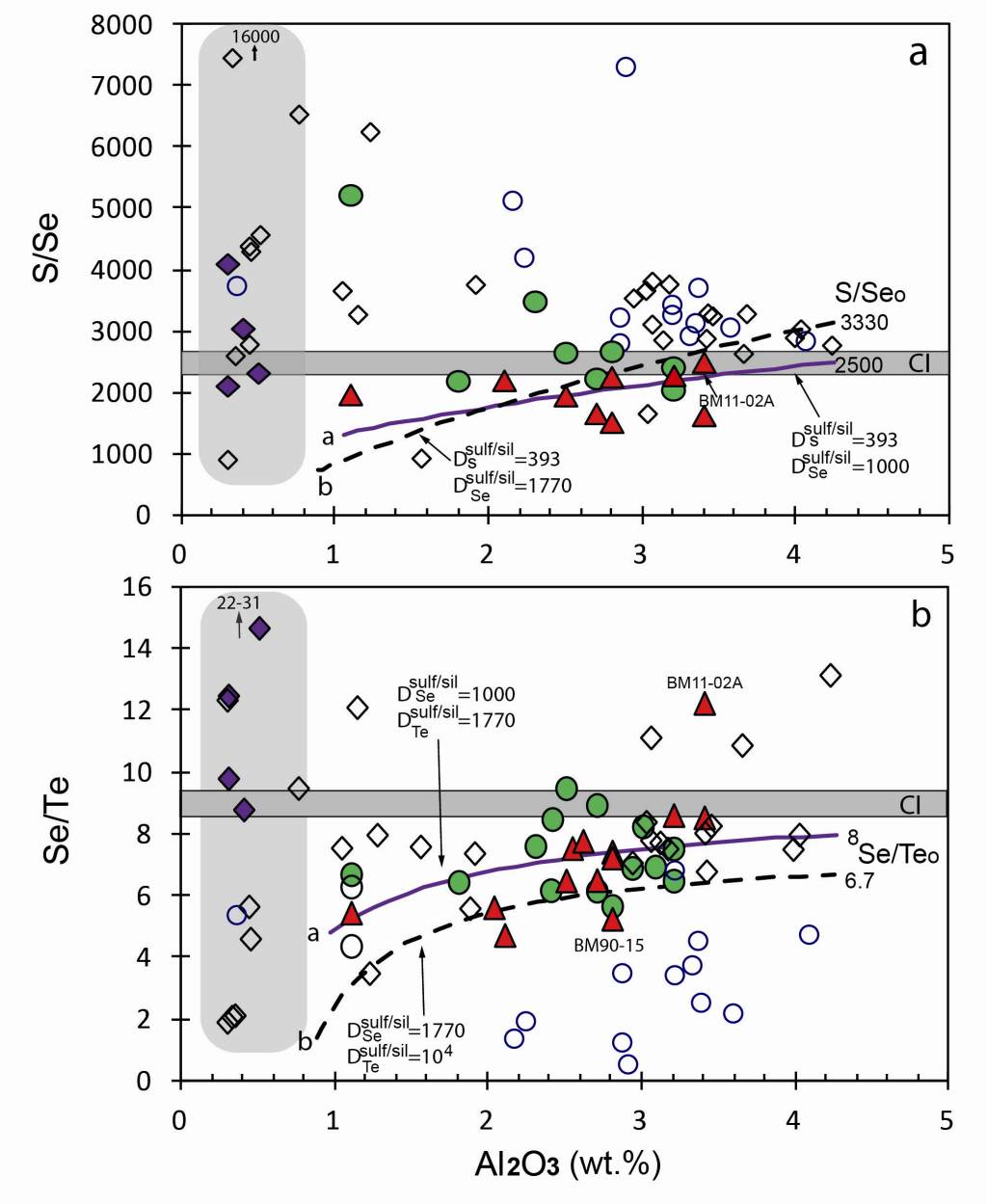

Figure 2.9 Ratios of S/Se and Se/Te vs Al_2O_3. S/Se in BD and BM lherzolites is relatively constant. An increase can be noted for depleted harzburgites, which is opposite to the expected trend, if sulfide-silicate melt partitioning controls the variations and $D_{Se} > D_S$ (a). S/Se in lherzolites display small but systematic differences for different locations, but the values are close to the ratio in CI chondrites (Dreibus et al., 1995). Se/Te ratios in lherzolites are more scattered and tend to be slightly lower than the ratio in CI chondrites (~9, this study and Palme and O'Neill, 2003). Modeling curves of sulfide-silicate partitioning using different partition coefficients and initial ratios are given (a-a, $S/Se_{initial}$=2500, Ds=393, D_{Se}=1000; a-b, $S/Se_{initial}$=3300, Ds=393, D_{Se}=1770; b-a, $Se/Te_{initial}$=8, D_{Se}=1000, D_{Te}=770; b-b, $Se/Te_{initial}$=6.7, D_{Se}=1770, D_{Te}=10000). Variable and high S/Se and Se/Te ratios in the dunites may reflect variable proportions of refractory MSS and secondary sulfides precipitated from melts with high S/Se and Se/Te. Symbols as Figure 2.8.

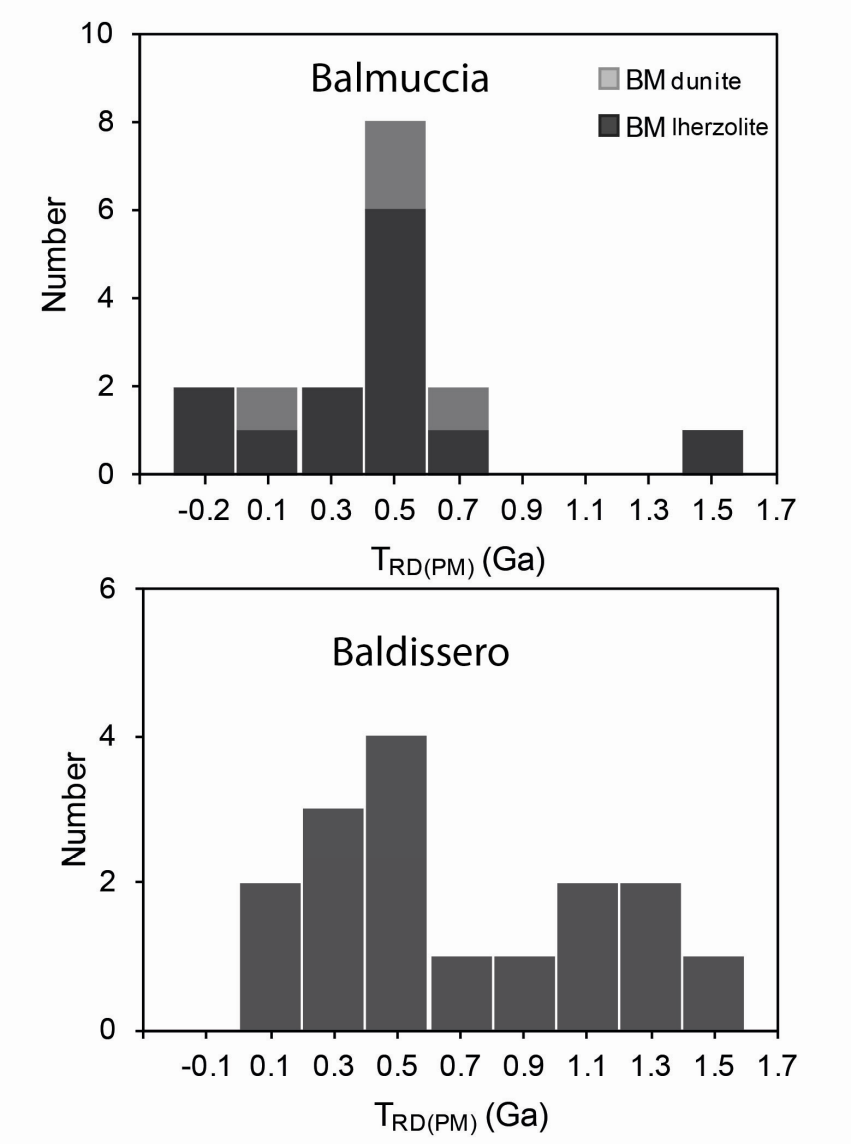

Figure 2.10 Distribution of Re depletion model ages in BM and BD peridotites. Both locations yield predominantly Paleozoic model ages, with BD showing better preservation of ancient Re depletion ages due to incomplete re-equilibration and resetting by percolating mantle melts. BD data also include results of peridotites away from dikes by Mazzucchelli et al. (2010).

2.7.6 Melt percolation

A few peridotites display somewhat elevated abundances of S, Se and Te given their Al_2O_3 contents, implying local sulfide metasomatism. On the other hand, dunites which formed by melt-rock reaction at high melt/rock ratios, have very low incompatible HSE, S, Se, Te abundances, and also relatively low compatible HSE abundances. These data suggest sulfide dissolution rather than addition.

2.7.6.1 Silicate melt percolation in replacive dunites

Melt percolation in mantle peridotites can significantly change abundances and ratios of HSE depending on magma composition, melt/rock ratios and pressure-temperature conditions (e.g., Becker et al., 2001a; Büchl et al., 2002; Pearson et al., 2004; Reisberg et al., 2005; Lorand et al., 2009, 2010). For instance, dunites from the Oman and Troodos Ophiolites are of replacive origin and formed at high melt/rock ratios (Kelemen et al., 1997). These rocks display enrichment of Re and Pd (Büchl et al., 2002; Hanghøj et al., 2010), and, at the same time, lower Os and Ir contents compared to lherzolites. It is believed that the high melt/rock ratios have lead to a more or less complete replacement of the original HSE composition by the composition of the melt (Büchl et al., 2002). In these rocks, HSE and chalcogen budgets are dominated by sulfides segregated from sulfide-saturated melt with a radiogenic Os signature.

Occurrence of relict websterite lenses in spinel bearing dunites at Balmuccia (Mazzucchelli et al., 2009) and gradual dissolution of pyroxenes from harzburgite BM11-03 into dunite BM11-03A indicate BM dunite formation relatively later than lherzolites. Similar Sr-Nd isotopic compositions of clinopyroxene separates from BM dunite and Cr-diopside websterite veins that cut the lherzolites also have been interpreted to indicate that BM dunites formed after re-equilibration of BM lherzolites (Mazzucchelli et al., 2009). BM dunites are characterized by fractionated HSE abundances, but the patterns differ substantially from dunites in ophiolites. Initial $^{187}Os/^{188}Os$ data of Balmuccia dunites are slightly subchondritic to chondritic, similar to the BM lherzolites (Figure 2.5). This also contrasts with more radiogenic dunites from ophiolites that formed in subduction zone settings. Incompatible HSE, S, Se and Te are highly depleted, whereas compatible HSE have low and variable concentrations, resulting in low ratios of incompatible HSE/compatible HSE (Figures 2.4a and 2.6). The HSE composition and low S suggest either that the BM dunites have equilibrated with HSE depleted magmas or that sulfide dissolution was promoted by sulfur undersaturated magmas.

Incompatible HSE and chalcogens in the dunites decrease in equal proportion (Table 2.1), which is consistent with the main control being preferential dissolution of interstitial sulfides. This process differs from fractionation by equilibrium partial melting because abundances of compatible HSE in dunites are much lower than in lherzolites and harzburgites (Figure 2.4a). Sample BM11-05 has higher Ir, Ru and Rh, even than the lherzolites, but the enrichment of compatible HSE is evidently not due to sulfide addition, because abundances of the chalcogens and incompatible HSE are low. This observation hints at the possibility of precipitation of HSE rich alloys at high melt/rock ratios (e.g., Finnigan et al., 2008). Experimental results indicate that

platinum group minerals (including metal alloys and laurite) tend to form at the mineral-melt interface during re-equilibration or growth of Cr-spinel in molten silicate (Finnigan et al., 2008). Such alloys only precipitate from S-undersaturated magma (Brenan and Andrews, 2001), in turn supporting S-undersaturated conditions during the formation of BM dunites.

In thin sections it is evident that tiny sulfides are hosted by olivine, but many sulfide grains (<20 μm) also occur on grain boundaries with olivine and spinel, consistent with our interpretation (see the Supplement). We interpret the observed HSE, and chalcogen systematics of Balmuccia dunites to be the result of mixing of small amounts of residual sulfides or alloys with minor secondary sulfides, the latter crystallized from sulfur-undersaturated melts that were entrapped in the dunites. The high S/Se and Se/Te of the dunites are most easily explained if the chalcogen budget of the dunites is controlled by secondary sulfides precipitated from basaltic melt during the final stages of melt migration. The minor enrichment of Re relative to Au indicates the presence of such minor quantity of trapped melt, but the overall shape of the dunite HSE patterns from Balmuccia requires that either the melts were depleted in incompatible HSE, or residual phases are present (Figure 2.4a). HSE data on some suites of mantle xenoliths also have been interpreted to reflect melt percolation by S undersaturated melts that did not result in the addition of radiogenic Os (Ackerman et al., 2009; Liu et al., 2010, 2011). This indicates that reaction of sulfur-undersaturated melt with peridotite mostly removes primary sulfides. Therefore, if percolating melts are sulfur-undersaturated, they may not substantially affect the Os isotopic composition of mantle rocks, but may themselves be strongly modified by the incorporation of unradiogenic Os from mantle peridotites. This will lead to decoupling of HSE and chalcophile systematics from lithophile elements and their radiogenic isotopes both in strongly modified mantle rocks (e.g. replacive dunites and harzburgites), and the resulting melts.

In summary, the data on BM peridotites indicate that different mechanisms of transport and removal of sulfides by silicate melt have occurred at different times. Pervasive infiltration of pyroxene and sulfide saturated melt and simultaneous melt extraction led to the formation of lherzolites from Proterozoic harzburgites with compositions, consistent with melting residues. At a later time, localized porous flow of sulfide and pyroxene undersaturated melt resulted in zones of tabular dunites within the lherzolites. In the dunites, Re, Au, Pd, Pt, S, Se and Te were mostly removed by dissolution of grain boundary sulfides into sulfur-undersaturated melt at high melt fractions and high permeability, whereas MSS inclusions in olivine, may have survived. At high melt fractions and if dissolution-reprecipitation of olivine

becomes important, Os, Ir and Ru bearing alloys may form during melt percolation in the course of the dissolution of sulfides in sulfur-undersaturated melts.

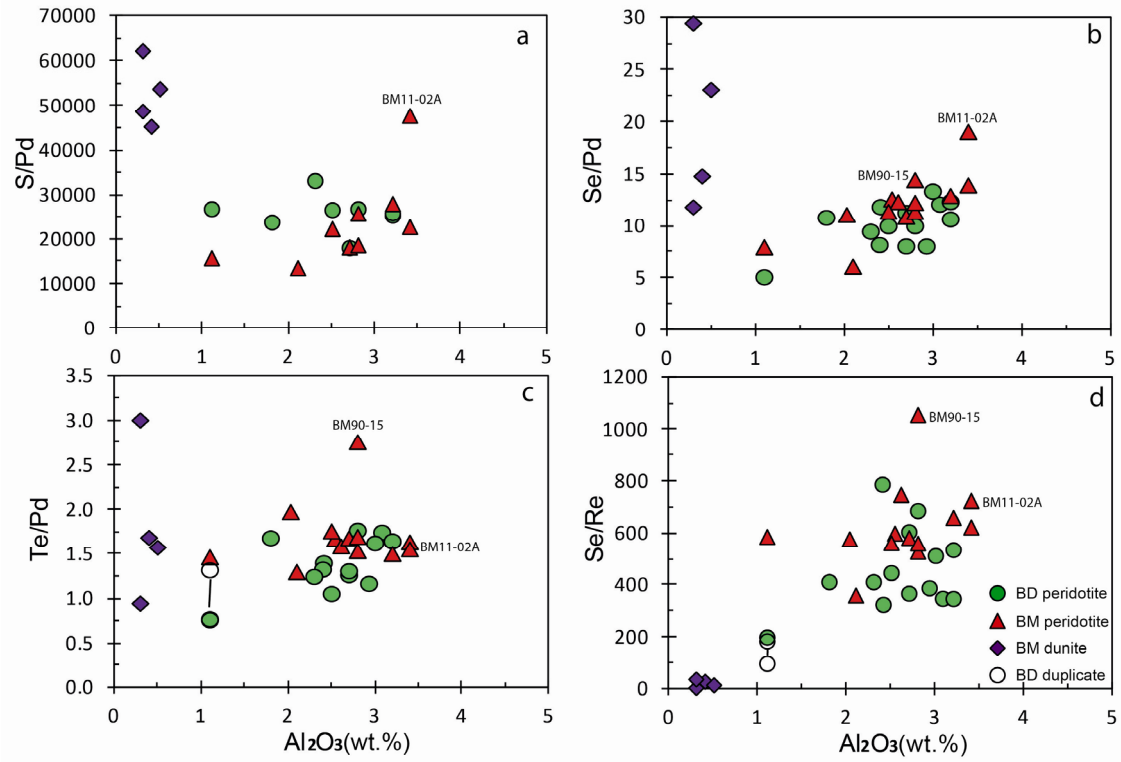

Figure 2.11 Variation of chalcogen/HSE ratios to assess the relative compatibility of chalcogens and HSE during magmatic processes in the mantle. S/Pd, Se/Pd and Te/Pd all slightly decrease with depletion, suggesting that chalcogen elements are more incompatible than Pd. Se/Re remains relatively constant with depletion, suggesting that Se and Re, behave similarly. BM dunites have different ratios compared with lherzolites and harzburgites, implying that in these rocks, melt/rock reaction has lead to fractionation of incompatible HSE with chalcogens.

2.7.6.2 The role of sulfide melt percolation

Two lherzolites from Balmuccia, BM11-02A and BM90-15 display considerably higher chalcogen abundances compared to other lherzolites (Table 2.1, Figures 2.6 and 2.8). BM11-02A may indeed record local mobilization of sulfide, as indicated by the high S (349 ppm) and Se (139.6 ppb) contents, and abundant interstitial sulfides (Supplement). No substantial fractionation of S from Se occurred in this case (S/Se = 2510) compared to other BM lherzolites, but Se/Te (12.2) is somewhat higher than in other lherzolites (Figure 2.9). This process did not modify HSE abundances, because Pt, Pd, Re and Au contents are similar to other lherzolites and their ratios relative to compatible HSE are not elevated (Figures 2.3, 2.7 and 2.11). In the sulfide bearing agent or melt S and Se must have been enriched, and Te and the HSE more depleted. This behavior is different from what would be expected from

basaltic melts near sulfide saturation. Thus, although this process seems to be not common, local migration of sulfide melt may occur. Although this process may produce modest fractionation of HSE from the chalcogens, it does not appear to change ratios of incompatible to compatible HSE. BM90-15 has comparatively high Te (20.5 ppb), but Se is similar to other lherzolites. We note that only few samples display such anomalies that may result from localized redistribution processes during cooling or late stage melt or fluid transport (e.g., Alard et al., 2011). Samples from Baldissero with high Pt and Pd contents and chondritic Os isotopic composition (BD90-4 and BM11-01) do not show anomalous S, Se and Te contents (Table 2.1). This observation, along with other data discussed earlier indicate that enrichments of Pt, Pd, Re and Au in peridotites do not always reflect mixing and sulfide addition, as has been proposed in some recent work (e.g., Alard et al., 2000; Lorand et al., 2010).

2.7.6.3 Compositional variations of infiltrating melts

Lherzolites from Lherz (Pyrenees), are thought to have formed by melt infiltration of harzburgites ("refertilization", Le Roux, et al., 2007). In the S-Se and Se-Te diagrams, most harzburgites and lherzolites from Lherz lie on the same positive linear trend, although with substantial scatter (Figure 2.8). Peridotites from Balmuccia show distinctly lower S/Se than peridotites from Lherz, whereas Baldissero samples lie in between the two trends. This observation is matching the stronger depletion of Re and the lithophile elements Na and Ti in BM compared to BD for a given Al_2O_3 or MgO content (Figures 2.1 and 2.2). The data are consistent with somewhat stronger enrichment of mildly incompatible elements in infiltrating melt at Lherz and Baldissero, compared to Balmuccia. At Balmuccia, more complete chemical and isotopic homogenization by infiltrating melt, tabular dunites and a strong foliation suggest that these processes occurred in an asthenospheric environment. Baldissero peridotites either represent ancient unequilibrated asthenospheric mantle accreted to the lithosphere during early Permian asthenospheric upwelling, or Proterozoic continental lithospheric mantle infiltrated by asthenospheric melts. Rhenium displays good correlations with S, Se and Te during partial melting, although in detail, there are hints for decoupling of these elements in BD samples (e.g., Figure 2.7b), which may reflect Paleozoic addition of melt with fractionated Re/chalcogen ratios.

2.8 Conclusions

Precise HSE, S, Se and Te contents and $^{187}Os/^{188}Os$ in peridotites from Balmuccia and Baldissero were determined by ID-ICPMS and N-TIMS to study the effects of partial melting and melt percolation on their abundances and chemical and

isotopic re-equilibration by porous melt flow. Balmuccia peridotites display predominantly Paleozoic Re depletion model ages with a distribution peak at 0.3-0.5 Ga. Baldissero displays a similar model age distribution peak, but more samples record Proterozoic depletion ages. The Paleozoic model ages are consistent with constraints from Sm-Nd ages of clinopyroxenes from the peridotites and the regional tectonic evolution, indicating major mantle melting events during that time. Depletions of incompatible HSE relative to compatible HSE in BD and BM are similar to results of low to moderate degrees of partial melting but more likely reflect variable re-equilibration of lherzolites with infiltrating incompatible element depleted melt. The homogeneous composition and Os model age distribution of lherzolites at BM indicates extensive homogenization by incompatible element depleted melt. Significantly more scattered HSE contents of BD samples probably reflects variable melt infiltration into Proterozoic melting residues and limited equilibration of harzburgites and depleted lherzolites. Os/Ir, Ru/Ir and Pd/Pt ratios in fertile lherzolites from both localities overlap with primitive mantle values, but Au, Re and S are more depleted. In the harzburgites and dunites, compatible HSE are heterogeneously distributed and tend to be more strongly fractionated compared to lherzolites. The chalcogens S, Se and Te are moderately incompatible during igneous processes in the peridotites. For both suites, S displays linear correlations with Al_2O_3, which roughly fits modeling assuming extraction of S saturated basaltic melts during partial melting. This behavior reflects solubility dependent sulfide removal or co-precipitation of sulfides with pyroxenes and spinel. At low to moderate degrees of partial melting, the relationship of the chalcogens with Re, Pt and Pd suggest decreasing compatibility in the order of Pt > Pd > Te ≥ Se ≥ S ≈ Re. The data indicate that MSS-sulfide melt partitioning does not control the HSE systematics of fertile and depleted lherzolites. At low to moderate degree of partial melting, sulfide-silicate melt partitioning seems to be the main control on Pd, Re, Au, S, Se and Te. Significant variations of S/Se and Se/Te in harzburgites are interpreted to result from heterogenous distribution of minor residual MSS and the variable presence of secondary sulfides that were precipitated from melts with high S/Se and high Se/Te.

Melt percolation may result in significant changes of HSE, and chalcogen abundances in reacted rocks and in produced melts. The HSE and chalcogen composition of BM dunites are consistent with melt-rock reaction and high fluxes of S undersaturated melt. The incompatible HSE and chalcogens in the BM dunites are notably more depleted than dunites in subduction-related ophiolites (Büchl et al., 2002; Zhou et al., 2005; Hanghøj et al., 2010). Very low contents of incompatible HSE and chalcogens, high S/Se and Se/Te and $^{187}Os/^{188}Os$ similar to BM lherzolites are consistent with the preservation of residual HSE and chalcogen composition after

reaction of BM lherzolites with S-undersaturated incompatible element depleted melts. The process of sulfide dissolution by S-undersaturated melts in BM dunites differs from sulfide removal during partial melting of the harzburgites because of much lower compatible HSE contents in BM dunites than in typical residual harzburgites.

Acknowledgments

We thank R. Naumann for XRF analyses of major and trace elements at GFZ Potsdam, U. Wiechert for providing the K_2SO_4 reference powder, K. Hammerschmidt and M. Feth for help and support in the TIMS and clean labs, and S. Hohl and C. Meyer for their assistance during sample collection in Italy. A. Greshake of the Museum für Naturkunde Berlin provided the Orgueil aliquot. Special thanks go to F. Wombacher and A. Ziegler for discussions and their initial efforts in establishing Se-Te analysis methods at FUB. A. Hofmann, G. Brügmann and S. Galer provided access to some samples from the early 1990s. W. Obermiller is acknowledged for a pdf version of his doctoral thesis and some spirited discussions in the early 1990s. Constructive comments from Associate Editor R. J. Walker, and A. Gannoun, L. Ackerman and an anonymous reviewer have improved the manuscript. This work was supported by a China Scholarship Council fellowship to Z. C. Wang and funds of Freie Universität Berlin.

Table 2.1 HSE, S, Se, Te, Al_2O_3, $^{187}Os/^{188}Os$ and model ages of Balmuccia and Baldissero peridotites

Sample	Rock	Al_2O_3 (w.t. %)	Re (ng/g)	Os (ng/g)	Ir (ng/g)	Ru (ng/g)	Rh (ng/g)	Pt (ng/g)	Pd (ng/g)	Au (ng/g)	$^{187}Re/^{188}Os$(2SE)	$^{187}Os/^{188}Os$(2SE)	$\gamma_{(Os)}$	$T_{Ma(PM)}$ Ga	$T_{RD(PM)}$ Ga	S(μg/g) a	S(μg/g) b	Se(ng/g) a	Se(ng/g) b	Te(ng/g) a	Te(ng/g) b
Baldissero																					
BD-13	L	3.08	0.22	4.35	3.65	7.37	1.22	6.91	6.35	0.65	0.244(2)	0.12808(1)	1.5	0.46	0.20			77.8	80.2	10.7	11.6
BD-16	L	2.41	0.27	4.26	3.70	7.41	1.37	7.61	***7.46***	1.26	0.307(2)	0.12876(3)	1.8	0.37	0.11			90.2	90.7	10.5	10.5
duplicate	L			3.86	3.45	6.62	1.13	7.01	***3.80***	1.93		0.12889(1)						85.0		12.4	
BD-17	H	1.1	0.03	***2.48***	***3.40***	5.43	0.93	6.83	1.33	0.40	0.066(3)	0.11826(1)	-5.7	1.82	1.55			7.0		1.0	
duplicate	H		0.03	***4.18***	***2.38***	6.89	0.84	5.93	1.27	0.19	0.038(2)	0.12808(1)	2.2	0.22	0.20			6.4		***1.0***	
duplicate	H		0.07	***3.68***	***2.50***	6.19	1.06	4.45	1.16	0.22	0.088(2)	0.11776(1)	-6.2	2.02	1.62	35.8		6.8		***1.5***	
BD90-3	L	2.93	0.17	4.43	3.92	7.86	1.38	10.51	8.26	1.27	0.186(2)	0.12543(1)	-0.4	0.99	0.57			68.4		9.7	
BD90-9	L	3.00	0.10	3.60	3.16	6.90	1.07	5.27	4.00	0.66	0.140(2)	0.12199(1)	-3.0	1.53	1.04			55.2	54.5	6.5	
BD90-4	L	2.4	0.11	4.03	3.64	7.21	1.25	8.09	10.12	1.91	0.126(2)	0.126130(4)	0.4	0.66	0.47			85.3		13.5	
BD90-10	L	2.7	0.12	4.48	4.13	8.18	1.41	7.88	6.44	0.99	0.129(2)	0.123030(5)	-2.1	1.27	0.90			75.4	74.2	8.2	
BD11-07	L	2.8	0.09	3.66	3.49	7.45	1.28	6.50	6.36	0.61	0.122(2)	0.12672(3)	0.8	0.55	0.40	171	170	67.1	63.7	10.0	
BD11-12	L	2.3	0.09	3.10	2.83	5.73	0.99	4.84	3.74	0.10	0.133(2)	0.12041(1)	-4.3	1.81	1.26	124	120	36.8	36.0	4.7	
BD11-13	L	2.5	0.12	4.03	3.26	7.25	1.24	6.93	5.35	0.27	0.143(2)	0.122231(7)	-2.9	1.50	1.01	143	138	57.3	52.7	5.4	5.9
BD92-2	H	1.8	0.09	3.55	3.02	6.88	1.18	4.33	3.41	0.32	0.121(2)	0.11986(1)	-4.7	1.84	1.33	81.4	78.3	39.2	36.7	5.0	6.5
BD11-01	L	2.7	0.20	4.05	3.91	8.03	1.37	10.87	8.96	1.09	0.233(2)	0.12454(6)	-1.4	1.50	0.70	162	162	73.5	74.9	11.8	
BD11-05	L	3.2	0.16	3.32	3.33	6.39	1.10	7.66	7.02	0.76	0.234(2)	0.12935(5)	2.5	0.08	0.04	178	177	89.0	88.9	11.6	
BD11-08	L	3.2	0.21	3.90	3.82	7.52	1.29	8.12	6.95	0.81	0.262(2)	0.127697(6)	1.1	0.66	0.26	180		76.1		11.5	
Balmuccia																					
BM90-5	L	2.03	0.13	3.99	3.74	7.53	1.30	8.10	6.68	1.01	0.153(2)	0.12565(1)	-0.1	0.83	0.54			76.4	75.6	13.0	13.5
duplicate	L		0.11	4.02	3.84	7.50	1.28	7.27	6.67	0.78	0.137(2)	0.12572(1)	0.0	0.78	0.53			78.0		12.8	
BM90-25	L	2.54	0.15	4.10	3.46	6.91	1.33	8.33	7.03	1.19	0.171(2)	0.12832(1)	1.9	0.28	0.17			91.0	91.0	11.8	11.8
duplicate	L			4.14	3.72	6.91	1.18	8.39	7.00	1.20		0.128314(5)						90.6		11.5	
BM90-41	L	2.61	0.10	3.70	3.31	6.26	1.02	6.91	5.89	0.80	0.124(2)	0.12653(1)	0.7	0.58	0.42			74.8	74.2	9.4	
duplicate	L		0.10	4.06	3.83	7.50	1.28	7.82	6.34	0.78	0.118(2)	0.12548(1)	-0.2	0.78	0.57			76.5	75.2	10.4	10.5
BM90-15	L	2.8	0.10	4.22	3.83	7.97	1.36	8.71	7.42	1.25	0.116(2)	***0.12578(1)***	0.1	0.71	0.52			110	110	20.6	20.5
duplicate	L		0.10	4.57	3.84	7.81	1.34	7.70	7.17	1.99	0.108(2)	***0.17783(1)***	41.7	-9.26	-7.07			112	116	20.4	20.4
BM11-11	L	2.1	0.11	4.06	4.00	8.10	1.39	10.58	6.48	0.45	0.131(2)	0.12493(1)	-0.7	0.92	0.64	88.2	88.1	40.1	41.8	8.6	8.3
BM-09	L	3.4	0.18	4.13	3.97	8.02	1.37	8.84	7.96	1.07	0.208(2)	0.13125(1)	4.1	-0.43	-0.23	182		114		13.1	
BM11-08	L	3.2	***0.12***	3.88	4.10	7.50	1.28	7.98	6.04	0.89	0.147(2)	0.12734(1)	1.2	0.47	0.31	***125***		80.2		9.1	
duplicate	L		***0.22***	4.28	3.93	7.45	1.27	8.46	6.68	1.11	0.252(2)	0.12745(1)	0.9	0.71	0.30	***170***		80.4		10.1	
BM11-09	L	2.7	0.13	4.02	3.92	7.80	1.33	9.33	6.97	0.76	0.157(2)	0.12613(1)	0.2	0.75	0.48	127		78.2		11.8	
BM11-03B	H	1.1	0.07	3.99	4.32	7.67	1.31	6.18	4.78	0.44	0.079(2)	0.11914(1)	-5.1	1.74	1.43	75.7		39.0	39.4	7.1	
BM11-04	L	2.5	0.14	3.94	3.86	7.63	1.31	8.59	6.86	0.90	0.170(2)	0.12667(1)	0.6	0.66	0.40	153		80.4		12.1	
BM11-18	L	2.8	0.14	3.63	3.63	7.13	1.22	8.49	6.50	0.79	0.186(2)	0.12649(1)	0.4	0.75	0.43	168		76.6	75.7	10.0	
BM11-10	L	2.8	0.16	4.08	3.93	7.74	1.32	8.95	7.13	0.88	0.184(2)	0.12702(1)	0.8	0.62	0.36	134		89.9		12.2	
BM11-02A	L	3.4	0.19	3.80	3.89	7.52	1.29	8.80	7.30	1.15	0.243(2)	0.13167(1)	4.3	-0.66	-0.29	349		***143***		11.4	
duplicate	L		0.21	4.15	3.69	7.27	1.25	7.53	6.81	1.10	0.239(2)	0.13104(3)	3.8	-0.44	-0.20	349		***124***		12.4	
BM11-03A	D	0.3	0.07	2.39	3.79	5.68	0.98	0.88	0.48	0.03	0.137(3)	0.12379(3)	-1.6	1.16	0.80	23.3		5.8		0.46	0.45
BM11-05	D	0.4	0.03	4.12	5.06	9.38	1.60	1.42	0.63	0.06	0.041(2)	0.12616(2)	0.7	0.52	0.47	***28.7***		9.6		1.1	1.0
duplicate	D		0.06	4.21	4.71	8.68	1.48	1.49	0.72	0.05	0.071(2)	0.12605(1)	0.5	0.58	0.49	***18.9***		8.7		1.5	
BM11-07A	D	0.3	0.09	1.17	1.98	3.89	0.68	2.29	1.18	0.18	0.373(7)	0.12625(3)	-0.5	3.20	0.46	73.4		35.5		3.5	3.6
BM11-24A	D	0.5	0.05	0.89	0.72	2.83	0.50	1.61	0.52	0.08	0.259(9)	0.12946(5)	2.5	0.04	0.02	27.9		12.3		0.89	

Duplicate: replicate digestion of the same sample powder; bold and italics indicate large variations between duplicates.
L: Lherzolite; H: Harzburgite; D: dunite.
a and b: re-analyses of different aqua regia solution from the same digestion for data quality evaluation of S, Se and Te. Average values are used for figures and discussion.
Re depletion age: values of PM $^{187}Os/^{188}Os$ =0.1296 and $^{187}Re/^{188}Os$=0.434 used for the calculation of T_{RD} and T_{MA} ages (Meisel et al., 2001b).
Os: calculated for an emplacement age of 280 Ma.
See precisions for each element in text. Typically, precisions for elements are better than 1-2 % (2 RSD). Values in brackets are in-run precisions (2SE) for $^{187}Re/^{188}Os$ and $^{187}Os/^{188}Os$ and precisions for $^{187}Re/^{188}Os$ are calculated from blank contribution and errors of Re and Os contents.

Table 2.2 Comparison of whole rock S, Se and Te analyses for UB-N and Orgueil

	S (µg/g)	Methods	Se (ng/g)	Methods	Te (ng/g)	Methods	References
UB-N	200±66						(Govindaraju, 1982)
	152-174	ICP-AES					(Okai et al., 2001)
	134±8 (n=5)	ICP-OES					(Ackerman et al., 2012)
	206±14 (n=5)	Combustion					(Ackerman et al., 2012)
	138-141	Combustion	113-123	HG-ICPMS	8.4-8.9	HG-ICPMS	(Lorand et al., 2008b; Lorand and Alard, 2010)
			112±3 (n=3)	HG-AAS	8±2	Liq. extraction GF-AAS	(Terashima and Imai, 2000; Terashima, 2001)
			174±58	TCF-INAA			(Savard et al., 2009)
			117±12 (n=8)				(Savard et al., 2009)
			126±3 (n=3)	TCP-ID-HG-MC-ICPMS	9.67±0.02 (n=3)	TCP-ID-HG-ICPMS	(König et al., 2012)
	155	**ID-ICPMS**	**127**	**HG-ID-ICPMS**	**10.6**	**HG-ID-ICPMS**	**This study**
	S (wt. %)		**Se (µg/g)**		**Te (µg/g)**		
CI Chondrite	5.41±0.27	compilation	21.4±1.07	compilation	2.27±0.23	compilation	(Palme and O'Neill, 2003)
	5.41±0.37(n=5)		19.7±0.4 (n=4)		2.33±0.18(n=3)		(Lodders, 2003)
	5.41		21.3	INAA			(Dreibus et al., 1995)
Orgueil	5.25 (n=2)	compilation	18.2 (n=12)	compilation	2.27 (n=12)	compilation	(Anders and Grevesse, 1989)
	5.39-5.49	0.05g sample	21.4	INAA			(Dreibus et al., 1995)
	5.35±0.25(n=7)		19.5±1.9(n=26)		2.26±0.17(n=17)		(Lodders, 2003)
			20.92±0.17(n=4)	**HG-ID-ICPMS**	**2.31±0.01(n=4)**	**HG-ID-ICPMS**	**This study**

All precision data for multiple analyses is given as one standard deviation (1 sd).
2.5 g of UB-N was digested. Orgueil (0.05g) was analyzed four times using aqua regia solution from the same digestion.

2.9 Supplement

2.9.1 Brief description of samples

Here, 27 peridotites of variable fertility from Baldissero and Balmuccia and four samples from tabular dunite bodies from Balmuccia were analyzed. Eleven peridotites have been analyzed previously for major elements, trace elements and Sr-Nd-O isotopes of clinopyroxene separates and all of them were collected distant to mafic dikes (Obermiller, 1994; Rivalenti et al., 1995). Clinopyroxene from peridotites show LREE depleted patterns; Sr-Nd isotopic compositions are MORB like, and $\delta^{18}O$ of 5.14 for BM samples are similar to mantle rocks (Obermiller, 1994; Rivalenti et al., 1995). Baldissero and Balmuccia peridotites have been interpreted to be results of fractional melting during upwelling of asthenosphere (Obermiller, 1994; Rivalenti et al., 1995; Mazzucchelli et al., 2010). The other samples, collected in 2011 (some by using a rock coring device), are also macroscopically unweathered and unaltered and were collected far from dikes (generally >0.3 m). The following are detailed coordinates and brief description of newly collected samples.

2.9.2 Baldissero

Most samples collected in 2011 are from outcrops in the active and abandoned areas of the main quarry at Baldissero. Samples are macroscopically unaltered, display granular texture, and were collected at some distance from pyroxenites dikes/veins.

BD11-01: fertile lherzolite, very fresh, fine to medium grain (0.5-2 mm). Collected at 30-40 cm distance from an Al-augite dike (1-2cm wide) that was crosscutting the foliation of cpx-rich lherzolite.

BD11-05: fertile lherzolite, coarse grained (3-5mm) and homogenous. A 1-2 cm wide discordant dike occurs > 1 m from the sampling site.

BD11-07: fertile lherzolite, near the entrance to old quarry, north side of road, homogenous.

BD11-08: fertile lherzolite, near south end of second level in the new quarry. Nearby peridotite is very homogenous and occurs along 200 m long road, lithology displays no noticeable change, no dikes.

BD11-12: lherzolite (drill core) with minor serpentinized cracks, collected along the gorge bank which locates at eastern of quarry. In thin section, tiny Fe oxides (10-30 μm) occur in serpentinized cracks.

BD11-13: lherzolite (drill core) with minor serpentinized cracks, similar to BD11-12, collected at the gorge bank which locates at eastern of quarry.

2.9.3 Balmuccia

Balmuccia peridotites collected in 2011 are from the main quarry and from the southern bank from the Sesia river.

BM11-02A: fertile lherzolite, fine grained, homogenous. Two small dikes occur around 50 cm far away.

BM11-03A (dunite) and **BM11-03B** (harzburgite): harzburgite-dunite transition. Harzburgite displays decreasing orthopyroxene abundance and becomes dunitic. BM11-03A and BM11-03B each were sampled at about 20 cm distance from the gradational boundary. Dunite BM11-03A is cut by 3 to 5 mm wide Cr diopside rich clinopyroxenite veinlets which contain abundant sulfides. Granular samples without cpx veinlets were used for analysis.

BM11-05: homogenous dunite from a tabular dunite body with local veins containing coarse amphibole (3-10 mm) or websterite veins (1-2 cm). Dunite was sampled > 40 cm far way from veins.

BM11-07A: fresh dunite cut by a 40 cm wide orthopyroxenite dike (BM11-07B). The orthopyroxenite displays a sharp boundary with the dunite and contains abundant and sometimes large sulfide grains. The orthopyroxenite cumulates appear to have formed after the dunite and display a coarse-grained texture (around 5mm). The dunite was sampled 40 cm far from the contact to orthopyroxenite.

BM11-04, BM11-08, BM11-09, BM11-10, BM11-11 and BM11-18: fertile lherzolites, very fresh and homogenous with no dikes in the vicinity (> 0.5 m).

BM11-24A: dunite sampled by drill core. This dunite body outcropping on the eastern bank of the Sesia river was studied by Mazzucchelli, et al. (2009). It is rich in spinel layers and Cr diopside veins. Dunite BM11-24A was sampled in 2 cm distance from spinel layer BM11-24B.

Table S2.1 Major and trace element XRF concentrations of peridotites from Baldissero and Balmuccia

	Rock	SiO_2 (wt.%)	TiO_2 (wt.%)	Al_2O_3 (wt.%)	Fe_2O_3 (wt.%)	MnO (wt.%)	MgO (wt.%)	CaO (wt.%)	Na_2O (wt.%)	LOI (wt.%)	Sum (wt.%)	Cr (µg/g)	Ni (µg/g)	V (µg/g)	Zn (µg/g)	Mg#
Baldissero																
BD 11-01	Lherzolite	43.9	0.08	2.7	8.82	0.13	40.57	2.44	0.13	0.62	99.35	2294	2189	66	55	90.2
BD 11-05	Lherzolite	45.1	0.10	3.2	8.64	0.13	38.39	2.98	0.15	0.54	99.29	2632	2004	78	55	89.9
BD 11-08	Lherzolite	44.2	0.09	3.2	8.72	0.13	39.40	2.93	0.13	0.50	99.30	2524	2101	83	54	90.0
BD 92-2	Harzburgite	42.7	0.07	1.8	9.26	0.13	42.74	1.26	0.04	1.47	99.45	1824	2325	43	51	90.2
BD 11-07	Lherzolite	43.9	0.09	2.8	9.06	0.13	39.19	2.78	0.11	1.27	99.33	2294	2072	68	52	89.6
BD 11-12	Lherzolite	41.9	0.06	2.3	8.24	0.11	40.23	1.67	0.10	4.67	99.25	2803	2184	54	67	90.7
BD 11-13	Lherzolite	43.3	0.08	2.5	8.75	0.13	39.23	2.32	0.11	2.95	99.34	2056	2085	71	49	90.0
BD-17	Harzburgite	42.8	0.02	1.1	8.77	0.12	43.73	0.67	<0.01	2.14	99.33	2438	2345	31	46	90.9
BD 90-4	Lherzolite	44.0	0.06	2.4	8.89	0.13	39.32	2.71	0.04	1.71	99.26	2576	2068	64	51	89.8
BD 90-10	Lherzolite	44.8	0.09	2.7	8.89	0.13	39.85	2.60	0.13	0.16	99.27	2685	2114	57	52	90.0
BD-13#	Lherzolite	44.7	0.09	3.1	9.20	0.13	39.95	2.92			100.09					89.7
BD-16#	Lherzolite	43.7	0.08	2.4	9.24	0.13	42.26	2.09	0.08		100.02					90.1
BD-90-3#	Lherzolite	44.6	0.09	2.9	9.01	0.13	40.37	2.79	0.10		99.97					90.0
BD90-9#	Lherzolite	44.3	0.09	3.0	8.92	0.13	39.65	2.97	0.15		99.24					89.9
Balmuccia																
BM 90-15	Lherzolite	43.3	0.07	2.8	9.11	0.13	39.93	2.57	0.06	1.27	99.21	2850	2156	67	58	89.8
BM -09	Lherzolite	45.3	0.09	3.4	8.87	0.13	37.64	3.25	0.11	0.49	99.30	2573	1942	78	57	89.5
BM 11-08	Lherzolite	45.1	0.08	3.2	8.72	0.13	38.60	2.81	0.10	0.60	99.29	2857	1977	81	63	89.9
BM 11-09	Lherzolite	44.1	0.07	2.7	9.09	0.13	40.13	2.57	0.09	0.50	99.34	2324	2186	64	50	89.8
BM 11-10	Lherzolite	44.2	0.07	2.8	8.83	0.13	39.78	2.87	0.11	0.53	99.32	2512	2184	69	52	90.0
BM 11-04	Lherzolite	43.7	0.06	2.5	9.04	0.13	39.94	2.78	0.09	0.99	99.26	2427	2167	70	55	89.8
BM 11-02A	Lherzolite	45.1	0.08	3.4	8.82	0.13	37.64	3.06	0.08	1.04	99.31	2586	2020	78	53	89.5
BM 11-18	Lherzolite	43.8	0.07	2.8	9.12	0.13	39.58	2.68	0.09	1.11	99.30	2394	2089	67	53	89.7
BM 11-03B	Harzburgite	43.1	0.03	1.1	8.99	0.13	44.06	0.96	0.02	0.96	99.35	2267	2265	38	52	90.7
BM 11-11	Lherzolite	42.3	0.06	2.1	9.38	0.14	39.43	1.60	0.03	4.26	99.33	2344	1984	55	118	89.4
BM90-5*	Lherzolite	44.0	0.06	2.0	9.02	0.13	42.49	2.23	0.04		99.97	2758	2296			90.4
BM90-25*	Lherzolite	44.7	0.06	2.5	8.83	0.13	41.14	2.51	0.07		99.99	3035	2171			90.3
BM90-41*	Lherzolite	44.7	0.07	2.6	9.21	0.13	40.51	2.71	0.05		99.99	2826	2139			89.8
BM 11-24A	Dunite	39.7	0.02	0.5	9.60	0.13	48.40	0.19	<0.01	0.65	99.24	2821	2934	21	36	91.0
BM 11-07A	Dunite	39.9	0.02	0.3	9.91	0.13	48.14	0.20	<0.01	0.75	99.42	1730	2742	10	47	90.7
BM 11-05	Dunite	39.7	0.01	0.4	9.53	0.13	48.50	0.23	<0.01	0.57	99.08	3806	2720	20	58	91.1
BM 11-03	Dunite	39.9	0.01	0.3	9.80	0.13	48.37	0.23	<0.01	0.53	99.29	2317	2697	17	55	90.8

Note: data of samples with # symbol from Obermiller (1994) and * symbol from Rivalenti, et al (1995).

Table S2.2 Coordinates of Baldissero and Balmuccia samples collected in 2011

Samples	Latitude	Longitude	Elevation (m)
Baldissero			
BD 11-01	45°25′11″	7°44′41″	508
BD 11-05	45°25′13″	7°44′45″	497
BD 11-07	45°25′19″	7°45′6″	469
BD 11-08	45°25′20″	7°45′4″	488
BD 11-12	45°25′6″	7°45′11″	342
BD 11-13	45°25′5″	7°45′10″	343
Balmuccia			
BM 11-08	45°49′17″	8°9′5″	627
BM 11-09	45°49′18″	8°9′5″	634
BM 11-10	45°49′18″	8°9′6″	628
BM 11-04	45°49′17″	8°9′3″	627
BM 11-02A	45°49′24″	8°9′22″	604
BM 11-18	45°49′21″	8°9′10″	620
BM 11-03B	45°49′16″	8°9′3″	630
BM 11-11	45°49′18″	8°9′6″	623
BM 11-24A	45°49′12″	8°9′13″	549
BM 11-07A	45°49′16″	8°9′3″	635
BM 11-05	45°49′16″	8°9′3″	631
BM 11-03	45°49′16″	8°9′3″	630

2.9.4 Sulfide occurrences

Most of sulfides in Baldissero and Balmuccia peridotites are interstitial and anhedral with 20-500 μm across and commonly occurring with olivine, spinel and pyroxene (Figure S2.2 and S2.3). Dominant pentlandite and subordinate chalcopyrite are the major base metal sulfides (>95 % by volume), and are intergrown in different proportions. A few tiny (<20 μm) sulfide grains are enclosed in silicate minerals, mostly in olivine at both BD and BM, but BD samples seem to have more inclusions than BM samples. Sulfides in dunites are sparse and also tiny. Some are hosted by olivine but most occur interstitial with spinel.

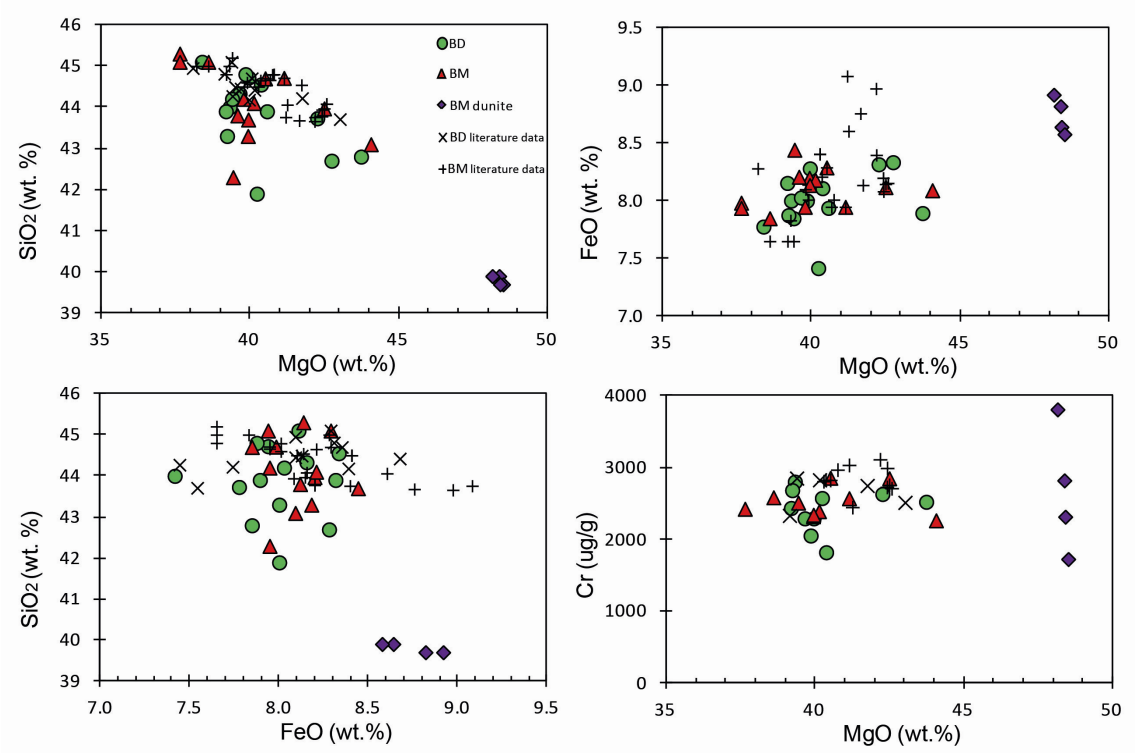

Figure S2.1 Variation diagrams of major element and Cr concentrations (literature data are same as in Figure 2.1).

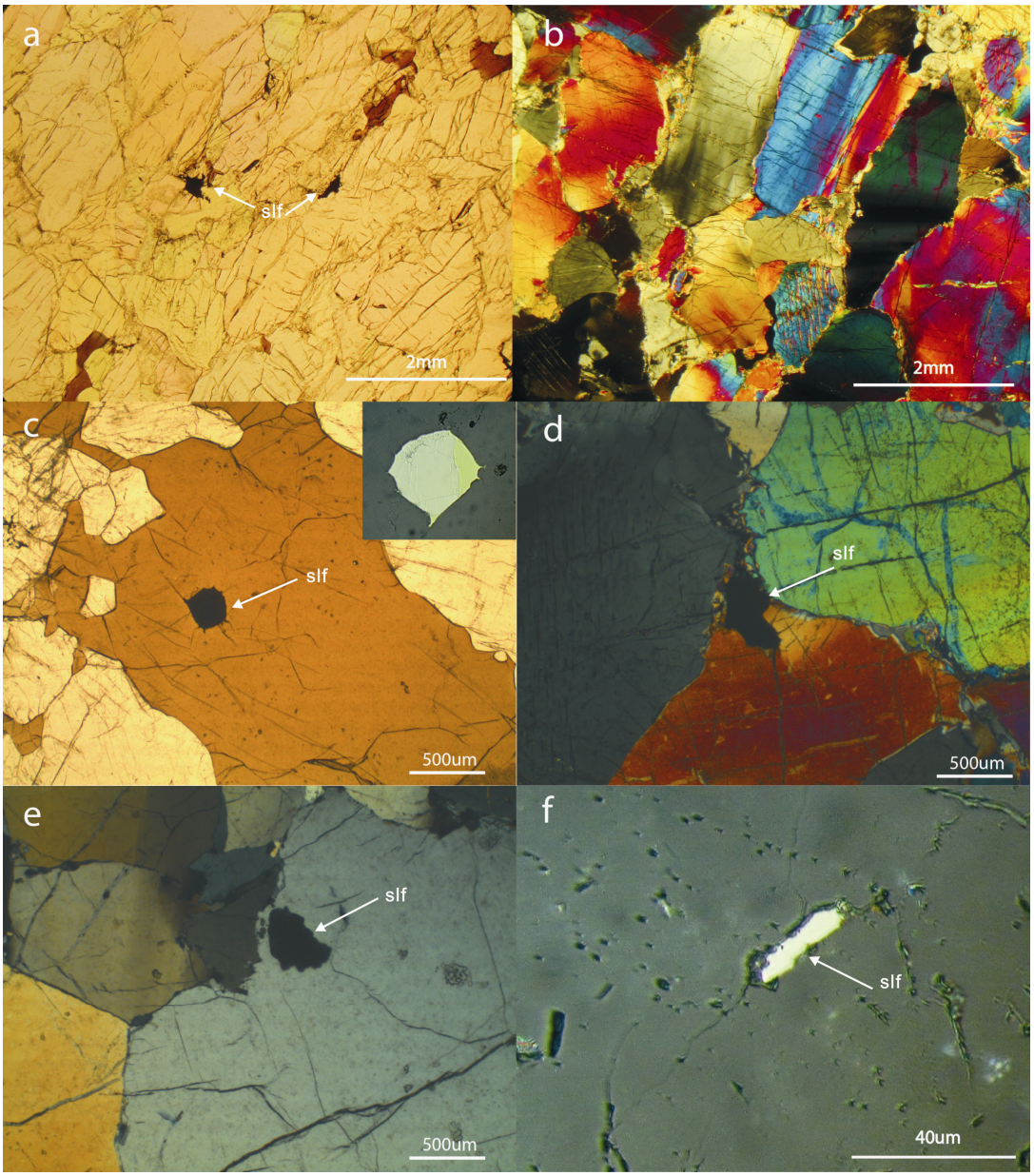

Figure S2.2 Microscopic textures of BD and BM peridotites, showing negligible alteration, typical granular textures and predominantly interstitial sulfides in BD and BM peridotite (a, b and d). Many sulfides occur with spinel, e.g., inclusion of pentlandite and chalcopyrite in spinel (upper right corner of c). A few sulfides with different sizes are also enclosed by olivine (e and f). slf, sulfide. a from BM11-09 (single-polarized light); b from BM11-08 (crossed-polarized light); c from BD11-05 (single-polarized light); d from BD11-05 (crossed-polarized light); e from BD11-05 (crossed-polarized light); and f from BD11-12 (reflected light).

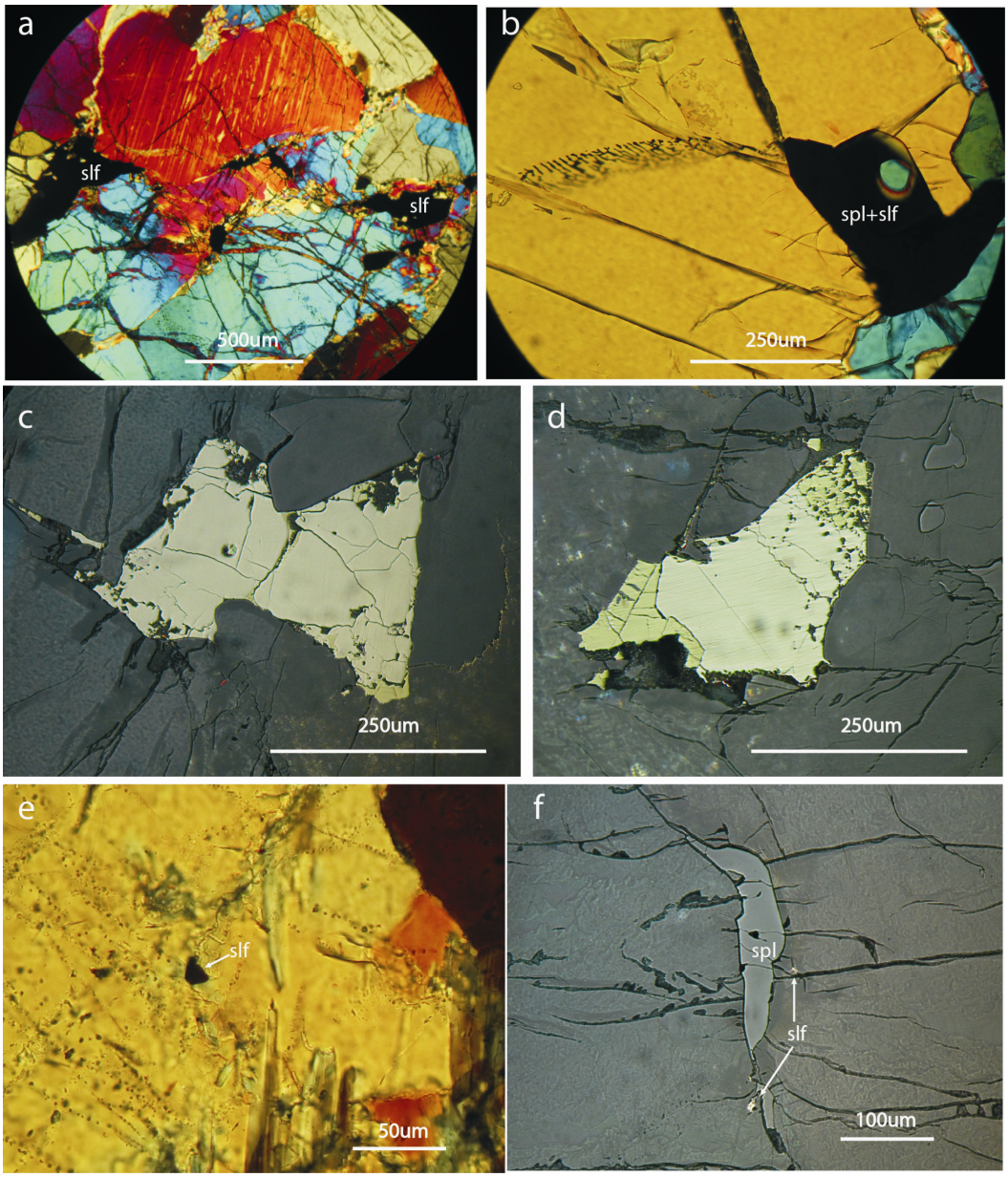

Figure S2.3 Microscopic photographs of sulfides in BD and BM peridotites, showing predominantly interstitial sulfides (a, b, c and d) with minor enclosed grains (e). Interstitial sulfides are commonly intergrowth of pentlandite and chalcopyrite with different proportions (c and d), interpreted as exsolutions from sulfide melts with cooling. A few sulfides enclosed by olivine occur in both of BD and BM and normally have small sizes (e). Elongate sulfide grains in dunite are very small (<30 μm) and most are interstitial and occur with spinel (f). spl, spinel; slf, sulfide. a from BM11-02A (crossed-polarized light); b from BM11-10 (crossed-polarized light); c and d from BM11-09 (reflected light); e from BM11-04 (crossed-polarized light); and f from dunite BM11-24A (reflected light).

2.9.5 Details of Se-Te measurements by hydride generation

Se and Te were measured using the low mass solution mode on the Element XR combined with a HG sample introduction system by reacting the sample solution with 1 % m/m $NaBH_4$ in 0.05 M NaOH (Rouxel et al., 2002; Elwaer and Hintelmann,

2008b). The HG technique significantly reduces memory effects and facilitates the efficiency of Se and Te transfer to the plasma and the ionization yield. Because of the formation of volatile hydrides, the effective separation of the gaseous hydrides of Se and Te from potential interferences can be easily achieved. Although transition metals can inhibit the hydride formation reaction, these elements have been removed by chemical separation. The transition metals do not form spectral interferences on Se and Te isotopes. Argon from the plasma is a major concern for Se isotopes because the formation of Ar-based polyatomic ions on m/z of 76, 78, and 80 is well known (Elwaer and Hintelmann, 2008a). Therefore, in order to avoid potential bias from fluctuations of the Ar background, we have chosen $^{77}Se/^{82}Se$ and $^{125}Te/^{126}Te$ to calculate Se and Te concentrations by isotope dilution. The raw data were corrected by subtraction of the background blank contribution, followed by correction of mass discrimination by a mixed Se-Te standard solution. Small contributions from Kr and Xe contaminants from the Ar gas could interfere with ^{82}Se and ^{126}Te, respectively. High purity Ar gas (≥99.999 %) was used in the study, and no interference of ^{126}Xe on ^{126}Te has been detected, when compared with measurements of Te isotopes in Nanopure water using HG and a regular glass spray chamber. Small amounts of ^{82}Kr were indeed detected (<2 % of samples). The $^{82}Kr/^{83}Kr$ of the acid blank measured in a glass spray chamber yielded nearly the natural ratio and the isotopic proportions in the gas background was relatively constant from sample to sample. These contributions were thus simply corrected by subtraction of the gas blank during HG measurements. If Se isotopes are measured by aspiration from a glass spray chamber, the predominant interferences are $^{40}Ar^{36}ArH$ and $^{40}Ar^{37}Cl$ on ^{77}Se. Even for acid blank and Nanopure water, significant intensity of mass 77 was detected, indicating the presence of strong $^{40}Ar^{36}ArH$ interference induced by Ar gas. Fortunately, this interference is relatively constant during measurement periods. The $^{40}Ar^{37}Cl$ interference on ^{77}Se was not observed in our study because we used HNO_3 rather than HCl as solvent. Therefore, for Ar-based polyatomic interferences, subtraction of gas blank followed by mass discrimination correction are sufficient for accurate Se and Te data reduction, when applying $^{77}Se/^{82}Se$ and $^{125}Te/^{126}Te$ to concentration calculation. The $^{77}Se/^{82}Se$ ratios of a 10 ng/g Se standard solution for testing, after acid background subtraction were nearly same (<0.5 % variation) during measurement period, thus further supports the effectiveness of our method. Acid blanks were detected before and after Se and Te standard solutions and every two samples.

Other possible inferences could be derived from the formation of $^{76}SeH^+$ and $^{125}TeH^+$ and may be caused by H_2 gas derived from the HG reaction (Elwaer and Hintelmann, 2008b). Elwaer and Hintelmann (2008b) observed an average $^{82}SeH^+/^{82}Se^+$ ratio of 3.4 % using SF-ICPMS and applied it to subtract the $^{76}SeH^+$

interference on their ^{77}Se signal. However, their monitor mass 83 ($^{82}SeH^+$) may have also reflected contributions from ^{83}Kr, rather than $^{82}SeH^+$. In practice, intensities of monitored mass 83 did not show any noticeable increase (<1 %) if the acid blank was compared with the 4 ng/g Se standard solution. We also have used the ^{125}Te spike solution to monitor $^{125}TeH^+$ and did not observe a significant extra contribution on mass 126 (<0.5 % of ^{125}Te), indicating negligible TeH^+. Consequently, we assume that SeH^+ formation can be neglected likewise. Due to variations in the gas flow during HG, the Se and Te intensities were not as stable as for the HSE and S, typically yielding 3-8 % RSD for samples. Standard errors of the mean of $^{77}Se/^{82}Se$ and $^{125}Te/^{126}Te$ were better than 0.1 % (2RSE) using peak dwell times of 5 ms and sample gas flow of 1.195 L/min and n = 6000 and 9000 scans, respectively.

Chapter 3

Magmatic fractionation of highly siderophile and chalcogen elements in the mantle: constraints from pyroxenites in the Balmuccia peridotite massif

Zaicong Wang and Harry Becker

Freie Universität Berlin, Institut für Geologische Wissenschaften,
Malteserstrasse 74-100, 12249 Berlin, Germany

3.1 Abstract

Mantle pyroxenites are cumulates of migrating melts in the mantle, which have been affected by reactive infiltration, fractional crystallization and mixing. Pyroxenites are also possible sources of mantle melts. The formation history and the role of pyroxenites during melting of heterogeneous mantle have been difficult to unveil by major elements and lithophile incompatible elements. Magmatic fractionation of the highly siderophile (HSE) and chalcogen (S, Se, Te) elements and Os isotopes in websterites and spinel clinopyroxenites of the Balmuccia peridotite massif (Ivrea-Verbano Zone, Italian Alps) sheds new insight on these processes.

High concentrations of the HSE and chalcogens in websterites and their ratios (notably, Se/Te, Pd/Ir) are consistent with early accumulation and sulfide segregation from primitive S saturated melts. In contrast, clinopyroxenites have MORB-like HSE and chalcogen compositions and high S, Se and Re contents similar to websterites, but lower abundances and stronger fractionations of the PGE and Te than websterites. Subparallel HSE patterns with variations over several orders of magnitude, and S/Se and Se/Te ratios, suggest that the clinopyroxenites formed from evolved melts that have undergone different extents of sulfide segregation in the mantle. Concentrations of the PGE in clinopyroxenites are higher than predicted by sulfide-silicate equilibration, indicating variable replenishment of these elements by reaction of the melts with grain boundary sulfides in peridotites. Re-Os errorchron and model ages imply that the clinopyroxenites formed during the Jurassic, significantly later than some websterites, which may have formed in the late Paleozoic.

The websterites, and calculated HSE abundances in their sulfides, share many similarities with element ratios of metasomatic interstitial sulfides of refertilized peridotites, e.g., Re/Os, Pd/Ir, S/Re, S/Se, Se/Te and moderately suprachondritic initial $^{187}Os/^{188}Os$. The similarities in sulfide compositions from websterites and grain boundary sulfides in peridotites indicate that preferential dissolution of interstitial sulfides in peridotites into migrating silicate melts should be an important mode of melt extraction and melt-peridotite reaction. The HSE and chalcogens in these melts are not fully equilibrated with peridotitic mantle. The fractionation of the HSE and chalcogens, particularly the strong fractionation of Re/Os relative to Pd/Ir in pyroxenites and upper and lower oceanic crust indicates that most of the compositional variation of these elements may reflect magma transport and reaction in the mantle. Incomplete equilibration of infiltrating melts with peridotites and selective remelting of pyroxenites or veined peridotites explain Os isotopic disequilibrium and heterogeneity in the mantle.

3.2 Introduction

Chemical and isotopic heterogeneity recorded in mantle rocks and in mantle-derived igneous rocks is a natural result of partial melting, crust formation and its alteration by surface processes and recycling of subducted lithosphere into the Earth's mantle (e.g., Hofmann, 1997). Transport of magma within the mantle can contribute both to chemical heterogeneity and homogenization, depending on spatial scales. Pyroxenite is a minor lithology (presumably < 5-10 % by volume) of the upper mantle and represents the mineralogical manifestation of major and trace element and isotopic heterogeneity (e.g., Suen and Frey, 1987; Pearson et al., 1991; Becker, 1996; Becker et al., 2004; Pearson and Nowell, 2004; Downes, 2007; van Acken et al., 2008, 2010b; Borghini et al., 2013). Because of their lower solidus temperatures compared to peridotite, pyroxenites and eclogites should melt preferentially during mantle upwelling and form considerable fractions of pyroxenite derived melts (Kogiso and Hirschmann, 2001; Pertermann and Hirschmann, 2003; Lambart et al., 2009), and have been proposed as an important source rock for the genesis of basaltic magma (Hirschmann and Stolper, 1996; Sobolev et al., 2005, 2007). Major, trace element and Os isotopic data indicate that most mantle pyroxenites are products of crystal accumulation of mantle-derived melts that variably reacted with mantle peridotite (e.g., Sinigoi et al., 1983; Suen and Frey, 1987; Becker et al., 2001a, 2004; Pearson and Nowell, 2004; Downes, 2007; van Acken et al., 2008, 2010b). Thus, the composition of mantle pyroxenites reveals information about the creation and destruction of the chemical and isotopic signatures of mantle heterogeneity and about early element fractionation during transport of magma in the mantle.

Some details of processes involved in pyroxenite genesis remain controversial and incompletely understood (Bodinier and Godard, 2003; Downes, 2007). The origin of pyroxenites as cumulates from peridotite derived partial melts or partial melts of heterogeneous peridotite-eclogite lithologies involving recycled materials and melt-peridotite reaction is debated (e.g., Allegre and Turcotte, 1986; Voshage et al., 1988; Blichert-Toft et al., 1999; Garrido and Bodinier, 1999; Obata et al., 2006; Dantas et al., 2007; Downes, 2007; Sobolev et al., 2007; Bodinier et al., 2008; van Acken et al., 2010b). The controversy reflects the difficulty to distinguish elemental and isotopic signatures of partial melting of peridotites from reaction of eclogite or pyroxenite-derived melt with peridotite. The mineralogical and chemical diversities of pyroxenites formed in different geological settings display their variable origins, e.g., pyroxenites from Beni Bousera and Ronda (e.g., Pearson et al., 1991; Garrido and Bodinier, 1999; Bodinier and Godard, 2003; Pearson and Nowell, 2004; Downes, 2007; Gysi et al., 2011).

The occurrence of pyroxenites is often associated with chemical and isotopic evidence for the infiltration of pyroxene saturated melts into surrounding peridotite and refertilization of the latter (Bodinier and Godard, 2003; Le Roux et al., 2007; Bodinier et al., 2008; Rampone and Borghini, 2008). The Sr-Nd isotopic signatures of these infiltration processes may reflect recycled sediment (Pearson et al., 1993; Becker, 1996; Marchesi et al., 2013) or middle ocean ridge basalt (MORB, or depleted mantle) like isotopic compositions (e.g., Mukasa and Shervais, 1999; van Acken et al., 2010a). In contrast, Os isotopic data of pyroxenites are nearly always suprachondritic and suggest the presence of components of recycled crust with high Re/Os (e.g., Reisberg et al., 1991; Becker et al., 2001a, 2004; Pearson and Nowell, 2004; Luguet et al., 2008; van Acken et al., 2008, 2010b).

Interstitial sulfides in refertilized peridotites commonly also display radiogenic initial $^{187}Os/^{188}Os$ and enrichments of Pt, Pd, Re, Te and Se relative to Os-Ir-Ru (e.g., Alard et al., 2000, 2002, 2005; Luguet et al., 2004; Harvey et al., 2011). Such interstitial sulfides likely were precipitated from melts with fractionated patterns of highly siderophile elements (HSE, including platinum group element (PGE), Re and Au). In mantle peridotites, empirical bulk peridotite-melt partition coefficients are Os $\geq$ Ir $\geq$ Ru > Rh $\geq$ Pt > Pd > Te (>Au?) > Se $\geq$ S $\approx$ Re, leading to strong fractionation of these elements in melts (Pearson et al., 2004; Becker et al., 2006; Fischer-Gödde et al., 2011; Wang et al., 2013). Subsequent processes such as sulfide segregation during fractional crystallization (Rehkämper et al., 1999b; Yi et al., 2000; Bézos et al., 2005) further modify HSE and chalcogen abundances of melts. Thus, it is likely that primitive partial melts and infiltrating melts in the mantle have abundances and ratios of HSE and chalcogens different from most MORB, but how much different is not clear.

In the present study, we present new highly siderophile element and chalcogen element abundance data that clearly show the connection between the reactive infiltration of mantle peridotites and pyroxenite formation, and the impact of early fractionation on the abundances of HSE and the chalcogens S, Se and Te in derivative magmas.

The Balmuccia peridotite massif (BM) in the Ivrea-Verbano zone, Italian Alps underwent partial melting and refertilization in the late-Paleozoic, presumably in the aftermath of the Hercynian orogeny (Voshage et al., 1988; Shervais and Mukasa, 1991; Obermiller, 1994; Rivalenti et al., 1995; Mukasa and Shervais, 1999; Mazzucchelli et al., 2009; Wang et al., 2013). The well-constrained evolution history of the host peridotites, crosscutting relationships of different generations of pyroxenite dikes, and negligible low-temperature alteration make Balmuccia pyroxenites ideal samples for understanding the nature of parent melts and processes from which

different types of pyroxenite layers formed. Previous studies have shown that BM pyroxenites are cumulates crystallized from mantle-derived magmas with similar Sr-Nd-Pb isotopic compositions as those of host Balmuccia peridotites (e.g., Sinigoi et al., 1983; Voshage et al., 1988; Shervais and Mukasa, 1991; Rivalenti et al., 1995; Mukasa and Shervais, 1999). Here, HSE and chalcogens data and Os isotopic compositions are reported that indicate an origin of Al augite rich pyroxenites from MORB like magmas and a more primitive nature of melts that were responsible for websterites. It is shown that sulfide-silicate partitioning as the major controlling process during melt evolution and that most of the HSE and chalcogen fractionation in basalts may occur in the mantle.

3.3 Geological setting

The Balmuccia peridotite massif was interpreted as a fragment of subcontinental lithospheric mantle which was tectonically emplaced into lower crustal granulite facies metabasites of the Ivrea-Verbano Zone (IVZ) in the western Italian Alps. Emplacement occurred presumably during the Carboniferous or Permian in the waning stage of the extensional Hercynian orogeny, and was exhumed in the course of the Mesozoic extension and subsequent Alpine compression (e.g, Zingg et al., 1990; Shervais and Mukasa, 1991; Handy et al., 1999; Mukasa and Shervais, 1999). Many studies have indicated that the voluminous Mafic Complex that hosts the BM massif intruded into lower-crustal, high-grade paragneiss of the Kinzigite Formation approximately at 280-290 Ma with cooling extending at least to 210 Ma (e.g, Peressini et al., 2007). Present exposure and orientation of the Balmuccia massif are mainly consequences of high degree tilting and uplift during Alpine collision (Handy et al., 1999).

The BM massif consists of fresh, unserpentinized spinel facies lherzolites with minor dunite and harzburgite, which are cross-cut by abundant pyroxenitic and gabbroic layers and dikes (Shervais and Mukasa, 1991; Mukasa and Shervais, 1999). The predominance of Paleozoic Re depletion ages with a peak at 300-500 Ma is consistent with Sm-Nd errorchron ages of clinopyroxenes from lherzolites and some websterites, indicating late Paleozoic partial melting of the peridotites (Voshage et al., 1990; Obermiller, 1994; Wang et al., 2013). In recent models, BM lherzolites have been interpreted to reflect open system melt infiltration and melting with incompatible elements indicating on average about 3-5 % fractional melting (Rivalenti et al., 1995; Mazzucchelli et al., 2009; Wang et al., 2013). Discordant relationships with the lherzolites and harzburgitic reaction zones indicate that replacive dunites formed at a later stage by focused melt percolation (Mazzuchelli et al. 2009; Wang et al. 2013).

Crosscutting relationships indicate that pyroxenites and other magmatic rocks in the BM peridotites formed at different times, approximately from oldest to youngest: green Cr-diopside suite websterites and gray Al-augite suite clinopyroxenites, late gabbro suite and veins containing abundant hydrous phases (hornblendite and phlogopite rich veins) (Shervais and Mukasa, 1991; Mukasa and Shervais, 1999). Initial Sr-Nd-Pb isotopic compositions of clinopyroxenes from websterites and clinopyroxenites calculated at 250 Ma are similar to each other and are indistinguishable from clinopyroxenes of BM lherzolites, indicating their derivation from source regions isotopically similar to depleted mantle and significant isotopic equilibration of these elements (Voshage et al., 1988; Mukasa and Shervais, 1999). Although clinopyroxene from 'evolved' clinopyroxenites (the Al augite group) have slightly higher REE, Sr, Zr, Y concentrations than those from websterites, concentrations in clinopyroxenes are LREE-depleted and overlap with REE patterns of clinopyroxenes from host lherzolites (Rivalenti et al., 1995; Mukasa and Shervais, 1999). The changes in trace element and isotopic compositions of dikes from the Cr diopside series towards gabbros have been interpreted to reflect changes from predominantly ocean island basalt (OIB) like magma to MORB like magma compositions, in response to thinning of the lithosphere and upwelling of the asthenosphere and uplift of the Balmuccia subcontinental lithospheric mantle to crustal levels (Mukasa and Shervais, 1999).

3.4 Samples and petrology

In the literature, BM pyroxenites were subdivided into Cr-diopside suite and younger Al-augite suite on the basis of both chemical and cross-cutting relationships, however, it is clear that the Cr diopside group also has formed at different times and presumably at a range of conditions (Shervais, 1979; Shervais and Mukasa, 1991; Mukasa and Shervais, 1999). Overall, the two groups correspond to dark green websterites, sometimes associated with orthopyroxenites and clinopyroxenites, and gray colored spinel clinopyroxenites that often cut websterites (Supplementary Figure S3.1). Al-augite suite layers have a large range of Al_2O_3 contents of 6.0 to 14.0 wt.%, some close to websterite compositions (Table 3.1 and Figure 3.1). Samples from the same vein can display large compositional variations in major elements (e.g., sample BM11-28), making classifications on the basis of Al contents somewhat arbitrary. In this paper, the distinction of websterites and clinopyroxenites is based on petrography and their visual appearance in the outcrop, mostly consistent with Cr-diopside suite and Al-augite suite, respectively. Centimeter-wide lenses and dikes of Cr-diopside websterite and Cr-spinel layers in spinel-rich dunite were interpreted to be related to

melts that formed the replacive dunites (Mazzucchelli et al., 2009), with some of the websterites also crosscutting the dunite structures. Hence, although folded Cr diopside websterites within the dunites may be regarded as early, other websterites appear to have formed after the dunites.

Most pyroxenites in this study were drilled from vein centers with drill core diameter of 3.2 cm and length of about 10 cm. Samples BM11-28 A, B, C are from the same spinel clinopyroxenite with decreasing spinel abundances from A to C. BM11-07B is an orthopyroxenite dike crosscutting dunite with sharp contacts. Chromium diopside rich websterites BM11-12 and BM11-14 formed 40 to 50 centimeter wide layers and contain large pyroxene grains up to 5 cm in size, and occasionally phlogopite. They show gradual transitions, both across layering and along strike, from peridotites containing thin and rather diffuse pyroxene layers to websterites, sometimes with a few centimeter wide olivine rich transition zones. Other layers are of variable widths, showing sharp boundaries to the host rock and occur parallel or slightly discordant to peridotite foliations. Accessory sulfides can be identified in most hand specimen. The sulfides, which predominantly occur on grain boundaries, are mostly intergrown aggregates of pentlandite, pyrrhotite and chalcopyrite. Sample BM11-24B is from a spinel rich layer in dunite body (spinel > 70-80 % by volume with minor clinopyroxene and olivine). Detailed petrographic information is given in Supplementary Table S3.1. Drill core samples and some hand specimen were cut using a diamond-steel saw blade. Sample surfaces were abraded with silica emery paper and washed with purified water. Up to 50-150 g of sample pieces were crushed with a hammer. Pieces were wrapped in paper to ensure protection from contamination by the hammer. The small pieces were processed to fine powder (about 10-30 μm) using an agate disc mill.

3.5 Analytical methods

Bulk rocks of six websterites, eleven spinel clinopyroxenites and one spinel rich vein from dunite were analyzed for major elements, selected lithophile trace elements, the HSE, S, Se and Te concentrations and Os isotopes. Two duplicates were also analyzed. Bulk rock composition for major elements and lithophile trace elements were determined by X-ray fluorescence analysis at GFZ, Potsdam as in Fischer-Gödde et al. (2011). The HSE, S, Se and Te data (except Rh and Au by internal standardization) were obtained from 2.5 g sample aliquot by isotope dilution methods after digestion in a high-pressure asher (HPA-S). Details of the methods, sample digestion in the HPA-S, chromatographic separation, and measurement by ICP-MS or negative TIMS, have been described in detail elsewhere (Fischer-Gödde et

al. 2010, 2011, Wang et al. 2013, Wang and Becker, 2013, In press), so only a brief description of the methods is given in Supplement. The methods have been applied to chondrites, peridotites and geological reference materials (Wang and Becker, In press) with variable compositions such as ultramafic and mafic to felsic igneous rocks, and sediments at Freie Universität Berlin.

3.6 Results

Major elements of websterites and clinopyroxenites are similar to literature values (Figure 3.1 and Supplementary Table S3.2). With an exception of orthopyroxenite BM11-07B, major elements, Ni, Cr and V contents in websterites show limited variations (for instance 2.7-5.1 wt.% Al_2O_3). Clinopyroxenites also display limited variations in major element composition, except for large variations in Al_2O_3 contents (6.0-14.0 wt.%). Sample BM11-28A has much higher Al_2O_3 (14.0 wt.%) than another two samples from the same vein (BM11-28 B and C, 6.0 wt.%), consistent with lower abundances of spinel in the latter samples. No systematic differences in Ca, Fe and Mg contents of websterites and clinopyroxenites occur. The main differences of websterites and clinopyroxenites are in their Na_2O, Ti_2O, Al_2O_3 and Cr contents, and are caused by differences in clinopyroxene composition and in the modal abundance of spinel. Contents of Na_2O, TiO_2 and Al_2O_3 correlate with each other and negatively with MgO (Figure 3.1).

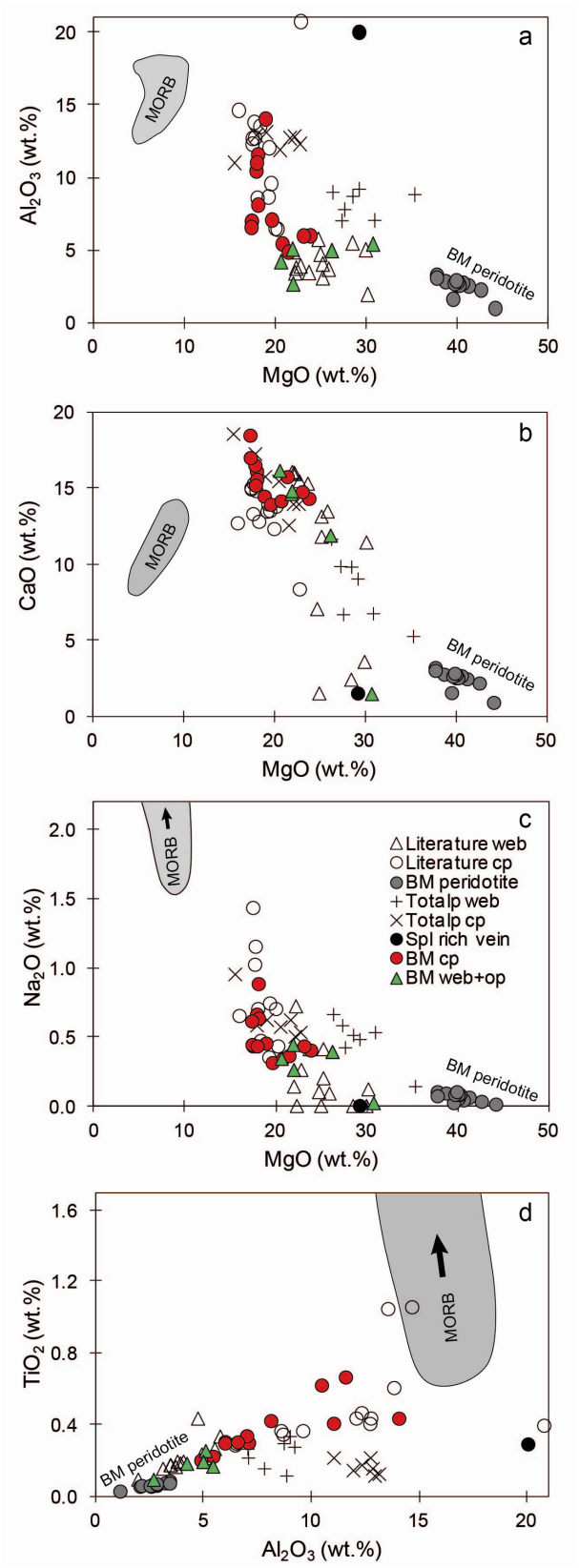

Figure 3.1 Major elements of pyroxenites in Balmuccia massif (a-d). Literature data of pyroxenites are in Balmuccia from (Rivalenti et al., 1995; Mukasa and Shervais, 1999) and in the Totalp massif from (van Acken et al., 2010b). Data for comparison are from Balmuccia peridotites (Wang et al., 2013) and MORB (Jenner and O'Neill, 2012). Web, websterites; op, orthopyroxenite; cp, clinopyroxenite; spl rich vein, spinel rich vein.

Whole rock S contents from XRF analysis, although systematically about 10-20 % lower than isotope dilution results, show a good linear correlation with our isotope dilution values, except for sample BM11-21 (Supplementary Table S3.2 and Figure S3.2). This correlation indicates that sulfides are distributed homogeneously in pyroxenite powders of this study. This is also reflected by reproducible S of duplicates of BM11-14 and BM11-26. Duplicates of BM11-14 have very reproducible contents of the HSE and chalcogens except Os and Re, whereas BM11-26 has poor reproducibility for most elements with low abundances, except high abundance S and Re. This reflects variable heterogeneity of chalcophile elements in samples, particularly at low abundances (Meisel and Moser, 2004a; Wang and Becker, In press).

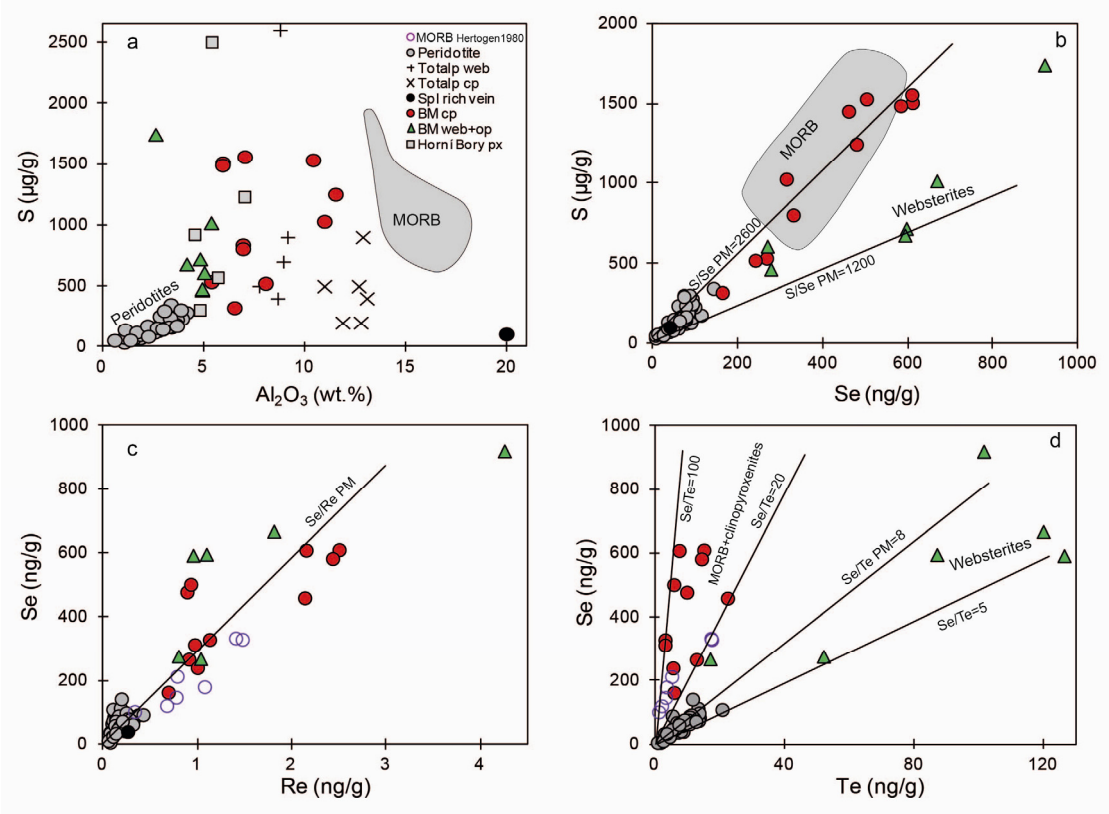

Figure 3.2 Correlations of Al_2O_3, Re, S, Se and Te. a) Broad correlation of S and Al_2O_3 for peridotites, pyroxenites and MORB. b) High abundances of S and Se in websterites and clinopyroxenites relative to peridotites. Ratios of S/Se in clinopyroxenites overlap with the value of the primitive mantle (PM), but are slightly higher than in S/Se in websterites. c) Se and Re also show broad positive correlations for peridotites, pyroxenites and MORB. d) Websterites and peridotites have Se/Te ratio close to the PM value, but clinopyroxenites and MORB have significantly higher Se/Te, presumably related to sulfide segregation (Hertogen et al., 1980; Yi et al., 2000). Literature data for peridotites are from (Lorand and Alard, 2010; König et al., 2012; Wang and Becker, 2013; Wang et al., 2013), MORB from (Hertogen et al., 1980; Jenner and O'Neill, 2012) and pyroxenites from Totalp (van Acken et al., 2010b) and Horní Bory (Ackerman et al., 2013). Web, websterites; op, orthopyroxenite; cp, clinopyroxenite; spl rich vein, spinel rich vein; px, pyroxenite.

In websterites and clinopyroxenites, S contents vary from 323 μg/g to 1745 μg/g and extend the correlation with Al_2O_3 of peridotites to higher concentrations, albeit with considerably scatter (Table 3.1, Figure 3.2). Websterites and clinopyroxenites have similar ranges of S, Se and Re abundances, which are commonly higher than in peridotites. Tellurium contents of websterites (16.8 to 126 ng/g) are significantly higher than in peridotites and MORB and correlate positively with Se (Figure 3.2). In contrast, clinopyroxenites have lower Te contents, mostly below 20 ng/g, with Se/Te ratios much higher than in lherzolites, but similar to ratios in MORB (Figures 3.2 and 3.3). S/Re and Se/Re ratios are relatively constant in peridotites, pyroxenites and MORB. S/Se and Se/Te ratios of websterites are systematically low, compared to BM clinopyroxenites, which display ratios similar to those of MORB (Figures 3.2 and 3.4).

Compared to the chalcogens and Re, websterites and clinopyroxenites display large variations of abundances of other HSE, up to several orders of magnitude (Figure 3.3). Overall, websterites have higher HSE contents and display less fractionation of Pt, Pd and Au (incompatible HSE, because these elements tend to be depleted in depleted peridotites) relative to Os, Ir and Ru (compatible HSE) than clinopyroxenites. Remarkably, Pt, Pd, Te and Au contents in websterites are higher than in peridotites and MORB. Clinopyroxenites mimic MORB patterns for the HSE and chalcogens, with similar concentration variations and fractionations (Figure 3.3). A spinel rich vein from dunite BM11-24B has an HSE and chalcogen pattern similar to the dunites (Wang et al., 2013), showing high Os, Ir and Ru contents but low abundances of other HSE and chalcogens (Figure 3.3).

$^{187}Re/^{188}Os$ and $^{187}Os/^{188}Os$ of websterites and clinopyroxenites display large variations, notably also in the three subsamples from the same vein BM11-28A, B, C (Table 3.1). Eight out of eleven clinopyroxenites define a Re-Os errorchron age of 141 Ma with initial $^{187}Os/^{188}Os$ of 0.142±0.047 (2σ, Supplementary Figure S3.3), and consistent with Mesozoic Re-Os model ages. Two clinopyroxenites (BM11-23 and BM11-29) and websterites (BM11-25 and BM11-19) have high initial $^{187}Os/^{188}Os$ at 280 Ma (γOs from +255 to +854). In contrast, the phlogopite-bearing websterites BM11-12 and BM11-14 have low γOs at 280 Ma of -6.4 to +8.5. Initial $^{187}Os/^{188}Os$ of other clinopyroxenites at 140 Ma are highly variable because of their high Re/Os and the effect of age correction, and if calculated at 280 Ma, would be too low with strongly negative γOs. Initial $^{187}Os/^{188}Os$ of websterites at 140 Ma or 280 Ma are also variable but most are slightly suprachondritic at 280Ma. The spinel vein from the dunite with 8.8 ng/g Os and subchondritic Re/Os has a γOs at 280 Ma of +6.2.

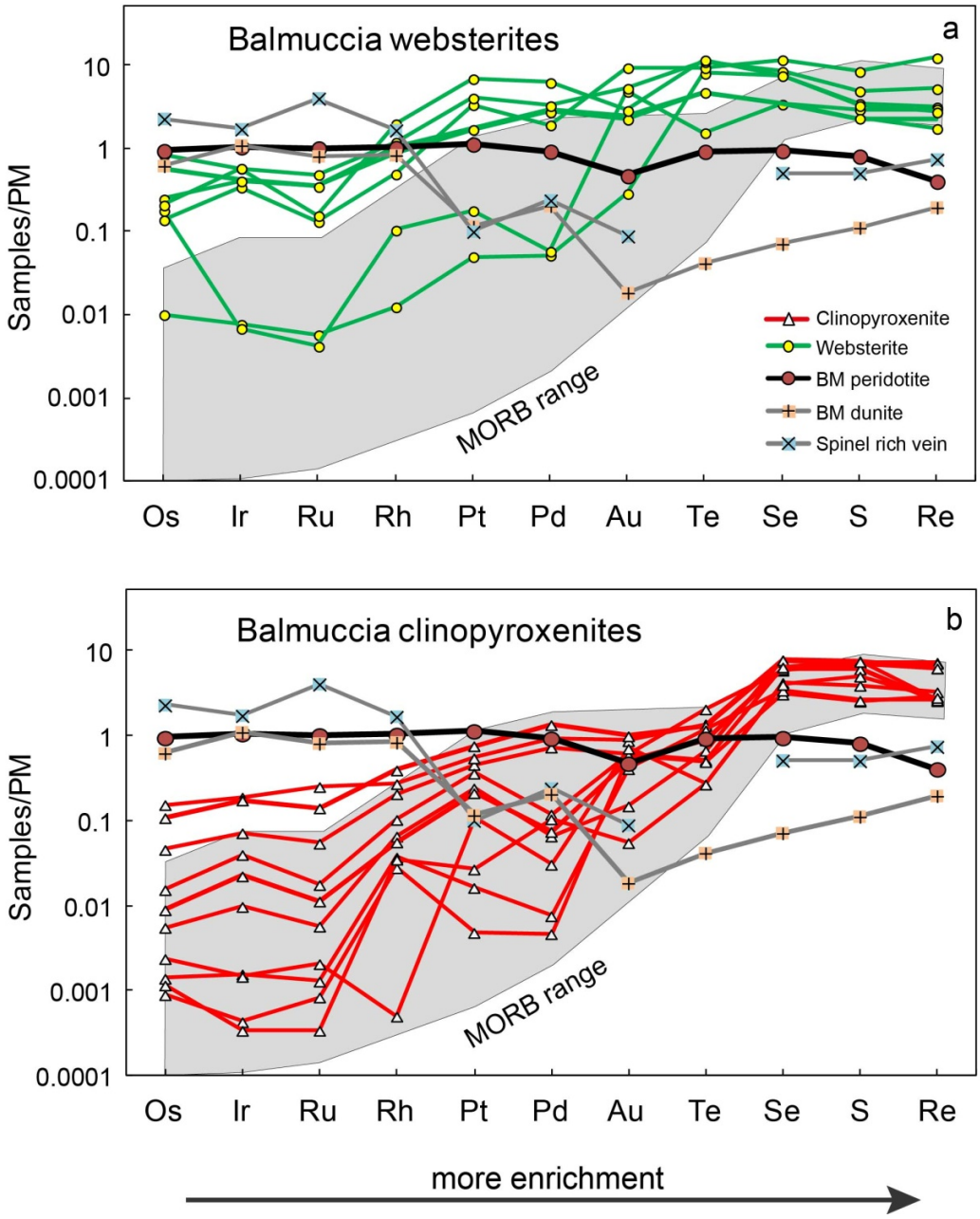

Figure 3.3 Primitive mantle normalized HSE and chalcogens patterns for BM websterites (a) and clinopyroxenites (b). Websterites and clinopyroxenites show similar Re, S and Se contents but large variations for other HSE and Te. Most websterites have higher abundances of Pt, Pd, Au and Te than in both peridotites and the MORB. The element sequence follows enrichment trend in pyroxenites. Shown for comparison are BM lherzolite (BM11-18) , dunite BM11-03A (Wang et al., 2013) and a spinel rich vein (BM11-24B) in BM dunite and MORBs (Hertogen et al., 1980; Rehkämper et al., 1999b; Yi et al., 2000; Bézos et al., 2005; Gannoun et al., 2007; Dale et al., 2008; Jenner and O'Neill, 2012). PM values are from (Becker et al., 2006; Fischer-Gödde et al., 2011; Wang and Becker, 2013).

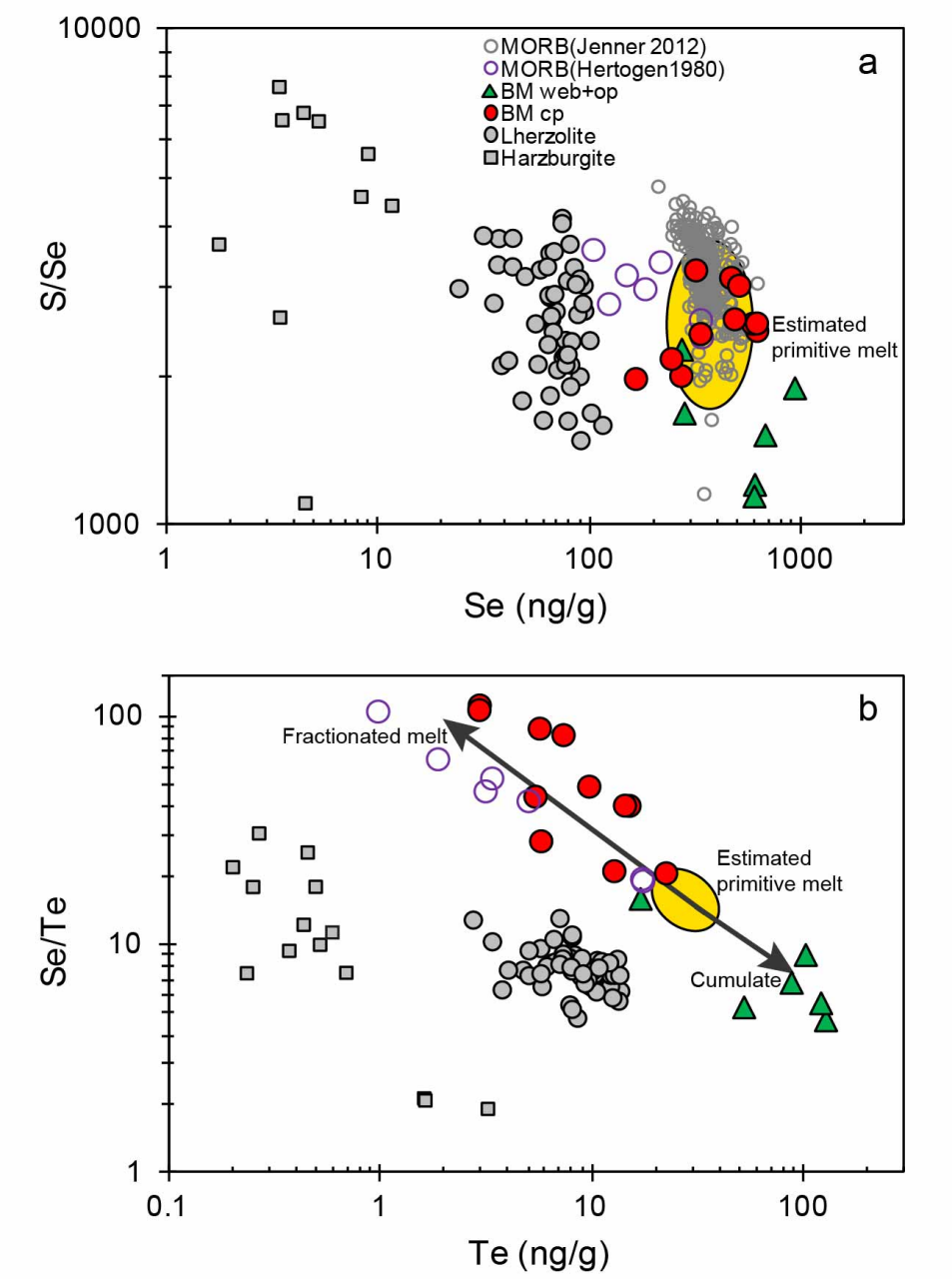

Figure 3.4 Fractionation of S, Se and Te in pyroxenites, suggesting relative sulfide-silicate partition coefficients of $D_S \leq D_{Se} < D_{Te}$ (apparent $D_{Te}/D_{Se} \approx 5 \pm 1.4$, 2σ, see Supplementary Figure S3.5) during segregation of sulfides from parent melts (Jenner et al., 2012; Wang and Becker, 2013; Patten et al., In press). a) Overall, websterites have slightly lower S/Se ratios than clinopyroxenites and MORB. b) Most websterites display Se/Te ratios significantly lower than clinopyroxenites and MORB (Hertogen et al., 1980; Jenner and O'Neill, 2012). Estimated compositions of primitive melt are assumed with 600-1000 μg/g S, 300-600 ng/g Se and 20-30 ng/g Te based on empirical partial melting of mantle peridotites and MORB (Jenner and O'Neill, 2012; Wang and Becker, 2013). Web, websterites; op, orthopyroxenite; cp, clinopyroxenite.

3.7 Discussion

3.7.1 The likely intrusion age of clinopyroxenite veins

Clinopyroxenites often crosscut websterites and their boundaries to host peridotites are sharp, implying that intrusion of these dikes into peridotites occurred relatively late. Re-Os errorchron age of most clinopyroxenites indicate a formation age of about 140 Ma, which is consistent with their model ages (Table 3.1, Supplementary Figure S3.3). No such young magmatic activity in the area has been reported. The main intrusion of the Mafic Complex Formation that host Balmuccia lherzolite may have occurred at 288±4 Ma (Peressini et al., 2007) and subsequent cooling lasted to 210 Ma, but it is much older that Re-Os errorchron age of clinopyroxenites. Sm-Nd errorchron ages of 270 Ma to 600 Ma for pyroxenites yielded no age significance (Voshage et al., 1990; Obermiller, 1994). Some early websterite dikes may have formed in the spinel lherzolite facies during magmatism related to late Paleozoic intrusion of the Mafic Complex, which is supported by the Re-Os systematics of a minority of the websterites (Voshage et al., 1988; Mukasa and Shervais, 1999).

Initial γOs of most clinopyroxenites calculated at 280 Ma yield very negative values (Table 3.1), which are considered to be unrealistic. This would imply too high Re relative to Os. High S contents and good correlations of S, Se and Re in clinopyroxenite veins suggest no later addition of Re by remelting or alteration after their formation. Ultraslow opening of the Ligurian Tethys ocean occurred during the Jurassic and lithosphere extension and thinning caused partial melting of the asthenosphere, and production of MORB type melts that have intruded overlying lithospheric peridotites (Müntener et al., 2004; Piccardo, 2008; Handy et al., 2010). The Re-Os data suggest that the Balmuccia lherzolite may have been affected by intrusion of such melts, which produced the clinopyroxenite cumulates with LREE depletion and Sr-Nd-Pb isotopic compositions similar to MORB (Mukasa and Shervais, 1999). The formation of BM clinopyroxenites during the opening of Liguria ocean is consistent with the widespread occurrence of pyroxenite and gabbro dikes that predominantly intruded at 165-160 Ma in nearby other peridotite massifs and ophiolites of northern Italy (e.g., Müntener et al., 2004; Tribuzio et al., 2004; Kaczmarek et al., 2008; Rampone and Borghini, 2008; van Acken et al., 2010b; Rampone and Hofmann, 2012).

3.7.2 HSE and chalcogen element partitioning in mantle processes

Major element compositions (Figure 3.1), sharp contacts with host rocks and modal variations such as the gradual decrease in spinel abundances within clinopyroxenite layers indicate that these rocks are cumulates. Websterite bands BM11-12 and BM11-14 display gradual contacts with peridotites. Their composition and the presence of megacrystic pyroxenes also reflect predominant crystal accumulation. Websterites and clinopyroxenites have similar ranges of S, Se and Re abundances and overlap with compositions of MORBs. This indicates precipitation of sulfide from S saturated melts (Mavrogenes and O'Neill, 1999) during transport in the upper mantle. Heterogeneous sulfide distribution in the cumulates is indicated by hand specimen and variable bulk rock S contents in different layers (Figure 3.2 and Supplementary Figure S3.1).

Websterites and spinel clinopyroxenites formed from S saturated parent melts with systematically different abundances and fractionation of chalcophile elements. Significantly, higher abundances of most HSE and Te but less fractionated HSE and chalcogens in websterites contrast with lower abundances but more strongly fractionated HSE and chalcogens in clinopyroxenites (Figure 3.3). Because of high abundances of Se and Te, S/Se and Se/Te ratios of websterites are systematically low, similar to values of lherzolites or even lower (in case of Se/Te). Because of low Te (and PGE) concentrations, the composition of clinopyroxenites (high S/Se and Se/Te) is similar to compositions of MORBs and complementary to the websterites (Figure 3.4). In contrast, S/Re of both websterites and clinopyroxenites are similar to lherzolites. Clinopyroxenites are depleted in Pt, Pt, Te and Au relative to websterites, but display stronger fractionation of Pd/Ir, Re/Os and Se/Te (Figures 3.3-3.5). This observation requires that these elements had been depleted in parent melts by previous sulfide segregation in the mantle.

The behavior of the chalcogens and the HSE in the different types of pyroxenites is consistent with expected trends for cumulates that precipitated from primitive magmas (the websterites) and cumulates that formed from magmas that already have precipitated sulfides (the clinopyroxenites). Parent melts of clinopyroxenites underwent sulfide removal that depleted the PGE and Te, however, abundances of Re, S and Se are similar to websterites, suggesting negligible effects of early sulfide fractionation on these elements. This can be easily explained with moderately high and similar sulfide-silicate partition coefficients of Re, S and Se on the order of 300-1000 and relative sulfide-silicate partition coefficients of $D_{Re} \approx D_S \leq D_{Se} < D_{Te}$, consistent with data on peridotites (Wang and Becker, 2013; Wang et al., 2013), MORBs (Hertogen et al., 1980; Peach et al., 1990; Yi et al., 2000; Gannoun et

al., 2007; Jenner et al., 2012; Patten et al., In press) and experiments (Choi and Cho, 1997; Brenan and McDonogh, 2006; Fonseca et al., 2007; Brenan, 2008). Negligible fractionation of Re relative to S or Se in both early websterites and late clinopyroxenites (Figure 3.2) does not support dominant control of Re by silicate melts rather than sulfide phases. Otherwise, clinopyroxenites which formed from more evolved melts would display higher Re contents than given S contents compared to in websterites when both of their parent melts were S saturated. Depletion of Te relative to Se and Se slightly relative to S in both clinopyroxenites and MORB are mirrored by elevated Te/Se and Se/S in websterites and match sulfide-silicate partition coefficients of Te > Se ≥ S with $D_{Te}/D_{Se} \approx 5 \pm 1.4$ (2σ) in the mantle (Figure 3.4 and Supplementary Figure S3.4). Recent data on MORB glass and sulfide droplets indicate D_{Te}/D_{Se} slightly higher (about 5-20) during shallow oceanic crust evolution (Patten et al., In press).

Fractionation of the HSE and chalcogens in cumulate pyroxenites also indicates, during melt evolution dominant control by sulfide-silicate partitioning rather than monosulfide solid solution (MSS)-sulfide melt partitioning. If the latter process would be significant, remaining sulfide melts in clinopyroxenites would become significantly enriched in Au, Te, Pd and Pt contents relative to S, Se and Re, because of relative $D^{MSS\text{-}sulfide\ melt}$ of Ir (0.9-10) ≈ Os (1.9-6.7) ≥ Re (1.8-3.9) > S (1.2) > Se (0.65) > Pd ≈ Pt (0.01-0.16) ≥ Te (0.02) > Au (<0.01) (Bockrath et al., 2004; Ballhaus et al., 2006; Helmy et al., 2010; Li and Audétat, 2013). MSS-sulfide melt fractionation also would lead to Pd/Ir ratios significantly larger than Re/Os in melt products (Ballhaus et al., 2006), which is opposite to natural fractionation (Figures 3.5 and 3.6). During melt evolution, Pd and Ir contents in pyroxenites, MORBs and Oman gabbros have variations up to 4 or 5 orders of magnitude, but minor fractionation occurs for Pd and Ir, e.g., apparent bulk $D_{Pd}/D_{Ir} \approx 0.95 \pm 0.11$ (2σ, Figures 3.5 and 3.6 and Supplementary Figure S3.6). Rhenium contents from these melt products are rather constant and contrast Os that has similar relative MSS-sulfide melt partition coefficients with Re but concentration variations up to 4 or 5 orders of magnitude. Sulfide-silicate partitioning is also consistent with fractional crystallization of MORB where precipitated sulfides are immiscible droplets (Patten et al., In press) and experimental results (Li and Audetat, 2012). Subsequent exsolution of sulfide droplets with cooling will lead to further fractionation within immiscible sulfide melts where MSS-sulfide melt fractionation becomes important (Piña et al., 2012; Patten et al., In press).

3.7.3 Incomplete equilibration of sulfide melts during magma transport

However, the variably depleted abundances of the HSE such as Pt and Pd in mantle peridotites, the enrichment of these elements in websterite and depletion in clinopyroxenites cannot be explained by equilibrium sulfide-silicate partitioning if the extremely high partition coefficients of up to 10^4 to 10^6 for these elements are correct (Peach et al., 1994; Fleet et al., 1999; Fonseca et al., 2009; Mungall and Brenan, In press). Parent melts of the BM clinopyroxenites and MORB have undergone sulfide segregation and thus, if sulfide-silicate partition coefficients of 10^4 to 10^6 and equilibrium partitioning are applicable, theses rocks should have much lower Pt, Pd and Te contents than websterites. The abundance difference for Pt, Pd, Au and Te between the clinopyroxenites and websterites is between only about one and three orders of magnitude (Table 3.1 and Figure 3.3).

The concentration data for the pyroxenites reveals incomplete equilibration of sulfide melts with silicate melts. One possible explanation for apparent lower partition coefficients in natural melt products relative to experimental results is 'R factor', the mass ratio of silicate melts to equilibrated sulfide melts (Campbell and Naldrett, 1979; Campbell and Barnes, 1984; Mungall, 2002; Mungall and Brenan, In press). When R is smaller than experimental partition coefficient $D_i^{\text{sulfide-silicate}}$, the HSE concentration in sulfide melts depends on R rather than $D_i^{\text{sulfide-silicate}}$. Different $D_i^{\text{sulfide-silicate}}$ values of the HSE, Te, Se and S (from $>10^4$ to hundreds) lead to their kinetic fractionation in the sulfide liquid and different apparent enrichment.

The more plausible way is by compositional changes of melts during transport in the mantle. Reaction with peridotite and changes in P and T can lead to changes in sulfide solubility (Mavrogenes and O'Neill, 1999; Li, 2005). Kinetically controlled dissolution of peridotite sulfides in migrating melts, as has occurred in the replacive dunites of the Balmuccia massif (Wang et al., 2013), will re-enrich PGE and Te in melts that had low abundances due to previous sulfide segregation. Spinel rich vein in dunites, though with 8.8 ng/g Os contents, has slightly suprachondritic $\gamma Os_{(280Ma)}$ of +6.2 and recorded fractionated Re/Os feature of percolating melts.

Websterites mostly have lower concentrations of compatible HSE such as Os, Ir, and Ru, but higher Pt, Pd, Au and Te than host peridotites, similar to websterites from other locales (van Acken et al., 2010b). In the study of van Acken et al (2010b), reaction zones of peridotites and websterites and radiogenic initial Os isotopes were modeled by mixing of host peridotite with partial melts of subducted oceanic crust to explain the HSE composition of websterites. Such simple mixing cannot explain websterites that have similar or higher concentrations of Pt, Pd, Au, and particularly

Te than both peridotites and MORB (Figures 3.2 and 3.3). Rather, early accumulation of websterites sequesters most highly chalcophile elements in early precipitating sulfides. Another process that may enhance HSE and chalcogen concentrations could be mixing of entrained sulfides in extracted melts from the host rocks (e.g., Ballhaus et al., 2006 and discussion in the next section). The latter process is indicated by the presence of sulfides with peridotite- and melt-like HSE ratios in pyroxenites (van Acken et al., 2010b; Gawronski et al., 2013).

The subparallel patterns of the HSE and chalcogens in the clinopyroxenites and the large abundance variations convey another important message. These compositions suggest a wide spectrum of HSE and chalcogen abundances in primitive mantle magmas, and, for reasons discussed in the previous paragraph, these compositions cannot be in equilibrium with mantle peridotites. Variations in initial γOs in different clinopyroxenite layers support this view (Table 3.1). We speculate that during transient reaction processes, mostly Pt-Pd-Re enriched grain boundary sulfides may be dissolved in the melts. Crystal accumulation may occur during or after melt infiltration into peridotite and subsequent extraction of reacted melt. In summary, HSE and chalcogen abundances of the pyroxenite layers reflect previous sulfide fractionation of the parent melts, but also subsequent reaction with peridotite and sulfide dissolution, however, without complete chemical equilibration.

3.7.4 Common origin of grain boundary sulfides in websterites and peridotites

It has been shown that during refertilization of depleted peridotites, infiltrating melts lead to precipitation of interstitial sulfides with spinel and pyroxene or olivine (Le Roux et al., 2007; Lorand and Alard, 2010; Van Den Bleeken et al., 2010), indicating infiltrating melts were S saturated. Because S, Se, Te and HSE are predominantly hosted in sulfides in pyroxenites and fertile peridotites, we use whole rock S contents to convert whole rock data to contents of HSE, Se and Te in sulfides assuming all these elements are hosted in sulfides (Figure 3.5 and Supplementary Figure S3.6).

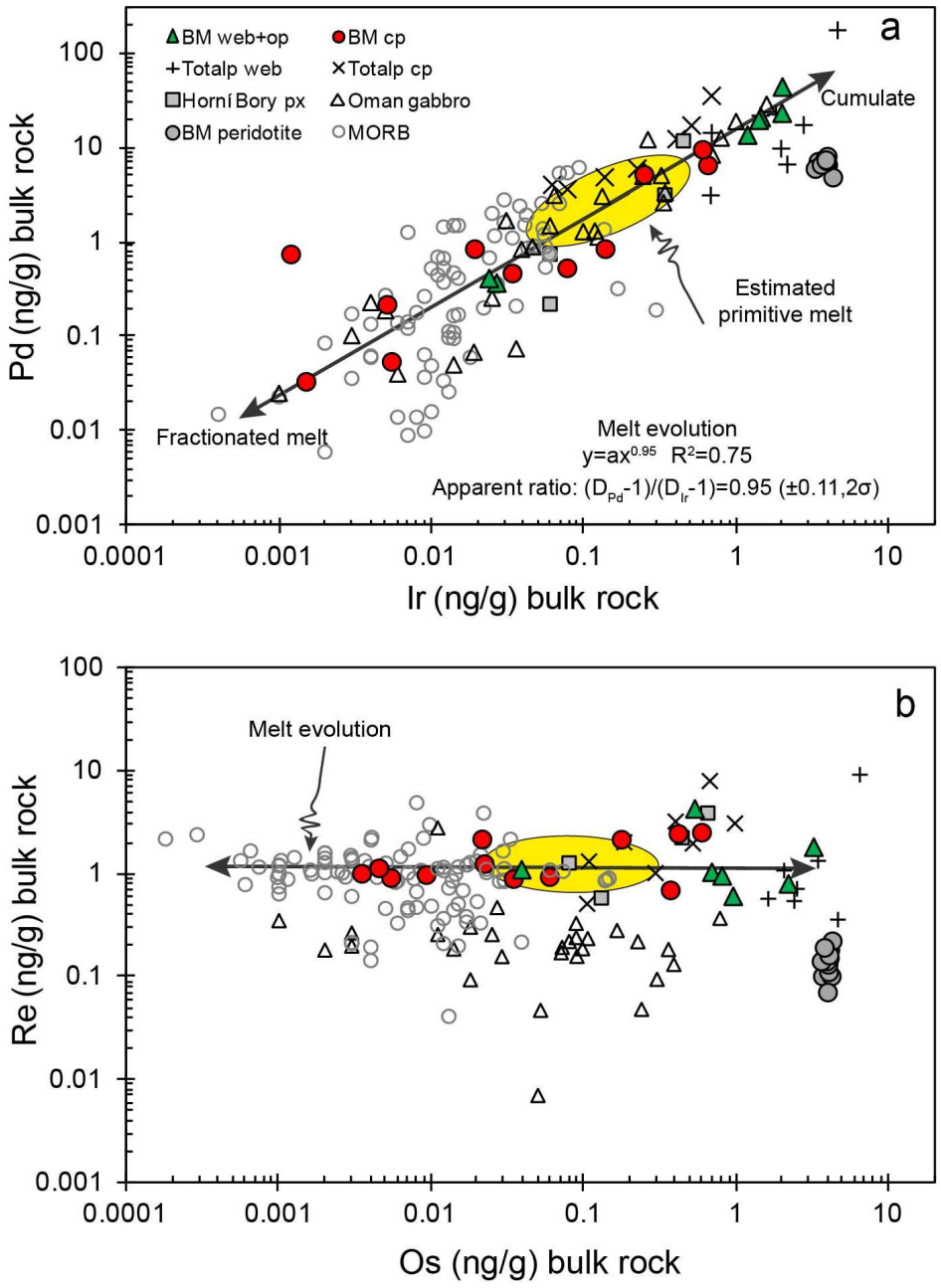

Figure 3.5 Comparison of bulk rock abundances of Pd, Ir, Re and Os in pyroxenites, peridotites, Oman lower crustal gabbros and MORB (including upper oceanic crust). a) Palladium and Ir contents in most websterites are several orders of magnitude higher than in clinopyroxenites which are similar to MORB, but minor fractionation of Pd and Ir occurs during melt evolution, as indicated by apparent bulk partitioning $D_{Pd}/D_{Ir} \approx 0.95 \pm 0.11$ (2σ) that is derived from pyroxenites, Oman gabbros and MORB. b) Rhenium contents have limited variations compared to Os, Ir and Pd contents. Data for comparison are from BM peridotites (Wang et al., 2013), pyroxenites from Horní Bory (Ackerman et al., 2013) and Totalp (van Acken et al., 2010b), Oman gabbro (Peucker-Ehrenbrink et al., 2012) and MORB (Rehkämper et al., 1999b; Peucker-Ehrenbrink et al., 2003; Bézos et al., 2005; Gannoun et al., 2007; Dale et al., 2008). Web, websterites; op, orthopyroxenite; cp, clinopyroxenite; px, pyroxenite.

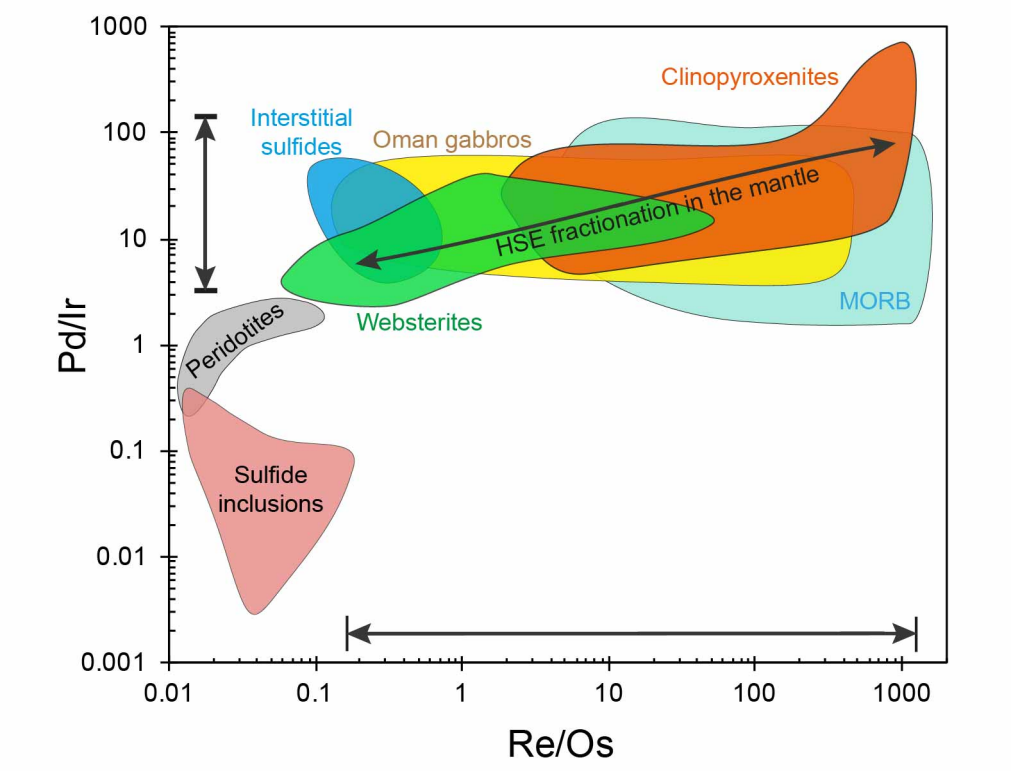

Figure 3.6 Strong fractionation of Re/Os relative to Pd/Ir during melt evolution in the mantle. Pd/Ir ratios that have minor variation (e.g., in single section of Oman gabbros) overlap for interstitial sulfides, websterites and Oman gabbros but differ from sulfide inclusions, indicating common origins of sulfide melts and preferential removal of interstitial sulfides during partial melting. Large variations of Re/Os in pyroxenites indicate that if long-lived and remelted, pyroxenites have potential to produce heterogeneous Os isotopes in melts. Data sources are same as for Figure 3.5, except sulfide inclusion and interstitial sulfides (Alard et al., 2005).

We note that concentrations and ratios of the HSE and Os isotopes of calculated sulfides in websterites and are similar to secondary/metasomatic interstitial sulfides of peridotites and different from unequilibrated sulfide inclusions enclosed in peridotite minerals (e.g., Alard et al., 2000, 2002, 2005; Luguet et al., 2004; Harvey et al., 2011) (Figure 3.6 and Supplementary Figure S3.6). For instance, Re/Os and Pd/Ir ratios and Se contents of the websterites are very similar to metasomatic interstitial sulfides in peridotites from the Kane fracture zone and External Ligurian peridotites (Luguet et al., 2004; Alard et al., 2005). Suprachondritic Os isotopic compositions of interstitial sulfides from peridotites are also consistent with values for the websterites (Alard et al., 2005; Harvey et al., 2010, 2011) and suggest that those sulfides were precipitated from similar melts with high Re/Os. Associations of websterite layers with fertile peridotites, such as in Balmuccia (this work, Rivalenti et al., 1995; Mazzuchelli et al., 2009; Wang et al., 2013), Beni Bousera (Pearson and Nowell, 2004; Gysi et al., 2011), Ronda (Garrido and Bodinier, 1999; Bodinier et al., 2008), Lherz (Le Roux et al., 2007) and Totalp (van Acken et al., 2008) indicate strong links between websterite formation in lherzolites and refertilization. Sr-Nd-Pb isotopic

compositions of clinopyroxenes from BM websterites are indistinguishable from peridotites, indicating that in contrast to the HSE and chalcogens, lithophile elements were equilibrated during the reactive infiltration of silicate melts (Mukasa and Shervais, 1999).

In this scenario, melts for refertilization and pyroxenite formation probably have instinct relationship. Refertilization as porous melt flow is a process of migration and redistribution of partial melts with sulfide droplets from upwelling asthenosphere to overlying lithospheric mantle in an open system via dissolution and re-precipitation reaction or melt stagnation (Le Roux et al., 2007; Müntener et al., 2010; Van Den Bleeken et al., 2010). Most intergranular Fe-Ni-Cu sulfides precipitated from infiltrating melts, which have evolved to dominant pentlandite and chalcopyrite with minor pyrrhotite during cooling, are enriched in incompatible HSE and chalcogen and can supplement previous Os-Ir-Ru alloy in depleted peridotites (e.g., Alard et al., 2000, 2005; Luguet et al., 2003, 2004; Lorand et al., 2008a, 2010; Wang et al., 2009; Lorand and Alard, 2010), making no noticeable differences but variably scattered HSE and chalcogen contents in affected peridotites (Lorand and Alard, 2010; Fischer-Gödde et al., 2011; Wang and Becker, 2013; Wang et al., 2013). The net effects are rejuvenation of refractory and ancient mantle by newly formed melts. Websterites that are associated with fertile peridotites are interpreted as cumulates of melts that have undergone reaction with peridotites and incorporated grain boundary sulfides. These melts should most closely resemble 'primitive' melts, with least fractionated HSE and chalcogen element compositions. Melts that have evolved from primitive melts by fractional crystallization and minor reaction with peridotite may form clinopyroxenites and lower crustal olivine gabbro, displaying MORB-like HSE and chalcogen compositions (Figure 3.3). Because websterites and clinopyroxenites in peridotites occur at conditions ranging from the spinel to garnet lherzolite facies (this work, Suen and Frey, 1987; Becker, 1996; Becker et al., 2001a, 2004; Pearson and Nowell; 2004; van Acken et al., 2010b), it appears that substantial fractionation and modification of the HSE and chalcogens occurs during melt transport in the mantle.

3.7.5 Melting of mixed pyroxenite-peridotite sources and the origin of Os isotopic variations in basalts and the mantle

Sulfides in websterites and clinopyroxenites have S, Se and Re compositions similar to interstitial sulfides in peridotites, hence, melting of pyroxenite-veined or unveined peridotites make no noticeable differences in these elements during open system melting. However, other HSE and Te abundances in websterites and clinopyroxenites display variations of up to several orders of magnitude and can produce compositional diversity of hybrid partial melts generated from mixed

pyroxenite-peridotite sources. In particular, clinopyroxenite layers in a matrix of peridotite are likely to produce MORB like melts after high degree melting.

Partial melting of recycled mafic oceanic crust and sediments in the mantle have been proposed to explain suprachondritic initial $^{187}Os/^{188}Os$ of mantle pyroxenites (Becker et al., 2001a; Pearson and Nowell, 2004; van Acken et al., 2010b) and some ocean island basalts (Reisberg et al., 1991; Lassiter and Hauri, 1998; Becker, 2000). The data in Figure 3.6 shows that igneous fractionation during magma transport in the mantle also produces strong fractionation of Re and Os, as indicated by the large range of compositions of mantle pyroxenites and interstitial sulfides in peridotites (e.g., Harvey et al., 2011). If long-lived, e.g., as part of the lithosphere or the convecting mantle, such heterogeneities may produce suprachondritic Os isotopic ratios.

Some plume-derived magmas from Hawaii, Gorgona Island and Norilsk display coupled suprachondritic $^{186}Os/^{188}Os$ and $^{187}Os/^{188}Os$ (Brandon et al., 1998, 1999, 2003). Such enrichments require mantle sources with moderately high Re/Os and Pt/Os, and high Pt/Re ratios of at least 88 to 100. Contribution of a small amount of outer core materials has been proposed as a viable, but controversial, model (Brandon et al., 1998, 1999). Luguet et al. (2008) have proposed that melting of recycled mantle pyroxenites may be an alternative explanation, because sulfides from pyroxenites of the Beni Bousera peridotite massif have the proper Pt/Re ratios to explain the coupled enrichment of ^{186}Os and ^{187}Os in these plume-derived magmas. However, bulk rock analyses of pyroxenites have not supported this model. Most pyroxenite layers in the Totalp ultramafic massif (van Acken et al., 2010b), Horní Bory, Bohemian Massif (Ackerman et al., 2013) and Hawaiian pyroxenite xenoliths (Sen et al., 2011) do not possess the required Re/Os, Pt/Os and Pt/Re. Highly differentiated clinopyroxenites from Balmuccia show high Re/Os of 1.9 to 285 and Pt/Os of 2.1 to 87 due to low Os contents, and will produce highly suprachondritic ^{186}Os and ^{187}Os isotopes after long-term isolation time, but the low Pt/Re (< 3) will produce a range of $^{186}Os/^{188}Os$ and $^{187}Os/^{188}Os$ that are inconsistent with data from the plume magmas. Some websterites have much higher Pt/Re of 0.35-54, but still less than required range of 88 to 100. Therefore, remelting of different types of pyroxenites such as websterites and clinopyroxenites which display a range of suprachondritic Re/Os and Pt/Os would produce variable and suprachondritic $^{186}Os/^{188}Os$ and $^{187}Os/^{188}Os$ for the heterogeneity of Os isotopes in ocean island basalts, but not the specific coupling of suprachondritic ^{186}Os-^{187}Os in the picrites from Hawaii and Norilsk, and the Gorgona komatiites. We note the compositions and ratios of the HSE in lower crustal olivine gabbros from Oman (Peucker-Ehrenbrink et al., 2012) cover those of websterites and clinopyroxenites in the mantle and MORBs

(Figures 3.5 and 3.6). Such feature indicates that the former may have formed from magmas that have undergone sulfide segregation in the mantle or in the lower oceanic crust. Their moderately suprachondritic initial $^{187}Os/^{188}Os$ of 0.146 may indicate that the parent melts formed in mantle that contained a minor proportion of material with high Re/Os. Melting veined or unveined peridotites via preferential removal of interstitial sulfides and modification of such magmas by reaction with peridotite during transport can explain these and other slightly radiogenic Os isotopic compositions of sulfides in some abyssal peridotites and in MORBs (Alard et al., 2005; Gannoun et al., 2007; Harvey et al., 2011).

3.8 Conclusions

Early websterites ('Cr-diopside suite') and later spinel clinopyroxenites ('Al-augite suite') of the Balmuccia peridotite massif were formed as cumulates during multi-stage late Paleozoic and Mesozoic melt influx into continental lithospheric mantle of the Ivrea-Verbano Zone (Italian Alps). Magmatism is related to continental extension and evolution of a passive continental margin evolution of the Ligurian Tethys realm. Re-Os model ages and Sm-Nd errorchron ages of peridotites and websterites are consistent with late Paleozoic magmatic equilibration of these systems (Shervais and Mukasa, 1991; Obermiller, 1994; Mazzucchelli et al., 2009; Wang et al., 2013), whereas the clinopyroxenites yield evidence from Re-Os data for Jurassic formation ages (this work). Sr-Nd-Pb isotopic compositions and trace elements suggest that the parent melts of the pyroxenites originated from upwelling asthenospheric melts (Rivalenti et al., 1995; Mukasa and Shervais, 1999; Mazzucchelli et al., 2009). Websterites and clinopyroxenites display contrasting abundances and ratios of highly siderophile elements (HSE) and chalcogens (S, Se and Te) and initial $^{187}Os/^{188}Os$. Websterites have higher abundances and display less fractionation of HSE and chalcogens than clinopyroxenites. HSE and chalcogen compositions of the clinopyroxenites are comparable to MORB compositions. Parent melts of the clinopyroxenites must have undergone sulfide segregation, but also variable re-enrichment of PGE by reaction with peridotite and sulfide dissolution. Abundances of Pt, Pd, Au, Re, S, Se and Te in the pyroxenites and the behavior of ratios such as Re/Os, Pd/Ir, S/Se and Se/Te indicate that the magmatic fractionation of the HSE and chalcogens during fractional crystallization and magma evolution in the mantle is significant. Concentration variations and element ratios in different lithologies indicate that fractionation during formation of the pyroxenites is predominantly controlled by sulfide-silicate partitioning. The lower apparent sulfide-silicate partition coefficients obtained from the pyroxenite data compared to

experimental values likely reflects the fact that the pyroxenites are not really cogenetic, which is indicated by heterogeneous initial $^{187}Os/^{188}Os$ calculated at appropriate ages. Clinopyroxenites have low PGE and Te contents, suggesting loss of these elements by sulfide segregation from precursor melts. However, abundances of these elements are still too high, because sulfide-silicate partition coefficients of the PGE are 10^4 to 10^6 (Peach et al., 1994; Fleet et al., 1999; Fonseca et al., 2009; Mungall and Brenan, In press). We infer that parent melts of clinopyroxenites have undergone re-enrichment of PGE by dissolution of grain boundary sulfides during melt-peridotite reaction.

The HSE and chalcogen abundances and Os isotopic compositions of sulfides of websterites show similarities with interstitial sulfides in refertilized peridotites, suggesting that the sulfide assemblages in these rocks form by related reactive infiltration processes. We interpret websterites as precipitates of the most 'primitive' magmas, because their HSE and chalcogen abundances suggest so. However, in reality, they are products of hybrid melts that reflect substantial interaction of precursor melts with peridotite.

It is difficult to distinguish melting of pyroxenites or veined mantle from partial melting of homogeneous peridotite on the basis of major element compositions of basalts (Lambart et al., 2013), S, Se and Re. However, this distinction becomes viable on the basis of the PGE and Te abundances, and in particular Os isotopic compositions due to the different fractionation of these elements in pyroxenites. As the present study shows, the different styles of fractionation of the HSE and the chalcogens in different types of mantle pyroxenites provide constraints on melt compositions and the importance of sulfide segregation, reactive transport, mixing and disequilibrium during magma transport in the mantle.

Acknowledgments

We thank R. Naumann for XRF analyses of major and some trace elements, K. Hammerschmidt, M. Feth, T. Gawronski and S. Hohl for help and support in the TIMS, ICPMS and clean labs, and S. Hohl and C. Meyer for their assistance during sample collection in Italy. Many thanks go to T. Gawronski for discussions about pyroxenites. This work was supported by funds of Freie Universität Berlin and a China Scholarship Council fellowship to Z. Wang.

Table 3.1 Concentrations of the HSE, S, Se and Te, Os isotopes, selected major elements and ratios for Balmuccia websterites and clinopyroxenites.

Samples	Type	Al_2O_3	MgO	Cr	S	Se	Te	Re	Os	Ir	Ru	Rh	Pt	Pd	Au	Se/Te	Re/Os	Pd/Ir	Pt/Re	$^{187}Re/^{188}Os$	$^{187}Os/^{188}Os$	2SE	2SD	γ(Os)	γ(Os)	$T_{MA(PM)}$
		(%)	(%)	(μg/g)	(μg/g)	(ng/g	(ng/g	(ng/g)	(ng/g)	(ng/g)	(ng/g)	(ng/g)	(ng/g)	(ng/g	(ng/g)						measured			@140Ma	@280Ma	Ga
BM11-28A	Sp-cpx	14.0	18.8	577	1456	460	22.2	2.13	0.177	0.249	0.382	0.245	3.43	5.11	1.04	21	12	20	1.6	59.2	0.2662	0.0004	0.0012	1.7	-108	0.14
BM11-28B	Sp-cpx	6.0	23.7	957	1509	610	14.9	2.50	0.595	0.653	1.764	0.322	4.10	6.44	1.46	41	4.2	10	1.6	20.4	0.1724	0.0007	0.0014	-0.9	-38	0.13
BM11-28C	Sp-cpx	6.0	23.0	1100	1490	583	14.2	2.43	0.418	0.604	0.990	0.466	5.69	9.40	1.66	41	5.8	16	2.3	28.3	0.2051	0.0002	0.0005	10	-42	0.16
BM11-27	Sp-cpx	7.1	19.5	376	1559	609	7.27	2.15	0.022	0.034	0.041	0.078	1.82	0.46	0.250	84	100	14	0.84	563	1.440	0.004	0.03	1.5	-1052	0.14
BM11-15	Sp-cpx	11.6	18.0	609	1250	479	9.62	0.887	0.035	0.078	0.080	0.067	1.60	0.52	0.870	50	26	6.7	1.8	129	0.4718	0.0009	0.008	36	-204	0.16
BM11-16A	Sp-cpx	10.4	17.8	908	1532	502	5.62	0.926	0.060	0.139	0.125	0.122	2.71	0.84	1.03	89	15	6.0	2.9	76.8	0.3445	0.0009	0.004	31	-112	0.17
BM11-20	Sp-cpx	5.4	20.7	2040	537	268	12.6	0.906	0.005	0.005	0.009	0.044	0.12	0.05	0.683	21	166	10	0.14	1106	3.027	0.003	0.29	258	-1812	0.16
BM11-22	Sp-cpx	8.1	18.0	423	523	241	5.36	0.998	0.004	0.002	0.006	0.033	0.04	0.03	0.989	45	285	22	0.04	2391	5.803	0.004	1.1	85	-4396	0.14
BM11-26	Sp-cpx	7.0	17.3	480	836	—	6.20	1.24	0.022	0.002	0.004	0.006	0.47	—	0.004		55		0.38	306	1.225	0.002	0.03	307	-263	0.22
duplicate	Sp-cpx	—	—	—	805	330	2.93	1.13	0.005	0.001	0.002	0.042	0.20	0.74	0.093	113	248	613	0.18	4301	20.05	0.13	6.2	7856	-147	0.28
BM11-23	Sp-cpx	11.0	17.9	432	1028	314	2.91	0.966	0.009	0.005	0.015	0.001	0.81	0.22	1.19	108	104	42	0.83	825	5.052	0.003	0.35	2378	854	0.36
BM11-29	Sp-cpx	6.6	17.3	860	323	164	5.71	0.688	0.371	0.019	0.136	0.116	0.78	0.84	0.234	29	1.9	43	1.1	9.55	0.6485	0.0004	0.0009	397	383	3.3
BM11-25	Web	4.9	21.4	4890	722	596	86.8	1.09	0.039	0.027	0.041	0.015	0.38	0.37	0.484	6.9	28	14	0.35	153	1.158	0.001	0.01	536	255	0.40
BM11-19	Web	5.1	21.8	4982	611	270	16.8	1.03	0.692	0.024	0.030	0.124	1.35	0.41	8.15	16	1.5	17	1.3	7.67	0.6529	0.0007	0.0015	404	393	4.2
BM11-21	Web	2.7	21.9	5382	1745	921	101	4.25	0.535	1.19	0.930	0.586	25.2	13.5	15.7	9.1	7.9	11	5.9	38.7	0.2186	0.0001	0.0004	1.8	-70	0.14
BM11-12	Web	4.2	20.5	4993	680	593	126	0.952	0.809	2.01	1.10	2.35	51.7	43.5	4.81	4.7	1.2	22	54	5.68	0.1438	0.0002	0.0004	3.5	-6.4	0.16
BM11-14	Web	5.0	26.1	5425	468	278	51.8	0.797	2.20	1.46	2.51	1.26	12.9	20.6	4.13	5.4	0.4	14	16	1.75	0.1440	0.0001	0.0003	11	8.5	0.65
duplicate	Web	—	—	—	479	—	51.3	0.603	0.955	1.41	2.45	1.02	12.7	19.3	3.77		0.6	14	21	3.05	0.1441	0.0001	0.0003	8.6	3.7	0.33
BM11-07B	Op	5.4	30.6	4307	1017	668	120	1.81	3.22	2.00	3.42	1.41	30.4	22.9	8.87	5.6	0.6	11	17	2.71	0.1393	0.0001	0.0002	5.5	1.2	0.25
BM11-24B	Spinel	20.0	29.1	115800	105	40.5	—	0.259	8.80	5.94	28.2	1.98	0.76	1.69	0.150		0.03	0.3	2.9	0.142	0.1335	0.0001	0.0002	5.7	6.2	-0.82

Note: Sp-cpx, spinel clinopyroxenite; Web, websterite; Op, othopyroxenite; Spinel, spinel rich vein in dunite

Values of PM $^{187}Os/^{188}Os = 0.1296$ and $^{187}Re/^{188}Os = 0.434$ used for calculation of T_{MA} ages (Meisel et al., 2001b).

γ(Os): calculated for at 280 Ma and 140 Ma of clinopyroxenite Re-Os errorchron age

2SE: in-run precisions for $^{187}Os/^{188}Os$; 2SD: precisions for $^{187}Os/^{188}Os$, including blank contribution.

3.9 Supplement

3.9.1 Brief description of Balmucia pyroxenites

Six websterites, eleven spinel clinopyroxenites and one spinel rich vein from dunite body were sampled in Balmuccia peridotite body in 2011. The brief petrologic description of these rocks is given in Table S3.1 and some examples of field occurrence and hand specimen are shown in Figure S3.1.

The major elements and some trace elements were analyzed by XRF methods at GFZ, Potsdam and the results are listed in Table S3.2. Whole rock S data from XRF analysis are systematically about 10-20 % lower than isotope dilution results, but show a good linear correlation with our isotope dilution values, except for sample BM11-21 (Figure S3.2). This correlation indicates that sulfides are distributed homogeneously in pyroxenite powders of this study.

Table S3.1 Petrographic features of Balmuccia layers of websterites and spinel clinopyroxenites of this study

Sample number	Pyroxenite type	Color	Vein width	Note	Sulfides-spinel in hand specimen	Description
BM11-28A	spinel clinopyroxenite	gray	6 cm	drill core	3-5 % spinel	the same vein BM11-28 with different modal abundance of spinel, deceasing from A to C and subparallel to foliation; 28A: rich in dark spinel minerals; 28B: less spinel; 28C (no dark spinel, but drill core has visible sulfides); distance of AB is 100 cm and BC is 20 cm
BM11-28B	spinel clinopyroxenite	gray	6 cm	drill core	1-2 % spinel	
BM11-28C	spinel clinopyroxenite	gray	6 cm	drill core	visible sulfides, little spinel	
BM11-26	spinel clinopyroxenite	gray	10 cm	drill core	visible sulfides, variable spinel (1-5 %)	clinopyroxenite veins with different widths from 0.5-31cm crosscut each other, subparallel (10 degree oblique) to foliation of lherzolite. BM11-26 cuts early clinopyroxenite veinlets
BM11-27	spinel clinopyroxenite	gray	31 cm	drill core	visible sulfides, little spinel	features similar to BM11-26 and half meter away from it
BM11-15	spinel clinopyroxenite	gray	> 8 cm	float block	visible sulfides, 1-3 % spinel	sharp boundary to lherzolite
BM11-16A	spinel clinopyroxenite	gray	8 cm	float block	visible sulfides, 1-3 % spinel	sharp boundary to lherzolite
BM11-20	spinel clinopyroxenite	gray	5-8 cm	drill core	visible sulfides, little spinel	sharp boundary to lherzolite
BM11-22	clinopyroxenite	gray	5 cm	drill core	little spinel	sharp boundary to lherzolite, 2-3 meters away from BM11-21
BM11-23	spinel clinopyroxenite	gray	8 cm	drill core	0.5 mm sulfide grains, 2-5 % spinel	sharp boundary to lherzolite, several centimeters away from BM11-22
BM11-29	spinel clinopyroxenite	gray	4 cm	drill core	0.2 mm sulfide grains, 1-2 % spinel	35 cm away from BM11-28, subparallel to BM11-28 and foliation of lherzolite
BM11-25	websterite	green	10 cm	drill core	visible sulfides, no spinel	crosscut replacive dunite with sharp boundary
BM11-19	websterite	green	8 cm	drill core	sparse sulfides, no spinel	sharp boundary to lherzolite
BM11-21	websterite	green	15 cm	drill core	visible sulfides, no spinel	host lherzolite contains websterite veins with different width (from <1cm to 15cm) and the sample drilled from one 15cm wide dike
BM11-12	websterite	green	40-50 cm	float block	0.1 mm sulfides, no spinel	40-50 cm wide band, green pyroxene predominant, megacrysts of pyroxene (3-5cm), phlogopite bearing, visible sulfides, gradual transition from peridotites containing thin and rather diffuse pyroxene layers to websterites containing thin olivine rich filaments, contact to peridotites is sometimes comprised of dunite.
BM11-14	websterite	green	> 40 cm	float block	visible sulfides, no spinel	similar to BM11-12, phlogopite bearing
BM11-07B	orthopyroxenite	green-dark	30-40 cm	float block	visible sulfides, no spinel	crosscut dunite with sharp boundary
BM11-24B	spinel rich vein	dark	4 cm	drill core	>70-80 % spinel	spinel rich layer with minor olivine and clinopyroxene, in replacive dunite body

Note：Except for modal variations in spinel abundances, clinopyroxenites display no noticeable macroscopic differences from each other: gray, interstitial sulfides bearing, olivine free, sharp boundary and subparallel or discordant to foliation of the host peridotites, variable spinel abundances (mostly <5 vol.%) and vein width (0.5 cm to 31 cm). Websterites show green color, sulfide bearing, and contain no or only little spinel and olivine, and mostly dikes with sharp contact with host peridotites. Some websterite layers have gradual boundaries to peridotites, e.g. BM11-12 and BM11-14. Websterites are cut by spinel clinopyroxenites.

Table S3.2 Major and trace elements of Balmuccia pyroxenites

Sample Name	Rock type	SiO_2 (%)	TiO_2 (%)	Al_2O_3 (%)	Fe_2O_3 (%)	MnO (%)	MgO (%)	CaO (%)	Na_2O (%)	K_2O (%)	P_2O_5 (%)	H_2O (%)	CO_2 (%)	Total (%)	Ba (μg/g)	Cr (μg/g)	Ni (μg/g)	Sr (μg/g)	V (μg/g)	Zn (μg/g)	Zr (μg/g)	S* by XRF (μg/g)	S by ID (μg/g)
BM11-28A	cpx	42.8	0.439	14.0	6.63	0.123	18.82	14.50	0.46	<0.01	<0.01	1.24	0.33	99.31	30	577	846	27	356	106	23	1400	1456
BM11-28B	cpx	47.0	0.309	6.0	6.29	0.113	23.74	14.35	0.41	<0.01	<0.01	0.78	0.27	99.21	16	957	1313	22	248	35	20	1336	1509
BM11-28C	cpx	47.5	0.301	6.0	6.10	0.113	23.00	14.79	0.44	<0.01	<0.01	0.75	0.29	99.26	41	1100	1195	23	267	33	19	1299	1490
BM11-27	cpx	49.9	0.303	7.1	7.57	0.151	19.52	13.97	0.32	<0.01	<0.01	0.50	0.14	99.43	24	376	624	25	281	32	18	1381	1559
BM11-15	cpx	46.1	0.669	11.6	5.15	0.108	17.98	16.14	0.89	0.03	<0.01	0.52	0.24	99.42	34	609	849	47	341	64	37	1009	1250
BM11-16A	cpx	47.4	0.624	10.4	5.23	0.114	17.80	16.54	0.67	<0.01	<0.01	0.35	0.14	99.32	31	908	732	46	342	51	35	1299	1532
BM11-20	cpx	51.2	0.227	5.4	6.08	0.132	20.67	14.19	0.35	0.01	<0.01	0.93	0.17	99.38	35	2040	650	25	233	24	14	448	537
BM11-22	cpx	49.0	0.426	8.1	6.33	0.138	18.00	15.61	0.64	0.03	<0.01	1.17	0.21	99.67	21	423	528	28	308	25	26	450	523
BM11-26	cpx	49.7	0.341	7.0	6.66	0.145	17.30	17.03	0.45	<0.01	<0.01	0.54	0.36	99.54	17	480	440	29	292	26	20	679	805
BM11-23	cpx	46.1	0.411	11.0	7.22	0.138	17.86	15.22	0.44	<0.01	<0.01	1.01	0.13	99.50	21	432	467	31	348	66	25	856	1028
BM11-29	cpx	50.1	0.307	6.6	4.83	0.119	17.26	18.50	0.62	0.01	0.010	0.96	0.35	99.59	30	860	466	34	291	17	19	393	323
BM11-25	web	50.5	0.205	4.9	5.46	0.128	21.35	15.78	0.37	<0.01	<0.01	0.26	0.09	98.97	16	4890	887	23	194	23	14	544	722
BM11-19	web	49.7	0.259	5.1	6.01	0.125	21.78	14.67	0.45	<0.01	<0.01	0.66	0.23	98.94	15	4982	958	32	183	30	23	545	611
BM11-21	web	52.9	0.099	2.7	5.19	0.119	21.85	14.86	0.27	<0.01	<0.01	0.55	0.17	98.63	29	5382	1459	26	128	26	12	1057	1745
BM11-12	web	51.8	0.188	4.2	5.10	0.123	20.51	16.19	0.35	<0.01	<0.01	0.29	0.21	98.95	29	4993	847	22	180	22	15	592	680
BM11-14	web	48.2	0.198	5.0	6.62	0.127	26.09	11.94	0.40	<0.01	<0.01	0.27	0.13	98.88	<10	5425	1217	19	169	34	17	377	468
BM11-07B	op	52.4	0.172	5.4	7.76	0.140	30.62	1.54	0.03	<0.01	<0.01	—	0.91	98.91	14	4307	1532	<10	128	43	12	—	1017
BM11-24B	spinel	15.5	0.296	20.0	15.94	0.140	29.10	1.57	0.01	<0.01	<0.01	—	0.38	82.96	45	115800	2161	<10	532	336	<10	—	105

Note: cpx, spinel clinopyroxenites; web, websterites; op, orthopyroxenite; spinel, spinel rich vein in dunite. ID, isotope dilution

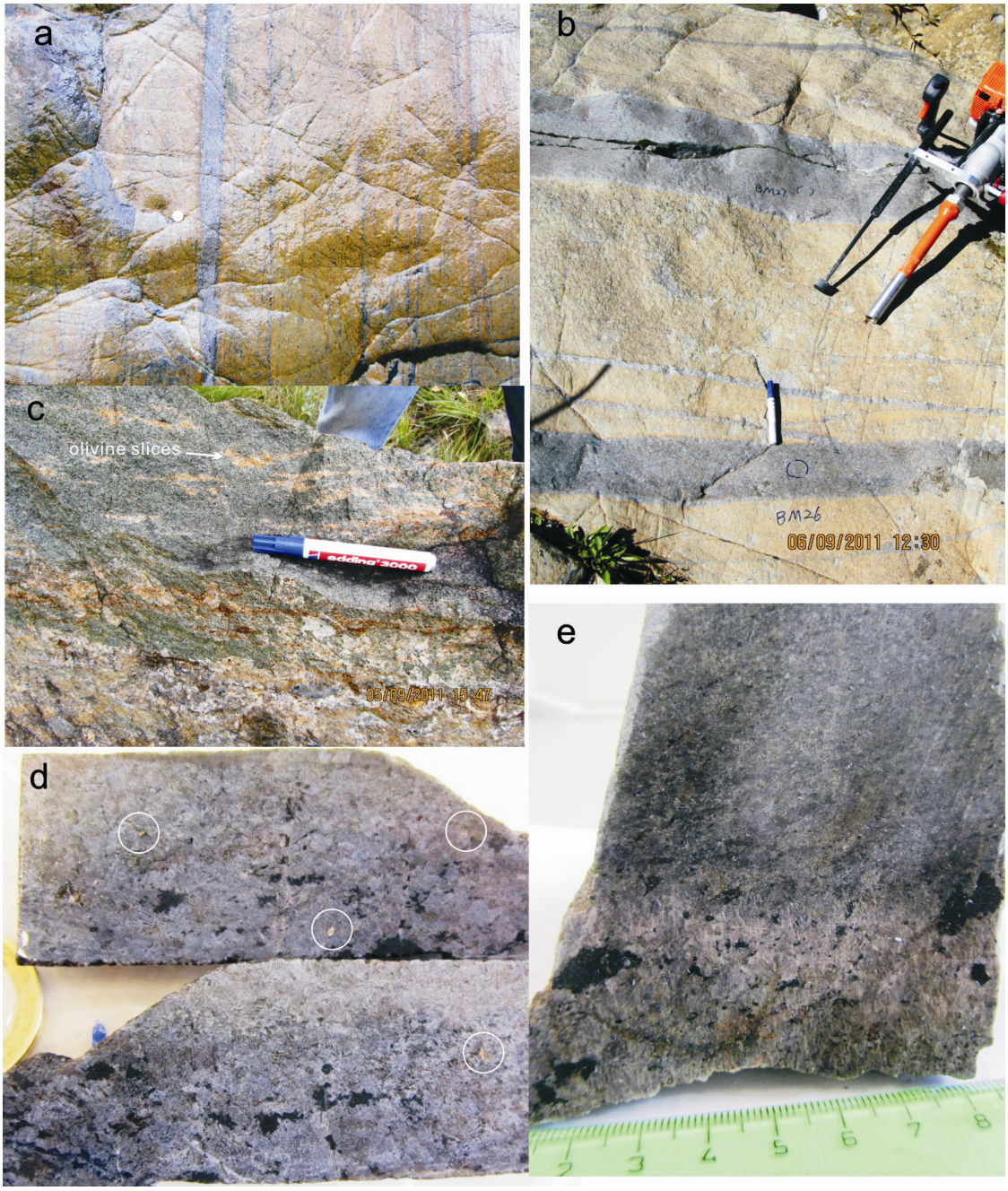

Figure S3.1 Examples of websterites and spinel clinopyroxenites from Balmuccia peridotite body. a) Sub-parallel layers of spinel clinopyroxenites in host peridotites (1 Euro coin as scale). b) Crosscutting relationships of different generation clinopyroxenites. BM11-26 and BM11-27 were drilled from vein centers. c) Websterites (BM11-14) contain filaments of olivine rich aggregates (yellow color from weathering) and megacrysts of pyroxene. These websterites show gradual transition to peridotites. d) Typical spinel clinopyroxenite (BM11-23) display heterogenous distribution of sulfides (0.5 mm, in white circles) and spinel (dark color), 1 Euro coin as scale. e) Sharp boundary of spinel clinopyroxenite (BM11-15) with host peridotites.

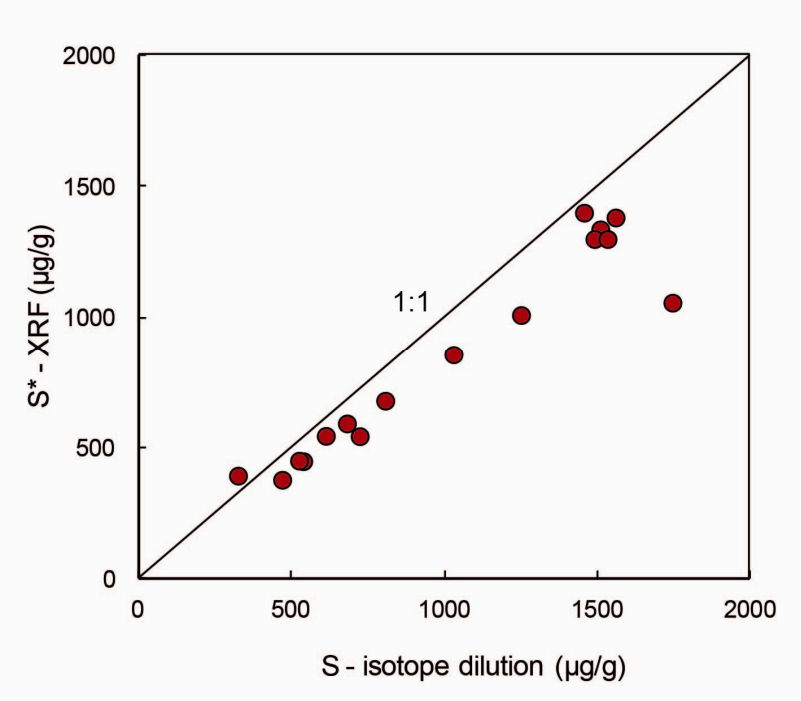

Figure S3.2 Good correlation of S contents from isotope dilution and XRF analysis, indicating homogenous distribution of sulfides in sample powder of this study.

3.9.2 Brief analytical methods of HSE, chalcogens and Os isotopes

Mixed ^{191}Ir-^{99}Ru-^{194}Pt-^{105}Pd, ^{77}Se-^{125}Te, and individual^{185}Re, ^{190}Os and ^{34}S spike solutions were weighed into 90 ml quartz glass digestion vessels, followed by about 2.5 g sample powder, 5 ml 14 mol l^{-1} HNO_3 and 2.5 ml 9 mol l^{-1} HCl. The vessels were sealed immediately with Teflon tape and samples were digested for 16 hours at 320 °C and 100 bar. After digestion, osmium was extracted into chloroform (Cohen and Waters, 1996), and further purified by micro distillation (Birck et al., 1997). About 40 % of the digestion solution was used for separation of the HSE fraction and 20 % for S-Se-Te separation.

Chemical separation of the HSE fraction from matrix was performed on columns filled with 10 ml of pre-cleaned Eichrom 50W-X8 (100-200 mesh) cation exchange resin (Fischer-Gödde et al., 2011). This fraction was collected in 14 ml 0.5 mol l^{-1}HCl-40 % (v/v) acetone and split into a fraction for analysis of Au, Re, Ir and Pt, and another fraction for analysis of Rh, Ir, Ru, Pt and Pd. The Pd fraction was further purified in 0.2 mol l^{-1}HCl on 2 ml Eichrom 50W-X8 (100-200 mesh) resin and analyzed the Element XR using an Aridus-I desolvator at an oxide formation rate < 0.3-0.4 % (CeO^+/Ce^+). The Au fraction was analyzed in 1 mol l^{-1} HCl using a Scott type glass spray chamber after reducing the volume of the solution to 2 ml.

A two-step ion exchange chromatography method was used for separation of S, Se and Te, and S-Se and Te fractions were obtained. Sulfur isotopic measurements were performed on the S-Se fraction at medium mass resolution mode (m/Δm=4000) on the Element XR. Selenium and Te were measured using a double pass Scott type glass spray chamber at low mass resolution mode on the Element XR, combined with a hydride generation sample introduction system by reacting the sample solution with 1 % m/m $NaBH_4$ in 0.05 M NaOH (see Wang et al., 2013, for details).

Osmium isotopic ratios were determined as OsO_3^- in negative mode using the Triton TIMS at Freie Universität Berlin. Signals of the spike isotope ^{190}Os of samples were typically at 15,000 to 800,000 cps using the secondary electron multiplier mode on a Thermo Finnigan Triton TIMS. About 160 scans were collected in each measurement. Raw data were corrected for isobaric OsO_3^- interferences, mass fractionation using the $^{192}Os/^{188}Os$ ratio of 3.08271, and spike contribution. Repeated measurements of about 100 pg of the University of Maryland Os standard solution yielded $^{187}Os/^{188}Os$=0.11402±0.00006 (2s, standard deviation, n=5) over the analysis period of the samples.

During this study, the total procedural blanks were as follows (n=5, 1s): Re=5.7±2.7 pg; Os=0.8±0.5 pg with $^{187}Os/^{188}Os$ ratios of 0.50±0.08; Ir=0.6±0.4 pg; Ru=0.2±0.2 pg; Rh=5±3 pg; Pt=32±15 pg; Pd=20±18 pg; Au=2±1 pg; Te=25±11 pg; Se=2.5±0.7 ng; S=3.0±0.8 μg. The relative higher Pd and Pt blanks in this study compared to previous work from our lab result from a new batch of cation resin with higher blank levels for these elements. Samples were corrected for total procedural blanks using mean values. Blanks are negligible (< 0.1 %) for Re, S, Se and Te in all samples. Blank corrections of Pt and Pd are only significant for BM11-22 (< 40 %), and several percent for a few low concentration samples. Blanks of Os, Ir, Ru and Rh are mostly negligible (< 0.5 %), but significant for BM11-20, BM11-22, BM11-23 and BM11-26 (< 30 %).

3.9.3 Supplementary discussion

3.9.3.1 Re-Os errorchron age of clinopyroxenites

Re-Os errorchron of 8 out of 11 clinopyroxenites (excluding BM11-26, BM11-23 and BM11-29) defines a 141 Ma 'age' (Figure S3.3), and the 'age' is similar to their Mesozoic Os model age (130-170 Ma). The correlation of $^{187}Os/^{188}Os_{present\ day}$ versus 1/Os indicates possible mixing features for some of samples.

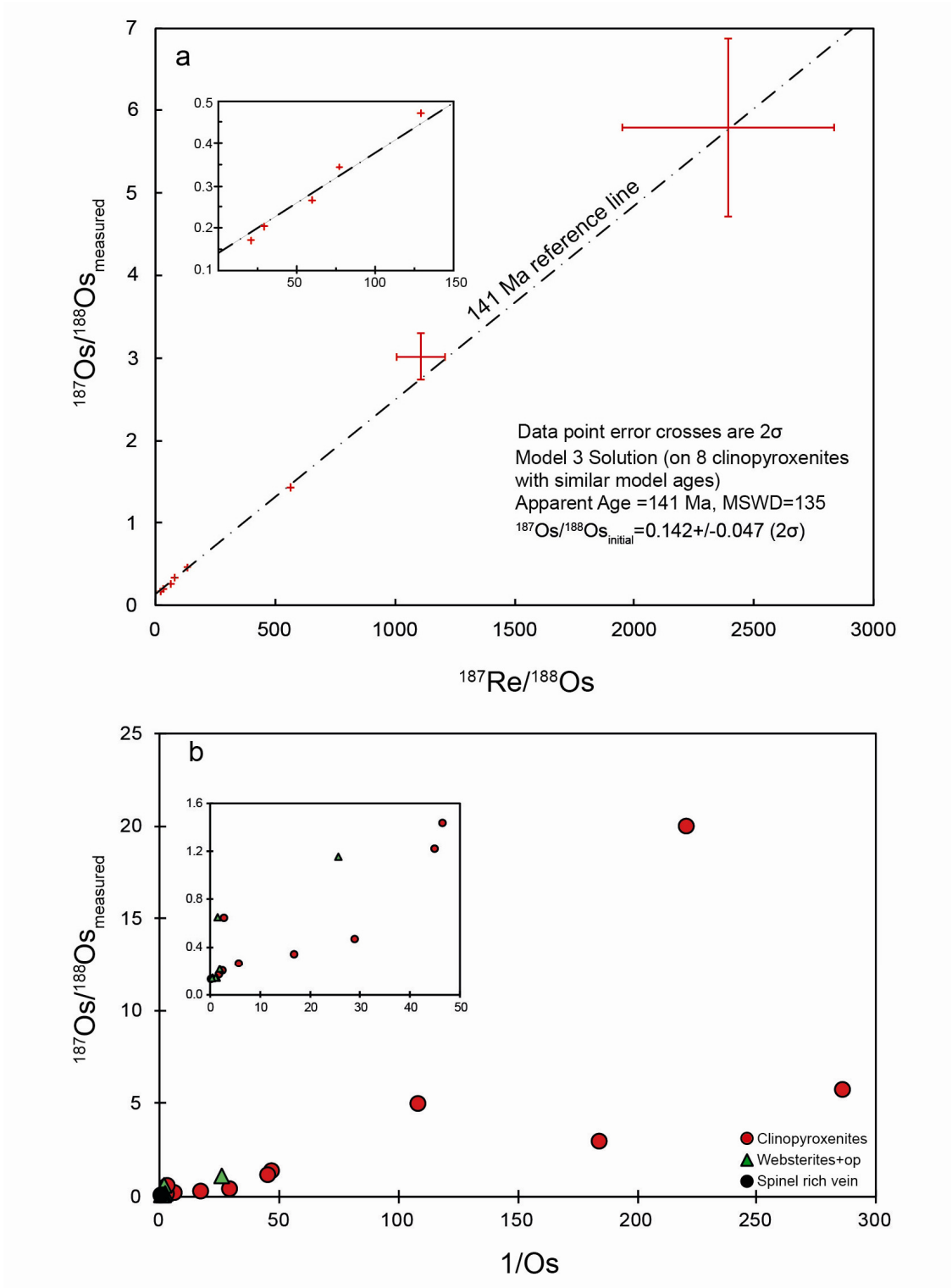

Figure S3.3 Re-Os errorchron age of clinopyroxenites from Balmuccia. a) Re-Os errorchron of 8 selected clinopyroxenites (excluding BM11-26, BM11-23 and BM11-29) that have similar Mesozoic Os model age defines a 141 Ma 'age'. Regression obtained, using the Isoplot 4.1 program (Berkeley Geochronology center, http://www.bgc.org/isoplot_etc/isoplot.html). Most errors reflect uncertainties of the blank contribution. b) $^{187}Os/^{188}Os_{present\ day}$ versus 1/Os.

3.9.3.2 Relative sulfide-silicate melt partition coefficients of Se and Te

Both of websterites and clinopyroxenites are cumulates with sulfide precipitation, thus Se and Te concentrations in sulfides can reflect sulfide-silicate melt partitioning, irrespectively of different concentrations of their parent melts. Concentrations of Se and Te in the sulfides were calculated based on whole rock S contents assuming all Se and Te in sulfides. Data on websterites and clinopyroxenites show apparent relative sulfide-silicate melt partition coefficients of $D_{Te}/D_{Se} \approx 5.0 \pm 1.4$ (2σ) during melt fractionation in the mantle (Figure S3.4).

It should be noted that websterite and clinopyroxenite dikes formed at different ages and have different initial γOs. Correlations of initial γOs with Se/Te, Pd/Ir and Re/Os in clinopyroxenites indicate that parent melts of some pyroxenites have inhomogeneous γOs and are probably products of mixing (Figures S3.4 and S3.5). However, websterites and clinopyroxenites still have similar fractionation process of Se and Te (Figure S3.4), probably implying independence of such sulfide-silicate melt fractionation on initial γOs or history of their parent melts.

3.9.3.3 HSE contents of sulfides in pyroxenites and other rocks

Because HSE are predominantly hosted in sulfides in pyroxenites and fertile peridotites, we use whole rock S contents to convert whole rock data to contents of HSE in sulfides assuming all these elements are hosted in sulfides (Figure S3.6). Calculated contents in sulfides of websterites have abundances and ratios of Os, Ir, Pd, Re close to metasomatic/interstitial sulfides and early formed olivine gabbro of the lower oceanic crust of the Oman ophiolite, whereas sulfides in clinopyroxenites have more evolved characteristics and are similar to sulfides in MORB. Minor fractionation of Pd and Ir occurs during melt evolution, as indicated by apparent sulfide-silicate partitioning $D_{Pd}/D_{Ir} \approx 0.95 \pm 0.11$ (2σ, Figure 3.5). Rhenium contents in sulfides have limited variations compared to Os, Ir and Pd content with several orders of magnitude.

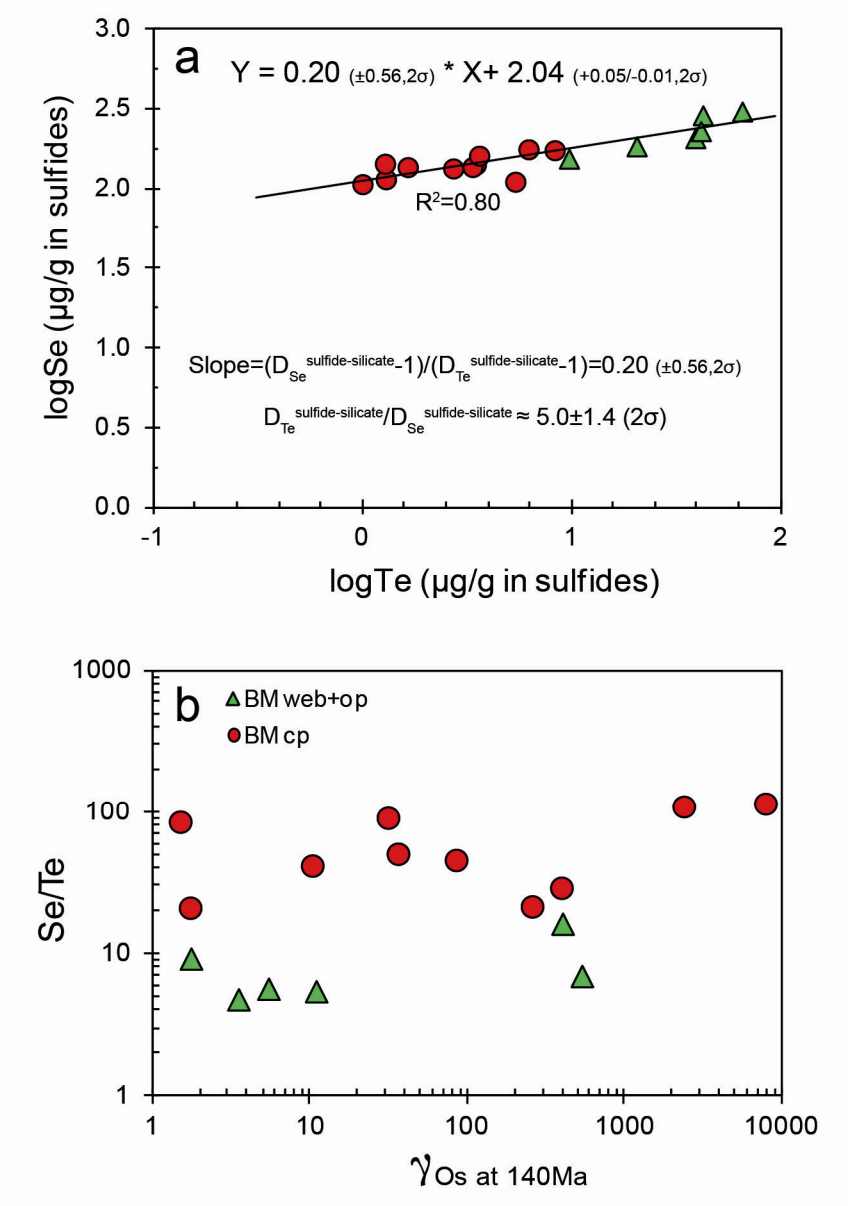

Figure S3.4 Apparent relative sulfide-silicate melt partitioning coefficient of Se and Te during melt fractionation at mantle depth (a), which is defined by the slope of Se and Te concentrations in sulfides. b) Correlation of Se/Te with $\gamma Os_{initial}$ reflects possible different sources of their parent melts.

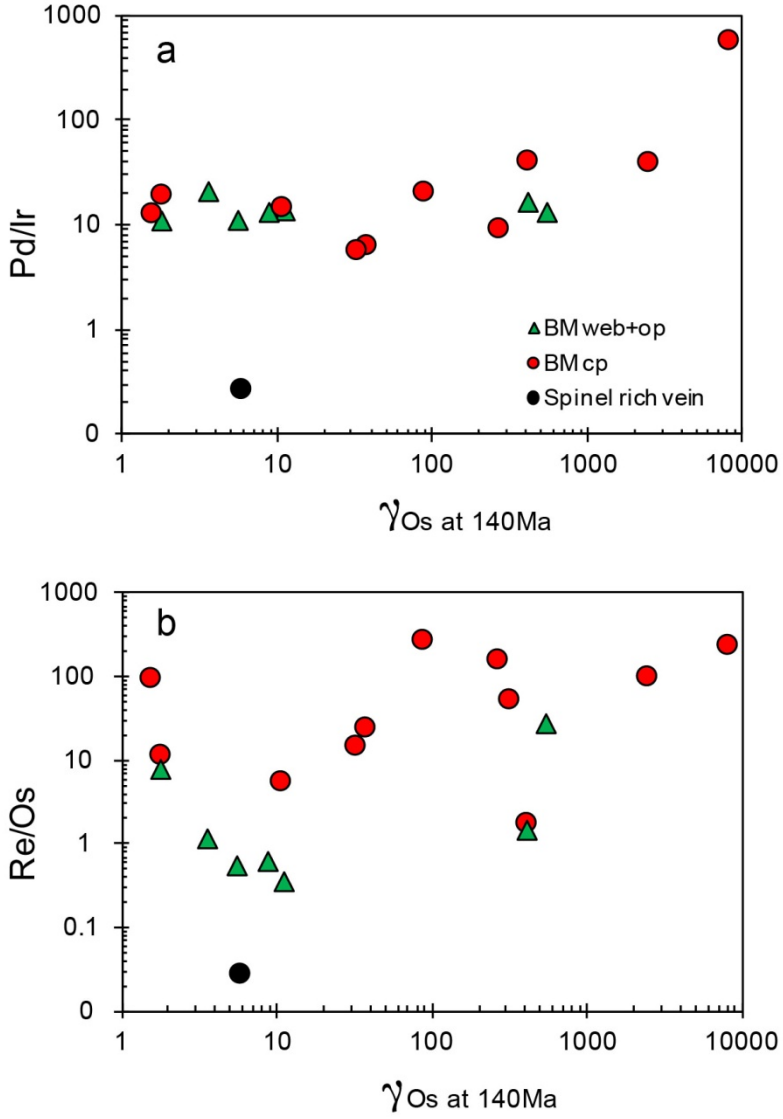

Figure S3.5 Correlations of $\gamma Os_{(140Ma)}$ with Pd/Ir (a) and Re/Os (b) in Balmuccia pyroxenites, showing inhomogeneous γOs for pyroxenites which sources have long-term fractionated Re/Os.

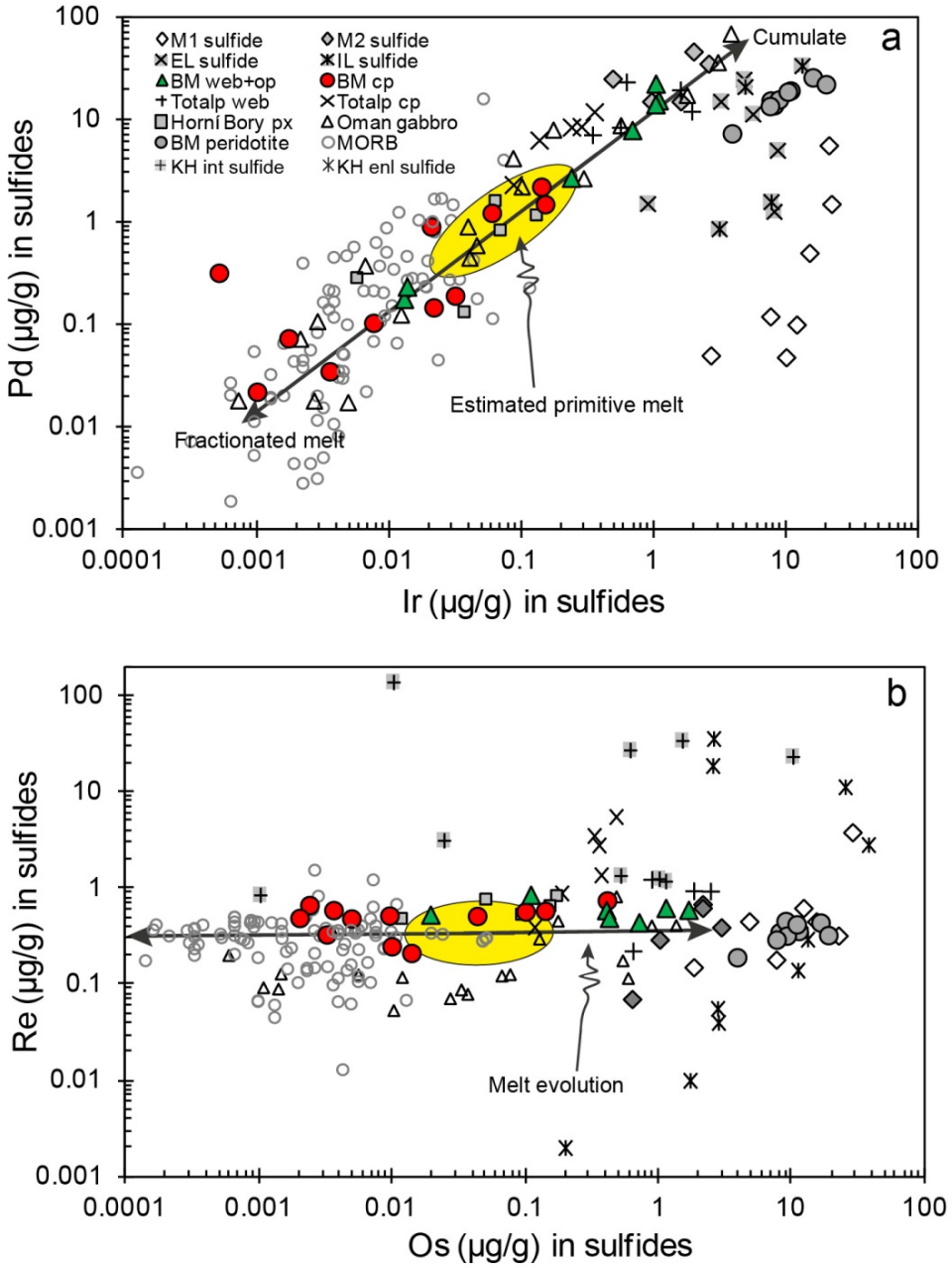

Figure S3.6 Comparison of abundances of Re, Pd, Os and Ir of calculated and measured sulfides in pyroxenites, peridotites, Oman gabbros and MORB (including upper oceanic crust). Because of known bulk rock S contents, contents of sulfides, if unknown, are estimated assuming that all HSE retain in sulfides with 35 wt.% sulfur, including for MORB. Subsolidus exsolution of sulfides during cooling may lead to strong depletion of Pt, Te and Au in sulfides (Luguet et al., 2004; Lorand and Alard, 2010; Lorand et al., 2010) so that laser ablation ICP-MS values do not necessarily represent the bulk composition of high-temperature sulfides and thus are not shown. Mass balance of contents in whole rock and sulfides suggest subsolidus exclusion of sulfides during cooling have limited effects on Os, Ir, Pd and probably Re (Luguet et al., 2004; Lorand and Alard, 2010; Harvey et al., 2011). M1-sulfides are early generation enclosed sulfides and M2 sulfides are metasomatic interstitial sulfides from the Kane fracture zone, Mid Atlantic Ridge (Alard et al., 2005), EL sulfide and IL sulfide are sulfides in peridotites from External Ligurides and Internal Ligurides, respectively (Luguet et al., 2004). Also shown are interstitial and enclosed sulfides in peridotites xenoliths from Kilbourne Hole (KH), New

Mexico (Harvey et al., 2011). Sulfide compositions were estimated from bulk rock contents with known S contents for BM peridotites, pyroxenites from Horní Bory (Ackerman et al., 2013) and Totalp (van Acken et al., 2010b), Oman lower crustal gabbros (Peucker-Ehrenbrink et al., 2012) and MORB (Rehkämper et al., 1999b; Peucker-Ehrenbrink et al., 2003; Bézos et al., 2005; Gannoun et al., 2007; Dale et al., 2008) assuming 1100 µg/g S if unknown.

Chapter 4

Ratios of S, Se and Te in the silicate Earth require a volatile-rich late veneer

Zaicong Wang and Harry Becker

Freie Universität Berlin, Institut für Geologische Wissenschaften,
Malteserstrasse 74-100, 12249 Berlin, Germany

This chapter has been published as:

Wang Z. and Becker H. (2013) Ratios of S, Se and Te in the silicate Earth require a volatile-rich late veneer. *Nature* 499, 328-331. Doi: 10.1038/nature12285.

(Note: *Letters to Nature* has no sub-headers and the content has been modified to follow the format of the thesis.)

4.1 Main content

The excess of highly siderophile (iron-loving) elements (HSE) and chondritic ratios of most HSE in the bulk silicate Earth (BSE) may reflect accretion of a chondritic 'late veneer' of about 0.5 % of Earth's mass after core formation (Walker, 2009; Mann et al., 2012). The amount of volatiles delivered by the late veneer is a key constraint for the budget and the origin of the volatiles in the Earth. At high pressure-temperature (P-T) conditions, the moderately volatile chalcogen elements sulfur, selenium and tellurium are moderately to highly siderophile, thus, if depleted by core formation, their mantle abundances should reflect the volatile composition of the late veneer (Yi et al., 2000; Rose-Weston et al., 2009). Here we determined ratios and abundances of S, Se and Te in the mantle based on new isotope dilution data for post-Archean mantle peridotites. The mean S/Se (2690±700, 1σ) and Se/Te (7.9±1.6, 1σ) of mantle lherzolites overlap with CI (Ivuna-type) carbonaceous chondrite values (Dreibus et al., 1995; Lodders, 2003). Se/Te of ordinary and enstatite chondrites are significantly different. The chalcogen/HSE ratio of the BSE is similar to that of CM (Mighei-type) carbonaceous chondrites, consistent with the view that the HSE signature of the BSE reflects a predominance of slightly volatile-depleted, carbonaceous-chondrite-like material, possibly with a minor proportion of non-chondritic material (Fischer-Gödde and Becker, 2012). Depending on the estimates for the abundances of water and carbon in the BSE (Marty, 2012), the late veneer may have supplied 20 % to 100 % of the budget of hydrogen and carbon in the BSE.

Understanding the history of the delivery of volatile elements, particularly water and carbon, is of fundamental importance for understanding planetary evolution (Abe et al., 2000). The Earth formed during collisions of protoplanetary embryos with compositions that may have evolved from reducing and volatile poor to oxidizing and presumably volatile rich (the heterogeneous accretion model) (Wood et al., 2006; Schönbächler et al., 2010; Rubie et al., 2011). The detailed origin and history of moderately volatile and atmophile elements in the Earth remains uncertain, mostly due to considerable element redistribution during core formation and silicate differentiation (Albarède, 2009; Schönbächler et al., 2010; Wood and Halliday, 2010; Marty, 2012). It is likely that a fraction of the atmophile element budget of the Earth was delivered after core formation, but little agreement exists on sources and mass fractions of volatiles delivered late (Albarède, 2009; Wood and Halliday, 2010). Some information about the composition of materials that accreted after core formation ('late veneer') has been derived from highly siderophile elements (the platinum group elements, Re and Au) (Becker et al., 2006; Walker, 2009; Fischer-Gödde et al., 2011;

Fischer-Gödde and Becker, 2012). The HSE should have partitioned into the metallic core of the Earth nearly quantitatively, leaving the BSE strongly depleted in HSE. High P-T experiments indicate significantly lower partition coefficients for the HSE during terrestrial core formation, but a late veneer is still required (Mann et al., 2012).

With the exception of Pd and Au, which are slightly volatile, most HSE are refractory elements. The $^{187}Os/^{188}Os$ of the BSE reflects its time integrated Re/Os and has been interpreted in that the late veneer may have been mostly comprised of water and carbon depleted ordinary or enstatite chondrites (Meisel et al., 2001b; Walker et al., 2002). More recent work has revealed that the BSE is characterized by an excess of Pd and Ru of 40-50 % and 30 %, respectively, relative to Ir, Os and Pt (Becker et al., 2006). The Pd excess may be attributed to mixing of a chondritic late veneer with mantle that displays a small Pd excess inherited from core-mantle equilibrium partitioning, however, the excess of Ru can neither be explained by metal-silicate segregation at high P-T, nor by chondritic late veneer models (Becker et al., 2006; Walker, 2009; Mann et al., 2012). The chalcogen/HSE ratio of the BSE is similar to that of CM (Mighei-type) carbonaceous chondrites, consistent with the view that the HSE signature of the BSE reflects a predominance of slightly volatile-depleted, carbonaceous-chondrite-like material, possibly with a minor proportion of non-chondritic material (Becker et al., 2006; Walker, 2009). HSE data from pre-3.8 Ga lunar impact rocks related to large basin forming impacts provide hints that the late veneer accreted to the Earth may have been comprised of carbonaceous chondrite like material with a minor contribution from a non-chondritic component (Fischer-Gödde and Becker, 2012). These data suggest that if the late veneer represents a mixture of materials with different compositions, the $^{187}Os/^{188}Os$ and HSE composition of the BSE cannot provide stringent constraints on the composition and class of chondritic material in the late veneer.

Sulfur, selenium and tellurium have similar and rather low 50 % condensation temperatures near 700 K in a canonical solar nebula composition (Lodders, 2003). An important property of the chalcogens is that they become more siderophile with increasing pressure and are moderately to highly siderophile during metal-silicate segregation at high P-T conditions (Rose-Weston et al., 2009). As for the HSE, the experimental data predict that S, Se and Te in the BSE should predominantly derive from the late veneer, if metal-silicate segregation occurred at high P-T and equilibrium conditions (Rose-Weston et al., 2009). Because different classes of chondrites display variable fractionation behavior of moderately volatile elements, the chalcogens can distinguish contributions from carbonaceous, ordinary or enstatite chondrite like materials in the late veneer. Notably, different carbonaceous chondrite groups all display Se/Te similar to the chemically most primitive chondrites (CI

chondrites, Se/Te = 8.5±0.7) (Lodders, 2003), irrespectively of the extent of depletion of the chalcogens; whereas ordinary and enstatite chondrites are characterized by significantly higher Se/Te (11-30) than carbonaceous chondrites (for details see Supplementary Table S4.6). In addition, the abundance of the chalcogens relative to the refractory HSE in the BSE may constrain the depletion of the chalcogens in the late veneer, the type of primitive material, and its likely contribution to highly volatile elements such as water and carbon.

Abundances of the chalcogens in the BSE have been estimated previously on the basis of a limited number of mantle peridotites, however, owing to analytical difficulties, abundance estimates of Se and Te in the BSE were based on very little data, and thus reliable data for S/Se and Se/Te have been scarce (McDonough and Sun, 1995; Palme and O'Neill, 2003; Lorand and Alard, 2010). In order to obtain an improved database for the chalcogen composition of the mantle, we present new precise S, Se and Te concentration data obtained by isotope dilution-ICPMS for the same digestion aliquot of fresh mantle peridotites (Figures 4.1 and 4.2; Supplementary Table S4.2). The new data will be compared with lithophile element data and precise HSE data obtained on the same samples, to evaluate the behavior of the chalcogens relative to these elements during mantle processes.

As in previous work (Morgan, 1986; Becker et al., 2006; Lorand and Alard, 2010), the data show a linear decrease of sulfur abundances with decreasing Al_2O_3 contents, an indicator of progressive depletion by melting, both for the whole data set of mantle peridotites, and for individual suites of peridotites (Figure 4.1a). Notably, the linear correlation of S with Al_2O_3 occurs in suites of peridotites that display different states of equilibration of $^{187}Os/^{188}Os$ and HSE abundances (Lorand and Alard, 2010; Fischer-Gödde et al., 2011). Similarly, Se and Te also display positive trends with Al_2O_3 and S contents, although with larger scatter (Figures 4.1 and 4.2). The coupled behavior of the chalcogens with Al_2O_3, HSE (also see Supplementary information) and the limited fractionation of S/Se and Se/Te in lherzolites provide a solid base for the determination of ratios and abundances of these elements in the BSE. S/Se ratios in lherzolites (Al_2O_3 >1.5 wt.%) display some scatter with a mean S/Se of 2690±700 (1σ, n=53, including Lherz (Lorand and Alard, 2010)), consistent with a value of 2600±700 (1σ) derived from linear regression of the correlation of S with Se (Figure 4.1c, Supplementary Table S4.5). Se/Te ratios yield a mean Se/Te of 7.9±1.6 (1σ, n=63), and slightly decrease with depletion, implying that Se is slightly more incompatible than Te (Figure 4.2c). The scatter in chalcogen element abundances and ratios between different suites of fertile lherzolites likely reflects different extents of magmatic re-equilibration of mantle domains during melt migration and open-system partial melting, and thus mantle heterogeneity. Infiltration and trapping of silicate

melt in peridotitic melting residues are now recognized as widespread processes in the mantle (Bodinier and Godard, 2003). Petrographic, major element, HSE and $^{187}Os/^{188}Os$ data indicate that many samples of this study probably were affected by such processes (Fischer-Gödde et al., 2011). Nonetheless, these processes appear to have very similar effects on abundances of S, Se and Te as equilibrium partitioning during open system melting (Wang et al., 2013). The limited variations suggest that the average S/Se and Se/Te of lherzolites should provide robust constraints on the composition of the BSE, irrespectively of the detailed mantle processes.

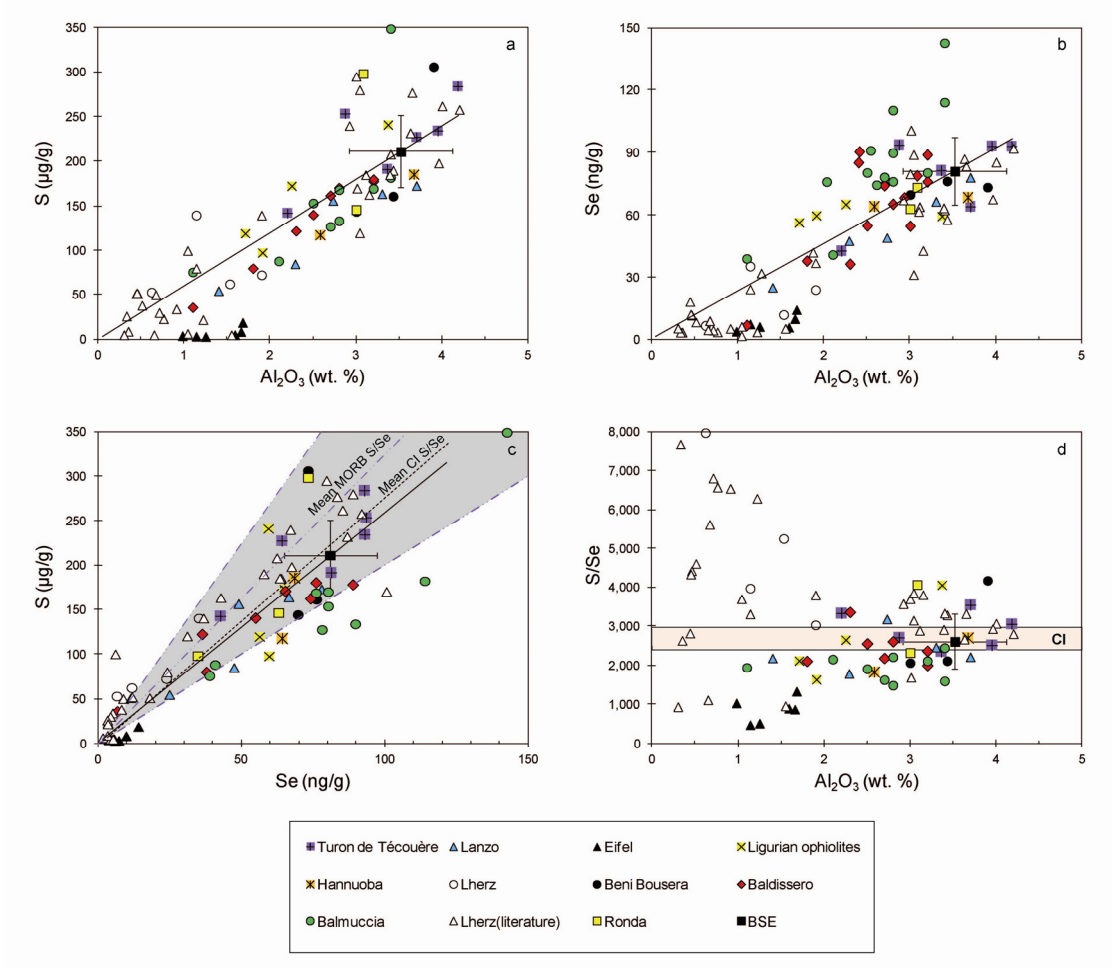

Figure 4.1 Correlation of S and Se contents of terrestrial peridotites with Al_2O_3 contents as indicator of depletion. (a-c) S, Se and Al_2O_3 display positive correlations with each other for mantle peridotites from different geological settings (lines in a to c are linear regression lines of the data). Shaded region in c is the range of S/Se of ocean ridge baslts (MORB) with a mean value of 3230±560 (1σ, n=279) (Jenner and O'Neill, 2012), somewhat higher than the mean S/Se of mantle peridotites. (d) S/Se ratios in lherzolites (Al_2O_3 > 1.5 wt. %) display scatter, but change little with depletion. In contrast, S/Se in harzburgites are much more variable. The mean S/Se (2690±700, 1σ, n=53) of the lherzolites is indistinguishable from the CI chondrite value (mean S/Se = 2750±200 (Lodders, 2003)). The Al_2O_3 concentration of the BSE given here is based on recent statistical evaluation of peridotite data (Lyubetskaya and Korenaga, 2007), and should be viewed as a minimum value (see Supplementary discussion). Literature data for Lherz are from (Lorand and Alard, 2010; König et al., 2012) and data

for Balmuccia and Baldissero from. Precisions of chalcogen concentrations are within symbol size and error bars of the BSE are 1σ.

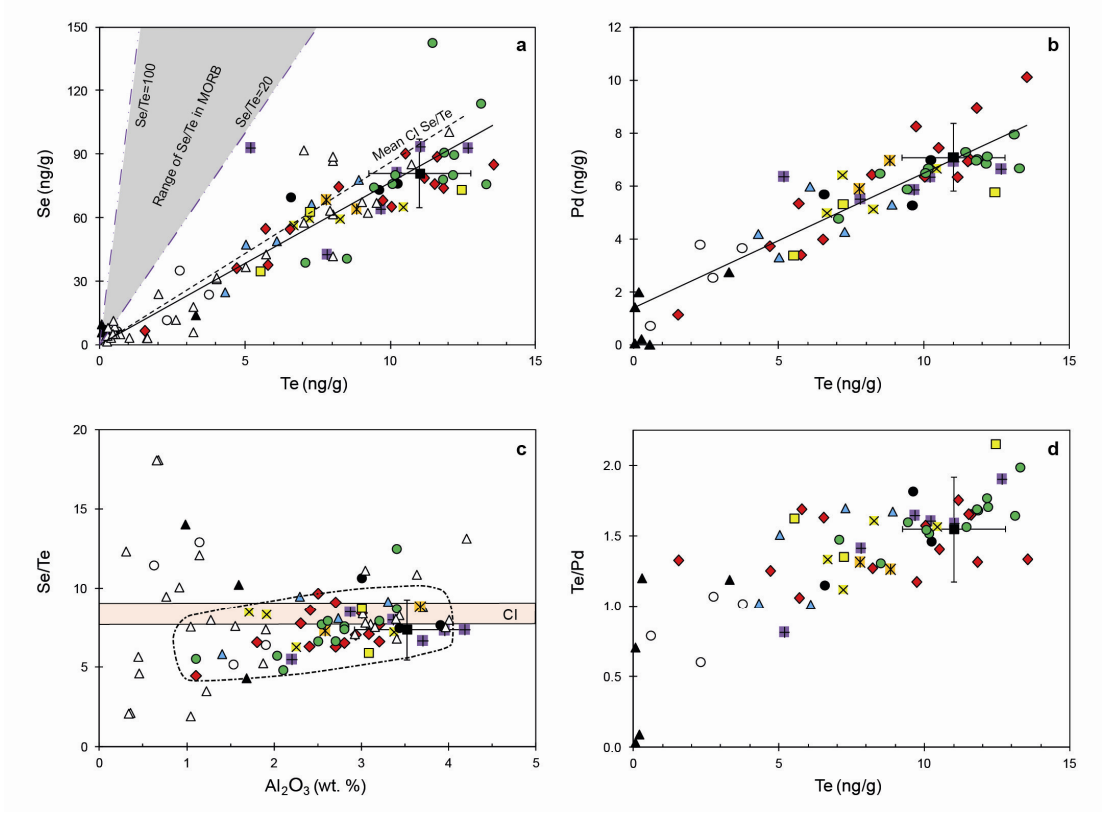

Figure 4.2 Correlations of Te with Se and Pd contents. (a, b) Tellurium displays positive correlations with Se and Pd (regression lines are solid). Dashed lines in (a) labelled Se/Te=20 and 100 reflect the range of Se/Te ratios in ocean ridge basalts (MORB) for comparison (Hertogen et al., 1980). (c) In lherzolites, Se/Te is decreasing slightly with decreasing Al_2O_3 (outlined region), but the mean value of fertile (Al_2O_3-rich) lherzolites overlaps with CI chondrite data within uncertainties (mean CI Se/Te = 8.5±0.7) (Lodders, 2003). Only few lherzolites have somewhat higher Se/Te than the CI value. As for S/Se, harzburgites display highly variable Se/Te ratios at low concentrations of these elements. (d) Te/Pd ratios decrease with decreasing Te contents, indicating that Te is more incompatible than Pd. Symbols and minimum Al_2O_3 content of BSE as in Figure 4.1. Precisions of concentrations are similar or smaller than symbol size and error bars of the BSE are 1σ.

Mantle heterogeneity only moderately affects linear correlations of S and Se with Al_2O_3 in peridotites (Figure 4.1). Thus, regressions can constrain abundances of S and Se in the BSE, provided the Al_2O_3 content of the BSE is known. A recent re-evaluation of the Al_2O_3 content of the BSE yielded 3.52±0.60 wt.% (Lyubetskaya and Korenaga, 2007), 20-30 % lower than previous estimates (4.0-4.5 wt. % Al_2O_3) (McDonough and Sun, 1995; Palme and O'Neill, 2003). The lower Al_2O_3 content yields *minimum* estimates for S and Se abundances in the BSE. The uncertainty in Al_2O_3 has negligible effects on the estimate of S/Se in the BSE (Figure 4.1, Supplementary Table S4.5). After excluding data from mantle xenoliths which have been affected by secondary processes (see Supplementary information), the lower value for Al_2O_3 in the BSE yields minimum S and Se abundances of the BSE that are

slightly lower, but still within uncertainty of previous estimates (S=211±40 µg/g and Se=80±17 ng/g, 1σ; or 0.0040±0.0008×CI chondrites) (McDonough and Sun, 1995; Palme and O'Neill, 2003). Tellurium is more compatible than Al during igneous processes in the mantle, and thus abundances display more scatter for a given Al_2O_3 content (Supplementary Figure S4.1). Te/Pd ratios in mantle peridotites decrease with decreasing Te contents, indicating that Te is more incompatible than Pd during mantle processes (Figure 4.2d). The relative sequence of empirical bulk partition coefficients of residue/melt during magmatic processes in the upper mantle is thus: $D_{Pd} > D_{Te} > D_{Se} \geq D_S \approx D_{Re} \approx D_{Al2O3}$ (Figures 4.1 and 4.2; Supplementary Figure S4.2) (Wang et al., 2013). This sequence also seems to be valid for peridotites affected by melt infiltration. Because the incompatibility of Te is between Pd and Se, upper and lower bounds of Te abundances in the BSE were obtained from regression of correlations with these elements (Te = 11.0±1.7 ng/g, 1σ, Figure 4.2 and Supplementary Tables S4.4 and S4.5) .

High metal-silicate partition coefficients during core formation at high P-T conditions indicate that the chalcogens would have been almost completely lost to the core (Rose-Weston et al., 2009). If significant amounts of chalcogen had been retained in the BSE after core formation, they would display non-chondritic ratios (Rose-Weston et al., 2009); the carbonaceous-chondrite-like ratios of the chalcogens in the BSE therefore support the late veneer as their main source. Within their uncertainties, the S/Se and Se/Te ratios of the BSE agree with values of CI chondrites (Figs 1-3 and Supplementary Tables S4.5 and S4.6), and accordingly, the late veneer must have consisted mostly of carbonaceous-chondrite-like material. The data in Figure 4.2 hint that the Se/Te ratio of the BSE may be 10 % lower than that of CI chondrites, but a difference cannot be resolved given the scatter of the data. CI-chondrite-normalized S/Ir, Se/Ir and Te/Ir ratios are similar to each other and match the volatile-element depletion trend of CM chondrites but not that of H (high-iron-type) chondrites or any other ordinary chondrite group (O'Neill, 1991; Palme and O'Neill, 2003) (Figure 4.3).

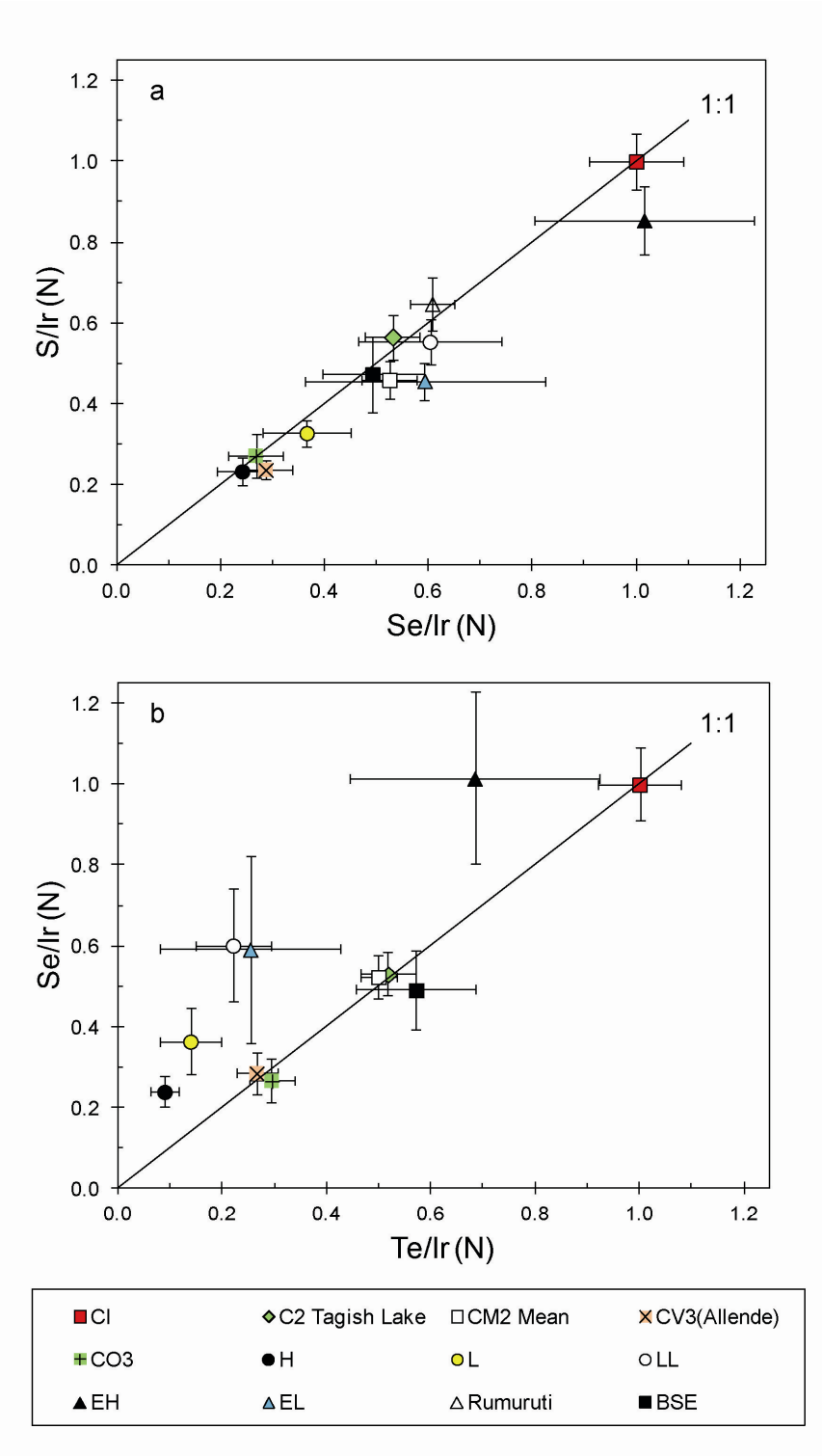

Figure 4.3 CI chondrite normalized ratios of moderately volatile chalcogens relative to the refractory highly siderophile element Ir for different groups of chondrites and the BSE (data sources see Supplementary Table S4.6). (a, b) Because of the depletion of the chalcogens relative to the HSE, the BSE has S/Ir, Se/Ir and Te/Ir ratios similar to CM carbonaceous chondrites. Ordinary and enstatite chondrites have significantly higher Se/Te or different chalcogen/HSE ratios than carbonaceous chondrites and the BSE (b). Error bars are 1σ.

The carbonaceous-chondrite-like chalcogen composition of the BSE lends further support to recent models of the composition of the late veneer based on HSE ratios in the BSE and in ancient lunar impact rocks. A mixed provenance of the late veneer with a large fraction of carbonaceous-chondrite-like material and a minor proportion of non-chondritic material-possibly differentiated meteoritic metal-could be a likely explanation (Fischer-Gödde and Becker, 2012). The minor contribution from metal that might explain the HSE systematics in the BSE may have limited effects on the chalcogens (Supplementary Information). Alternatively, relatively volatile-rich, primitive material with suprachondritic Ru/Ir and Pd/Ir ratios may explain the HSE composition of the BSE (Becker et al., 2006; Walker, 2009; Fischer-Gödde and Becker, 2012). Material with such a composition is different from known primitive meteorites.

The CM chondrite like chalcogen composition of the late veneer yields constraints on the origin and timing of delivery of highly volatile (atmophile) elements on the Earth. If all sulfur of the late veneer was delivered by comets, this would exceed most estimates of the abundances of atmophile elements in the BSE and should have resulted in significantly lower H/C ratios in the BSE (Supplementary Table S4.7). D/H and $^{15}N/^{14}N$ ratios of the Earth's surface inventory are similar to CI or CM carbonaceous chondrites, but different from solar and presumably also cometary compositions (Alexander et al., 2012; Marty, 2012). However, considerable uncertainties exist regarding the ranges of light stable isotope ratios in comets (Marty, 2012). Combined isotopic and compositional data indicate that carbonaceous chondrite like material was the most likely source of a large fraction of the Earth's noble gases, H, N, and presumably also C (Alexander et al., 2012; Marty, 2012). Conservative estimates of the abundances of water and carbon in the mantle and in surface reservoirs imply that the late veneer may be the dominant source for water and carbon in the BSE (see Supplementary discussion). On the basis of noble gas budgets and correlations, it has been suggested that the abundances of water and carbon in BSE may be as high as 1000-3000 μg/g and 500 μg/g, respectively, equivalent to 2±1 % of Earth's mass of CI or CM chondrite like material (Marty, 2012). In this case, the contribution of the late veneer to the Earth's budget of water and carbon may be only 20-50 %. If correct, these estimates require accretion of CI or CM chondrite like materials during core formation. Larger quantities of atmophile elements in the Earth's interior would be consistent with the proposed accretion of volatile bearing carbonaceous chondrite-like material near the end of accretion, as suggested by modeling of Ag isotopic data (Schönbächler et al., 2010) and heterogeneous accretion models (Rubie et al., 2011). A late veneer predominantly composed of volatile rich carbonaceous chondrite like materials then simply may reflect the tail of the late phase

of terrestrial planet accretion, as proposed by recent dynamical models (Bottke et al., 2010).

Method summary

Concentrations of S, Se, Te and HSEs in bulk rocks of peridotites and some carbonaceous chondrites (Supplementary Information) were determined by isotope dilution and inductively coupled plasma mass spectrometry (ICP-MS) using high pressure asher (HPA-S) digestion. The details have been described elsewhere (Fischer-Gödde et al., 2011; Wang et al., 2013).

About 2.5 g of peridotite powder or 50–70 mg of meteorite sample powder were digested by HPA-S in 5 ml of 14M HNO3 and 2.5 ml of 9M HCl at 100 bar and 320 ℃ for 16 h after addition of mixed ^{77}Se–^{125}Te and ^{34}S spike solutions for all samples, and a mixed ^{191}Ir–^{99}Ru–^{194}Pt–^{105}Pd spike solution for some samples to obtain duplicate data for comparison with literature values. After digestion, one third of the digestion solution was used for chemical separation of Ir, Ru, Pt and Pd as described elsewhere (Fischer-Gödde et al., 2011), and about one-quarter of the remaining solution was used for S–Se–Te separation.

The S–Se and Te fractions were obtained by separation on anion-exchange resin using 6M HCl, 9M HCl, 5M hydrofluoric acid and 1M HNO3 (Wang et al., 2013). The separated S–Se fraction was purified on cation-exchange resin using 0.1M HNO3. Sulfur measurements were performed on the S–Se fraction using a Scott-type glass spray chamber in medium-mass-resolution mode (m/Δm=4,000) on the Element XR ICP-MS at Freie Universität Berlin (Wang et al., 2013). Selenium and Te were measured in low mass-resolution mode on the Element XR, using a double-pass Scott-type glass spray chamber, combined with a hydride-generation sample-introduction system by reacting the sample solution with 1% m/m $NaBH_4$ in 0.05M NaOH (Wang et al., 2013). Procedural blanks for the chalcogens were in most cases insignificant (<1%; 3±1.5 mg S, 1.5±1 ng Se and 20±15 pg Te).

Methods

Concentrations of S, Se, Te and the HSE in bulk rocks of peridotites and some carbonaceous chondrites (Supplementary Information) were determined by isotope dilution and inductively coupled plasma mass spectrometry using HPA-S digestion. Details of the techniques have been described elsewhere (Fischer-Gödde et al., 2011; Wang et al., 2013). Additional data on duplicates of peridotites, reference materials and some carbonaceous chondrites are presented in Supplementary Tables S4.1–

S4.3. About 2.5 g of peridotite powder or 50–70 mg of meteorite sample powder were digested by HPA-S in 5 ml of 14 M HNO_3 and 2.5 ml of 9 M HCl at 100 bar and 320 °C for 16 h after addition of a mixed ^{77}Se-^{125}Te and a ^{34}S spike solution for all samples, and a mixed ^{191}Ir-^{99}Ru-^{194}Pt-^{105}Pd spike for some samples to obtain duplicate data for comparison with literature values. After digestion, one third of the digestion solution was used for HSE chemical separation (Supplementary Table S4.1) and about one-quarter of the remaining solution was used for S-Se-Te separation.

Chemical separation

A two-step anion- and cation-exchange chromatography method was used for the separation of S-Se from Te and matrix elements. The digestion solution was evaporated, repeatedly treated with 9 M HCl and dried to reduce Se and Te to the quadrivalence state. After dissolution of the residue in 4 ml of 6 M HCl, the solution was loaded on 3 ml of pre-cleaned Eichrom 1-X8 (100–200 mesh) anion resin (Fehr et al., 2004; Wang et al., 2013). Sulfur and Se and part of the matrix were collected in 7 ml of 6 M HCl. The resin was further washed with 5 ml of 5 M hydrofluoric acid and 4 ml of 9 M HCl to elute remaining matrix. Finally, Te was eluted in 7 ml of 1 M HNO_3, ready for mass spectrometric analysis. The S–Se fraction was dried at 85 °C and the residue dissolved in 4 ml of 0.1 M HNO_3. The S–Se fraction was purified on 3 ml of Eichrom 50W-X8 (100–200 mesh) cation resin and collected in 7 ml of 0.1 M HNO_3. We added 1 ml of 7 M HNO_3 to facilitate the hydride generation reaction. Sulfur and Se show high recovery (>80 %), but Te yields were variable, ranging from 10 % to >95 % depending on the composition of the matrix: they were typically around 10–40 % for peridotites, >80 % for chondrites and >95 % for procedural blanks. The low Te yield for peridotites is probably due to incomplete reduction of Te. Yields of Te can be improved by heating the S-Se fraction at 85 °C for two hours and reloading on the anion resin after washing the resin in 5 M hydrofluoric acid and 9 M HCl. Precise and accurate Te data can be obtained using the isotope dilution method and hydride generation (see details in chapters 2 and 5).

Inductively coupled plasma mass spectrometry

Sulfur isotopic measurements were performed on the S–Se fraction using a Scott-type glass spray chamber on the Element XR ICP-MS at Freie Universität Berlin in medium-mass-resolution mode ($m/\Delta m$ = 4,000). Precisions of ^{32}S/^{34}S were greater than ±0.1 % (twice the relative standard error (2 r.s.e.)) using n = 800 scans and a sample time of 10 ms. Selenium and Te were measured in low-mass-resolution mode on the Element XR, using a double-pass Scott-type glass spray chamber, combined with a hydride-generation sample-introduction system, by reacting the sample solution with 1 % m/m $NaBH_4$ in 0.05 M NaOH (Wang et al., 2013). Owing to

variations in the gas flow during hydride generation, the Se and Te intensities were not as stable as for the HSE and S, with a typical uncertainty of 3–8 % relative standard deviations (r.s.d.) for samples. Standard errors of the mean of $^{77}Se/^{82}Se$ and $^{125}Te/^{126}Te$, which were used for concentration calculation, were less than 0.1 % (2 r.s.e.) using sample times of 5 ms and n = 6,000 and 9,000 scans, respectively. $^{77}Se/^{82}Se$ and $^{125}Te/^{126}Te$ ratios of Se and Te standard solutions changed little (typically 0.1 % to <1 %) during the measurement period, leading to variations in Se and Te concentrations of <1–2 %.

Procedural blanks

The S blank was typically 3 ± 1.5 µg (1 r.s.d., n = 11; mainly from the cation resin), the Se blank was typically 1.5 ± 1 ng (1 r.s.d., n = 10) and the Te blanks were typically 20 ± 15 pg (1 r.s.d., n = 10) during the analysis period. Procedural-blank corrections for the chalcogens were always applied and were in most cases insignificant (<1 %). For depleted harzburgites, procedural blanks may comprise up to 5–25 % for S, Se and Te when using 2.5 g of sample powder.

Acknowledgements

Some peridotite and meteorite samples were provided by Shan Gao, Konrad Hammerschmidt, Jean-Pierre Lorand, Glenn MacPherson and Meenakshi Wadhwa. We thank Frank Wombacher and Claudia Funk for discussions and Monika Feth, Konrad Hammerschmidt and Marc Weynell for technical assistance. This work was supported by funds from Freie Universität Berlin and a China Scholarship Council fellowship to Z. Wang.

4.2 Supplementary Information

The supplementary information includes information on samples and analytical methods with supplementary 2 figures and 7 tables, and supplementary discussion.

4.2.1 Materials and data quality

4.2.1.1 Samples

Samples analyzed in this study are fresh post-Archean mantle peridotites from different geological settings, including massif type peridotites from Ronda, Lanzo, Beni Bousera, the External and Internal Ligurian ophiolites, Lherz (eastern Pyrenees) and Turon de Técouère (western Pyrenees). Also included are a few alkali basalt hosted xenoliths from the Eifel (Germany) and Hannuoba (China), as well as some carbonaceous chondrites and reference materials (UB-N, a serpentinized lherzolite from Alsace, and Allende, a CV3 type carbonaceous chondrite). Chalcogen element abundances in peridotites from Baldissero and Balmuccia, and Lherz samples have been previously determined (Lorand and Alard, 2010; König et al., 2012; Wang et al., 2013).

The mantle peridotites of this study have been intensively studied, especially for highly siderophile elements (HSE) and Os isotopes (Fischer-Gödde et al., 2011; Wang et al., 2013). Previous results indicate that the peridotites underwent partial melting processes and possible subsequent different degree melt infiltration by reactive infiltration of silicate melts and variable Os isotopic equilibration. For selected peridotites, HSE data were obtained together with S, Se and Te on the same sample aliquot. The HSE results show excellent reproducibility with previous data obtained on the same sample powder (Becker et al., 2006; Fischer-Gödde et al., 2011) (mostly <5 %, Table S4.1). Thus, we used literature HSE data (Fischer-Gödde et al., 2011) obtained on the same sample powders for the comparison of HSE, S, Se and Te data (Table S4.2).

4.2.1.2 Evaluation of data quality

The accuracy and reproducibility of HSE, Se and Te abundance measurements have been discussed elsewhere (Fischer-Gödde et al., 2011; Wang et al., 2013), using the Allende CV3 chondrite standard powder and the CI chondrite Orgueil, the reference material UB-N, and sample duplicates and reanalysis of aqua regia digestion solutions from same digestion. Here, we present further duplicates of samples and

reanalysis of aqua regia digestion solutions, and new data on some carbonaceous chondrites (Tables S4.2 and S4.3). Multiple analysis of the S concentration in aqua regia solution from the same digestion (Table S4.2, column a and b) yielded good reproducibility within 0.5-2 %. Analysis of sample duplicates also produced <5 % variations for S. Duplicates of the reference material UB-N also yield reproducible results (Table S4.3). Importantly, sulfur data of most samples from Turon de Técouère are within 5 % of other data using high temperature combustion (Fischer-Gödde et al., 2011). Some samples, however, show larger variations in S abundances (>5-30 %), probably due to heterogeneously distributed sulfides. For Se and Te, UB-N, Murchison duplicates and other carbonaceous chondrites also display good reproducibility within a few percent (Table S4.3). A few cases of large abundance variations for Se and Te in peridotite duplicates are probably because of heterogeneous sample powders.

4.2.2 Supplementary discussion

4.2.2.1 Behavior of S, Se, Te and Pd in mantle peridotites

Linear correlations between S, Se, Te and Al_2O_3 in mantle peridotites have been recorded in previous studies (Morgan, 1986; Lorand and Alard, 2010; Wang et al., 2013) and the new data confirm the general relevance of such correlations (Figures 4.1 and 4.2). According to these data, the chalcogen elements are mildly incompatible during depletion of mantle peridotites. In mantle rocks, S, Se, Te and Pd are dominantly controlled by accessory sulfides and their breakdown products (Luguet et al., 2004; Lorand and Alard, 2010), and their relative incompatibility is slightly different. In different lherzolite suites, S and Se display linear correlations of slightly different slope. For instance, S/Se of Lherz and Baldissero peridotites is slightly higher than for peridotites from Balmuccia (Figure 4.1c). This can be explained if sulfur is slightly more incompatible than Se during igneous processes in the mantle (Wang et al., 2013), and is supported by data on ocean ridge basalts (MORB) (Peach et al., 1990; Jenner et al., 2010; Jenner and O'Neill, 2012). Mean S/Se ratios of MORB are 3230±560 (1σ, n=279) (Jenner and O'Neill, 2012), only slightly higher than the mean obtained here for mantle rocks. S/Se in MORB tend to increase slightly with fractional crystallization of MORB (Jenner et al., 2012).

Se/Te ratios in mantle peridotites slightly decrease with decreasing Al_2O_3 contents, which is used as indicator of mantle depletion, implying that Se is slightly more incompatible than Te during partial melting (Wang et al., 2013) (Figure 4.2c). This is consistent with experimental results of $D^{sulfide\text{-}silicate}$ for Se and Te(Choi and Cho, 1997; Brenan and McDonogh, 2006). The strong fractionation of Se from Te

with very high and variable Se/Te in MORB relative to mantle peridotites (Hertogen et al., 1980; Yi et al., 2000; Jenner and O'Neill, 2012) indicates the importance of additional fractionation processes after melt extraction in the mantle. Te/Pd ratios in peridotites decrease with decreasing Te contents, indicating that Te is more incompatible than Pd (Wang et al., 2013) (Figure 4.2d). The relative sequence of empirical bulk partition coefficients of residue/melt during magmatic processes in the upper mantle is thus: $D_{Pd} > D_{Te} > D_{Se} \geq D_S$ (Figures 4.1 and 4.2). Melt infiltration and refertilization of peridotites involve co-precipitation of grain boundary sulfides with pyroxenes and spinels from infiltrating melts (Le Roux et al., 2007; Lorand and Alard, 2010). These processes appear to have very similar effects on abundances of S, Se and Te as open system melting (Wang et al., 2013). Therefore, the mean S/Se and Se/Te of unaltered mantle peridotites from different geological settings should provide a reasonable estimate of these ratios in the BSE. The small difference of S/Se in average MORB, compared to the mean values of lherzolites, and nearly identical S/Se in primitive MORB and lherzolites strongly support the conclusions from the peridotite data (Jenner and O'Neill, 2012; Jenner et al., 2012). The scatter in element abundances and ratios between different suites of fertile lherzolites likely reflects different extents of magmatic re-equilibration of mantle domains during melt migration and open-system partial melting.

4.2.2.2 Al_2O_3 content of the BSE and its effect on mantle abundances of the chalcogens

Most previous estimates of the Al_2O_3 content of the BSE have been in the range between 4.0 and 4.5 wt. % (e.g., 4.45±0.44 wt.% (McDonough and Sun, 1995) or 4.51±0.36 wt.% (Palme and O'Neill, 2003)). A recent statistical evaluation of essentially the same peridotite data base has yielded a significantly lower value of 3.52±0.60 wt.% (Lyubetskaya and Korenaga, 2007). Which value will be used, the low or the high estimate, will slightly influence estimates of concentrations of elements such as S and Se in the BSE that correlate with Al. Abundances of Al, Ca, S and other mildly incompatible elements in the depleted mantle should be nearly identical with the BSE when considering the mass balance of bulk mantle and crust. For instance, the average Al_2O_3 content of the crust is 15-16 wt.% (Rudnick and Gao, 2003), but the crustal budget hardly changes the Al_2O_3 content of the BSE, because the crust accounts for only 0.5 wt.% of the mantle. Mantle convection and particularly melt infiltration may produce a statistically valid sample representative of a homogeneous bulk mantle, but efficiencies of these processes are unknown, and thus uncertainties difficult to quantify. Out of more than 1700 samples of mantle peridotites, only 5 % have Al_2O_3 contents of more than 4.0 wt.% (Canil, 2004). Some samples that have very fertile compositions likely reflect melt infiltration, as for

instance at Lherz (Le Roux et al., 2007). Thus, the abundance of Al_2O_3 in the BSE (Lyubetskaya and Korenaga, 2007), likely carries an uncertainty of 20-30 %. Here we use lower and upper bounds for Al_2O_3 contents in the BSE for calculation of the concentrations of S, Se and Te in BSE (Tables S4.4 and S4.5). The correct choice of the Al_2O_3 content of the BSE will affect absolute abundances of S and Se when relying on linear correlations of S and Se with Al_2O_3, but the S/Se ratio of lherzolites does not change as a function of Al_2O_3 content (Figure 4.1, Table S4.5). In spite of these limitations, the 20-30 % uncertainty of the Al_2O_3 content of the BSE only translates into a similar uncertainty of the extent of volatile depletion of the late veneer but does not change the picture of accretion of a volatile rich late veneer. The lower Al_2O_3 content yields minimum estimates for S and Se (and indirectly Te) abundances in the BSE, implying a late veneer at least as volatile rich as CM carbonaceous chondrites. Higher Al_2O_3 values would lead to 20-30 % higher volatile element abundances in the late veneer, but still more similar to CM than to CI carbonaceous chondrites.

4.2.2.3 Preference of peridotite tectonites over xenoliths or data on mantle sulfides for estimates of the abundances of the chalcogens in the mantle

The focus of the present study has been on peridotite massifs with compositions ranging from fertile lherzolites to depleted harzburgites. Peridotite xenoliths were largely avoided, because previous studies indicate that mantle xenoliths often have been affected by complex secondary processes that have changed abundances of chalcogens and the HSE. These processes may include cryptic metasomatism, assimilation and infiltration by melts/fluids and supergene weathering (Lorand, 1990; Lorand et al., 2003; Pearson et al., 2004; Reisberg et al., 2005; Ackerman et al., 2009; Lorand and Alard, 2010; Fischer-Gödde et al., 2011). Previous studies show that these processes can lead to significant S loss (in most cases) or enrichment, and fractionation of S/Se (Lorand, 1990; Handler et al., 1999; Lorand et al., 2003; Lorand and Alard, 2010, 2011; Alard et al., 2011). This is probably why many mantle xenoliths commonly have highly variable S/Se ratios and low S and Se contents compared with samples from peridotite massifs (Lorand et al., 2003; Alard et al., 2011). For instance, xenoliths from the Eifel in this study have much lower S and Se contents than massif type peridotites with similar Al_2O_3 contents (Figure 4.1). The Eifel samples are also less depleted than harzburgites from Lherz according to Al_2O_3 contents, but have similar or even lower S and Se contents (Figure 4.1). Eifel xenoliths underwent recent modification by metasomatic fluids and/or melts and their S and Se contents are likely to have been affected by such processes, as indicated by their HSE data (Schmidt et al., 2003; Fischer-Gödde et al., 2011). Lherzolite xenoliths from the SW USA and other locales in the pioneering work by Morgan

(1986) have noticeably lower Se/Te (0.5-6.8, most near 3) and a larger range in S/Se (2800-7000) than massif type peridotites. Besides lower precision and accuracy of the Se and Te data obtained by radiochemical neutron activation, the unusually low S in some of these samples and low abundances of the HSE may reflect the above mentioned fluid or late-stage alteration processes (Becker et al., 2006; Fischer-Gödde et al., 2011). We emphasize, as others did before, that because of these complications and their effects on chalcogen and HSE ratios, xenolith data must be viewed with caution. Not all peridotite xenoliths have been affected by such processes. For instance, the xenoliths from Hannuoba (China), which are included in the present study, display HSE (Gao et al., 2002) and chalcogen variations indistinguishable from those in peridotite massifs. For the reasons noted above, we used linear regressions based predominantly on massif peridotites for mantle abundance estimates of chalcogens.

The quality of the analytical data and methods used also has an influence on the scatter of the data. For instance, S/Se ratios determined by Garuti et al. (1984) on samples from the Ivrea zone are considerably lower than data obtained by isotope dilution on samples from the same peridotite bodies(Wang et al., 2013), likely reflecting inaccurate Se concentrations in the former study. Because the chalcogens are hosted by trace sulfide phases, heterogeneous distribution and settling in sample powders may add to scatter in concentration data (‘nugget effect’). The advantage of the present data set is that all three elements were determined in the same digestion aliquot, thus limiting the nugget effect, and related analytical scatter, which is likely if S, Se and Te were determined by different methods/aliquots as in some previous work (e.g., Lorand and Alard, 2010; König et al., 2012) and differences of sulfur contents between compiled and our new isotope dilution data in Table S4.2). Concentration data of S, Se and Te determined for sulfides in mantle rocks were not included in regressions, because of the relatively large uncertainties of Se and particularly Te data and the possibility of bias from sulfide exsolution and element redistribution during cooling. For instance, some mantle sulfides from peridotitic mantle xenoliths (Hattori et al., 2002) and sulfide inclusions in diamond (Bulanova et al., 1996) are characterized by low Se/Te (2-10); whereas laser ablation-ICPMS data on sulfides from Ligurian peridotites and from the Lherz peridotite massif indicate much higher Se/Te than the CI ratio (e.g., mostly >10-50) (Luguet et al., 2004; Lorand and Alard, 2010). Some Te may not reside in sulfides, but in discrete microphases that have exsolved from Cu–Ni-rich sulfide melts during cooling (Luguet et al., 2004; Lorand and Alard, 2010; Lorand et al., 2010). Regressions were calculated for data without and with literature peridotite data from Lherz (Lorand and Alard, 2010; König et al., 2012) (method a and b in Table S4.4, respectively). Both regressions yield nearly

identical results, indicating that melt infiltration and mantle heterogeneity produce systematic variations that are, for mildly incompatible elements, on average indistinguishable from partial melting processes (see also the detailed discussion of these processes and their influence on HSE and chalcogens elsewhere (Wang et al., 2013)).

4.2.2.4 Composition of the late veneer

The volatile element composition of the late veneer is best constrained by volatile elements such as Se and Te, which also behave very siderophile during core formation at high P-T conditions (Rose-Weston et al., 2009). Rose-Weston et al. (2009) have shown that during metal-silicate partitioning at high P-T conditions, $D_{Se}^{metal\text{-}silicate}$ (>10^4) and $D_{Te}^{metal\text{-}silicate}$ (>10^5) will be high enough so that the mantle after core formation should be strongly depleted in Se and Te if core-mantle equilibration was achieved (Rose-Weston et al., 2009). However, $D_S^{metal\text{-}silicate}$ should have been lower than Se and Te, which might have lead to retention of minor sulfur in the mantle before arrival of the late veneer. If we assume metal-silicate equilibrium, $D_S^{metal\text{-}silicate}$ = 700-800 during the final stages of core formation (Rose-Weston et al., 2009), and a maximum sulfur content in the core of 1.7 wt. % (Dreibus and Palme, 1996), the mantle would retain about 20-25 µg/g sulfur. This minor sulfur retention is about 10 % of the sulfur in the BSE and within uncertainty of the S/Se of the BSE (±27 %), as determined in the present work. The observed abundances and ratios of S, Se and Te in the BSE are notably different from abundances and ratios expected from high P-T experimantl results (Rose-Weston et al., 2009), thus requiring a late veneer.

The BSE value of S/Se is within error of the limited range in chondrites. Se/Te in BSE is matching the value of carbonaceous chondrites, irrespectively of the degree of volatile depletion of the C chondrite group, but is lower than values in ordinary and enstatite chondrites (Figure 4.3, Table S4.6). Because of the uncertainty of the BSE value (Se/Te=7.9±1.6, 1σ), it is difficult to precisely estimating the maximum fraction of ordinary and enstatite chondrite like material in a late veneer of mixed provenance. For a Se/Te in the BSE of less than 9.5 (upper bound of Se/Te of the BSE), and assuming a mixture of CI or CM chondrites with different proportions of ordinary or enstatite chondrites, less than 20 % mass of the late veneer may be derived from ordinary or enstatite chondrite like material (calculated using data from Table S4.6). Thus the CI chondritic S/Se and Se/Te of BSE and chalcogen/HSE fractionation indicated in this study, support carbonaceous chondrite like material at least as volatile rich as CM chondrites as dominant composition of the late veneer.

At first glance, these results might seem to contradict conclusions derived from the Os isotopic composition of chondrites and the BSE. It is well known that

$^{187}Os/^{188}Os$ (0.1296±0.0008) (Meisel et al., 2001b), reflecting time integrated Re/Os in the BSE is more similar to anhydrous ordinary (0.127 to 0.133) and enstatite (0.1281±0.0004) chondrites rather than carbonaceous chondrites (0.1262±0.0006) (Walker et al., 2002; Horan et al., 2003; Fischer-Gödde et al., 2010). These differences in isotopic ratios are matched by an about 8 % lower measured Re/Os concentration ratio of carbonaceous chondrites compared to average ordinary and enstatite chondrites (Horan et al., 2003). $^{186}Os/^{188}Os$ of the Earth's mantle (reflecting time integrated Pt/Os) are also indistinguishable from H-group ordinary and some enstatite chondrites (Brandon et al., 2006). For a while, these data were the strongest evidence for anhydrous ordinary or enstatite chondrites as dominant composition of the late veneer. However, the BSE is also characterized by suprachondritic Ru/Ir (30 % excess relative to CI normalized abundances of Ir) and Pd/Ir (40-50 % excess relative to CI chondrites) (Becker et al., 2006). These data are difficult to explain by chondritic late veneer models or metal-silicate segregation at high P-T conditions (Mann et al., 2012). Hence, additional processes or somewhat different refractory element compositions of the late veneer compared to known chondrites are required (Becker et al., 2006; Walker, 2009; Mann et al., 2012). Some indications indeed exist. The ungrouped volatile rich Tagish Lake carbonaceous chondrite has somewhat higher Ru/Ir (1.63±0.08) and $^{187}Os/^{188}Os$ (0.12564-0.12802) compared to other carbonaceous chondrites and hints at possible HSE fractionations in primitive meteorites beyond of what is known from most chondrites (Brandon et al., 2005). Refractory element depleted CAIs (those with "Group II" rare earth element patterns) in carbonaceous chondrites display systematically high $^{187}Os/^{188}Os$ of up to 0.138, which reflects Re/Os fractionation 4.56 b. y. ago (Becker et al., 2001b). These "suprachondritic" ratios in components of chondrites may reflect very early fractional condensation of components in primitive meteorites (Walker et al., 2002; Horan et al., 2003; Fischer-Gödde et al., 2010). Thus, it cannot be taken for granted that the compositional range of refractory elements in known bulk chondritic material covers the complete spectrum of compositions. Modest deviations should not be surprising.

Recent HSE data from ancient (> 3.8 Ga) lunar impact rocks display slightly suprachondritic $^{187}Os/^{188}Os$, Pd/Ir, Ru/Ir that are similar to those in the BSE (Norman et al., 2002; Puchtel et al., 2008; Fischer-Gödde and Becker, 2012). At least some prevalent meteoritic components in lunar impact rocks are chemically distinct from known chondrite types (Puchtel et al., 2008) and some have compositions similar to non-chondritic differentiated metal (Fischer-Gödde and Becker, 2012). On the basis of the lunar impact rock data, Fischer-Gödde and Becker (2012) have proposed that a carbonaceous chondrite like late veneer (>75 %) with a minor contribution from a differentiated component (<25 %, e.g., iron meteorites) might explain the HSE

composition of the BSE (Fischer-Gödde and Becker, 2012). Currently, no data on all three chalcogen elements in iron meteorites have been reported, so it is unclear what the effects of such mixing processes on the chalcogens will be. Tellurium (presumably also Se) seems to be predominantly enriched in sulfides, as is indicated by 12.1 µg/g Te in sulfides versus 0.18 µg/g Te in metal of the Canyon Diablo iron meteorite (Fehr et al., 2005). The S content in metal is also at trace level (<0.05 wt. %) in comparison to 36 wt.% S in meteoritic sulfides (D'Orazio et al., 2009). Canyon Diablo troilite has roughly CI chondritic S/Se and Se/Te of 3000 and 9.8, respectively (120 µg/g Se (Sutton et al., 1986) and 12.2±0.4 µg/g Te (Fehr et al., 2005), assuming S =36.1 wt. %, similar to troilite in the Sahara 03505 sulfide-rich iron meteorite (D'Orazio et al., 2009)). Thus, S, Se and Te may be predominantly enriched in sulfides. Therefore, minor contributions from differentiated meteoritic metal that were proposed to explain the HSE systematics in the BSE may have limited effects on the chalcogens.

4.2.2.5 Contribution of the late veneer to the water and carbon budget in the BSE

Ratios of highly volatile elements, such as hydrogen (in water), carbon, and noble gases (with the exception of Xe) may be similar to ratios in carbonaceous chondrites, although uncertainties on the abundances of some of these elements in the BSE are large (Marty, 2012). Besides D/H and $^{15}N/^{14}N$ ratios of the Earth's surface inventory (Alexander et al., 2012; Marty, 2012), the Kr and Xe isotopic composition of mantle-derived materials also indicate that the Earth acquired volatiles from materials similar to average carbonaceous chondrites (Holland et al., 2009). If a late veneer of 0.5 % of Earth's mass contains 3-3.5 wt.% sulfur, 10±2 (1σ) wt.% water, 1.9±0.6 (1σ) wt.% carbon and 0.10±0.04 (1σ) wt.% nitrogen, similar to average CM chondrites (Dreibus et al., 1995; Alexander et al., 2012), the maximum water, carbon and nitrogen in the BSE derived from the late veneer should be 600-800 µg/g, 100-150 µg/g and 6-10 µg/g, respectively, assuming ratios of S, H_2O, C and N as in carbonaceous chondrites (Table S4.7). The value for water is consistent with the sum of 150±50 µg/g for the depleted mantle (Saal et al., 2002; Marty, 2012) and 400 µg/g for near-surface reservoirs (total 1.6×10^{24}g water in 4×10^{27}g bulk silicate Earth, including the crust, oceans and atmosphere) (Hirschmann and Dasgupta, 2009). The delivered amount of carbon is likely to exceed the minimum estimates of 20±8 µg/g for depleted mantle (Marty, 2012) and 25±3 µg/g for the less well-constrained surface reservoirs ($9.3\pm0.9\times10^{22}$g) (Hirschmann and Dasgupta, 2009). Nitrogen from the late veneer also exceeds its budget from the current abundance estimate in the BSE (1.9±0.7 µg/g) (Marty and Dauphas, 2003). The apparent depletion of carbon and nitrogen in the BSE relative to other volatiles may reflect degassing after impact, or the difficulties in obtaining accurate estimates in the mantle, for instance because of trapping of nitrogen in the mantle (Marty, 2012). These estimates show that the late

veneer may have supplied most of the atmophile elements in the BSE, if no significant loss of highly volatile elements occurred during accretion of the late veneer. However, on the basis of noble gas budgets and correlations with carbon, the abundances of water and carbon in the BSE may be as high as 1000-3000 μg/g and 500 μg/g (Marty, 2012), provided losses during accretion were small. This would require considerable accretion (up to 2 % of Earth's mass) of CI or CM chondrite like materials before core formation was completed. Consequently, a CM chondrite like late veneer may have supplied at least 20 % to 100 % of the budget of these elements in the BSE, depending on the accuracy of estimates of water and carbon in the BSE. If the late veneer was delivered by comets similar in composition to Comet Halley, the amounts of water, carbon and nitrogen would significantly exceed the budget of these volatiles in the BSE (Table S4.7).

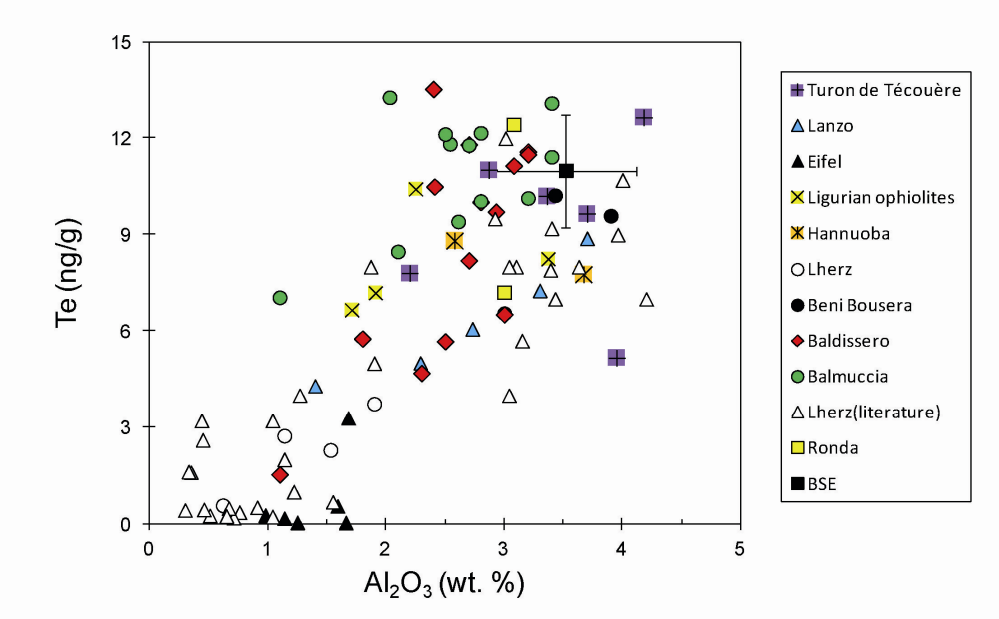

Figure S4.1 Correlation of Te with Al_2O_3 contents. This displays broadly positive relationship with larger variation than S-Al_2O_3 and Se-Al_2O_3 correlations (Figure 4.1). Lherz literature data are from (Lorand and Alard, 2010; König et al., 2012). Errors are similar to or smaller than symbol sizes.

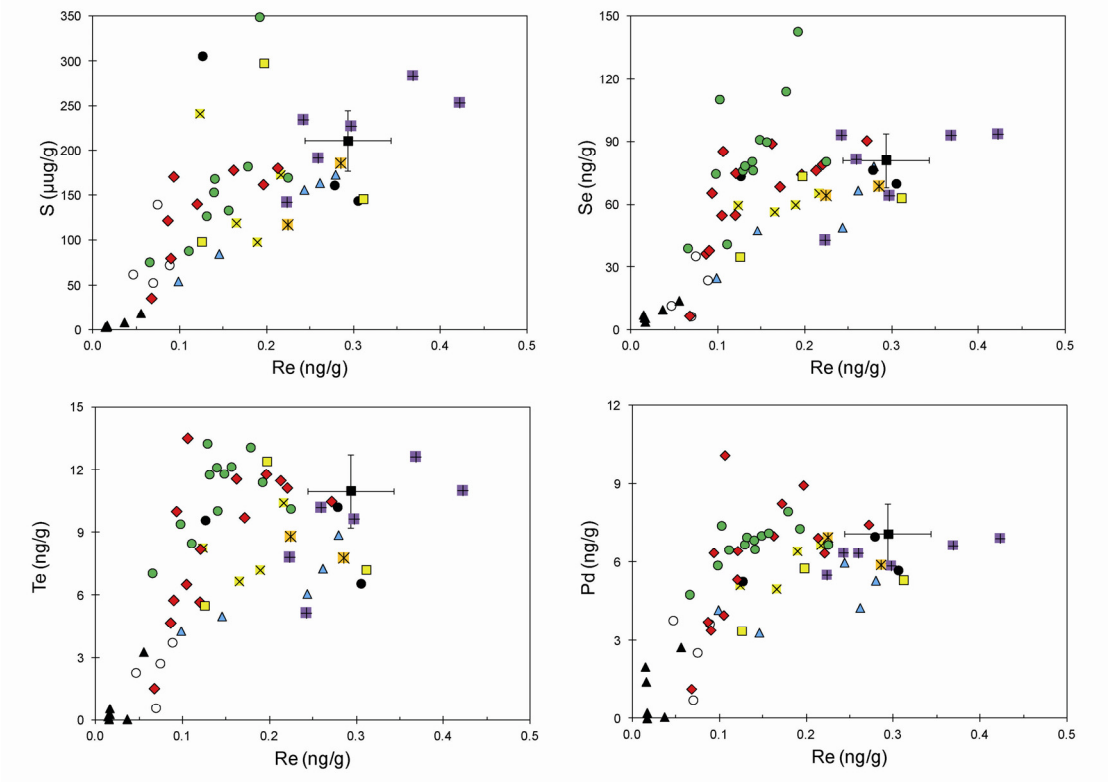

Figure S4.2 Correlations of Re with chalcogens and Pd. Sulfur and Re display a broad linear correlation. The abundances in the BSE are based on a minimum estimate for Al_2O_3 in the BSE (Lyubetskaya and Korenaga, 2007) of 3.52±0.60 wt.% and thus should be considered as minimum estimates. Symbols as Figure S4.1, errors within symbols and error bars of the BSE is 1σ.

4.2.3 Supplementary Tables

Table S4.1 Comparison of HSE results of duplicates analyzed in this study

Samples	Ir	Ru	Rh	Pt	Pd
	ng/g	ng/g	ng/g	ng/g	ng/g
TUR 7 Replicate	3.30	6.53	1.12	7.28	6.65
TUR7[a]	3.23	6.56	1.12	7.51	6.60
TUR7[b]	3.59	7.22		7.20	6.54
TUR 14 Replicate	3.24	6.63	1.14	6.93	6.36
TUR 14 [a]	3.11	6.37	1.21	7.06	6.22
TUR 14 [b]	3.26	6.82		6.90	6.35
TUR 16 Replicate	4.23	8.68	1.49	6.50	5.52
TUR 16 [a]	4.23	8.96	1.19	6.55	5.59
TUR 16 [b]	4.38	8.62		6.49	5.25
TUR 23 Replicate	3.10	6.25	1.08	6.51	5.87
TUR 23 [a]	3.19	6.44	1.16	6.60	5.91
TUR 23 [b]	3.07	6.10		6.39	5.62
71-325 Replicate	4.08	5.81	1.00	4.54	0.73
71-325 [a]	3.96	7.07	1.03	5.04	0.72
UB-N Replicate	3.14	6.33	1.09	7.08	5.79
UB-N [a]	3.16	6.43	1.10	7.31	5.85
DM59 Replicate	4.16	8.09	1.38	8.58	6.97
DMP59 [a]	4.09	7.98	1.43	8.46	6.60
DM60 Replicate	3.45	6.82	1.17	7.61	5.91
DMP60 [a]	3.50	6.79	1.19	7.27	6.00
DMP60 [b]	3.59	7.24		7.31	6.21
L217 Replicate	3.47	6.72	1.15	6.24	5.31
L217 [a]	3.29	6.48	1.11	5.79	5.18
L217 [b]	3.59	7.28		5.83	5.38
BB3A Replicate	3.53	7.57	1.30	6.70	5.70
BB3A [a]	3.42	7.10	1.22	6.69	5.56
BB2G Replicate	4.27	8.39	1.44	8.68	7.00
BB2G [a]	3.99	8.02	1.38	8.62	6.72
IL1 Replicate	4.15	8.76	1.50	7.50	6.42
IL 1 [a]	4.12	8.68	1.32	7.01	6.45

Note: Replicate data from this study show good reproducibility (mostly <5 %, a from (Fischer-Gödde et al., 2011), b from (Becker et al., 2006)). Data sets were measured by isotope dilution ICPMS after HPA-S digestion in this study and (Fischer-Gödde et al., 2011) or high temperature digestion (345 °C) (Becker et al., 2006).

Table S4.2 New and compiled HSE, S, Se and Te concentration data of mantle peridotites

	Al_2O_3	Re	Os	Ir	Ru	Rh	Pt	Pd	Au	S (µg/g)				Se	Te	S/Se	Se/Te
	(w.t.%)	ng/g	ng/g	ng/g	ng/g	ng/g	ng/g	ng/g	ng/g	a	b	average	c	ng/g	ng/g		
TUR 7	4.2	0.37	3.73	3.30	6.53	1.12	7.28	6.65	1.59	281	287	284	270	93.0	12.7	3053	7.4
TUR 14	4.0	0.24	3.45	3.24	6.63	1.14	6.93	6.36	1.71	234	235	234	240	99.2	13.4	2363	7.4
TUR14*										239	234	236		90.7	5.17	2606	17.5
TUR 16	2.2	0.22	4.93	4.23	8.68	1.49	6.50	5.52	0.83	141	145	143	140	42.8	7.80	3329	5.5
TUR 23	3.7	0.30	3.58	3.10	6.25	1.08	6.51	5.87	1.34	224	231	227	220	64.2	9.65	3542	6.7
TUR11	3.4	0.26	4.32	3.94	7.89	1.19	7.74	6.35	1.01	193	190	192	190	81.4	10.2	2353	8.0
TUR11*											198	198		83.7	11.8	2369	7.1
TUR21	2.9	0.42	4.43	3.98	7.62	1.52	8.20	6.93	2.24	253	254	254	155	93.6	11.0	2709	8.5
LZ71-325	0.6	0.07	4.98	4.08	5.81	1.00	4.54	0.73	0.28		52.9	52.9	5	6.6	0.58	8015	11.4
LZ82-4	1.1	0.07	4.72	3.53	5.96	0.95	4.82	2.55	0.47		140	140	80	35.3	2.73	3966	12.9
LZ71-107	1.9	0.09	4.88	4.45	7.48	1.56	6.19	3.67	1.49	71.4	72.4	71.9	158	23.9	3.74	3008	6.4
LZ71-322	1.5	0.05	4.03	4.45	7.82	1.32	6.42	3.80	0.47	61.0	62.2	61.6	56	11.8	2.29	5220	5.2
DM59	2.6	0.22	4.45	4.16	8.09	1.38	8.58	6.97	1.16		118	118	200	64.3	8.82	1830	7.3
DM60	3.7	0.29	3.79	3.45	6.82	1.17	7.61	5.91	2.16		186	186	320	68.6	7.77	2706	8.8
BB3A	3.0	0.31	3.90	3.53	7.57	1.30	6.70	5.70	0.78		144	144	100	69.8	6.56	2063	10.6
BB3A *										152	150	151		77.5	9.13	1947	8.5
BB2G	3.4	0.28	4.49	4.27	8.39	1.44	8.68	7.00	0.99		161	161	114	76.3	10.2	2111	7.5
BB2C	3.9	0.13	3.28	2.96	5.97	1.04	6.42	5.28	0.80	305	307	306	407	73.4	9.59	4169	7.7
BB2C*											306	306		86.7	10.6	3534	8.2
EL1	3.4	0.12	3.66	3.21	6.51	1.09	6.47	5.13	0.74	246	236	241	315	59.5	8.25	4052	7.2
EL1*											242	242		77.7	10.0	3120	7.7
IL1	1.9	0.19	4.83	4.15	8.76	1.50	7.50	6.42	0.77		97.6	97.6	88	59.8	7.19	1632	8.3
IL2	1.7	0.17	3.23	2.86	5.87	0.87	6.70	4.99	0.72		119	119	104	56.4	6.66	2117	8.5
IL3	2.3	0.22	4.00	3.23	7.17	1.20	6.89	6.66	0.91		173	173	228	65.2	10.4	2647	6.3
L52	1.4	0.10	3.65	2.75	6.56	0.75	5.38	4.20	0.58		54.6	54.6	80	25.0	4.29	2184	5.8
L213	3.3	0.26	3.25	2.54	5.00	0.79	5.05	4.28	0.84	162	165	164	200	66.6	7.26	2459	9.2
L215	2.7	0.24	3.67	2.23	5.85	1.19	8.27	5.99	0.83	157	155	156	215	49.1	6.07	3181	8.1
L216	2.3	0.15	3.41	2.61	5.63	0.91	4.67	3.32	0.38	84.6	85.1	84.9	100	47.5	5.01	1787	9.5
L217	3.7	0.28	3.90	3.47	6.72	1.15	6.24	5.31	0.85	168	178	173	210	78.1	8.89	2214	8.8
RO126	3.0	0.31	3.91	3.34	6.65	1.20	7.25	5.33	0.89		146	146	160	63.0	7.21	2321	8.7
RO307	3.1	0.20	3.49	3.27	6.25	1.06	6.71	5.78	0.60	296	301	298		73.3	12.4	4068	5.9
RO310		0.13	5.10	4.14	9.11	1.54	4.58	3.39	0.30		98.1	98.1		34.9	3.36	2811	10.4
LeyX1	1.1	0.01	3.13	2.70	6.42	0.80	4.46	2.00	0.05	3.3	3.7	3.5	< 50	7.3	0.18	480	40.6
LeyX2	1.7	0.06	2.25	2.40	5.25	0.75	3.93	2.76	0.25	19.0	18.8	18.9	< 50	14.2	3.28	1331	4.3
LeyX3	1.6	0.02	0.30	0.18	2.88	0.23	0.17	0.02	0.04	5.2	5.1	5.1	< 50	5.7	0.56	895	10.2
LeyX4	1.3	0.02	3.16	2.43	5.68	0.67	4.05	1.44	0.04	2.8	3.5	3.2	< 50	6.1	0.05	525	122
Ley1-06	1.7	0.04	0.11	0.14	1.39	0.11	0.16	0.07	0.11		8.6	8.6	< 50	9.9	0.05	868	198
Ley1-08	1.0	0.02	3.26	2.67	6.74	0.66	2.75	0.23	0.05		4.0	4.0	< 50	3.9	0.28	1026	13.9
BD-13	3.1	0.22	4.35	3.65	7.37	1.22	6.91	6.35	0.65					79.0	11.2		7.1
BD-16	2.4	0.27	4.26	3.70	7.41	1.37	7.61	7.46	1.26					90.5	10.5		8.6
BD-17	1.1	0.07	3.68	2.50	6.19	1.06	4.45	1.16	0.22	35.8		35.8		6.8	1.53	5265	4.5
BD90-3	2.9	0.17	4.43	3.92	7.86	1.38	10.5	8.26	1.27					68.4	9.72		7.0
BD90-9	3.0	0.10	3.60	3.16	6.90	1.07	5.27	4.00	0.66					54.8	6.52		8.4
BD90-4	2.4	0.11	4.03	3.64	7.21	1.25	8.09	10.12	1.91					85.3	13.5		6.3
BD90-10	2.7	0.12	4.48	4.13	8.18	1.41	7.88	6.44	0.99					74.8	8.20		9.1
BD11-07	2.8	0.09	3.66	3.49	7.45	1.28	6.50	6.36	0.61	171	170	171		65.4	10.0	2609	6.5
BD11-12	2.3	0.09	3.10	2.83	5.73	0.99	4.84	3.74	0.10	124	120	122		36.4	4.69	3359	7.8
BD11-13	2.5	0.12	4.03	3.26	7.25	1.24	6.93	5.35	0.27	143	138	141		55.0	5.68	2555	9.7
BD92-2	1.8	0.09	3.55	3.02	6.88	1.18	4.33	3.41	0.32	81.4	78.3	79.9		37.9	5.77	2106	6.6
BD11-01	2.7	0.20	4.05	3.91	8.03	1.37	10.9	8.96	1.09	162	162	162		74.2	11.8	2182	6.3
BD11-05	3.2	0.16	3.32	3.33	6.39	1.10	7.66	7.02	0.76	178	177	178		89.0	11.6	1999	7.7
BD11-08	3.2	0.21	3.90	3.82	7.52	1.29	8.12	6.95	0.81	180		180		76.1	11.5	2366	6.6
BM90-5	2.0	0.13	3.99	3.74	7.53	1.30	8.10	6.68	1.01					76.0	13.3		5.7
BM90-25	2.5	0.15	4.10	3.46	6.91	1.33	8.33	7.03	1.19					91.0	11.8		7.7
BM90-41	2.6	0.10	3.70	3.31	6.26	1.02	6.91	5.89	0.80					74.5	9.41		7.9
BM90-15	2.8	0.10	4.22	3.83	7.97	1.36	8.71	7.42	1.25					110	20.5		5.4
BM11-11	2.1	0.11	4.06	4.00	8.10	1.39	10.58	6.48	0.45	88.2	88.1	88.1		40.9	8.48	2154	4.8
BM-09	3.4	0.18	4.13	3.97	8.02	1.37	8.84	7.96	1.07	182		182		114	13.1	1595	8.7
BM11-08	3.2	0.22	4.28	3.93	7.45	1.27	8.46	6.68	1.11	170		170		80.4	10.1	2111	7.9
BM11-09	2.7	0.13	4.02	3.92	7.80	1.33	9.33	6.97	0.76	127		127		78.2	11.8	1627	6.6
BM11-03B	1.1	0.07	3.99	4.32	7.67	1.31	6.18	4.78	0.44	75.7		75.7		39.0	7.05	1941	5.5

	Al_2O_3	Re	Os	Ir	Ru	Rh	Pt	Pd	Au	S (µg/g)				Se	Te	S/Se	Se/Te
	(w.t.%)	ng/g	ng/g	ng/g	ng/g	ng/g	ng/g	ng/g	ng/g	a	b	average	c	ng/g	ng/g		
BM11-04	2.5	0.14	3.94	3.86	7.63	1.31	8.59	6.86	0.90	153		153		80.4	12.1	1909	6.6
BM11-18	2.8	0.14	3.63	3.63	7.13	1.22	8.49	6.50	0.79	168		168		76.1	10.1	2211	7.6
BM11-10	2.8	0.16	4.08	3.93	7.74	1.32	8.95	7.13	0.88	134		134		89.9	12.2	1486	7.4
BM11-02A	3.4	0.19	3.80	3.89	7.52	1.29	8.80	7.30	1.15	349		349		143	11.4	2446	12.5

Note: All BD and BM data from (Wang et al., 2013), other Al_2O_3 contents, column c of sulfur and most HSE data compiled from (Fischer-Gödde et al., 2011), and HSE data of samples RO307 and RO310 were analyzed in this study. Colunm a and b of sulfur from reanalysis of different aqua regia solution from the same digestion, S, Se and Te results and duplicates (*) are from this study, except for BD and BM. All abundance data, except for Rh and Au, were determined by isotope dilution methods. BD=Baldissero, BM=Balmuccia; Ley=Eifel xenoliths; RO=Ronda; L=Lanzo; BB=Beni Bousera; EL and IL=External and Internal of Ligurian ophiolites; DM= Hannuoba xenoliths; TUR=Turon de Técouère of Western Pyrenees; LZ=Lherz.

Table S4.3 S, Se and Te results of some carbonaceous chondrites and reference material UB-N analyzed in this study in comparison with previous data

Samples	Type	S (m/m %)	Methods for S	Se (µg/g)	Te (µg/g)	S/Se	Se/Te	Methods for Se&Te	Sources
Mighei	CM2			**13.5**	**1.49**		9.05	ID-HG-ICPMS	**This study**
Murchison	CM2			**14.0**	**1.56**		9.02	ID-HG-ICPMS	**This study**
Murchison duplicate				**14.1**	**1.56**		9.03	ID-HG-ICPMS	**This study**
		3.03	CSA	12.8		2370		INAA	(Dreibus et al., 1995)
		2.70	ID-ICPMS	12.3	1.32	2200	9.32	ID-ICPMS	(Makishima and Nakamura, 2009)
				12.6-13.1	1.60-1.66		8.2	RNAA and ICPMS	(Friedrich et al., 2002)
					1.52±0.15			ID-TIMS	(Smith et al., 1977)
					1.53±0.15			ID-TIMS	(Smith et al., 1977)
					1.52-1.79			ICPMS	(Fehr et al., 2005)
Allende	CV3			**8.63**	**0.929**		9.29	ID-HG-ICPMS	**This study**
Allende duplicate		**2.05**	ID-ICPMS	**8.74**	**1.10**	2340	7.95	ID-HG-ICPMS	**This study**
		2.06	CSA	9.1		2270		INAA	(Dreibus et al., 1995)
					0.92±0.17			ID-TIMS	(Smith et al., 1977)
					1.11±0.07			ID-TIMS	(Smith et al., 1977)
					0.95-0.97			ID-TIMS	(Loss et al., 1984)
					0.91-1.08			ICPMS	(Fehr et al., 2005)
		2.07	ID-ICPMS	7.94	0.859	2610	9.24	ID-ICPMS	(Makishima and Nakamura, 2009)
Orgueil	CI	5.39-5.49	CSA	21.4		2550		INAA	(Dreibus et al., 1995)
				20.9	2.31		9.06	ID-ICPMS	(Wang et al., 2013)
					2.44-2.55			ICPMS	(Fehr et al., 2005)
					2.24±0.05			ID-TIMS	(Loss et al., 1984)
				18.8-21.1	2.26-2.50			RNAA and ICPMS	(Friedrich et al., 2002)
Mean CI		5.41±0.37	Compilation	19.7±0.4	2.33±0.18	2750	8.5	Compilation	(Lodders, 2003)
		5.41	CSA	21.3		2540		INAA	(Dreibus et al., 1995)
		S (µg/g)		**Se (ng/g)**	**Te (ng/g)**				
UB-N		155	ID-ICPMS	127	10.6			ID-HG-ICPMS	(Wang et al., 2013)
UB-N duplicate		**157**	ID-ICPMS	**131**	**10.6**			ID-HG-ICPMS	**This study**
UB-N				126±3	9.67±0.02			ID-HG-ICPMS	(König et al., 2012)
		138-141	CSA						(Lorand et al., 2008b)
		152-174	ICP-AES						(Okai et al., 2001)
		134±8; 206±14	ICP-OES or CSA						(Ackerman et al., 2012)

Note: Sample weights were about 50-70 mg for chondrites and 1.5 or 2.5 g for UB-N. Due to application of hydride generation reaction which has relatively unstable intensities, typical precisions for Se and Te are 1-2 % (2 RSD). Most duplicates have good reproducibility, but Te in Allende may be distributed heterogeneously, because duplicates display up to 19 % variation and literature data by ID-TIMS also show such large variations (Smith et al., 1977). Allende: Smithsonian standard powder (USNM 3529, Split 18 position 1); Murchison: No. 9 19 0455, Universität Tübingen Collection; Mighei: No. 1456 # 46, Field Museum (Chicago). Method abbrevations: ID= isotope dilution; ICPMS= inductively coupled plasma mass spectrometry; TIMS= thermal ionization mass spectrometry; HG= hydride generation; INAA= instrumental neutron activation analysis; RNAA= radiochemical neutron activation analysis; AES= atomic emission spectroscopy; OES= optical emission spectrometry; CSA = carbon-sulfur analyzer.

Table S4.4 New estimates of the *minimum* abundances of chalcogen elements in the BSE using different regressions of element pairs

Elements	Estimate methods	Note	Results	Regression functions	R^2
S (µg/g)	S- Al_2O_3	a	S=206±38(1σ,n=41) @ Al_2O_3=3.52%	y = 58.5x	R^2 = 0.67
		b	S=211±40 (1σ,n=74) @ Al_2O_3=3.52%	y = 59.9x	R^2 = 0.77
Se (ng/g)	Se-Al_2O_3	a	Se=86.0±17.0 (1σ,n=51) @ Al_2O_3=3.52%	y = 24.4x	R^2 = 0.52
		b	Se=80.0±17.1 ng/g (1σ,n=84) @ Al_2O_3=3.52%	y = 22.7x	R^2 = 0.71
	S-Se	a	Se=85.1±17.2 (1σ,n=42) @ S=206 µg/g	y = 2.42x	R^2 = 0.48
		b	Se=81.2±16.2 (1σ,n=75)@ S=211 µg/g	y = 2.60x	R^2 = 0.71
Te (ng/g)	Te-Al_2O_3	a	Te=11.4±3.1 (1σ,n=51) @ Al_2O_3=3.52%	y = 3.23x	R^2 = 0.23
		b	Te=10.3±3.0 (1σ,n=85) @ Al_2O_3=3.52%	y = 2.92x	R^2 = 0.55
	Se-Te	a	Te=11.5±1.7 (1σ,n=52) @ Se=85.1 ng/g	y = 7.38x	R^2 = 0.71
		b	Te=10.8±1.6 (1σ,n=85) @ Se=80.0 ng/g	y = 7.52x	R^2 = 0.85
	Pd-Te	a	Te=11.3±1.7 (1σ,n=52) @ Pd=7.1 ng/g	y = 0.472x + 1.75	R^2 = 0.74

Note: a: sample data base in Table S4.2, excluding Eifel mantle xenoliths and BM11-02A and BM90-15, both of which have anomalously high S, Se or Te, probably due to localized sulfide redistribution processes (Wang et al., 2013). Excluding these samples only affects uncertainties of results. b: data from a and including peridotites from Lherz (Lorand and Alard, 2010; König et al., 2012), because these samples from Lherz were clearly affected by melt infiltration (Le Roux et al., 2007; Lorand and Alard, 2010). Both regressions show nearly the same results, indicating little difference between melt infiltration and melt extraction on abundance estimates of chalcogens in the BSE.

Table S4.5 Abundances of chalcogens in the BSE using regressions a and b from Table S4.4, compared to previous estimates

	New estimates from a using Al_2O_3=3.52 wt.%	**New estimates from b using Al_2O_3=3.52 wt.%**	**New estimates from b using Al_2O_3=4.45 wt.%**	**McDonough and Sun 1995**	**Palme and O'Neill 2003**
S (µg/g)	S=206±38 (1σ,n=41)	S=211±40 (1σ,n=74)	S=267±50 (1σ)	S=250±50 (1σ)	S=200±40 (1σ)
Se (ng/g)	Se=86.0±17.0 (1σ,n=51)	Se=80.0±17.1 (1σ,n=84)	Se=101±21 (1σ)	Se=75±50 (1σ)	Se=79 (1σ > 40)
	Se=85.1±17.2 (1σ,n=42)	Se=81.2±16.2 (1σ,n=75)	Se=103±20 (1σ)		
Te (ng/g)	Te=11.4±1.7(1σ)	Te=11.0±1.7(1σ)	Te=12.5±2.5 (1σ)	Te=6-24	Te=8 (1σ > 4)
S/Se	2420	2600	2600	3330	2530 (chondritic)
Se/Te	7.4	7.4	8.1	6.3	"chondritic"

Empirically, the bulk partition coefficient of Te during magmatic processes in the mantle is likely between Se and Pd (Figure 4.2). Accordingly, estimates of Te in the BSE are based on average values obtained from regressions of Se-Te and Pd-Te correlations (Table S4.4) because they constrain upper and lower limits of Te concentration of the BSE, respectively. In the new estimate from regression b, the Te value obtained from Se-Te is slightly lower than from Pd-Te (Table S4.4), which reflects the scatter of the data. The lower Te value derived from data set b and S/Se and Se/Te ratios obtained from S-Se and Se-Te diagrams, are also consistent with mean values of lherzolites with Al_2O_3 >1.5 wt.%, respectively (S/Se= 2690±700, 1σ, n=53 and Se/Te=7.9±1.6, 1σ, n=63). Palme and O'Neill 2003 have *assumed* CI chondritic S/Te.

Table S4.6 HSE and chalcogen data for the BSE and chondrites used in Figure 4.3

Group		Note	Ir	Te	Se	S	S/Se	Se/Te	data sources*
			ng/g	µg/g	µg/g	µg/g			
BSE			3.5	0.011	0.080	211	2600	7.4	(Becker et al., 2006), this study
		1SD	0.4	0.0017	0.017	40			
		RSD (%)	11%	16%	20%	19%			
Mean CI			424	2.33	19.7	54100	2750	8.5	(Lodders, 2003; Fischer-Gödde et al., 2010)
		1SD		0.18	0.4	3650			
		RSD (%)	4%	8%	9%	7%			
Carbonaceous Chondrites									
CI	CI	Orgueil	435	2.26±0.17	19.5±1.9	53500± 2530	2740	8.6	(Lodders, 2003; Fischer-Gödde et al., 2010)
				2.31	20.9			9.1	(Wang et al., 2013)
					21.4	54400	2540		(Dreibus et al., 1995)
				2.22	18.5			8.3	(Wolf et al., 2005)
				2.26-2.50	18.8-21.1			8.4	(Friedrich et al., 2002)
	C2	Tagish Lake	547	1.5	14.3	38000	2660	9.5	(Brown et al., 2000)
			507	1.67	14.0			8.4	(Friedrich et al., 2002; Brandon et al., 2005)
				1.52	12.6			8.3	(Wolf et al., 2005)
CM	CM2	Murchison	569	1.56	14.1			9.0	(Fischer-Gödde et al., 2010),This study
					12.8	30300	2370		(Dreibus et al., 1995)
				1.60	13.1			8.2	(Friedrich et al., 2002)
				1.52	12.5			8.2	(Wolf et al., 2005)
	CM2	Mighei	545	1.49	13.5			9.1	(Fischer-Gödde et al., 2010),This study
	CM2	Nogoya	548		13.5	34600	2560		(Dreibus et al., 1995; Fischer-Gödde et al., 2010)
CM2 Mean			554	1.52	13.5	32450	2410	8.8	
	CM1	EET83334		1.51 (1.38)	12.3 (12.2)			8.1	(Friedrich et al., 2002)
	CM1-2	ALH 83100		1.48 (1.27)	12.5 (9.64)			8.4	(Friedrich et al., 2002)
	CM2	MAC 88100		1.50 (1.29)	14.1(14.5)			9.4	(Friedrich et al., 2002)
	CM2	Y-793321		1.67(1.41)	13.3(14.7)			8.0	(Friedrich et al., 2002)
	CM	EET96010		0.61	8.3±5.0				(Moriarty et al., 2009)
	CM	WIS91600		1.00	8.3±3.5				(Moriarty et al., 2009)
	CM	MET01070		1.30	8.9±1.7				(Moriarty et al., 2009)
	CM	LAP02277		1.20	7.7±2.7				(Moriarty et al., 2009)
CV	CV3	Allende	684		9.1	20600	2260		(Dreibus et al., 1995; Fischer-Gödde et al., 2010)
				0.929	8.63			9.3	This study
				1.10	8.74	20500	2340	8.0	This study
				0.859	7.94	20700	2610	9.2	(Makishima and Nakamura, 2009)
	CV	LAP 02206		1.00	8.8±0.9				(Moriarty et al., 2009)
CO	CO3	Kainsaz	660		8.2	22800	2780		(Dreibus et al., 1995; Fischer-Gödde et al., 2010)
	CO3	ALH 83108		0.96 (0.89)	7.03 (5.14)			7.3	(Friedrich et al., 2002)
	C3	MAC88107		1.07(0.92)	8.21(8.67)			7.7	(Friedrich et al., 2002)
Ordinary chondrites									
H	average		733	0.36±0.10	8.2±1.3			22.8	(Lingner et al., 1987; Wolf and Lipschutz, 1995a, b; Wolf et al., 1997; Wang et al., 1999)
				0.26	7.7	20000	2600	29.6	(Wasson and Kallemeyn, 1988)
				0.35	8.28			23.5	(Wolf and Lipschutz, 1998)
					9.53	23500	2470		(Dreibus et al., 1995)
				0.33	8.15			24.7	(Schaefer and Fegley, 2010)
L	avera		537	0.41±0.17	9.1±2.1			22.2	(Binz et al., 1976; Walsh and Lipschutz,

Group	Note	Ir ng/g	Te µg/g	Se µg/g	S µg/g	S/Se	Se/Te	data sources*
	ge							1982; Huston and Lipschutz, 1984; Kaczaral et al., 1989; Friedrich et al., 2003; Friedrich et al., 2004)
			0.48	9	22000	2440	18.8	(Wasson and Kallemeyn, 1988)
				9.31	22800	2450		(Dreibus et al., 1995)
			0.37	9.04			24.4	(Schaefer and Fegley, 2010)
LL	avera ge	322	0.39±0.13	9.0±2.1			23.1	(Binz et al., 1976; Friedrich et al., 2003)
			0.49	9.9	23000	2320	20.2	(Wasson and Kallemeyn, 1988)
				9.55	22400	2350		(Dreibus et al., 1995)
			0.53	8.25			15.7	(Schaefer and Fegley, 2010)
Enstatite chondrites								
EH	avera ge	532	2.0±0.7	25.1±5.2			12.6	(Binz et al., 1974; Hertogen et al., 1983; Kallemeyn and Wasson, 1986; Wang and Lipschutz, 2005)
			2.23	25.5	58000	2280	11.4	(Wasson and Kallemeyn, 1988)
EL	avera ge	567	0.79±0.54	15.6±6.1			19.7	(Binz et al., 1974; Hertogen et al., 1983; Kallemeyn and Wasson, 1986; Wang and Lipschutz, 2005)
			0.8	13.5	33000	2440	16.9	(Wasson and Kallemeyn, 1988)
Rumuruti chondrites								
R	avera ge	493		13.9±1.0	40700	2930		(Bischoff et al., 2011)
				14.6	40700	2790		(Dreibus et al., 1995)

* Ir data for carbonaceous chondrites are from (Fischer-Gödde et al., 2010), except Tagish Lake (Brown et al., 2000; Brandon et al., 2005), values for ordinary, enstatite and Rumuruti chondrites are averages that are derived from (Horan et al., 2003; Fischer-Gödde et al., 2010). Concentrations of chalcogen elements for mean CI are from (Lodders, 2003) with a range of S/Se slightly higher than the range from (Dreibus et al., 1995). Selenium and Te data for ordinary, enstatite and Rumuruti chondrites are averages with errors (1σ) from original literature that have both Se and Te analyzed. These averages are similar to those given in compilations (Wasson and Kallemeyn, 1988; Schaefer and Fegley, 2010). Errors of S data for Tagish Lake, CO3, enstatite and Rumuruti chondrites for which only limited data are available, were assumed 10 % in Figure 4.3 because of high S concentrations. Recent isotope dilution data support previously published data that indicate that Se/Te of ordinary, enstatite and Rumuruti chondrites are consistently higher than the value for carbonaceous chondrites (Funk et al., 2012). The isotope dilution ICPMS data of carbonaceous chondrites are much more homogeous than earlier data and hints at a Se/Te for CI and other carbonaceous chondrites near 9 (see also Table S4.3) (Funk et al., 2012; Wang et al., 2013). CM2 Mean are results of Murchison, Mighei and Nogoya. Selenium and Te data of Antactic carbonaceous chondrites from (Xiao and Lipschutz, 1992) are not included because duplicates of some samples analyzed later (Friedrich et al., 2002) display 10-20 % variations, especially for Te with systematic lower values, such as EET 83334, ALH83100, MAC 88100, Y-793321, MAC 88107 and ALH 83108 listed in this table (values outside brackets by ICPMS (Friedrich et al., 2002) and values in brackets by RNAA (Xiao and Lipschutz, 1992)).

Table S4.7 Estimated contributions of volatiles to the BSE, assuming a late veneer comprised of CM chondrite or of material similar to Comet Halley's ice and dust

	Sulfur	**Water**	**Carbon**	**Nitrogen**	**Required mass fraction (% of Earth's mass)**
CI chondrite	5.4 wt. % (Lodders, 2003)	14 wt. % (Alexander et al., 2012)	3.6 wt. % (Alexander et al., 2012)	0.2 wt.% (Alexander et al., 2012)	
Mean CM chondrite	3%-3.5wt. % (Dreibus et al., 1995)	10±2 (1σ) wt.% (Alexander et al., 2012)	1.9±0.6 (1σ) wt.% (Alexander et al., 2012)	0.10±0.04 (1σ) wt.% (Alexander et al., 2012)	
Comet Halley ice & dust (Lodders and Bruce Fegley, 1998)	3.8wt. %	60 wt. %	20 wt. %	2.2 wt. %	
BSE	**210 µg/g**	550-3000 µg/g (Hirschmann and Dasgupta, 2009; Marty, 2012)	45-500 µg/g (Hirschmann and Dasgupta, 2009; Marty, 2012)	1.9±0.7 µg/g (Marty and Dauphas, 2003)	
CM chondrite contribution to the BSE	**210 µg/g**	630 µg/g	120 µg/g	7 µg/g	0.43%
Comet contribution to the BSE	**210 µg/g**	3300 µg/g	1100 µg/g	120 µg/g	0.37%

Note: 1) Assuming all H of comets is added in the form of water; 2) Contribution of the late veneer to the BSE for water, carbon and nitrogen is based on sulfur content constrained by this study and their ratios to sulfur in CM chondrites and cometary material, respectively, assuming no loss during accretion. Because of similar S contents, the required mass of cometary material is similar to CM chondrites.

Chapter 5

Abundances of sulfur, selenium, tellurium, rhenium and platinum group elements in eighteen reference materials by isotope dilution sector-field ICP-MS and negative TIMS

Zaicong Wang and Harry Becker

Freie Universität Berlin, Institut für Geologische Wissenschaften,
Malteserstrasse 74-100, 12249 Berlin, Germany

This chapter has been published as:

Wang Z. and Becker H. (In press) Abundances of sulphur, selenium, tellurium, rhenium and platinum group elements in eighteen reference materials by isotope dilution sector-field ICP-MS and negative TIMS. *Geostandards and Geoanalytical Research.* Doi: 10.1111/j.1751-1908X.2013.00258.x.

5.1 Abstract

Geological reference materials (RMs) with variable compositions and the NIST SRM 612 were analyzed by isotope dilution mass spectrometry for bulk rock concentrations of chalcogen elements (sulfur, selenium and tellurium), rhenium and platinum group elements (PGEs: Ru, Pd, Os, Ir and Pt), including the isotope ratio of $^{187}Os/^{188}Os$. All concentrations were obtained from the same aliquot after HCl-HNO_3 digestion in a high pressure asher at 320°C. Concentrations were determined after chemical separation by negative TIMS, ICP-MS and hydride generation ICP-MS (Se, Te). As in previous studies, concentrations of the PGEs in most RMs are highly variable, which may be ascribed to sample heterogeneity at the <1 gram level. In contrast, S, Se and Te display good precisions of concentrations data obtained after repeated digestions and measurements (RSD < 5 %) in most RMs, suggesting that part of PGE budget is controlled by different phases, compared to the chalcogen budgets. The method may minimize losses of volatile chalcogens during the closed-system digestion and indicates different extent of heterogeneity of chalcogens, Re and PGEs in the same sample aliquot. OKUM, SCo-1, MRG-1, DR-N and MAG-1 are useful RMs for the chalcogens. NIST SRM 612 displays homogenous distribution of S, Se, Te, Pt and Pd in 30 mg aliquots, in contrast to micro-scale heterogeneity of Se, Pd and Pt.

5.2 Introduction

The chalcogen elements sulfur, selenium and tellurium are of increasing importance as tracers in geological and cosmochemical processes, because of their chalcophile, siderophile and volatile behavior. The chalcogens (in this work, the term 'chalcogens' is used synonymously for S, Se and Te only) are critical tracers for understanding planetary processes such as the delivery of volatiles, core-mantle differentiation, magmatic processes in mantle and crust (e.g., Hertogen et al. 1980, Morgan 1986, Dreibus et al. 1995, de Hoog et al. 2001, Lorand et al. 2003, Lorand and Alard 2010, Wang and Becker 2013, Wang et al. 2013), and formation of magmatic Cu-Ni-platinum group elements (PGEs) sulfide deposits (e.g., Helmy et al. 2010, Piña et al. 2012). Similarly, the PGEs and Re are also important tracers for these processes (e.g., Shirey and Walker 1998, Becker et al. 2006, Walker 2009, Holwell and McDonald 2010). Because of similar geochemical properties, Se and Te can substitute for S in sulfides and were proposed as potential proxies to estimate primitive S contents or effects of secondary alteration/weathering on S contents, such as in magma before degassing (Jenner et al. 2010) and mantle rocks (e.g., Lorand et

al. 2003, Alard et al. 2011). The PGEs are mainly controlled by accessory platinum group minerals (PGM) and base metal sulfides, selenides and tellurides, which may lead to decoupling and fractionation of PGEs (or selected refractory PGEs such as Ir-Os-Pt in alloys) from Re and chalcogens during magmatic, ore-forming and other processes (e.g., Lorand et al. 2003, 2010, Luguet et al. 2004, Piña et al. 2012).

The chemical behavior of S and Se also has been intensively studied in environmental sciences (e.g., Halmer et al. 2002, Floor and Roman-Ross 2012). Some Se and Te species are potentially toxic and have an enormous impact on human and animal health (Cerwenka Jr and Cooper 1961). Thus, these wide applications increasingly require reliable concentration data of S, Se, Te and the PGEs in geological RMs.

Up to now, a limited number of concentration data of chalcogen element, Re and PGE data have been available for geological RMs, and most studies report data for individual elements, or selected groups of elements (e.g., some of the PGEs) only. The main reason has been analytical difficulties for the low abundance levels of most of these elements (e.g., Yi et al. 1998, Meisel and Moser 2004b, Bédard et al. 2008, Savard et al. 2009), such as typically in the ng g^{-1} to pg g^{-1} range for PGEs, Se and Te. Most data of S abundances in RMs with low concentrations show large variations and uncertainties (e.g., Bédard et al. 2008, Ackerman et al. 2012). Sulfur abundance data of RMs, such as peridotite UB-N and basalt BCR-2, have yielded precise results by the same method, but systematic and significant differences when different digestion or analytical methods were employed (Okai et al. 2001, Ackerman et al. 2012). For RMs with low sulfur contents, few sulfur concentration values are available. RMs with low Se, Te, Re and PGE contents were also rarely analyzed. Sample heterogeneity or incomplete digestion considerably affects the precision of PGE content data (e.g., Meisel et al. 2001b, 2003b, Meisel and Moser 2004b, Li et al. 2013), but to which extent this is also the case for S, Se and Te is not well known.

Digestion in concentrated HCl and HNO_3 in a high pressure asher system (HPA-S) at high temperatures of 300-320°C has been established as a method to obtain reproducible abundance data of the PGEs, Re and Au in peridotites and in chondrites (e.g., Meisel and Moser 2004a, Lorand et al., 2008, Fischer-Gödde et al. 2010, 2011). The same technique also yields precise data of the chalcogen elements in mantle peridotites (König et al. 2012, Wang and Becker 2013, Wang et al. 2013). Digestion in a closed system by a high pressure asher coupled with the isotope dilution mass spectrometry (ID-MS) method has great potential to minimize volatile loss of chalcogen elements and help achieve spike-sample equilibration. The method yields precise data, even for samples with low concentrations of these elements (e.g., mostly RSD for Se and Te <5 %, König et al. 2012). In this contribution, these

measurement procedures have been applied for the determination of concentrations of S, Se, Te, Re and the PGEs (excluding monoisotopic Rh) in selected geological RMs in the same digestion aliquot. We also report concentrations of S, Se, Te, Ru, Pd, Ir and Pt obtained by digestion in concentrated HF and HNO_3 for several bulk aliquots of NIST SRM 612 glass. NIST SRM 612 is now widely used as a RM for microanalysis of trace element abundances by LA-ICP-MS and SIMS but concentration data of chalcogen elements and PGEs are still limited (Pearce et al. 1997, Jochum et al. 2011). The new data will provide further constraints on concentrations and homogeneity of these elements in this RM.

5.3 Sample description

Geological RMs analyzed in this study have variable petrographic compositions ranging from ultramafic and mafic to felsic igneous rocks and also include sediments (Table 5.1). Most RMs have low PGE and Re contents (pg g^{-1} to ng g^{-1} range), and variable abundances of chalcogens (tens to thousands of μg g^{-1} for S; <1 ng g^{-1} to hundreds of ng g^{-1} for Se and Te).

For the present work, test portion sizes in the range of about 0.5 to 1 g geological RMs was digested and some RMs were digested and analyzed in duplicates or triplicates (Table 5.1). Four different glass splits, each about 30 mg, from two different wafers of NIST SRM 612 glass were analyzed. Prior to analysis of NIST SRM 612 glass chips, potential contamination from cutting was removed. Before crushing, the surface of the wafers was cleaned in cold ethanol, 0.7 mol l^{-1} HNO_3 and 18.2 MΩ-cm water in an ultrasonic bath for a few minutes. During crushing into small chips, the wafers were wrapped in Kimwipe paper as a protection against contamination.

5.4 Experimental

The measurement procedures used for the geological RMs have been applied to chondrites and ultramafic rocks such as mantle peridotites at Freie Universität Berlin. The methods, including sample digestion, chromatographic separation, and measurement by sector-field ICP-MS or negative TIMS, have been described in detail elsewhere (Fischer-Gödde et al. 2010, 2011, Wang and Becker 2013, Wang et al. 2013), so only an abridged description of the methods is given here. Minor changes in the procedures were made because of lower test portion size, compared to previous studies and lower PGE and variable chalcogen element contents.

5.4.1 Reagents and materials

Concentrated acids of HCl and HNO_3 for sample digestion, chemical separation and ICP-MS measurement were twice quartz distilled (2QD) and twice Teflon distilled (2TD) from analysis grade HCl and HNO_3. HNO_3 used for digestion was further treated by H_2O_2 oxidation and N_2 bubbling to reduce the Os blank. Concentrated HCl or HNO_3 acids (2QD2TD) were diluted using 18.2 MΩ-cm water. Commercially available 24 mol l^{-1} ultrapure HF (J. T. Baker®, ULTREX II) was used for digestion of NIST SRM 612 glass, and $NaBH_4$ (J. T. Baker®, reagent grade) for hydride generation reaction. High purity Ar gas (≥99.999 %) was used in the study for ICP-MS measurement and interferences from Kr and Xe contaminants from the Ar gas were negligible for ^{82}Se and ^{126}Te measurements, respectively (details in Wang et al. 2013).

All ion exchange resin (Eichrom 50W-X8, 100-200 mesh and Eichrom AG1-X8, 100-200 mesh) were pre-cleaned by clean water and different concentrations of HCl and HNO_3 (both 2QD, 1 mol l^{-1} and 6 mol l^{-1} twice) to reduce resin blanks. The anion resin used for separation of S, Se and Te, was discarded after one separation, whereas the cation resin was used 3 to 5 times. Cation resin (2-3 ml) in Biorad columns was used for clean up of S-Se and Pd. After separations, the resin was cleaned with three reservoirs (10 ml) of 6 mol l^{-1} HCl (2QD), followed by a backwash in water. After separation of the PGE and Re, the cation resin (10 ml) was cleaned in 3 times 25 ml 6 mol l^{-1} HCl (2QD), followed by a backwash in water.

Savillex Teflon® PFA (perfluoroalkoxy) beakers were used as containers for digested sample material and separated elements. After each use, they were cleaned using cotton swabs, and then boiled for at least 12 hours in half concentrated aqua regia, followed by half concentrated HNO_3, half concentrated HCl and clean water. After each cleaning step, beakers were rinsed in clean water three times.

5.4.2 Instrumentation

The HPA-S (Anton Paar, Austria) with 90 mL quartz glass vessels, the Element XR sector field ICP-MS (Thermo Scientific) and Triton TIMS (Thermo Scientific) at Freie Universität Berlin were used. Aridus desolvator I was used to limit oxide formation and increase sensitivity, with a CeO^+/Ce^+ ratio of 0.3-0.4 % and 3 to 4 million counts per second for ^{115}In of 1 ng g^{-1} indium tuning solution. A double pass Scott type glass spray chamber was used for the hydride generation (HG) measurements and a Scott type glass spray chamber was for measurements without HG reaction, with CeO^+/Ce^+ ratio < 3-4 %.

5.4.3 Calibration standards and spike solutions

The Ru, Pd, Ir, Pt, Re, Se and Te standard solution for calibration of instrumental mass discrimination are dilution of about 1000 µg ml^{-1} Plasma Standard Specpure® standard solutions from Alfa Aesar (A Johnson Matthey Company). The ICP-MS calibration standard solutions were diluted to concentrations of 0.1 ng g^{-1} for Re and 1 to 3 ng g^{-1} for Ru, Pd, Ir and Pt in a mixed element standard solution. The Se standard was diluted to a concentration of 4.4 ng g^{-1}. During HG measurement, Te has much higher intensity (but also stronger memory effects) than measurements without HG. A 0.1 ng g^{-1} Te standard solution was used for HG and a 1 ng g^{-1} Te was used for Te measurements without HG (in particular for measurement of NIST SRM 612). Because $^{32}S/^{34}S$ has a large ratio and is measured at medium solution, a standard solution with 10 µg g^{-1} S was prepared. The K_2SO_4 powder (Merck company, >99 %) used for the S standard has a $\delta^{34}S$ of 10.70±0.15‰ (2s) determined by gas source mass spectrometry. An Os standard solution (University of Maryland, UMD, Shirey and Walker 1998) was used to monitor the precision of Os isotope measurements of 100 pg Os aliquots during the analysis period of the samples.

Because geological RMs have variable concentrations for most elements analyzed in this study, suitable amounts of spike solutions with different concentrations were used to minimize error propagation of the ID-ICP-MS measurement uncertainty and to save spike solution. Mixed ^{99}Ru-^{105}Pd-^{191}Ir-^{194}Pt and ^{185}Re-^{190}Os (mixed from individual ^{185}Re and ^{190}Os) and sometimes individual Re and Os spikes have been used as in previous work on different types of samples (Becker et al. 2006, Fischer-Gödde et al. 2010, 2011, Fischer-Gödde and Becker 2012, Wang et al. 2013). ^{77}Se-^{125}Te and ^{34}S spikes also have been used for peridotites, chondrites and some RMs such as UB-N and the Smithsonian Allende standard powder (Wang and Becker 2013, Wang et al. 2013) and precise data on these samples have been obtained.

Here brief procedures for the S spike preparation and calibration will be explained, because S is particularly prone to loss by volatilization. One thousand milligram elemental sulfur-34 spike (enrichment: 98.80 %) from ISOFLEX USA was split in three aliquots, and each aliquot was digested in 7 ml 14 mol l^{-1} HNO_3 (2QD2TD) in a 90 ml quartz vessel in the HPA-S at 240 °C overnight. After combining the digestion solutions in a 60 ml Savillex beaker, 6.9 g high purity sodium chloride (99.999 %, Alfa Aesar, Puratronic) was added to prevent loss of S as sulfuric acid during heating (Mann and Kelly 2005). The solution was then evaporated to dryness at 100 °C and 5 ml 9 mol l^{-1} HCl (2QD2TD) was added and dried down twice at 100 °C. The spike solution was finally stored in 2 mol l^{-1} HCl. For S concentration calibration, three different calibration standard solutions and the reverse isotope

dilution method were used. The three calibration standards were obtained by diluting 1000 µg ml^{-1} ICP standard solutions from Alfa Aesar ($(NH_4)_2SO_4$ solution), Merck (dilute H_2SO_4) and Fluka (dilute H_2SO_4) using water. Twelve blends of S spike and standard in capped 15 ml Savillex beakers were equilibrated on a hotplate at 140 °C for 2 days, and were analysed directly after dilution. The calibrated concentration of the S spike has a high precision (2RSD of 0.6 %). Compared to the weighed and digested S spike mass, the calibrated S spike concentration was lower by only 0.7 %, indicating negligible loss of sulphur during HPA-S digestion.

5.4.4 Sample digestion

Mixed ^{99}Ru-^{105}Pd-^{191}Ir-^{194}Pt, ^{77}Se-^{125}Te, ^{185}Re-^{190}Os (or individual ^{185}Re, ^{190}Os depending on expected concentrations of samples) and ^{34}S spike solutions were weighed into 90 ml quartz glass digestion vessels, followed by 0.5-1 g RM powder, 3 ml 14 mol l^{-1} HNO_3 and 1.5 ml 9 mol l^{-1} HCl. Because spike solutions are dilute acids, the addition of samples after spike solutions can reduce possible trace loss of gaseous sulfur compounds (e.g., H_2S) during weighting. Spike solutions and samples were weighed to a precision of 0.05 mg. After the addition of digestion acids, the vessels were capped and sealed immediately with Teflon tape. Samples were digested at 320 °C and 100 bar in the HPA-S for 16 hours. After digestion, the sample solution usually showed a yellow color. A small amount of remaining slush was light grey for ultramafic to mafic samples, with minor precipitation of ferric iron compounds accumulating at the bottom of the digestion vessels. Sulfides and the oxides that host S, Se, Te, Re and the PGEs were digested easily in the reverse aqua regia whereas some silicate phases may not be completely digested. Although it has been suggested that a fraction of Re may be hosted in silicate phases in mantle rocks (Mallmann and O'Neill 2007), detailed investigation of different digestion methods (e.g., low temperature acid attacks, Carius tube, NiS fire assay and HPA-S) using UB-N, a serpentinized lherzolite RM indicates reproducible Re concentrations, independent of application of HF or not and of different digestion methods (Meisel et al. 2003a). The HPA-S method also yielded reproducible contents for the PGEs, although abundances of Os, Ir and Pt may display the influence of trace phase heterogeneity in the sample and in its powder (Lorand et al. 2008). After digestion, osmium was immediately extracted into CCl_4 (Cohen and Waters 1996) and further purified by micro distillation (Birck et al. 1997). After Os extraction, the digestion solution was centrifuged for 20 minutes. One third of the supernatant solution was used for separation of the Re-Ru-Pd-Ir-Pt fraction, and half for S-Se-Te separation.

5.4.5 Chemical separation

Chemical separation of the Re-Ru-Pd-Ir-Pt fraction from matrix was performed on columns filled with 10 ml of pre-cleaned Eichrom 50W-X8 (100-200 mesh) cation exchange resin (Fischer-Gödde et al. 2011). This fraction was collected in 14 ml 0.5 mol l^{-1} HCl-40ml/100ml acetone and dried down to 2-3 ml for the analysis of Re, Ir and Pt. The solution remaining after analysis was purified on 2 ml Eichrom 50W-X8 (100-200 mesh) resin and 3.5 ml 0.2 mol l^{-1} HCl was collected after loading sample solution and analyzed for Ru, Pd, Ir and Pt using an Aridus-I desolvator.

A two-step ion exchange chromatography method was used for the separation of S, Se and Te from matrix. In the first step, S, Se and Te were separated from iron and other elements on 2 ml Eichrom AG1-X8 (100-200 mesh) anion exchange resin after reduction of Se and Te to quadrivalence in concentrated HCl (Rouxel et al. 2002, Fehr et al. 2004, Wang and Becker 2013, Wang et al. 2013). Reduction of Se and Te which, after HCl-HNO_3 digestion, would predominantly occur in the hexavalent state is important because only Se^{4+} and Te^{4+} allow hydride generation. The digestion solution was dried down at 80-85 °C and 2 ml 9 mol l^{-1} HCl was added and dried down twice to convert aqua regia to chloride form and to reduce Se and Te. The still wet residue was dissolved in 2 ml 6 mol l^{-1} HCl. Sulfur, Se, and most of the matrix are not absorbed on the anion resin in 6 mol l^{-1} HCl, and were collected in 4 ml 6 mol l^{-1} HCl. The resin was washed in 5 ml of 5 mol l^{-1} HF, followed by 4 ml of 9 mol l^{-1} HCl to remove the remaining matrix (Fehr et al. 2004). Finally, Te was eluted in 6 ml of 1 mol l^{-1} HNO_3 and ready for analysis. The S-Se fraction was taken to near-dryness at 80-85 °C and redissolved in 2 ml of 0.1 mol l^{-1} HNO_3. This solution was purified on 2 ml Eichrom 50W-X8 (100-200 mesh) resin and collected in 5 ml 0.1 mol l^{-1} HNO_3. Another 1 ml 7 mol l^{-1} HNO_3 was added to increase acid concentration to facilitate reduction of Se^{4+} to Se^{2-} via the HG reaction.

5.4.6 Measurements and data reduction

Osmium isotopic ratios were determined as OsO_3^- in negative mode using the Triton TIMS. A secondary electron multiplier was used for all samples. Signals of the spike isotope ^{190}Os of samples and blanks were measured typically at 15,000 to 200,000 cps in pulse counting secondary electron multiplier mode. About 160 scans of relevant Os isotopes were collected in a measurement. Raw data were corrected for molecular OsO_3^- interferences, instrumental mass fractionation using the $^{192}Os/^{188}Os$ ratio of 3.08271, a linear fractionation law and UMD Os standard solution (Boelrijk, 1968, Luck and Allègre 1983), and subsequent subtraction of the spike contribution.

Repeated measurements of about 100 pg Os standard yielded $^{187}Os/^{188}Os$=0.11399±0.00012 (2s, standard deviation, n=8) over the analysis period of the samples. The precisions of the mean of $^{187}Os/^{188}Os$ for most RMs were better than 0.2 % (2 r. s. e.) and occasionally several percent for a few samples with very low Os contents such as DR-N, MA-N and RGM-1.

The intensities of other elements were measured by sector-field ICP-MS (Element XR), following the methods outlined in Fischer-Gödde et al. (2011) and Wang et al. (2013). Sulfur abundance measurements were performed in medium mass resolution mode (m/Δm=4000). The signals of Se and Te were measured in low mass resolution mode, using a double pass Scott type glass spray chamber and hydride generation by reacting the sample solution with 1g/100g $NaBH_4$ in 0.05 mol l^{-1} NaOH. Oxide formation rates during Re-Ir-Pt and S measurements were <3-4 % (CeO^+/Ce^+). Isotopic ratios used for isotope dilution were $^{99}Ru/^{101}Ru$, $^{105}Pd/^{106}Pd$, $^{185}Re/^{187}Re$, $^{190}Os/^{188}Os$, $^{191}Ir/^{193}Ir$, $^{194}Pt/^{195}Pt$, $^{34}S/^{32}S$, $^{77}Se/^{82}Se$ and $^{125}Te/^{126}Te$, respectively.

For signal measurements of Ru, Pd, Ir, Pt, Re, S, Se and Te with the Element XR, acid blank solutions with the same acid concentrations as sample solutions were measured before and after two samples to control background intensities and memory effects. Intensities of acid blanks were always subtracted. For most samples, background intensities for PGEs, Re, S, Se and Te were <0.5 % of samples signals, but for a few samples with very low concentrations, the subtraction of background intensities accounts for a few percent to about 20 percent (the precision of the value <50 %), such as Se, Pd, Pt and Ir in GS-N, NIM-D, NIM-L and RGM-1. Instrumental mass bias for PGEs, Re, S, Se and Te was determined and corrected by comparison of isotope ratios of RMs with isotope ratios of single element or mixed element standard solutions. Mean values used for these corrections were obtained by two or three analyses of these standard solutions during the measurement period. For multiple analyses of the same standard solution, isotopic ratios of Re and the PGEs in the standard solution were relatively stable (RSD <0.2 %). Sulfur measurements also displayed stable intensities. During the measurement period, the S standard solution yielded typical variations of $^{32}S/^{34}S$ by <0.5 % (RSD). Because of variations in the gas flow during HG, the Se and Te intensities were not as stable as for the PGEs and S so that ratios of $^{77}Se/^{82}Se$ and $^{125}Te/^{126}Te$ were measured at more scans using peak dwell times of 5 ms and n = 6000 and 9000 scans, respectively. Multiple analyses of Se and Te standard solution during each measurement period yielded precisions of $^{77}Se/^{82}Se$ and $^{125}Te/^{126}Te$ ratios in Se and Te standard solutions at 0.1 % to 1 % RSD (n=3).

Intensities of Te during HG were variable and often lower than expected from the Te yield. Mafic to ultramafic igneous rocks such as BHVO-1 (basalt), MRG-1

(gabbro) and OKUM (komatiite) sometimes had low Te intensities compared to other RMs, although Te contents in these samples are higher than in other RMs. It is possible that some residual cations of more abundant transition elements in the Te fraction inhibited the HG reaction and conversion of Te^{+4} into Te^{-2} (Yu et al. 1983). We found that sample matrix strongly affects Te yields and signal intensities of samples. For instance, aliquots of 2-3 g mantle peridotites digested in a HPA-S, corresponding to 0.5-1 g of sample, have lower Te chemistry yields than matrix free procedural blanks or chondrites corresponding to 0.01 g sample (Wang et al. 2013). Duplicates of BHVO-1 were analyzed by ICP-MS without HG. Precise $^{125}Te/^{126}Te$ data (RSD < 3 %) can be obtained by low resolution ICP-MS analysis in a Scott type spray chamber without HG if Te intensities are sufficiently high compared to dilute nitric acid blanks.

5.4.7 NIST SRM 612 glass

Different procedures were applied for the determination of concentrations in NIST SRM 612 glass. A suitable amount of mixed ^{99}Ru-^{105}Pd-^{191}Ir-^{194}Pt, ^{77}Se-^{125}Te and ^{34}S spike solutions were weighed into 15 ml PFA beakers, followed by 3 ml of 24 mol l^{-1} ultrapure HF and 1.5 ml of 14 mol l^{-1} HNO_3 (2QD2TD) and 25-30 mg of glass fragments. The glass was digested in capped beakers on a hotplate at 140 °C for 2 days. Solutions were dried down at 80-85 °C, converted to chloride form by addition of 2 ml of 9 mol l^{-1} HCl and taken to dryness. This procedure was repeated, and the residue dissolved in 5 ml 3 mol l^{-1} HCl. About 2 % (0.1 ml) of the solution was diluted in 1 ml 0.2 mol l^{-1} HCl and was purified on 2 ml Eichrom 50W-X8 (100-200 mesh) resin and 3.5 ml 0.2 mol l^{-1} HCl was collected, similar to the clean up procedure for the Ru-Pd-Ir-Pt fraction in geological RMs. The Ru-Pd-Ir-Pt fraction was analyzed using the Aridus coupled to the ICP-MS. Another 2 % of the digestion solution was diluted by a factor of about 50 and S, Se and Te were analyzed on the ICP-MS without chemical separation. Sulfur, Se, and Ru-Pd-Ir-Pt were determined on the ICP-MS following the setup for geological RMs. Because of the presence of high abundance levels on many trace elements in SRM 612 the HG reaction was inhibited and very low Te intensities were observed. For this reason, and because SRM 612 contains 20-30 μg g^{-1} Ag and Cd (Jochum et al. 2011), the Te fraction was reanalyzed using the solution at low resolution without HG, using first a Scott-type spray chamber and then the Aridus . Oxide interferences from ^{109}Ag, ^{110}Cd and ^{110}Pd on ^{125}Te and ^{126}Te were monitored. The Te concentrations obtained using both measurement modes at different oxide formation rates have little variation of <1.5 %, indicating negligible effects of oxide interferences on Te contents.

5.5 Results and discussions

5.5.1 Detection limits of the methods

Isotope dilution methods have been used in this study, and the detection limits for ID-ICP-MS were calculated by equation 4 from Yu et al. (2002), which provides a conservative estimate of limit of detection for ID-ICP-MS, not only related to ICP-MS instrumental capability but also the spike composition used. The detection limits for the two isotopes used for concentration calculation were calculated in the following way:

$$\text{Detection limit of one isotope} = 3^* \text{ SD} / \text{f}$$

where SD is the standard deviation of the reagent blank (dilute HCl or HNO_3) in counts per second (cps), and f is the cps/ng g^{-1} conversion factor, based on the sensitivity of the Element XR ICP-MS for a calibration standard solution with a known concentration (ng g^{-1}). The detection limits of the methods are listed in Table 5.2. Without HG, the detection limit for Te is about a factor of 10-20 higher. Procedural detection limits were also calculated by three times the standard deviation of total procedural blanks (see below and Table 5.2), which are similar (for Ru) or considerably higher (for other elements) than detection limits based on acid blank.

5.5.2 Total procedural blanks

Total procedural blanks based on 1 g aliquots were also determined by ID-MS methods together with samples digested in the same batch. The results were as follows (n=6, 1s, Table 5.2): Re=4.2±1.9 pg; Os=1.0±0.6 pg; Ir=0.7±0.5 pg; Ru=0.4±0.3 pg; Pt=26±12 pg; Pd=20±8 pg; Te=19±12 pg; Se=1.9±0.8 ng; S=4.0±1.2 μg (S blank mainly from the cation resin). Occasionally, total procedural blank results for individual elements produced unreasonably high values, for instance, Os (5.3 pg), Pt (118 pg), Pd (65 pg) and Te (83 pg). These values were much higher than most blank values, and reflect poor element yields or problem during measurements. These values were excluded from calculation of the blank mean values. RMs were corrected for total procedural blanks using mean values. The total procedural blanks of Pd, Os, Pt and Te including the anomalous values also were given in Table 5.2 for comparison. Total procedural blanks and their standard deviations are the main contributors to measurement uncertainty of the content of some elements, in particular for RMs with low concentrations (Tables 5.3 and 5.4). For instance, the S blank contributed >30 % of the total amount of S determined during analyses of RGM-1 replicates (14 and 17 μg g^{-1}), the Se blank contributed > 30 % to NIM-S and the Se content of RGM-1 is

below procedural detection limit. The PGEs also had significant blank contributions (typically a few percent) for RMs with low concentrations. Concentrations of Os, Ir and Ru of RGM-1are close to blank values.

5.5.3 Chalcogen elements

Sulfur abundances in geological RMs have been reported in many studies (e.g., Okai et al. 2001, Bédard et al. 2008, Andrade et al. 2009, Ackerman et al. 2012). However, different methods have yielded systematically different results for some samples (e.g., Okai et al. 2001, Ackerman et al. 2012). This may be due to different oxidation states of sulfur in some RMs (presence of sulfates and sulfides), which can lead to incomplete decomposition or partial loss of sulfur as H_2S or SO_2 during acid digestion (Okai et al. 2001, Ackerman et al. 2012). Another explanation of variable results may be heterogeneous distribution of sulfur-rich phases. This behavior is known from accessory sulfides in ultramafic and mafic rocks, in cases where the test portion size analyzed is too low (e.g., Meisel and Moser 2004a). By applying a HPA-S digestion system that approaches closed system conditions, combined with the ID method, data with relatively low measurement uncertainties can be obtained to evaluate the possible reasons. The RMs analyzed here have variable major element compositions and sulfur concentrations (tens of μg g^{-1} to several thousand μg g^{-1}). Most replicates display low variations in S concentrations at the < 5 % (RSD for n > 2) level, indicating homogeneous distribution of S in the powders and no evidence of significant S loss using this method. For instance, komatiite OKUM with the highest variation for S (with the exception of granite GS-N, RSD=38 %) has RSD < 4.2 % (n=6). The new ID results for sulfur are consistent with ranges of literature values, irrespectively of the concentration level (Table 5.3). Our new data suggest that gabbro MRG-1 and Cody shale SCo-1 have about 10 % higher S concentrations than indicated by literature results (Table 5.3). Multiple aliquots of GS-N, using test portion mass of up to 0.7 g, show 38 % RSD (n=3) for S contents of 184 μg g^{-1}. This large variation also appears in literature data (102-170 μg g^{-1}), suggesting that heterogeneity of the sample powder can to some extent affect S results in some RMs (Table 5.3). The S contents of BHVO-1 may also reflect heterogeneous distribution of S in the sample powder. Sulfur data of two BHVO-1 duplicates in this study yield 83 μg g^{-1}, about 10 %-15 % lower than an earlier compiled value (102 μg g^{-1}, Govindaraju, 1994) and ID-ICP-MS data (93 μg g^{-1}, Makishima and Nakamura, 2001), but noticeably higher than the results of 47 μg g^{-1} and 54 μg g^{-1} obtained by combustion elemental analyzer and ICP-MS, respectively (Erdman et al. 2013).

As for sulfur, Se and Te also yield precise results for most RMs that often agree well with literature data (e.g., BHVO-1 and SCo-1, Table 5.3). Some RMs

which yield very precise results (e.g., MAG-1 and OKUM) have 10-20 % higher Se contents than data from the literature. Only GS-N displays large variability for Se (RSD=45 %) and Te (RSD=27 %), probably because of the heterogenous distribution of sulfide in the sample powder. The good reproducibility of S, Se and Te abundances indicate that most RMs analyzed in this study are homogenous for chalcogen element abundances at the ±5 % level for 0.5-1 g of sample. In particular, OKUM, SCo-1, MRG-1, DR-N and MAG-1 are good candidates for quality control, method development and calibration of chalcogen element abundances in rock samples.

5.5.4 Platinum group elements and rhenium

Concentrations of the PGEs in the RMs show large concentration ranges, from the pg g^{-1} to ng g^{-1} level, and most have low concentrations (Table 5.4). Data of replicate analyses of BHVO-1, MRG-1, GS-N, RGM-1, SCo-1, MAG-1 and OKUM display large variations for most PGEs, and precisions vary from one element to another (Table 5.4). Overall, as in literature data, Re shows the lowest variations. For instance, SCo-1 displays <1 % RSD for Re, but much larger variations for the PGEs. Two OKUM sub-splits with different numbers have yielded very precise results for Ir, Ru and Pd abundances in the replicates (a few percent RSD, n=6). However, Re, Os and Pt abundances have large variations (RSD>20 %), implying heterogeneous distribution of discrete Os and Pt rich alloy phases in the sample powder at this test portion size. Other samples with high PGE contents also show considerable abundance variations between different digestions, consistent with previous isotope dilution data (Peucker-Ehrenbrink et al. 2003, Meisel and Moser 2004a, 2004b, Savard et al. 2010). As discussed in previous studies, the poor reproducibility for some elements in specific RMs likely reflects heterogeneity of the distribution of trace phases in 1 to 2 g aliquots of sample powder (Meisel et al. 2001b, Meisel and Moser 2004a, 2004b, Savard et al. 2010).

5.5.5 Sample heterogeneity

The HPA-S digestion method has been validated for the analysis of the PGEs and Re in mantle peridotites, but also for other terrestrial rocks with lower abundances of these elements (Meisel et al. 2001a, 2003a, Meisel and Moser 2004a, Lorand et al., 2008, Fischer-Gödde et al. 2011). However, heterogeneous distribution of the PGEs in trace phases (the “nugget effect”) is a major concern, especially for samples with low abundances of these elements (Meisel et al. 2001b, Meisel and Moser 2004b, Savard et al. 2010). In most rocks, the PGEs and Re occur in accessory sulfides, breakdown products of sulfides such as selenides and tellurides, and PGM (e.g., Luguet et al.

2004, Lorand et al. 2008, 2010, Piña et al. 2012). In particular, Ir, Os, Pt and Ru may occur in the form of discrete micro-PGM or alloys (Lorand et al. 2008, 2010). Gravitational settling and segregation of such accessory phases can lead to heterogeneous distributions of these trace elements in sample powders. The results in previous (Meisel and Moser 2004b) and the present study indicate that for such samples, 1-2 g material is not large enough to obtain abundance data at acceptable levels (e.g., 10 % RSD). Samples such as NIM-P and NIM-D with higher PGE contents are also not necessarily homogenous (Table 5.4). OKUM is relatively homogenous for Ir (RSD=8 %, n=6), Ru (RSD=2 %, n=6), and Pd (RSD=4 %, n=6), but not for Pt and Os at a test portion size < 1 g.

The systematics of the highly variable Os and Pt contents of OKUM require a closer inspection. Three replicates of OKUM4128/1164 have around 30 ng g^{-1} Pt, much higher than OKUM4210/1114 with about 11-15 ng g^{-1} Pt. Some replicates of both splits have anomalously high and variable Os contents (4-9 ng g^{-1} versus mostly 0.8 ng g^{-1}) and such high Os contents do not necessarily corresponds to high Pt contents. A large number of literature data for OKUM (Barnes and Fiorentini 2008, Maier et al. 2009, 2012, Savard et al. 2010) have shown reproducible results for Ru, Pd, Ir, Pt but more heterogeneity for Re and Os (Table 5.4). Some komatiites may have heterogeneous distribution of some PGEs or Re (e.g., Meisel et al. 2001b, Meisel and Moser 2004a), but obviously, it is necessary to explain why such significant differences exist for OKUM. The $^{187}Os/^{188}Os$ ratio can assist in understanding the heterogeneous distribution of PGEs and Re in sample powders (Meisel et al. 2001b). Replicates of OKUM with high Os contents also have relatively radiogenic $^{187}Os/^{188}Os$ of 0.52-0.57 compared to values between 0.27 and 0.31 in low Os replicates (Figure 5.1 and Table 5.4). Such high Os contents with radiogenic Os isotopes are obviously not related to differences in Re contents or Re/Os ratios of replicates. OKUM replicates were digested and measured in three different batches (Table 5.1) and during this period no samples with such high Os contents and with $^{187}Os/^{188}Os$ of 0.52-0.57 were digested in our lab (Tables 5.1 and 5.4). Two replicates of OKUM4128/1164 were digested and measured at different times, but have nearly identical $^{187}Os/^{188}Os$ of 0.57 with high and slightly different Os contents. Thus, accidental contamination during sample digestion, Os extraction and measurement is a very unlikely explanation for the poor precision data of some of these elements (but not others, e.g., Ru and Pd, Table 5.4). We note that Ir abundances also show some systematic variability that appears to correlate with Pt and less so with Os contents. The most likely explanation for the significant heterogeneity of Pt, Os and Re abundances and $^{187}Os/^{188}Os$ at the given test portion size of these splits of OKUM is heterogeneity of the powder with respect to PGM trace phases. The Re-Os systematics

also hints at a complicated history of this rock with two or more reservoirs of radiogenic Os (Figure 5.1).

The heterogeneity of the PGE data in most geological RMs contrasts with chalcogen element abundances, which are quite homogeneously distributed in the same sample powder (mostly, RSD <5 %). BHVO-1 (basalt), MRG-1 (gabbro) and OKUM (komatiite) display large variations for the PGEs, but mostly not for the chalcogens. Unlike for the PGEs, 0.5-1 g of sample can achieve very reproducible results for S, Se and Te in most samples. This difference suggests fractionation or decoupling of PGE and chalcogen abundances in natural samples of different major element compositions. The likely process that leads to such chemical fractionation is exsolution of secondary sulfides, selenides, tellurides or alloy phases during cooling of high-temperature magmatic or hydrothermal sulfides (e.g., Luguet et al. 2004, Lorand et al. 2008, Piña et al. 2012). In ultramafic rocks from the mantle, PGM phases that are relics of high degree melting may contribute to powder heterogeneity (e.g., Luguet et al. 2007, Lorand et al. 2010). However, where such secondary phases are absent or subordinate, determination of PGEs, Re and chalcogen element abundances from the same sample aliquot can be advantageous to better constrain the details of the fractionation of these elements in natural systems (e.g., Wang et al., 2013).

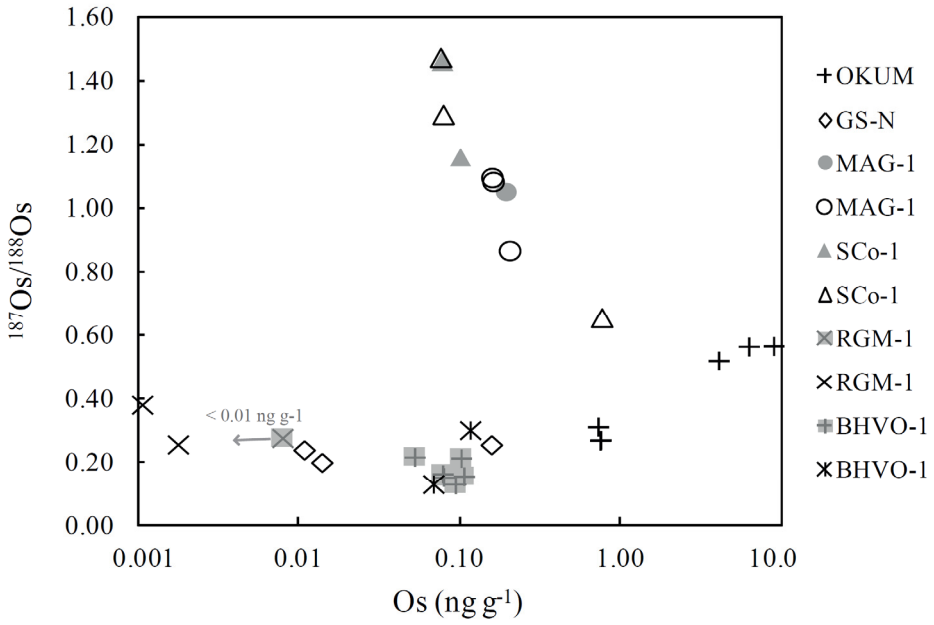

Figure 5.1. Osmium contents and $^{187}Os/^{188}Os$ in replicates of reference materials measured in this study (data from Table 5.4), showing some extent of sample heterogeneity. Six replicates of OKUM have different Os contents and $^{187}Os/^{188}Os$. Gray symbols are literature data from Table 5.4 for comparison. Precisions for $^{187}Os/^{188}Os$, including blank contribution, are in most cases smaller than the size of the symbols.

5.5.6 NIST SRM 612

The new isotope dilution results for selected elements in NIST SRM 612 are listed in Table 5.5. With the exception of a previous determination for Pd and Pt abundances in the glass by isotope dilution (Sylvester and Eggins 1997), the limited literature data for the PGEs, S and Se were obtained mostly by micro analytical methods, such as LA-ICP-MS, calibrated using other RMs (Table 5.5) (Jochum et al. 2011). Micro-analytically determined S contents show large variability with considerable uncertainty, ranging from 133 μg g^{-1} to 450 μg g^{-1} (Table 5.5). Our four ID determinations of the concentration in the bulk glass yield good precision (296±4 μg g^{-1}, RSD=1.4 %) and the values are close to the result of 270±100 μg g^{-1} obtained by EPMA (Jochum et al. 2011), but lower than most values obtained by LA-ICP-MS (e.g., 377 μg g^{-1}, Jochum et al., 2011). The new data for the Se contents (16.5±0.2 μg g^{-1}, 1s) matches a previous result obtained by LA-ICP-MS (16.3 μg g^{-1}, Jochum et al., 2011). Both determinations are slightly higher than the "preferred value" of 15.2±0.2 μg g^{-1} (1s), obtained by LA-ICP-MS (Jenner et al. 2009). The bulk glass values indicate homogenous S and Se distribution at the 25 to 30 mg test portion level. The precise Se value obtained in the present work is consistent with decreasing element heterogeneity with increasing test portion size (see Jochum et al. 2011). No Te data has been available before for SRM 612. The new Te data also indicates homogenous distribution of Te (RSD=2.4 %, n=4) for bulk glass samples. Palladium and Pt data are also relatively homogenous in this study, but our values are somewhat lower than literature data (Table 5.5). For instance, our mean result for Pt (2.41±0.05 μg g^{-1}, 1s) is a few percent lower than published 2.44 to 2.59 μg g^{-1}. The mean result for Pd (0.84±0.03 μg g^{-1}, 1s) is about 20 % lower than data from previous measurements, also obtained by isotope dilution (1.09±0.09 μg g^{-1}, 1s) (Sylvester and Eggins 1997) and LA-ICP-MS data, e.g., 1.03±0.04 μg g^{-1} (1s) calibrated to NIST SRM 610 (Hu et al. 2009), and 0.91±0.07 μg g^{-1} (1s, ^{105}Pd measured) or 0.99±0.07 μg g^{-1} (1s, ^{106}Pd and ^{108}Pd measured) calibrated to NIST SRM 614/615 (Sylvester and Eggins 1997) (Table 5.5). Values of NIST SRM 610 and 614/615 from Sylvester and Eggins (1997) used for calibration were determined by isotope dilution. The Pd concentrations calculated using ^{105}Pd/^{108}Pd and ^{105}Pd/^{106}Pd are very similar in this study (<2 % variation, Table 5.5). A possible reason of our systematic lower values might be some strong oxide interference on the spike isotope ^{105}Pd, such as ^{89}YO because of high concentration ratio of Y/Pd (38.3 μg g^{-1} versus 0.84 μg g^{-1}). However, this explanation can be excluded, because cation exchange resin was employed to remove most matrix elements (including Y), as indicated by the negligible amount of Cd (which interferes with ^{106}Pd and ^{108}Pd) in the PGE fraction. Furthermore, oxide formation rates were <0.3-0.4 % (CeO^+/Ce^+) with the Aridus. Alternatively, the Pd spike may not have

equilibrated completely with Pd in the glass during the HF-HNO_3 digestion. This could be a problem for any isotope dilution determination. The precise concentration results of different digestions (±3 % RSD) are difficult to reconcile with such a scenario, but it also cannot be excluded. Because a mixed Ru-Pd-Ir-Pt spike was used, and Ir and Ru contents in the glass are much lower than contents of Pt and Pd, Ir and Ru were strongly over-spiked and large uncertainties exist for their concentrations. Iridium values are 4.8±0.4 ng g^{-1} (1s), similar to 4.5±1.2 ng g^{-1} (1s) obtained by LA-ICP-MS data (Hu et al. 2009), and the Ru content should be below 2 ng g^{-1}.

5.6 Summary

Abundances of chalcogen elements (S, Se and Te), Re and most PGEs (Ru, Pd, Os, Ir, and Pt) have been determined in the same digestion aliquot in 0.5-1 gram of geological RMs of different compositions. The contents were analyzed by isotope dilution ICP-MS and negative TIMS, after digestion in concentrated HNO_3 and HCl in a high-pressure asher at 320°C. Replicate digestions of RMs yield precise results (mostly RSD < 5 %) for S, Se and Te, which are generally consistent with previous values, irrespectively of the concentration range. A few samples yielded somewhat higher S and Se contents (about 10-20 %) compared to literature data, suggesting the utility of the HPA-S digestion method for these volatile elements. In contrast, PGE contents in the same digestion aliquots of the RMs often display poor reproducibility, especially in low concentration samples. Different PGEs and Re display different degrees of heterogeneity. As in previous studies (e.g., Meisel and Moser 2004a, 2004b), the reproducibility of Re concentrations is commonly better than the reproducibility of PGE concentrations. The contrasting variations for different PGEs, in comparison to Re, S, Se and Te imply control by different accessory phases and heterogeneous distribution of these phases and their main elements in RM powders (for instance by gravitational settling). Determination of chalcogens and PGEs in the same sample aliquot can help identifying their fractionation and relationship in geological processes.

Abundances of S, Se, Te, Ru, Pd, Ir and Pt in NIST SRM 612 glass were determined by isotope dilution in bulk glass aliquots digested in concentrated HF and HNO_3 on a hotplate. Bulk glass concentrations of the chalcogen elements, Pt and Pd are homogenous for 25-30 mg aliquots and contrast with the known element heterogeneity of Se, Pd and Pt at the tens of micrometer scale (< 1 µg test mass), indicated by micro analysis (Jochum et al. 2011).

Acknowledgements

We thank Thomas Meisel for providing two powder aliquots of OKUM, his comments on the manuscript and editorial handling. Comments from two reviewers resulted in significant improvement of the manuscript. We thank Frank Wombacher and Claudia Funk for discussions, and Monika Feth, Timo Gawronski, Konrad Hammerschmidt and Simon Hohl for support in the lab. This work was supported by funds of Freie Universität Berlin and a China Scholarship Council fellowship to Z. Wang.

Table 5.1 Reference materials analyzed in this study

Sample	Rock type	Sample source	Replicate number	Test portion mass (g)	Digestion date	Analysis date for Os
BHVO-1	Basalt	USGS	a	0.76	2012-7-3	2012-7-9
			b	0.70	2012-9-12	2012-10-12
OKUM4128/1164	Komatiite	OGS	a	0.96	2012-5-7	2012-7-9
			b	0.69	2012-11-13	2012-11-21
			c	0.98	2012-9-19	2012-10-12
OKUM4210/1114	Komatiite	OGS	a	1.03	2012-5-7	2012-7-9
			b	0.71	2012-11-13	2012-11-21
			c	0.99	2012-9-19	2012-10-12
MRG-1	Gabbro	CCRMP	a	0.88	2012-7-3	2012-7-9
			b	0.90	2012-9-12	2012-10-12
			c	0.81	2012-11-23	2013-1-29
GS-N	Granite	ANRT	a	0.73	2012-7-10	2012-7-30
			b	0.83	2012-9-12	2012-10-12
			c	0.72	2012-11-13	2012-11-21
RGM-1	Rhyolite	USGS	a	0.79	2012-7-18	2012-7-30
			b	0.83	2012-11-23	2013-1-29
SCo-1	Cody shale	USGS	a	0.72	2012-7-31	2012-10-12
			b	0.79	2012-9-12	2012-10-12
			c	0.72	2012-11-13	2012-11-21
MAG-1	Marine mud	USGS	a	0.51	2012-7-31	2012-10-12
			b	0.50	2012-11-23	2013-1-29
			c	0.49	2012-11-23	2013-1-29
DR-N	Diorite	ANRT		0.66	2012-7-3	2012-7-9
AN-G	Anorthosite	GIT-IWG		1.03	2012-7-3	2012-7-9
MA-N	Granite	GIT-IWG		0.92	2012-7-18	2012-7-30
SO-3	Soil	CCRMP		1.02	2012-7-31	2012-10-12
NIM-P	Pyroxenite	MINTEK		0.84	2012-7-10	2012-7-30
NIM-D	Dunite	MINTEK		0.79	2012-7-10	2012-7-30
BM	Basalt	ZGI		0.72	2012-7-10	2012-7-30
NIM-S	Syenite	MINTEK		0.97	2012-7-18	2012-7-30
NIM-L	Lujavrite	MINTEK		1.01	2012-7-18	2012-7-30
TB	Shale	ZGI		0.69	2012-7-31	2012-10-12
NIST SRM 612	Silicate glass	NIST		0.030	2013-2-26	

Sample sources: USGS- United States Geological Survey, OGS- Ontario Geological Survey, Canada, CCRMP- Canadian Certified Reference Materials Project, ANRT- Association Nationale de la Recherche Technique, Paris, GIT-IWG- Groupe International de Travail-International Working group, MINTEK- Coucil for Mineral Technology, South Africa, ZGI- Zentrales Geologishes Institut, Berlin, NIST-National Institute of Standards and Technology. See the details in Govindaraju (1994).

Table 5.2 Limits of detection and total procedural blanks (TPB) of the methods used in the study

Elements	S	Se	Te	Ru	Pd	Ir	Pt	Re	Os
Detection limits of ID-ICP-MS (ng ml^{-1})	50		0.05	0.0005	0.002	0.0003	0.009	0.0004	
Detection limits of HG-ID-ICP-MS (ng ml^{-1})		0.06	0.003						
TPB (ng)	4000	1.9	0.030	0.0004	0.026	0.0007	0.039	0.0042	0.002
1s (ng, n=6)	1200	0.8	0.028	0.0003	0.020	0.0005	0.032	0.0019	0.002
Procedural detection limits (3s of TPB, ng)	3600	2.4	0.084	0.0009	0.06	0.0015	0.096	0.0057	0.006
Anomalously high TPB value (ng)			0.083		0.065		0.118		0.0053
TPB (ng) without the anomalous value			0.019		0.02		0.026		0.001
1s (ng, n=5)			0.012		0.008		0.012		0.0006
Procedural detection limits (3s of TPB, ng)			0.036		0.024		0.036		0.0018

Note: Detection limits of ID-ICP-MS is based on the equation of Yu et al. (2002). Procedural detection limits are expressed as three times the standard deviation of the procedural blanks.

Table 5.3 Concentration results of S, Se and Te obtained by isotope dilution methods in geological reference materials

Sample	Replicate	S (μg g^{-1})					Se (ng g^{-1})					Te (ng g^{-1})				
		This study		Literature			This study		Literature			This study		Literature		
		Values	RSD (%)	Values	Methods	Ref.	Values	RSD (%)	Values	Methods	Ref.	Values	RSD (%)	Values	Methods	Ref.
BHVO-1	a	83		93	ID-ICP-MS	M&N1	81		74	Compiled	Go	4.9		4.9	ID-ICP-MS	M&N9
	b	83		102	Compiled	Go	80		79	ID-HG-ICP-MS	Fo	5.0		6.4	Compiled	Go
				54	ICP-MS	Er			99	ID-ICP-MS	M&N9			6.4	ID-HG-ICP-MS	Fo
				47	CEA	Er			101	GF-AAS	Ma			8.0	ICP-MS	H&G
OKUM4128/1164	a	233		241	CEA	B	156		110	TCF-INAA	Sa	23.2				
	b	242					160		139	HG-ICP-MS	Sa					
	c	234					152									
OKUM4210/1114	a	233					147					23.9				
	b	257					144					25.3				
	c	231					156					26.7				
Mean		**238**	**4.2%**				**153**	**4.0%**				**24.8**	**7.1%**			
MRG-1	a	677		600	XRF	Gl	225		194	Compiled	Go	33.8		32	HG-ICP-MS	H&P
	b	663		610	Compiled	Go			199	HG-ICP-MS	H&P	34.2		46	Compiled	Go
	c	668							199	Compiled	Sa					
Mean		**669**	**1.1%**						209	TCF-INAA	Sa					
									210	GF-AAS	Ma					
GS-N	a	176		102	ICP-OES	Ac	10		4	HG-AAS	T&I	3.76		2.4	GF-AAS	Te
	b	118		133	ICP-AES	Ok	5		<20	GF-AAS	Ma	2.20				
	c	258		136	CEA	Ac	14					2.90				
Mean		**184**	**38%**	140	Compiled	Go	**10**	**45%**				**2.95**	**27%**			
				156	IC	M&V										
				170	CEA	An										
RGM-1	a	14		35	IC	M&V	<2		6	Compiled	Go	1.45		1.5	ICP-MS	H&G
	b	17		54	Compiled	Go	<2		<6	HG-ICP-MS	H&P	0.23		15	HG-ICP-MS	H&P
									<20	GF-AAS	Ma					
SCo-1	a	679		593	CEA	B	858		788	TCF-INAA	Sa	78.3		77	Compiled	Go
	b	693		630	Compiled	Go	874		823	HG-ICP-MS	H&P	80.5		76	ICP-MS	H&G
	c	728		570	CEA	An	897		841	Compiled	Sa	79.6		82	HG-ICP-MS	H&P
Mean		**700**	**3.6%**	640	CEA	An	**876**	**2.3%**	861	HG-ICP-MS	H&P	**79.5**	**1.4%**			
									890	Compiled	Go					
									890	GF-AAS	Ma					
MAG-1	a	3884		3500	CEA	An	1265		1010	GF-AAS	Ma	73.1		66	Compiled	Go
	b	3789		3900	Compiled	Go	1249		1013	TCF-INAA	Sa	72.6		75	HG-ICP-MS	H&P
	c	3879		4096	CEA	K	1247		1015	HG-ICP-MS	H&P	71.8				
Mean		**3850**	**1.4%**	3820	ICP-MS	Er	**1254**	**0.8%**	1060	Compiled	Sa	**72.5**	**0.9%**			
									1160	Compiled	Go					

Sample	Replicate	S (μg g^{-1})					Se (ng g^{-1})					Te (ng g^{-1})				
		This study		Literature			This study		Literature			This study		Literature		
		Values	RSD (%)	Values	Methods	Ref.	Values	RSD (%)	Values	Methods	Ref.	Values	RSD (%)	Values	Methods	Ref.
DR-N		438		350	Compiled	Go	89		82	GF-AAS	Ma	19.6		19	GF-AAS	Te
				390	IC	Ga			82	HG-AAS	T&I					
				433	ICP-AES	Ok			87	Compiled	Sa					
									100	TCF-INAA	Sa					
AN-G		152		138	ICP-AES	Ok	60		41	HG-AAS	T&I	3.03		3.1	GF-AAS	Te
				140	Compiled	Go			45	GF-AAS	Ma					
				155	CEA	B			46	TCF-INAA	Sa					
				160	IC	Ga			49	Compiled	Sa					
				205	IC	M&V			60	Compiled	Go					
MA-N		45		42	IC	M&V	12		7	HG-AAS	T&I	2.15		1.6	GF-AAS	Te
				51	ICP-AES	Ok			<20	GF-AAS	Ma					
				93	IC	M&V										
				100	Compiled	Go										
SO-3		132		132	Compiled	Go	26		25	HG-ICP-MS	H&P	11.8		10	HG-ICP-MS	H&P
NIM-P		134					32					3.85				
NIM-D		74					7					1.38				
BM		140					90					1.23				
NIM-S		35					3					1.97				
NIM-L		654					39					0.13				
TB		119					66					23.2				

Note: Mean values with RSD uncertainty are given when replicate number ≥ 3. Except Te data in BHVO-1 (by ID-ICP-MS), all Se and Te data in this study were analyzed by ID-HG-ICP-MS. S data by ID-ICP-MS. Precisions of total procedural blanks (Te=19±12 pg; Se=1.9±0.8 ng; S=4.0±1.2 μg) are the main contribution factor to measurement uncertainty of abundances, especially for samples with low concentration. Ion chromatography (IC), combustion elemental analyzer (CEA), optical emission spectrometer (OES), thiol cotton fiber (TCF), and graphite furnace (GF). Ref.: Ac - (Ackerman et al. 2012), An - (Andrade et al. 2009), B - (Bédard et al. 2008), Er- (Erdman et al. 2013), Fo - (Forrest et al. 2009), Ga - (Gazulla et al. 2009), Go - (Govindaraju 1994), Gl - (Glasby et al. 2004), H&G - (Hu and Gao 2008), H&P - (Hall and Pelchat 1997), K - (Kubota 2009), Ma - (Marin et al. 2001), M&N1 - (Makishima and Nakamura 2001), M&N9 - (Makishima and Nakamura 2009), M&V - (Michel and Villemant 2003), Ok - (Okai et al. 2001), Sa - (Savard et al. 2009), T&I - (Terashima and Imai 2000), Te - (Terashima 2001)

Table 5.4 Concentration results (ng g^{-1}) of Re, Os, Ir, Ru, Pt and Pd obtained by isotope dilution in geological reference materials

Sample	Replicate	Ru	RSD %	Pd	RSD %	Ir-a	Ir-b	Ir-Mean	RSD %	Pt-a	Pt-b	Pt-Mean	RSD %	Re	RSD %	Os	RSD %	$^{187}Os/^{188}Os$	±2s	data source
BHVO-1	a	0.064		2.74		0.135	0.102	0.118		4.72	4.12	4.42		0.329		0.069		0.132	0.003	this study
	b	0.139		3.39		0.056	0.061	0.059		1.70	1.60	1.65		0.328		0.117		0.303	0.003	this study
		0.186		2.98				0.097				2.67		0.307		0.080		0.154		(Meisel and Moser 2004b)
		0.162		3.08				0.081				2.72		0.297		0.079		0.164		(Meisel and Moser 2004b)
		0.131		3.08				0.079				2.34		0.301		0.107		0.157		(Meisel and Moser 2004b)
		0.215		2.99				0.061				2.85		0.297		0.053		0.218		(Meisel and Moser 2004b)
		0.381		3.16				0.107				4.81		0.287		0.103		0.215		(Meisel and Moser 2004b)
		0.23	4%	3.55	20%			0.031	36%			4.07	13%	0.55	61%					(Meisel and Moser 2004b)
				2.86	7%			0.095	15%			2.3	19%			0.095	7%	0.1314		(Peucker-Ehrenbrink et al. 2003)
				3				0.44				2								(Govindaraju 1994)
								<3												(Bédard and Barnes 2002)
OKUM4128/1164	a	4.48		11.5		0.869	0.873	0.871		32.3	32.3	32.3		0.356		0.755		0.2718	0.0006	this study
	b	4.47		12.3		1.05	0.980	1.02		27.4	27.8	27.6		0.395		6.30		0.5661	0.0001	this study
	c	4.61		11.8		0.942	0.956	0.949		30.1	29.4	29.7		0.526		9.00		0.5677	0.0004	this study
OKUM4210/1114	a	4.38		11.5		0.859	0.867	0.863		11.2	11.2	11.2		0.325		0.755		0.2704	0.0005	this study
	b	4.37		12.6		0.817	0.811	0.814		14.8	15.0	14.9		0.337		0.729		0.3139	0.0007	this study
	c	4.33		11.4		0.860	0.877	0.869		11.3	10.9	11.1		0.485		4.10		0.5213	0.0002	this study
Mean		**4.44**	**2%**	**11.8**	**4%**			**0.897**	**8%**			**21.1**	**46%**	**0.404**	**21%**	**3.61**	**97%**			
		4.33	12%	11.35	7%			1.00	13%			11.00	5%	0.16	60%	0.98	35%			(Savard et al. 2010)
		4.15	2%	12.20	6%			0.943	4%			11.44	2%	0.566	6%	0.790				(Savard et al. 2010)
		4.39	7%	11.43	7%			1	6%			10.4	3%			0.83	7%			(Maier et al. 2009)
		4.11	2%	12.24	3%			0.944	4%			11.47	3%			0.8				(Maier et al. 2009)
		4.53		11.93				0.99				11.44				0.78				(Maier et al. 2012)
		4.2	12%	11.8	3%			1.05	7%			11.6	3%							(Barnes and Fiorentini 2008)
MRG-1	a	0.138		5.76		0.112	0.116	0.114		5.73	5.65	5.69		0.435		0.082		0.295	0.004	this study

Sample	Replicate	Ru	RSD %	Pd	RSD %	Ir-a	Ir-b	Ir-Mean	RSD %	Pt-a	Pt-b	Pt-Mean	RSD %	Re	RSD %	Os	RSD %	$^{187}Os/^{188}Os$	±2s	data source
	b	0.058		5.93		0.102	0.104	0.103		5.77	5.77	5.77		0.310		0.045		0.450	0.010	this study
	c	0.044		5.60		0.100	0.093	0.097		7.31	7.30	7.30		0.370		0.061		0.397	0.007	this study
Mean		**0.08**	**64%**	**5.76**	**3%**			**0.104**	**9%**			**6.25**	**15%**	**0.372**	**17%**	**0.063**	**30%**			
GS-N	a	0.069		2.20		0.009	0.015	0.012		0.09	0.21	0.15		0.059		0.159		0.257	0.002	this study
	b	0.011		2.10		0.008	0.002	0.005		0.56	0.41	0.49		0.073		0.011		0.24	0.03	this study
	c	0.023		0.25		0.008	0.007	0.008		1.20	1.20	1.20		0.101		0.014		0.20	0.02	this study
Mean		**0.035**	**89%**	**1.52**	**72%**			**0.007**	**32%**			**0.61**	**88%**	**0.077**	**28%**	**0.061**	**138%**			
RGM-1	a	0.012		0.09		0.001	0.002	0.002		0.44	0.45	0.45		0.062		0.001		0.38	0.39	this study
	b	0.003		0.14		0.003	0.001	0.002		0.30	0.04	0.17		0.025		0.002		0.26	0.16	this study
				<0.01				<0.020				1.06	2%	0.044	55%	<0.010		0.278		(Meisel and Moser 2004b)
								<2												(Bédard and Barnes 2002)
SCo-1	a	0.063		1.93		0.015	0.023	0.019		0.53	0.53	0.53		1.04		0.770		0.658	0.001	this study
	b	0.032		1.96		0.024	0.015	0.019		1.12	1.09	1.11		1.03		0.077		1.48	0.02	this study
	c	0.027		1.80		0.022	0.009	0.016		2.30	2.25	2.28		1.04		0.080		1.30	0.02	this study
Mean		**0.041**	**47%**	**1.90**	**4%**			**0.018**	**11%**			**1.30**	**68%**	**1.04**	**0.4%**	**0.309**	**129%**			
		0.115		0.796				0.054				0.565		1.05		0.080		1.46		(Meisel and Moser 2004b)
		0.103		0.917				0.048				2.56		1.05		0.103		1.16		(Meisel and Moser 2004b)
		0.095		0.814				0.046				1.39		1.00		0.079		1.46		(Meisel and Moser 2004b)
		0.061		0.817				0.031				0.66		0.91		0.080		1.47		(Meisel and Moser 2004b)
		0.108		0.847				0.059				0.58		1.06						(Meisel and Moser 2004b)
								<3												(Bédard and Barnes 2002)
				1																(Govindaraju 1994)
MAG-1	a	0.109		0.90		0.034	0.039	0.037		1.04	1.05	1.05		4.11		0.206		0.869	0.007	this study
	b	0.099		2.69		0.024	0.033	0.029		1.59	1.57	1.58		3.90		0.160		1.097	0.012	this study
	c	0.082		1.24		0.036	0.032	0.034		2.18	2.16	2.17		3.85		0.163		1.085	0.012	this study
Mean		**0.097**	**14%**	**1.61**	**59%**			**0.033**	**12%**			**1.60**	**35%**	**3.95**	**4%**	**0.176**	**15%**			
		0.167	269%	1.24	36%			0.095	97%			1.45	29%	3.91	29%	0.198	39%	1.05		(Meisel and Moser 2004b)
								<2												(Bédard and Barnes 2002)
								<2.4												(Constantin 2009)
				1.7																(Govindaraju

Sample	Replicate	Ru	RSD %	Pd	RSD %	Ir-a	Ir-b	Ir-Mean	RSD %	Pt-a	Pt-b	Pt-Mean	RSD %	Re	RSD %	Os	RSD %	$^{187}Os/^{188}Os$	±2s	data source
																				1994)
DR-N		0.079		0.93		0.032	0.022	0.027		0.37	0.37	0.37		0.239		0.010		2.00	0.32	this study
								<3.8												(Constantin 2009)
AN-G		0.143		0.45		0.018	0.030	0.024		0.35	0.74	0.55		0.165		0.022		2.47	0.12	this study
								<3												(Bédard and Barnes 2002)
								<1.7												(Constantin 2009)
NIM-P		43.0		16.9		7.44	7.50	7.47		33.7	34.0	33.9		0.335		2.99		0.1332	0.0001	this study
		9.0		5.4				1.9				11								(Plessen and Erzinger 1998)
								7.8												(Constantin 2009)
NIM-D		1.64		0.64		0.228	0.229	0.228		14.8	14.8	14.8		0.077		0.093		0.208	0.003	this study
		1.9		0.88				0.44				13								(Plessen and Erzinger 1998)
		2.14		1.74				1.24				88.4		0.032		0.295				(Meisel and Moser 2004a)
		1.93		0.75				0.35				19.0		0.154		0.258				(Meisel and Moser 2004a)
		1.92		0.92				0.35				19.2		0.152						(Meisel and Moser 2004a)
		2.02		0.68				0.34				27.8		0.200						(Meisel and Moser 2004a)
								<1.1												(Constantin 2009)
BM		0.031		1.37		0.005	0.008	0.007		0.07	0.08	0.08		0.283		0.075		3.04	0.06	this study
		<0.002		0.1				<0.001				<0.005								(Plessen and Erzinger 1998)
NIM-S		0.209		0.56		0.025	0.025	0.025		0.53	0.56	0.54		0.053		0.031		0.223	0.007	this study
		<0.3		0.067				0.010				0.099								(Plessen and Erzinger 1998)
								<1.0												(Constantin 2009)
NIM-L		0.020		0.05		0.003	0.008	0.006		0.07	0.10	0.08		0.217		0.010		9.8	1.7	this study
								<1.5												(Constantin 2009)
TB		0.059		0.37			0.054	0.054		1.07	0.69	0.88		0.329		0.016		1.38	0.11	this study
		0.023		0.26				0.020				0.13								(Plessen and Erzinger 1998)
SO-3		0.030		0.28			0.012	0.012		0.87	0.44	0.65		0.115		0.510		0.635	0.001	this study
MA-N		0.055		0.31		0.007	0.016	0.011		0.90	1.00	0.95		0.094		0.003		0.75	0.22	this study

Note: Mean values with RSD uncertainty from this study are given when duplicate number ≥ 3. These RSD values often reflect heterogeneity within the sample powder and possible measurement uncertainty when sample intensities are low. For details on the precision of analyses, see main text. Previous detailed results of BHVO-1, SCo-1 and NIM-D are given for comparison to illustrate heterogeneity of PGE abundances within the sample powders. Iridium and Pt results are means of two analyses of Re-Ir-Pt fraction (a) and Ru-Pd-Ir-Pt fraction (b) using a Scott-type spray chamber and an Aridus desolvation unit, respectively. In most cases the different modes of analyses of Ir and Pt yielded similar concentrations. In a few cases with low signal intensities, the Pt data yielded large differences in concentrations. Values with such large variations are underlined. Uncertainty of Os isotopes (2s) includes blank correction.

Table 5.5 Isotope dilution results for four duplicates of NIST SRM 612 glass

Sample No.	Test size	S		Se		Te-a	Te-b	Te-Mean	Pt-a	Pt-b	Pd-a	Pd-b	Ir		Ru
	mg	µg g^{-1}		µg g^{-1}		µg g^{-1}	µg g^{-1}	µg g^{-1}	µg g^{-1}	µg g^{-1}	µg g^{-1}	µg g^{-1}	ng g^{-1}		ng g^{-1}
612waferA-1	28.7	300		16.7		31.7	30.8	31.3	2.34	2.33	0.870	0.842	5.2		0.1
612waferA-2	26.8	295		16.6		31.2	31.2	31.2	2.43	2.40	0.809	0.798	4.4		1.1
612waferB-1	30.8	299		16.3		30.0	29.7	29.9	2.45	2.43	0.829	0.819	4.7		2.0
612waferB-2	29.9	291		16.6		31.4	30.8	31.1							
Mean		**296**		**16.5**		**31.1**	**30.6**	**30.9**	**2.41**	**2.38**	**0.84**	**0.82**	**4.8**		**1.1**
SD		4		0.2		0.7	0.6	0.7	0.05	0.05	0.03	0.02	0.4		1.0
RSD		1.4%		0.9%		2.4%	2.0%	2.3%	2.3%	2.2%	3.7%	2.7%	8.4%		91%
Literature data		377	(Jochum et al. 2011)	16.3	(Jochum et al. 2011)				2.51	(Jochum et al. 2011)	1.05	(Jochum et al. 2011)	4.5	(Jochum et al. 2011)	
		270±100	(Jochum et al. 2011)	15.2±0.2	(Jenner et al. 2009)				2.49±0.05	(Hu et al. 2009)	1.03±0.04	(Hu et al. 2009)	4.5±1.2	(Hu et al. 2009)	
		350±35	(Jochum et al. 2006)	15.1±1.0	(Jenner et al. 2009)				*2.59±0.03*	(Sylvester and Eggins 1997)	*1.09±0.09*	(Sylvester and Eggins 1997)			
		440±40	(Guillong et al. 2008)	15.6±0.3	(Jenner et al. 2009)				2.44±0.03	(Sylvester and Eggins 1997)	0.96±0.07	(Sylvester and Eggins 1997)			
		450±50	(Guillong et al. 2008)	15-17	(Gagnon et al. 2008)				2.5	(Gagnon et al. 2008)	1.1	(Gagnon et al. 2008)			
		133±17	(Fitzpatrick et al. 2008)	20	(Fitzpatrick et al. 2008)										
		16	(Pearce et al. 1997)	14.8±0.7	(Savard et al. 2009)										

Note: Two duplicates are from NIST SRM 612 wafer A and B, respectively. Te-a and Te-b were measured from the same sample solution but using a Scott spray chamber (CeO^+/Ce^+ of 3 %-4 %) and Aridus (CeO^+/Ce^+ of 0.2 %-0.3 %), respectively. Different CeO^+/Ce^+ ratios do not change the results. Results a and b of Pt and Pd data are calculated from different isotope ratios (Pt-a: $^{194}Pt/^{196}Pt$; Pt-b:$^{194}Pt/^{19}5Pt$; Pd-a: $^{10}5Pd/^{108}Pd$; Pd-b: $^{105}Pd/^{106}Pd$) and have limited variations. Iridium and Ru were strongly over-spiked and have large uncertainties. The Ru concentration is below 2 ng g^{-1}. Uncertainty of literature data is 1s. Except for the italics and underlined Pt and Pd values (by ID-ICP-MS), all literature values were obtained by micro analysis, mostly LA-ICP-MS.

Chapter 6

Conclusions and Outlook

6.1 Conclusions

The major contribution of this dissertation has been to put constraints on effects of melt extraction and infiltration on abundances of the HSE and chalcogen elements and Os isotopes in mantle peridotites and magmatic fractionation of these elements during melt transport in the mantle, and finally on accretion of a volatile rich late veneer after the Earth's core formation. New methods have been developed to obtain precise data on the chalcogen elements S, Se and Te that may be affected by sample heterogeneity and volatile loss.

Isotope dilution mass spectrometry methods coupled with a closed system high pressure asher digestion have been newly developed in this work to obtain high precision data of the HSE and chalcogens, as well as Os isotopes in the same sample aliquots. Geological reference materials with variable compositions have been analyzed to verify the utility of the analytical methods. The results show that the method may minimize losses of volatile chalcogens and indicates different extent of heterogeneity of chalcogens and HSE, particularly at low test portion size.

Depletions of incompatible HSE relative to compatible HSE in Balmuccia (BM) and Baldissero (BD) likely reflect variable re-equilibration of lherzolites with infiltrating incompatible element depleted melt. The homogeneous composition and Paleozoic Re-Os model ages of lherzolites at BM indicate extensive homogenization by infiltrating incompatible element depleted melt. Significantly scattered HSE contents and coexistence of Paleozoic and Proterozoic model ages of BD samples probably reflects variable melt infiltration into Proterozoic melting residues and limited equilibration of harzburgites and depleted lherzolites. In the harzburgites and dunites, compatible HSE are heterogeneously distributed and tend to be more strongly fractionated compared to lherzolites.

Melt infiltration may result in significant changes of HSE and chalcogen abundances in reacted rocks and in produced melts. The HSE and chalcogen

composition of tabular replacive dunites within BM lherzolites are consistent with melt-rock reaction and localized high fluxes of S undersaturated melt.

Websterites (Cr-diopside suite) and spinel clinopyroxenites (Al-augite suite) form layers and dikes in the BM peridotite massif. The composition of the pyroxenites indicates that they represent cumulates of sulfide saturated melts and constrain magmatic fractionation of the HSE and chalcogens during magma transport in the mantle. High abundances of HSE and Te in the websterites are consistent with a cumulate origin and early sulfide segregation from 'primitive' melts. Clinopyroxenites have HSE and chalcogen element compositions and Sr-Nd-Pb isotopic compositions similar to MORB. The new data indicate early sulfide segregation of precursor melts of MORB like magmas. Websterites have high abundances of most HSE and Te and display less fractionated HSE and chalcogen ratios than in clinopyroxenites. The HSE, chalcogens and Os isotopes in sulfides of websterites show similar abundances and ratios as interstitial sulfides in refertilized peridotites, suggesting possible preferential melting and migration of interstitial sulfides during partial melting and melt-peridotite reaction. Melting of pyroxenites or pyroxenite-peridotite mantle may produce basalts with concentrations of major elements, S, Se and Re that are difficult to distinguish from basalt produced by partial melting of lherzolite. In contrast, melting of pyroxenites should produce heterogeneous abundances of HSE and Te, and variable Os isotopic compositions in basalts due to large abundance variations of these elements in pyroxenites from the mantle.

Data on the peridotites indicate that at low to moderate degrees of partial melting or melt infiltration, the HSE and chalcogens are dominantly controlled by a combination of sulfide-silicate partitioning and dissolution of poorly equilibrated sulfides on grain boundaries. The apparent compatibility of the elements is Pt > Pd > Te (> Au?) > Se ≥ S ≈ Re, as reflected by ratios of Re/Os, Pd/Ir, S/Se and Se/Te and abundances of Pt, Pd, Au, Re, S, Se and Te in mantle residues and melt products. The data yields lower apparent sulfide-silicate partition coefficients for elements such as Pd and Au (< 5000) compared to predicted experimental values (> 10^4 to 10^6, Peach et al., 1994; Fleet et al., 1999; Fonseca et al., 2009; Mungall and Brenan, In press). These discrepancies result from incomplete equilibration of silicate melts with sulfide melts, or from reaction of migrating melts with peridotites during magma transport in the mantle.

The net effects of dissolution of pyroxene and sulfides during partial melting and melt migration are rejuvenation of depleted mantle (some of it being ancient as indicated by unradiogenic $^{187}Os/^{188}Os$, e.g., Harvey, et al., 2006; Liu et al., 2008) by infiltrating melts to form refertilized peridotites during porous melt flow. Although

such processes may lead to multiple generations of sulfides, ratios of Os/Ir, Ru/Ir, Pd/Pt, Pd/Ir, S/Re, S/Se and Se/Te in bulk rock fertile lherzolites from BM, BD and other mantle peridotites, overlap within limited compositional ranges, indicating indistinguishable effects of partial melting and melt infiltration on chalcogen and HSE abundances.

Regression of abundances of S, Se, Te, Pd and Al_2O_3 contents in the peridotites yield minimum abundances of S, Se and Te in the PM, because the Al_2O_3 content of the mantle has an uncertainty of about 20 % (S=211±40 μg/g, Se=80±17 ng/g, Te =11.0±1.7 ng/g, 1σ; or 0.0040±0.0008×CI chondrites). S/Se and Se/Te in the fertile lherzolites change little with decreasing Al_2O_3, with a mean S/Se of 2690±700 (1σ, n=53) and Se/Te of 7.9±1.6 (1σ, n=63). The mean S/Se and Se/Te of mantle lherzolites overlap with CI chondrite values, and are significantly different from ordinary and enstatite chondrites. The chalcogen/HSE ratio of the PM is similar to CM group carbonaceous chondrites, consistent with the view that the HSE signature of the PM reflects a predominance of slightly volatile depleted carbonaceous chondrite like material, possibly with a minor proportion of non-chondritic material. Like the HSE and Os isotopes, the results from chalcogen elements support the late veneer hypothesis. Accretion of a volatile-rich late veneer may have provided between 20 % and 100 % of the budget of water and carbon on the Earth.

6.2 Outlook

The chalcogen elements S, Se and Te in the mantle peridotites suggest a volatile rich late veneer. This would also have supplied a significant amount of water and carbon on the Earth, ranging from 20 % to 100 %. The specific proportion relies on accurate estimates of the water and carbon contents of Earth' interior (Marty, 2012). Accurate estimates will help answer whether some water and carbon were accreted before the late veneer. A late veneer with 0.5 % of the Earth's mass cannot explain the Earth's budget of other siderophile volatile elements (McDonough and Sun, 1995; Palme and O'Neill, 2003), implying that late veneer was not the only source for these volatile elements. More precise data on siderophile volatile elements in the PM will constrain accretion of volatile elements to the Earth before the late veneer and the history of core-mantle fractionation (e.g., O'Neill and Palme, 2008; Schönbächler et al., 2010; Rubie et al., 2011; Ballhaus et al., 2013). For instance, high indium content of the PM was interpreted to reflect a preferential removal proto-crust by impacts (O'Neill and Palme, 2008; Witt-Eickschen et al., 2009). Additionally, recent S isotopic data of MORB have been interpreted to reflect the composition of the Earth's mantle with a slight difference compared to chondrites. The S isotopic

composition was interpreted to reflect metal-silicate fractionation during the segregation of metal into the core. This implies that half of the S content of the mantle was inherited from the main accretion stage of the Earth (Labidi et al., 2013). If correct, this should lead to suprachondritic S/Se in the mantle (Rose-Weston et al., 2009), which is in conflict with the data (Wang and Becker, 2013). Because most MORB have undergone sulfide segregation or degassing, fractionation of S isotopes during these processes cannot be ruled out. If such fractionations occur, S isotopic compositions of MORB may not represent mantle values. Therefore, S isotope data on mantle peridotites can be used to test this hypothesis and data on cumulate pyroxenites may constrain fractionation of S isotopes during melt transport and fractionation in the mantle.

Chapter 7

References

Abe Y., Ohtani E., Okuchi T., Righter K. and Drake M., 2000. Water in the Early Earth. In: Canup R. M. and Righter K. (Eds.), Origin of the Earth and Moon, Tucson, pp. 413-433.

Ackerman L., Walker R. J., Puchtel I. S., Pitcher L., Jelinek E. and Strnad L. (2009) Effects of melt percolation on highly siderophile elements and Os isotopes in subcontinental lithospheric mantle: A study of the upper mantle profile beneath Central Europe. *Geochimica et Cosmochimica Acta* **73**, 2400-2414.

Ackerman L., Rohovec J. and Šebek O. (2012) Determination of total sulfur in fifteen geological materials using inductively coupled plasma-optical emission spectrometry (ICP-OES) and combustion/infrared spectrometry. *Geostandards and Geoanalytical Research* **36**, 407-414.

Ackerman L., Pitcher L., Strnad L., Puchtel I. S., Jelinek E., Walker R. J. and Rohovec J. (2013) Highly siderophile element geochemistry of peridotites and pyroxenites from Horni Bory, Bohemian Massif: Implications for HSE behaviour in subduction-related upper mantle. *Geochimica et Cosmochimica Acta* **100**, 158-175.

Alard O., Griffin W. L., Lorand J. P., Jackson S. E. and O'Reilly S. Y. (2000) Non-chondritic distribution of the highly siderophile elements in mantle sulphides. *Nature* **407**, 891-894.

Alard O., Griffin W. L., Pearson N. J., Lorand J. P. and O'Reilly S. Y. (2002) New insights into the Re-Os systematics of sub-continental lithospheric mantle from in situ analysis of sulphides. *Earth and Planetary Science Letters* **203**, 651-663.

Alard O., Luguet A., Pearson N. J., Griffin W. L., Lorand J. P., Gannoun A., Burton K. W. and O'Reilly S. Y. (2005) In situ Os isotopes in abyssal peridotites bridge the isotopic gap between MORBs and their source mantle. *Nature* **436**, 1005-1008.

Alard O., Lorand J.-P., Reisberg L., Bodinier J.-L., Dautria J.-M. and O'Reilly S. Y. (2011) Volatile-rich metasomatism in Montferrier xenoliths (Southern France): Implications for the abundances of chalcophile and highly siderophile elements in the subcontinental mantle. *Journal of Petrology* **52**, 2009-2045.

Albarède F. (2009) Volatile accretion history of the terrestrial planets and dynamic implications. *Nature* **461**, 1227-1233.

Alexander C. M. O. D., Bowden R., Fogel M. L., Howard K. T., Herd C. D. K. and Nittler L. R. (2012) The Provenances of Asteroids, and Their Contributions to the Volatile Inventories of the Terrestrial Planets. *Science* **337**, 721-723.

Allegre C. J. and Turcotte D. L. (1986) Implications of a 2-Component Marble-Cake Mantle. *Nature* **323**, 123-127.

Anders E. and Grevesse N. (1989) Abundances of the elements: Meteoritic and solar. *Geochimica et Cosmochimica Acta* **53**, 197-214.

Andrade S., Ulbrich H. H., Janasi V. A. and Navarro M. S. (2009) The determination of total hydrogen, carbon, nitrogen and sulfur in silicates, silicate rocks, soils and sediments. *Geostandards and Geoanalytical Research* **33**, 337-345.

Büchl A., Brugmann G., Batanova V. G., Munker C. and Hofmann A. W. (2002) Melt percolation monitored by Os isotopes and HSE abundances: a case study from the mantle section of the Troodos Ophiolite. *Earth and Planetary Science Letters* **204**, 385-402.

Büchl A., Brügmann G. E., Batanova V. G. and Hofmann A. W. (2004) Os mobilization during melt percolation: The evolution of Os isotope heterogeneities in the mantle sequence of the troodos ophiolite, Cyprus. *Geochimica et Cosmochimica Acta* **68**, 3397-3408.

Bédard L. P. and Barnes S.-J. (2002) A comparison of N-type semi-planar and coaxial INAA detectors for 33 geochemical reference samples. *Journal of Radioanalytical and Nuclear Chemistry* **254**, 485-497.

Bédard L. P., Savard D. and Barnes S.-J. (2008) Total sulfur concentration in geological reference materials by elemental infrared analyser. *Geostandards and Geoanalytical Research* **32**, 203-208.

Bézos A., Lorand J. P., Humler E. and Gros M. (2005) Platinum-group element systematics in Mid-Oceanic Ridge basaltic glasses from the Pacific, Atlantic, and Indian Oceans. *Geochimica et Cosmochimica Acta* **69**, 2613-2627.

Ballhaus C., Bockrath C., Wohlgemuth-Ueberwasser C., Laurenz V. and Berndt J. (2006) Fractionation of the noble metals by physical processes. *Contributions to Mineralogy and Petrology* **152**, 667-684.

Ballhaus C., Laurenz V., Münker C., Fonseca R. O. C., Albarède F., Rohrbach A., Lagos M., Schmidt M. W., Jochum K.-P., Stoll B., Weis U. and Helmy H. M. (2013) The U/Pb ratio of the Earth's mantle—A signature of late volatile addition. *Earth and Planetary Science Letters* **362**, 237-245.

Barnes S.-J., Savard D., Bédard L. and Maier W. (2009) Selenium and sulfur concentrations in the Bushveld Complex of South Africa and implications for formation of the platinum-group element deposits. *Mineralium Deposita* **44**, 647-663.

Barnes S. J. and Fiorentini M. L. (2008) Iridium, ruthenium and rhodium in komatiites: Evidence for iridium alloy saturation. *Chemical Geology* **257**, 44-58.

Batanova V. G., Belousov I. A., Savelieva G. N. and Sobolev A. V. (2011) Consequences of Channelized and Diffuse Melt Transport in Supra-subduction Zone Mantle: Evidence from the Voykar Ophiolite (Polar Urals). *Journal of Petrology* **52**, 2483-2521.

Becker H. (1996) Geochemistry of garnet peridotite massifs from lower Austria and the composition of deep lithosphere beneath a Palaeozoic convergent plate margin. *Chemical Geology* **134**, 49-65.

Becker H. (2000) Re-Os fractionation in eclogites and blueschists and the implications for recycling of oceanic crust into the mantle. *Earth and Planetary Science Letters* **177**, 287-300.

Becker H., Shirey S. B. and Carlson R. W. (2001a) Effects of melt percolation on the Re-Os systematics of peridotites from a Paleozoic convergent plate margin. *Earth and Planetary Science Letters* **188**, 107-121.

Becker H., Morgan J. W., Walker R. J., MacPherson G. J. and Grossman J. N. (2001b) Rhenium-osmium systematics of calcium-aluminium-rich inclusions in carbonaceous chondrites. *Geochimica et Cosmochimica Acta* **65**, 3379-3390.

Becker H., Carlson R. W. and Shirey S. B. (2004) Slab-derived osmium and isotopic disequilibrium in garnet pyroxenites from a Paleozoic convergent plate margin (lower Austria). *Chemical Geology* **208**, 141-156.

Becker H., Horan M. F., Walker R. J., Gao S., Lorand J.-P. and Rudnick R. L. (2006) Highly siderophile element composition of the Earth's primitive upper mantle: Constraints from new data on peridotite massifs and xenoliths. *Geochimica et Cosmochimica Acta* **70**, 4528-4550.

Binz C. M., Kurimoto R. K. and Lipschutz M. E. (1974) Trace elements in primitive meteorites—V. Abundance patterns of thirteen trace elements and interelement relationships in enstatite chondrites. *Geochimica et Cosmochimica Acta* **38**, 1579-1606.

Binz C. M., Ikramuddin M., Rey P. and Lipschutz M. E. (1976) Trace-Elements in Primitive Meteorites .6. Abundance Patterns of 13 Trace-Elements and Interelement Relationships in Unequilibrated Ordinary Chondrites. *Geochimica et Cosmochimica Acta* **40**, 59-71.

Birck J. L., Barman M. R. and Capmas F. (1997) Re-Os isotopic measurements at the femtomole level in natural samples. *Geostandards Newsletter* **21**, 19-27.

Bischoff A., Vogel N. and Roszjar J. (2011) The Rumuruti chondrite group. *Chemie der Erde - Geochemistry* **71**, 101-133.

Blichert-Toft J., Albarede F. and Kornprobst J. (1999) Lu-Hf isotope systematics of garnet pyroxenites from Beni Bousera, Morocco: Implications for basalt origin. *Science* **283**, 1303-1306.

Bockrath C., Ballhaus C. and Holzheid A. (2004) Fractionation of the Platinum-Group Elements During Mantle Melting. *Science* **305**, 1951-1953.

Bodinier J. L. and Godard M., 2003. 2.04 - Orogenic, Ophiolitic, and Abyssal Peridotites. In: Holland H. D. and Turekian K. K. (Eds.), Treatise on Geochemistry. **2**, Oxford, pp. 1-73.

Bodinier J. L., Garrido C. J., Chanefo I., Bruguier O. and Gervilla F. (2008) Origin of pyroxenite-peridotite veined mantle by refertilization reactions: Evidence from the Ronda peridotite (Southern Spain). *Journal of Petrology* **49**, 999-1025.

Boelrijk N. A. I. M. (1968) A general formula for “double” isotope dilution analysis. *Chemical Geology* **3**, 323-325.

Borghini G., Rampone E., Zanetti A., Class C., Cipriani A., Hofmann A. W. and Goldstein S. L. (2013) Meter-scale Nd isotopic heterogeneity in pyroxenite-bearing Ligurian peridotites encompasses global-scale upper mantle variability. *Geology*. Doi: 10.1130/g34438.1.

Bottke W. F., Walker R. J., Day J. M. D., Nesvorny D. and Elkins-Tanton L. (2010) Stochastic Late Accretion to Earth, the Moon, and Mars. *Science* **330**, 1527-1530.

Brandon A. D., Walker R. J., Morgan J. W., Norman M. D. and Prichard H. M. (1998) Coupled Os-186 and Os-187 evidence for core-mantle interaction. *Science* **280**, 1570-1573.

Brandon A. D., Norman M. D., Walker R. J. and Morgan J. W. (1999) Os-186-Os-187 systematics of Hawaiian picrites. *Earth and Planetary Science Letters* **174**, 25-42.

Brandon A. D., Walker R. J., Puchtel I. S., Becker H., Humayun M. and Revillon S. (2003) Os-186-Os-187 systematics of Gorgona Island komatiites: implications for early growth of the inner core. *Earth and Planetary Science Letters* **206**, 411-426.

Brandon A. D., Humayun M., Puchtel I. S. and Zolensky M. E. (2005) Re-Os isotopic systematics and platinum group element composition of the Tagish Lake carbonaceous chondrite. *Geochimica et Cosmochimica Acta* **69**, 1619-1631.

Brandon A. D., Walker R. J. and Puchtel I. S. (2006) Platinum-osmium isotope evolution of the Earth's mantle: Constraints from chondrites and Os-rich alloys. *Geochimica et Cosmochimica Acta* **70**, 2093-2103.

Brenan J. M. and Andrews D. (2001) High-temperature stability of laurite and Ru-Os-Ir alloy and their role in PGE fractionation in mafic magmas. *Canadian Mineralogist* **39**, 341-360.

Brenan J. M. (2002) Re-Os fractionation in magmatic sulfide melt by monosulfide solid solution. *Earth and Planetary Science Letters* **199**, 257-268.

Brenan J. M. and McDonogh W. F. (2006) Sulfide-Silicate Partitioning of Mo, Sb, Pb, Se AND Te: Inital Results. *GAC-MAC Meeting, Montreal, Canada*.

Brenan J. M. (2008) Re-Os fractionation by sulfide melt-silicate melt partitioning: A new spin. *Chemical Geology* **248**, 140-165.

Brenan J. M. and McDonough W. F. (2009) Core formation and metal-silicate fractionation of osmium and iridium from gold. *Nature Geoscience* **2**, 798-801.

Brown P. G., Hildebrand A. R., Zolensky M. E., Grady M., Clayton R. N., Mayeda T. K., Tagliaferri E., Spalding R., MacRae N. D., Hoffman E. L., Mittlefehldt D. W., Wacker J. F., Bird J. A., Campbell M. D., Carpenter R., Gingerich H., Glatiotis M., Greiner E., Mazur M. J., McCausland P. J. A., Plotkin H. and Mazur T. R. (2000) The fall, recovery, orbit, and composition of the Tagish Lake meteorite: A new type of carbonaceous chondrite. *Science* **290**, 320-325.

Bulanova G. P., Griffin W. L., Ryan C. G., Shestakova O. Y. and Barnes S.-J. (1996) Trace elements in sulfide inclusions from Yakutian diamonds. *Contributions to Mineralogy and Petrology* **124**, 111-125.

Burton K. W., Schiano P., Birck J. L. and Allegre C. J. (1999) Osmium isotope disequilibrium between mantle minerals in a spinel-lherzolite. *Earth and Planetary Science Letters* **172**, 311-322.

Campbell I. H. and Naldrett A. J. (1979) The influence of silicate:sulfide ratios on the geochemistry of magmatic sulfides. *Economic Geology* **74**, 1503-1506.

Campbell I. H. and Barnes S. J. (1984) A model for the geochemistry of the platinum-group elements in magmatic sulfide deposits. *Canadian Mineralogist* **22**, 151-160.

Canil D. (2004) Mildly incompatible elements in peridotites and the origins of mantle lithosphere. *Lithos* **77**, 375-393.

Cerwenka Jr E. and Cooper W. C. (1961) Toxicology of selenium and tellurium and their compounds. *Arch. Environmental Health* **3**, 189-200.

Chesley J. T., Rudnick R. L. and Lee C. T. (1999) Re-Os systematics of mantle xenoliths from the East African Rift: Age, structure, and history of the Tanzanian craton. *Geochimica et Cosmochimica Acta* **63**, 1203-1217.

Choi N. and Cho W. (1997) Distribution behavior of cobalt, selenium, and tellurium between nickel-copper-iron matte and silica-saturated iron silicate slag. *Metallurgical and Materials Transactions B* **28**, 429-438.

Chou C. L. (1978). Fractionation of siderophile elements in the Earth's upper mantle. Lunar and Planetary Science Conference Proceedings. **9**, pp. 219-230.

Cohen A. S. and Waters F. G. (1996) Separation of osmium from geological materials by solvent extraction for analysis by thermal ionisation mass spectrometry. *Analytica Chimica Acta* **332**, 269-275.

Constantin M. (2009) Trace Element Data for Gold, Iridium and Silver in Seventy Geochemical Reference Materials. *Geostandards and Geoanalytical Research* **33**, 115-132.

Craddock P. R., Rouxel O. J., Ball L. A. and Bach W. (2008) Sulfur isotope measurement of sulfate and sulfide by high-resolution MC-ICP-MS. *Chemical Geology* **253**, 102-113.

D'Orazio M., Folco L., Chaussidon M. and Rochette P. (2009) Sahara 03505 sulfide-rich iron meteorite: Evidence for efficient segregation of sulfide-rich metallic melt during high-degree impact melting of an ordinary chondrite. *Meteoritics & Planetary Science* **44**, 221-231.

Dale C. W., Luguet A., Macpherson C. G., Pearson D. G. and Hickey-Vargas R. (2008) Extreme platinum-group element fractionation and variable Os isotope compositions in Philippine Sea Plate basalts: Tracing mantle source heterogeneity. *Chemical Geology* **248**, 213-238.

Dantas C., Ceuleneer G., Gregoire M., Python M., Freydier R., Warren J. and Dick H. J. B. (2007) Pyroxenites from the Southwest Indian Ridge, 9-16 degrees E: Cumulates from incremental melt fractions produced at the top of a cold melting regime. *Journal of Petrology* **48**, 647-660.

Dare S., Barnes S.-J., Prichard H. and Fisher P. (2011) Chalcophile and platinum-group element (PGE) concentrations in the sulfide minerals from the McCreedy East deposit, Sudbury, Canada, and the origin of PGE in pyrite. *Mineralium Deposita* **46**, 381-407.

Dawson J. B. (1984). Contrasting types of upper-mantle metasomatism? In: Kornprobst J. (Ed.), Kimberlites II. The Mantle and Crust-Mantle Relationships, Amsterdam, pp. 289-294.

Day J. M. D., Pearson D. G. and Taylor L. A. (2007) Highly siderophile element constraints on accretion and differentiation of the Earth-Moon system. *Science* **315**, 217-219.

de Hoog J. C. M., Mason P. R. D. and van Bergen M. J. (2001) Sulfur and chalcophile elements in subduction zones: Constraints from a laser ablation ICP-MS study of melt inclusions from Galunggung Volcano, Indonesia. *Geochimica et Cosmochimica Acta* **65**, 3147-3164.

Dick H. J. B., Lissenberg C. J. and Warren J. M. (2010) Mantle Melting, Melt Transport, and Delivery Beneath a Slow-Spreading Ridge: The Paleo-MAR from 23 degrees 15'N to 23 degrees 45'N. *Journal of Petrology* **51**, 425-467.

Downes H. (2007) Origin and significance of spinel and garnet pyroxenites in the shallow lithospheric mantle: Ultramafic massifs in orogenic belts in Western Europe and NW Africa. *Lithos* **99**, 1-24.

Drake M. J. and Righter K. (2002) Determining the composition of the Earth. *Nature* **416**, 39-44.

Dreibus G., Palme H., Spettel B., Zipfel J. and Wänke H. (1995) Sulfur and selenium in chondritic meteorites. *Meteoritics* **30**, 439-445.

Dreibus G. and Palme H. (1996) Cosmochemical constraints on the sulfur content in the Earth's core. *Geochimica et Cosmochimica Acta* **60**, 1125-1130.

Elwaer N. and Hintelmann H. (2008a) Comparing the precision of selenium isotope ratio measurements using collision cell and sector field inductively coupled plasma mass spectrometry. *Talanta* **75**, 205-214.

Elwaer N. and Hintelmann H. (2008b) Selective separation of selenium (IV) by thiol cellulose powder and subsequent selenium isotope ratio determination using multicollector inductively coupled plasma mass spectrometry. *Journal of Analytical Atomic Spectrometry* **23**, 733-743.

Erdman M. E., Lee C.-T. A., Yang W. and Ingram L. (2013) Sulfur concentration in geochemical reference materials by solution ICP-MS. *Geostandards and Geoanalytical Research*, Doi: 10.1111/j.1751-1908X.2013.00226.x.

Ernst W. G. (1978) Petrochemical Study of Lherzolitic Rocks from Western Alps. *Journal of Petrology* **19**, 341-392.

Fehr M. A., Rehkämper M. and Halliday A. N. (2004) Application of MC-ICPMS to the precise determination of tellurium isotope compositions in chondrites, iron meteorites and sulfides. *International Journal of Mass Spectrometry* **232**, 83-94.

Fehr M. A., Rehkämper M., Halliday A. N., Wiechert U., Hattendorf B., Günther D., Ono S., Eigenbrode J. L. and Rumble Iii D. (2005) Tellurium isotopic composition of the early solar system--A search for effects resulting from stellar nucleosynthesis, 126Sn decay, and mass-independent fractionation. *Geochimica et Cosmochimica Acta* **69**, 5099-5112.

Finnigan C. S., Brenan J. M., Mungall J. E. and McDonough W. F. (2008) Experiments and models bearing on the role of chromite as a collector of platinum group minerals by local reduction. *Journal of Petrology* **49**, 1647-1665.

Fischer-Gödde M., Becker H. and Wombacher F. (2010) Rhodium, gold and other highly siderophile element abundances in chondritic meteorites. *Geochimica et Cosmochimica Acta* **74**, 356-379.

Fischer-Gödde M., Becker H. and Wombacher F. (2011) Rhodium, gold and other highly siderophile elements in orogenic peridotites and peridotite xenoliths. *Chemical Geology* **280**, 365-383.

Fischer-Gödde M. and Becker H. (2012) Osmium isotope and highly siderophile element constraints on ages and nature of meteoritic components in ancient lunar impact rocks. *Geochimica et Cosmochimica Acta* **77**, 135-156.

Fitzpatrick A. J., Kyser T. K., Chipley D. and Beauchemin D. (2008) Fabrication of solid calibration standards by a sol-gel process and use in laser ablation ICPMS. *Journal of Analytical Atomic Spectrometry* **23**, 244-248.

Fleet M. E., Crocket J. H., Liu M. and Stone W. E. (1999) Laboratory partitioning of platinum-group elements (PGE) and gold with application to magmatic sulfide-PGE deposits. *Lithos* **47**, 127-142.

Floor G. H. and Roman-Ross G. (2012) Selenium in volcanic environments: A review. *Applied Geochemistry* **27**, 517-531.

Fonseca R. O. C., Mallmann G., O'Neill H. S. C. and Campbell I. H. (2007) How chalcophile is rhenium? An experimental study of the solubility of Re in sulphide mattes. *Earth and Planetary Science Letters* **260**, 537-548.

Fonseca R. O. C., Campbell I. H., O'Neill H. S. C. and Allen C. M. (2009) Solubility of Pt in sulphide mattes: Implications for the genesis of PGE-rich horizons in layered intrusions. *Geochimica et Cosmochimica Acta* **73**, 5764-5777.

Fonseca R. O. C., Laurenz V., Mallmann G., Luguet A., Hoehne N. and Jochum K. P. (2012) New constraints on the genesis and long-term stability of Os-rich alloys in the Earth's mantle. *Geochimica et Cosmochimica Acta* **87**, 227-242.

Forrest A., Kingsley R. and Schilling J. G. (2009) Determination of selenium and tellurium in basalt rock reference materials by isotope dilution hydride generation-inductively coupled plasma-mass spectrometry (ID-HG-ICP-MS). *Geostandards and Geoanalytical Research* **33**, 261-269.

Fountain D. M. (1976) Ivrea-Verbano and Strona-Ceneri Zones, Northern Italy - Cross-Section of Continental Crust - New Evidence from Seismic Velocities of Rock Samples. *Tectonophysics* **33**, 145-165.

Friedrich J. M., Wang M. S. and Lipschutz M. E. (2002) Comparison of the trace element composition of Tagish Lake with other primitive carbonaceous chondrites. *Meteoritics & Planetary Science* **37**, 677-686.

Friedrich J. M., Wang M. S. and Lipschutz M. E. (2003) Chemical studies of L chondrites. V: Compositional patterns for 49 trace elements in 14 L4-6 and 7 LL4-6 falls. *Geochimica et Cosmochimica Acta* **67**, 2467-2479.

Friedrich J. M., Bridges J. C., Wang M. S. and Lipschutz M. E. (2004) Chemical studies of L chondrites. VI: Variations with petrographic type and shock-loading among equilibrated falls. *Geochimica et Cosmochimica Acta* **68**, 2889-2904.

Funk C., Wombacher F., Becker H. and Bischoff A. (2012). Isotope dilution analysis of Selenium and Tellurium in chondrites. European Mineralogical Conference 2012. **1**, p. 642.

Gagnon J. E., Fryer B. J., Samson I. M. and Williams-Jones A. E. (2008) Quantitative analysis of silicate certified reference materials by LA-ICPMS with and without an internal standard. *Journal of Analytical Atomic Spectrometry* **23**, 1529-1537.

Gannoun A., Burton K. W., Parkinson I. J., Alard O., Schiano P. and Thomas L. E. (2007) The scale and origin of the osmium isotope variations in mid-ocean ridge basalts. *Earth and Planetary Science Letters* **259**, 541-556.

Gao S., Rudnick R. L., Carlson R. W., McDonough W. F. and Liu Y. S. (2002) Re-Os evidence for replacement of ancient mantle lithosphere beneath the North China craton. *Earth and Planetary Science Letters* **198**, 307-322.

Garrido C. J. and Bodinier J. L. (1999) Diversity of mafic rocks in the Ronda peridotite: Evidence for pervasive melt-rock reaction during heating of subcontinental lithosphere by upwelling asthenosphere. *Journal of Petrology* **40**, 729-754.

Garuti G., Gorgoni C. and Sighinolfi G. P. (1984) Sulfide Mineralogy and Chalcophile and Siderophile Element Abundances in the Ivrea-Verbano Mantle Peridotites (Western Italian Alps). *Earth And Planetary Science Letters* **70**, 69-87.

Gawronski T., Becker H. and Humayun M. (2013) Peridotite-Derived Sulfides in Pyroxenites from the Lanzo and the Lherz Ultramafic Massifs? *Mineralogical Magazine* **77**, 1149.

Gazulla M. F., Gomez M. P., Zumaquero E. and Vicente S. (2009) Sulfur determination in geological samples based on coupled analytical techniques: Electric furnace-IC and TGA-EGA. *Geostandards and Geoanalytical Research* **33**, 71-84.

Glasby G. P., Szefer P., Geldon J. and Warzocha J. (2004) Heavy-metal pollution of sediments from Szczecin Lagoon and the Gdansk basin, Poland. *Science of the Total Environment* **330**, 249-269.

Govindaraju K. (1982) Report (1967–1981) on Four ANRT Rock Reference Samples: Diorite DR-N, Serpentine UB-N, Bauxite BX-N and Disthene DT-N. *Geostandards Newsletter* **6**, 91-159.

Govindaraju K. (1994) 1994 compilation of working values and sample description for 383 geostandards. *Geostandards Newsletter* **18**, 1-158.

Guillong M., Latkoczy C., Seo J. H., Günther D. and Heinrich C. A. (2008) Determination of sulfur in fluid inclusions by laser ablation ICP-MS. *Journal of Analytical Atomic Spectrometry* **23**, 1581-1589.

Gysi A. P., Jagoutz O., Schmidt M. W. and Targuisti K. (2011) Petrogenesis of Pyroxenites and Melt Infiltrations in the Ultramafic Complex of Beni Bousera, Northern Morocco. *Journal of Petrology* **52**, 1679-1735.

Hall G. E. M. and Pelchat J.-C. (1997) Determination of As, Bi, Sb, Se and Te in fifty five reference materials by hydride generation ICP-MS. *Geostandards Newsletter* **21**, 85-91.

Halliday A. N. (2004) Mixing, volatile loss and compositional change during impact-driven accretion of the Earth. *Nature* **427**, 505-509.

Halmer M. M., Schmincke H. U. and Graf H. F. (2002) The annual volcanic gas input into the atmosphere, in particular into the stratosphere: A global data set for the past 100 years. *Journal of Volcanology and Geothermal Research* **115**, 511-528.

Handler M. R., Bennett V. C. and Dreibus G. (1999) Evidence from correlated Ir/Os and Cu/S for late-stage Os mobility in peridotite xenoliths: Implications for Re-Os systematics. *Geology* **27**, 75-78.

Handy M. R., Franz L., Heller F., Janott B. and Zurbriggen R. (1999) Multistage accretion and exhumation of the continental crust (Ivrea crustal section, Italy and Switzerland). *Tectonics* **18**, 1154-1177.

Handy M. R., Schmid S. M., Bousquet R., Kissling E. and Bernoulli D. (2010) Reconciling plate-tectonic reconstructions of Alpine Tethys with the geological-geophysical record of spreading and subduction in the Alps. *Earth-science Reviews* **102**, 121-158.

Hanghøj K., Kelemen P. B., Hassler D. and Godard M. (2010) Composition and Genesis of Depleted Mantle Peridotites from the Wadi Tayin Massif, Oman Ophiolite; Major and Trace Element Geochemistry, and Os Isotope and PGE Systematics. *Journal of Petrology* **51**, 201-227.

Hartmann G. and Wedepohl K. H. (1993) The composition of peridotite tectonites from the Ivrea Complex, northern Italy - Residues from melt extraction. *Geochimica Et Cosmochimica Acta* **57**, 1761-1782.

Harvey J., Gannoun A., Burton K. W., Rogers N. W., Alard O. and Parkinson I. J. (2006) Ancient melt extraction from the oceanic upper mantle revealed by Re-Os isotopes in abyssal peridotites from the Mid-Atlantic ridge. *Earth and Planetary Science Letters* **244**, 606-621.

Harvey J., Gannoun A., Burton K. W., Schiano P., Rogers N. W. and Alard O. (2010) Unravelling the effects of melt depletion and secondary infiltration on mantle Re-Os isotopes beneath the French Massif Central. *Geochimica et Cosmochimica Acta* **74**, 293-320.

Harvey J., Dale C. W., Gannoun A. and Burton K. W. (2011) Osmium mass balance in peridotite and the effects of mantle-derived sulphides on basalt petrogenesis. *Geochimica et Cosmochimica Acta* **75**, 5574-5596.

Hattori K. H., Arai S. and Clarke D. B. (2002) Selenium, tellurium, arsenic and antimony contents of primary mantle sulfides. *Canadian Mineralogist* **40**, 637-650.

Helmy H. M., Ballhaus C., Berndt J., Bocrath C. and Wohlgemuth-Ueberwasser C. (2007) Formation of Pt, Pd and Ni tellurides: experiments in sulfide-telluride systems. *Contributions to Mineralogy and Petrology* **153**, 577-591.

Helmy H. M., Ballhaus C., Wohlgemuth-Ueberwasser C., Fonseca R. O. C. and Laurenz V. (2010) Partitioning of Se, As, Sb, Te and Bi between monosulfide solid solution and sulfide melt - Application to magmatic sulfide deposits. *Geochimica et Cosmochimica Acta* **74**, 6174-6179.

Hertogen J., Janssens M. J. and Palme H. (1980) Trace elements in ocean ridge basalt glasses: implications for fractionations during mantle evolution and petrogenesis. *Geochimica et Cosmochimica Acta* **44**, 2125-2143.

Hertogen J., Janssens M.-J., Takahashi H., Morgan J. W. and Anders E. (1983) Enstatite chondrites: Trace element clues to their origin. *Geochimica et Cosmochimica Acta* **47**, 2241-2255.

Hirschmann M. M. and Stolper E. M. (1996) A possible role for garnet pyroxenite in the origin of the "garnet signature" in MORB. *Contributions to Mineralogy and Petrology* **124**, 185-208.

Hirschmann M. M. and Dasgupta R. (2009) The H/C ratios of Earth's near-surface and deep reservoirs, and consequences for deep Earth volatile cycles. *Chemical Geology* **262**, 4-16.

Hofmann A. W. and Hart S. R. (1978) An assessment of local and regional isotopic equilibrium in the mantle. *Earth and Planetary Science Letters* **38**, 44-62.

Hofmann A. W. (1997) Mantle geochemistry: The message from oceanic volcanism. *Nature* **385**, 219-229.

Holland G., Cassidy M. and Ballentine C. J. (2009) Meteorite Kr in Earth's Mantle Suggests a Late Accretionary Source for the Atmosphere. *Science* **326**, 1522-1525.

Holwell D. A. and McDonald I. (2010) A review of the behaviour of platinum group elements within natural magmatic sulfide ore systems. *Platinum Metals Review* **54**, 26-36.

Horan M. F., Walker R. J., Morgan J. W., Grossman J. N. and Rubin A. E. (2003) Highly siderophile elements in chondrites. *Chemical Geology* **196**, 27-42.

Hu Z. C. and Gao S. (2008) Upper crustal abundances of trace elements: A revision and update. *Chemical Geology* **253**, 205-221.

Hu Z. C., Liu Y. S., Li M., Gao S. and Zhao L. S. (2009) Results for rarely determined elements in MPI-DING, USGS and NIST SRM glasses using laser ablation ICP-MS. *Geostandards and Geoanalytical Research* **33**, 319-335.

Huston T. J. and Lipschutz M. E. (1984) Chemical studies of L chondrites—III. Mobile trace elements and 40Ar39Ar ages. *Geochimica et Cosmochimica Acta* **48**, 1319-1329.

Ionov D. A., Shirey S. B., Weis D. and Brügmann G. (2006) Os–Hf–Sr–Nd isotope and PGE systematics of spinel peridotite xenoliths from Tok, SE Siberian craton: Effects of pervasive metasomatism in shallow refractory mantle. *Earth and Planetary Science Letters* **241**, 47-64.

Ireland T. J., Walker R. J. and Garcia M. O. (2009) Highly siderophile element and Os-187 isotope systematics of Hawaiian picrites: Implications for parental melt composition and source heterogeneity. *Chemical Geology* **260**, 112-128.

Jenner F. E., Holden P., Mavrogenes J. A., O'Neill H. S. and Allen C. (2009) Determination of selenium concentrations in NIST SRM 610, 612, 614 and geological glass reference materials using the electron probe, LA-ICP-MS and SHRIMP II. *Geostandards and Geoanalytical Research* **33**, 309-317.

Jenner F. E., O'Neill H. S. C., Arculus R. J. and Mavrogenes J. A. (2010) The magnetite crisis in the evolution of arc-related magmas and the initial concentration of Au, Ag and Cu. *Journal of Petrology* **51**, 2445-2464.

Jenner F. E. and O'Neill H. S. C. (2012) Analysis of 60 elements in 616 ocean floor basaltic glasses. *Geochemistry, Geophysics, Geosystems* **13**, Q02005, Doi:02010.01029/02011 GC004009.

Jenner F. E., Arculus R. J., Mavrogenes J. A., Dyriw N. J., Nebel O. and Hauri E. H. (2012) Chalcophile element systematics in volcanic glasses from the northwestern Lau Basin. *Geochemistry, Geophysics, Geosystems* **13**, Q06014, Doi:06010.01029/02012GC004088.

Jochum K. P., Stoll B., Herwig K., Willbold M., Hofmann A. W., Amini M., Aarburg S., Abouchami W., Hellebrand E., Mocek B., Raczek I., Stracke A., Alard O., Bouman C., Becker S., Ducking M., Bratz H., Klemd R., de Bruin D., Canil D., Cornell D., de Hoog C. J., Dalpe C., Danyushevsky L., Eisenhauer A., Gao Y. J., Snow J. E., Goschopf N., Günther D., Latkoczy C., Guillong M., Hauri E. H., Hofer H. E., Lahaye Y., Horz K., Jacob D. E., Kassemann S. A., Kent A. J. R., Ludwig T., Zack T., Mason P. R. D., Meixner A., Rosner M., Misawa K. J., Nash B. P., Pfander J., Premo W. R., Sun W. D., Tiepolo M., Vannucci R., Vennemann T., Wayne D. and Woodhead J. D. (2006) MPI-DING reference glasses for in situ microanalysis: New reference values for element concentrations and isotope ratios. *Geochemistry Geophysics Geosystems* **7**, Doi 10.1029/2005gc001060.

Jochum K. P., Weis U., Stoll B., Kuzmin D., Yang Q., Raczek I., Jacob D. E., Stracke A., Birbaum K., Frick D. A., Günther D. and Enzweiler J. (2011) Determination of reference values for NIST SRM 610-617 glasses following ISO guidelines. *Geostandards and Geoanalytical Research* **35**, 397-429.

König S., Luguet A., Lorand J.-P., Wombacher F. and Lissner M. (2012) Selenium and tellurium systematics of the Earth's mantle from high precision analyses of ultra-depleted orogenic peridotites. *Geochimica et Cosmochimica Acta* **86**, 354-366.

Kaczaral P. W., Dodd R. T. and Lipschutz M. E. (1989) Chemical studies of L chondrites: IV. Antarctic/non-Antarctic comparisons. *Geochimica et Cosmochimica Acta* **53**, 491-501.

Kaczmarek M. A., Muntener O. and Rubatto D. (2008) Trace element chemistry and U-Pb dating of zircons from oceanic gabbros and their relationship with whole rock composition (Lanzo, Italian Alps). *Contributions to Mineralogy and Petrology* **155**, 295-312.

Kallemeyn G. W. and Wasson J. T. (1986) Compositions of enstatite (EH3, EH4,5 and EL6) chondrites: Implications regarding their formation. *Geochimica et Cosmochimica Acta* **50**, 2153-2164.

Keays R. R. (1995) The role of komatiitic and picritic magmatism and S-saturation in the formation of ore deposits. *Lithos* **34**, 1-18.

Kelemen P. B., Shimizu N. and Salters V. J. M. (1995) Extraction of Mid-Ocean-Ridge Basalt from the Upwelling Mantle by Focused Flow of Melt in Dunite Channels. *Nature* **375**, 747-753.

Kelemen P. B., Hirth G., Shimizu N., Spiegelman M. and Dick H. J. B. (1997) A review of melt migration processes in the adiabatically upwelling mantle beneath oceanic

spreading ridges. *Philosophical Transactions of the Royal Society a-Mathematical Physical and Engineering Sciences* **355**, 283-318.

Kogiso T. and Hirschmann M. M. (2001) Experimental study of clinopyroxenite partial melting and the origin of ultra-calcic melt inclusions. *Contributions to Mineralogy and Petrology* **142**, 347-360.

Kubota R. (2009) Simultaneous determination of total carbon, nitrogen, hydrogen and sulfur in twenty-seven geological reference materials by elemental analyser. *Geostandards and Geoanalytical Research* **33**, 271-283.

Labidi J., Cartigny P. and Moreira M. (2013) Non-chondritic sulphur isotope composition of the terrestrial mantle. *Nature* **501**, 208-211.

Lambart S., Laporte D. and Schiano P. (2009) An experimental study of pyroxenite partial melts at 1 and 1.5 GPa: Implications for the major-element composition of Mid-Ocean Ridge Basalts. *Earth and Planetary Science Letters* **288**, 335-347.

Lambart S., Laporte D. and Schiano P. (2013) Markers of the pyroxenite contribution in the major-element compositions of oceanic basalts: Review of the experimental constraints. *Lithos* **160**, 14-36.

Lassiter J. C. and Hauri E. H. (1998) Osmium-isotope variations in Hawaiian lavas: evidence for recycled oceanic lithosphere in the Hawaiian plume. *Earth and Planetary Science Letters* **164**, 483-496.

Le Roux V., Bodinier J. L., Tommasi A., Alard O., Dautria J. M., Vauchez A. and Riches A. J. V. (2007) The Lherz spinel lherzolite: Refertilized rather than pristine mantle. *Earth and Planetary Science Letters* **259**, 599-612.

Li C. S. (2005) Empirical equations to predict the sulfur content of mafic magmas at sulfide saturation and applications to magmatic sulfide deposits. *Mineralium Deposita* **40**, 218-230.

Li J., Zhong L.-F., Xu J.-F., Wang X.-C., Wang G.-Q. and Zhao P.-P. (2013) Determination of platinum-group elements and Re-Os isotopes using ID-ICP-MS and N-TIMS from a single digestion after two-stage column separation. *Geostandards and Geoanalytical Research*, Doi: 10.1111/j.1751-1908X.2013.00242.x.

Li Y. and Audetat A. (2012) Partitioning of V, Mn, Co, Ni, Cu, Zn, As, Mo, Ag, Sn, Sb, W, Au, Pb, and Bi between sulfide phases and hydrous basanite melt at upper mantle conditions. *Earth and Planetary Science Letters* **355**, 327-340.

Li Y. and Audétat A. (2013) Gold solubility and partitioning between sulfide liquid, monosulfide solid solution and hydrous mantle melts: Implications for the formation of Au-rich magmas and crust–mantle differentiation. *Geochimica et Cosmochimica Acta* **118**, 247-262.

Lingner D. W., Huston T. J., Hutson M. and Lipschutz M. E. (1987) Chemical studies of H chondrites. I: Mobile trace elements and gas retention ages. *Geochimica et Cosmochimica Acta* **51**, 727-739.

Liu C. Z., Snow J. E., Hellebrand E., Brugmann G., von der Handt A., Buchl A. and Hofmann A. W. (2008) Ancient, highly heterogeneous mantle beneath Gakkel ridge, Arctic Ocean. *Nature* **452**, 311-316.

Liu C. Z., Snow J. E., Brugmann G., Hellebrand E. and Hofmann A. W. (2009) Non-chondritic HSE budget in Earth's upper mantle evidenced by abyssal peridotites from Gakkel ridge (Arctic Ocean). *Earth and Planetary Science Letters* **283**, 122-132.

Liu J., Rudnick R. L., Walker R. J., Gao S., Wu F. and Piccoli P. M. (2010) Processes controlling highly siderophile element fractionations in xenolithic peridotites and their influence on Os isotopes. *Earth and Planetary Science Letters* **297**, 287-297.

Liu J., Rudnick R. L., Walker R. J., Gao S., Wu F.-y., Piccoli P. M., Yuan H., Xu W.-l. and Xu Y.-G. (2011) Mapping lithospheric boundaries using Os isotopes of mantle xenoliths: An example from the North China Craton. *Geochimica et Cosmochimica Acta* **75**, 3881-3902.

Lodders K. and Bruce Fegley J., 1998. The planetary scientist's companion. Oxford Universtiy Press, New York.

Lodders K. (2003) Solar system abundances and condensation temperatures of the elements. *Astrophysical Journal* **591**, 1220-1247.

Lorand J. P. (1989) Abundance and distribution of Cu-Fe-Ni sulfides, sulfur, copper and platinum-group elements in orogenic-type spinel lherzolite massifs of Ariège (northeastern Pyrenees, France). *Earth and Planetary Science Letters* **93**, 50-64.

Lorand J. P. (1990) Are spinel Iherzolite xenoliths representative of the abundance of sulfur in the upper mantle? *Geochimica et Cosmochimica Acta* **54**, 1487-1492.

Lorand J. P., Pattou L. and Gros M. (1999) Fractionation of platinum-group elements and gold in the upper mantle: a detailed study in Pyrenean orogenic lherzolites. *Journal of Petrology* **40**, 957-981.

Lorand J. P. and Alard O. (2001) Platinum-group element abundances in the upper mantle: New constraints from in situ and whole-rock analyses of Massif Central xenoliths (France). *Geochimica et Cosmochimica Acta* **65**, 2789-2806.

Lorand J. P., Alard O., Luguet A. and Keays R. R. (2003) Sulfur and selenium systematics of the subcontinental lithospheric mantle: Inferences from the Massif Central xenolith suite (France). *Geochimica et Cosmochimica Acta* **67**, 4137-4151.

Lorand J. P., Luguet A. and Alard O. (2008a) Platinum-group elements: A new set of key tracers for the earth's interior. *Elements* **4**, 247-252.

Lorand J. P., Luguet A., Alard O., Bezos A. and Meisel T. (2008b) Abundance and distribution of platinum-group elements in orogenic lherzolites; a case study in a Fontete Rouge lherzolite (French Pyrenees). *Chemical Geology* **248**, 174-194.

Lorand J. P., Alard O. and Godard M. (2009) Platinum-group element signature of the primitive mantle rejuvenated by melt-rock reactions: evidence from Sumail peridotites (Oman Ophiolite). *Terra Nova* **21**, 35-40.

Lorand J. P. and Alard O. (2010) Determination of selenium and tellurium concentrations in Pyrenean peridotites (Ariege, France): New insight into S/Se/Te systematics of the upper in mantle samples. *Chemical Geology* **278**, 120-130.

Lorand J. P., Alard O. and Luguet A. (2010) Platinum-group element micronuggets and refertilization process in Lherz orogenic peridotite (northeastern Pyrenees, France). *Earth and Planetary Science Letters* **289**, 298-310.

Lorand J. P. and Alard O. (2011) Pyrite tracks assimilation of crustal sulfur in Pyrenean peridotites. *Mineralogy and Petrology* **101**, 115-128.

Lorand J. P., Luguet A. and Alard O. (2013) Platinum-group element systematics and petrogenetic processing of the continental upper mantle: A review. *Lithos* **164-167**, 2-21.

Loss R. D., Rosman K. J. R. and Delaeter J. R. (1984) Mass-Spectrometric Isotope-Dilution Analyses of Palladium, Silver, Cadmium and Tellurium in Carbonaceous Chondrites. *Geochimica et Cosmochimica Acta* **48**, 1677-1681.

Luck J. M. and Allègre C. J. (1983) Re-187-Os-187 systematics in meteorites and cosmochemical consequences. *Nature* **302**, 130-132.

Luguet A., Alard O., Lorand J. P., Pearson N. J., Ryan C. and O'Reilly S. Y. (2001) Laser-ablation microprobe (LAM)-ICPMS unravels the highly siderophile element geochemistry of the oceanic mantle. *Earth and Planetary Science Letters* **189**, 285-294.

Luguet A., Lorand J. P. and Seyler M. (2003) Sulfide petrology and highly siderophile element geochemistry of abyssal peridotites: A coupled study of samples from the Kane Fracture Zone (45 degrees W 23 degrees 20N, MARK Area, Atlantic Ocean). *Geochimica et Cosmochimica Acta* **67**, 1553-1570.

Luguet A., Lorand J. P., Alard O. and Cottin J. Y. (2004) A multi-technique study of platinum group element systematic in some Ligurian ophiolitic peridotites, Italy. *Chemical Geology* **208**, 175-194.

Luguet A., Shirey S. B., Lorand J. P., Horan M. F. and Carlson R. W. (2007) Residual platinum-group minerals from highly depleted harzburgites of the Lherz massif (France) and their role in HSE fractionation of the mantle. *Geochimica et Cosmochimica Acta* **71**, 3082-3097.

Luguet A., Pearson D. G., Nowell G. M., Dreher S. T., Coggon J. A., Spetsius Z. V. and Parman S. W. (2008) Enriched Pt-Re-Os isotope systematics in plume lavas explained by metasomatic sulfides. *Science* **319**, 453-456.

Lyubetskaya T. and Korenaga J. (2007) Chemical composition of Earth's primitive mantle and its variance: 1. Method and results. *Journal of Geophysical Research-Solid Earth* **112**, B03211, Doi:03210.01029/02005JB004223.

Müntener O., Pettke T., Desmurs L., Meier M. and Schaltegger U. (2004) Refertilization of mantle peridotite in embryonic ocean basins: trace element and Nd isotopic evidence and implications for crust-mantle relationships. *Earth and Planetary Science Letters* **221**, 293-308.

Müntener O., Manatschal G., Desmurs L. and Pettke T. (2010) Plagioclase Peridotites in Ocean-Continent Transitions: Refertilized Mantle Domains Generated by Melt Stagnation in the Shallow Mantle Lithosphere. *Journal of Petrology* **51**, 255-294.

Maier W. D., Barnes S. J., Campbell I. H., Fiorentini M. L., Peltonen P., Barnes S.-J. and Smithies R. H. (2009) Progressive mixing of meteoritic veneer into the early Earth's deep mantle. *Nature* **460**, 620-623.

Maier W. D., Peltonen P., McDonald I., Barnes S. J., Barnes S.-J., Hatton C. and Viljoen F. (2012) The concentration of platinum-group elements and gold in southern African and Karelian kimberlite-hosted mantle xenoliths: Implications for the noble metal content of the Earth's mantle. *Chemical Geology* **302**, 119-135.

Makishima A. and Nakamura E. (2001) Determination of total sulfur at microgram per gram levels in geological materials by oxidation of sulfur into sulfate with in situ generation of bromine using isotope dilution high resolution ICPMS. *Analytical Chemistry* **73**, 2547-2553.

Makishima A. and Nakamura E. (2009) Determination of Ge, As, Se and Te in silicate samples using isotope dilution-internal standardisation octopole reaction cell ICP-QMS by normal sample nebulisation. *Geostandards and Geoanalytical Research* **33**, 369-384.

Mallmann G. and O'Neill H. S. C. (2007) The effect of oxygen fugacity on the partitioning of Re between crystals and silicate melt during mantle melting. *Geochimica et Cosmochimica Acta* **71**, 2837-2857.

Mann J. L. and Kelly W. R. (2005) Measurement of sulfur isotope composition (delta S-34) by multiple-collector thermal ionization mass spectrometry using a S-33-S-36 double spike. *Rapid Communications in Mass Spectrometry* **19**, 3429-3441.

Mann U., Frost D. J., Rubie D. C., Becker H. and Audetat A. (2012) Partitioning of Ru, Rh, Pd, Re, Ir and Pt between liquid metal and silicate at high pressures and high temperatures - Implications for the origin of highly siderophile element concentrations in the Earth's mantle. *Geochimica et Cosmochimica Acta* **84**, 593-613.

Marchesi C., Garrido C. J., Bosch D., Bodinier J.-L., Gervilla F. and Hidas K. (2013) Mantle refertilization by melts of crustal-derived garnet pyroxenite: Evidence from the Ronda peridotite massif, southern Spain. *Earth and Planetary Science Letters* **362**, 66-75.

Marin L., Lhomme J. and Carignan J. (2001) Determination of selenium concentration in sixty five reference materials for geochemical analysis by GFAAS after separation with thiol cotton. *Geostandards Newsletter* **25**, 317-324.

Marty B. and Dauphas N. (2003) The nitrogen record of crust-mantle interaction and mantle convection from Archean to present. *Earth and Planetary Science Letters* **206**, 397-410.

Marty B. (2012) The origins and concentrations of water, carbon, nitrogen and noble gases on Earth. *Earth and Planetary Science Letters* **313–314**, 56-66.

Mavrogenes J. A. and O'Neill H. S. C. (1999) The relative effects of pressure, temperature and oxygen fugacity on the solubility of sulfide in mafic magmas. *Geochimica et Cosmochimica Acta* **63**, 1173-1180.

Mazzucchelli M., Rivalenti G., Brunelli D., Zanetti A. and Boari E. (2009) Formation of Highly Refractory Dunite by Focused Percolation of Pyroxenite-Derived Melt in the Balmuccia Peridotite Massif (Italy). *Journal Of Petrology* **50**, 1205-1233.

Mazzucchelli M., Zanetti A., Rivalenti G., Vannucci R., Correia C. T. and Tassinari C. C. G. (2010) Age and geochemistry of mantle peridotites and diorite dykes from the Baldissero body: Insights into the Paleozoic-Mesozoic evolution of the Southern Alps. *Lithos* **119**, 485-500.

McDonough W. F. and Sun S. S. (1995) The composition of the Earth. *Chemical Geology* **120**, 223-253.

Meisel T., Moser J. and Wegscheider W. (2001a) Recognizing heterogeneous distribution of platinum group elements (PGE) in geological materials by means of the Re-Os isotope system. *Fresenius Journal of Analytical Chemistry* **370**, 566-572.

Meisel T., Walker R. J., Irving A. J. and Lorand J. P. (2001b) Osmium isotopic compositions of mantle xenoliths: A global perspective. *Geochimica et Cosmochimica Acta* **65**, 1311-1323.

Meisel T., Fellner N. and Moser J. (2003a) A simple procedure for the determination of platinum group elements and rhenium (Ru, Rh, Pd, Re, Os, Ir and Pt) using ID-ICP-MS with an inexpensive on-line matrix separation in geological and environmental materials. *Journal of Analytical Atomic Spectrometry* **18**, 720-726.

Meisel T., Reisberg L., Moser J., Carignan J., Melcher F. and Brugmann G. (2003b) Re-Os systematics of UB-N, a serpentinized peridotite reference material. *Chemical Geology* **201**, 161-179.

Meisel T. and Moser J. (2004a) Platinum-group element and rhenium concentrations in low abundance reference materials. *Geostandards and Geoanalytical Research* **28**, 233-250.

Meisel T. and Moser J. (2004b) Reference materials for geochemical PGE analysis: new analytical data for Ru, Rh, Pd, Os, Ir, Pt and Re by isotope dilution ICP-MS in 11 geological reference materials. *Chemical Geology* **208**, 319-338.

Michel A. and Villemant B. (2003) Determination of halogens (F, Cl, Br, I), sulfur and water in seventeen geological reference materials. *Geostandards Newsletter* **27**, 163-171.

Morgan J. W. (1986) Ultramafic xenoliths: Clues to Earth's late accretionary history. *Journal of Geophysical Research-Solid Earth* **91**, 12375-12387.

Moriarty G. M., Rumble D. and Friedrich J. M. (2009) Compositions of four unusual CM or CM-related Antarctic chondrites. *Chemie Der Erde-Geochemistry* **69**, 161-168.

Mukasa S. B. and Shervais J. W. (1999) Growth of subcontinental lithosphere: evidence from repeated dike injections in the Balmuccia lherzolite massif, Italian Alps. *Lithos* **48**, 287-316.

Mungall J. E. (2002) Kinetic Controls on the Partitioning of Trace Elements Between Silicate and Sulfide Liquids. *Journal of Petrology* **43**, 749-768.

Mungall J. E. and Brenan J. M. (In press) Partitioning of platinum-group elements and Au between sulfide liquid and basalt and the origins of mantle-crust fractionation of the chalcophile elements. *Geochimica et Cosmochimica Acta*.

Niu Y. L. (1997) Mantle melting and melt extraction processes beneath ocean ridges: Evidence from abyssal peridotites. *Journal of Petrology* **38**, 1047-1074.

Norman M. D., Bennett V. C. and Ryder G. (2002) Targeting the impactors: siderophile element signatures of lunar impact melts from Serenitatis. *Earth and Planetary Science Letters* **202**, 217-228.

O'Neill H. S. C. (1991) The origin of the moon and the early history of the earth—A chemical model. Part 2: The earth. *Geochimica et Cosmochimica Acta* **55**, 1159-1172.

O'Neill H. S. C. and Palme H. (2008) Collisional erosion and the non-chondritic composition of the terrestrial planets. *Philosophical Transactions of the Royal Society a-Mathematical Physical and Engineering Sciences* **366**, 4205-4238.

O'Reilly S. and Griffin W. L. (2013). Mantle Metasomatism. In: Harlov D. and Austrheim H. (Eds.), Metasomatism and the Chemical Transformation of Rock, pp. 471-533.

Obata M., Hirajima T. and Svojtka M. (2006) Origin of eclogite and garnet pyroxenite from the Moldanubian Zone of the Bohemian Massif, Czech Republic and its implication to other mafic layers embedded in orogenic peridotites. *Mineralogy and Petrology* **88**, 321-340.

Obermiller W. A. (1994). Chemical and isotopic variations in the Balmuccia, Baldissero and Finero peridotite massifs (Ivrea-Zone, Italy). **PhD dissertation**, p. 191.

Okai T., Terashima S. and Imai N. (2001) Determination of total sulfur in thirty one geochemical reference materials using an inductively coupled plasma-atomic emission spectrometer fitted with a semiconductor photodiode detector. *Geostandards Newsletter* **25**, 133-136.

Palme H. and O'Neill H. S. C., 2003. 2.01 - Cosmochemical Estimates of Mantle Composition. In: Holland H. D. and Turekian K. K. (Eds.), Treatise on Geochemistry. **2**, Oxford, pp. 1-38.

Patten C., Barnes S.-J., Mathez E. A. and Jenner F. E. (In press) Partition coefficients of chalcophile elements between sulfide and silicate melts and the early crystallization

history of sulfide liquid: LA-ICP-MS analysis of MORB sulfide droplets. *Chemical Geology*.

Pattou L., Lorand J. P. and Gros M. (1996) Non-chondritic platinum-group element ratios in the Earth's mantle. *Nature* **379**, 712-715.

Peach C. L., Mathez E. A. and Keays R. R. (1990) Sulfide melt-silicate melt distribution coefficients for noble metals and other chalcophile elements as deduced from MORB: Implications for partial melting. *Geochimica et Cosmochimica Acta* **54**, 3379-3389.

Peach C. L., Mathez E. A., Keays R. R. and Reeves S. J. (1994) Experimentally Determined Sulfide Melt-Silicate Melt Partition-Coefficients for Iridium and Palladium. *Chemical Geology* **117**, 361-377.

Pearce N. J. G., Perkins W. T., Westgate J. A., Gorton M. P., Jackson S. E., Neal C. R. and Chenery S. P. (1997) A compilation of new and published major and trace element data for NIST SRM 610 and NIST SRM 612 glass reference materials. *Geostandards Newsletter* **21**, 115-144.

Pearson D. G., Davies G. R., Nixon P. H., Greenwood P. B. and Mattey D. P. (1991) Oxygen Isotope Evidence for the Origin of Pyroxenites in the Beni Bousera Peridotite Massif, North Morocco - Derivation from Subducted Oceanic Lithosphere. *Earth and Planetary Science Letters* **102**, 289-301.

Pearson D. G., Davies G. R. and Nixon P. H. (1993) Geochemical Constraints on the Petrogenesis of Diamond Facies Pyroxenites from the Beni Bousera Peridotite Massif, North Morocco. *Journal of Petrology* **34**, 125-172.

Pearson D. G. and Nowell G. M. (2004) Re-Os and Lu-Hf isotope constraints on the origin and age of pyroxenites from the Beni Bousera peridotite massif implications for mixed peridotite-pyroxenite mantle sources. *Journal of Petrology* **45**, 439-455.

Pearson D. G., Irvine G. J., Ionov D. A., Boyd F. R. and Dreibus G. E. (2004) Re-Os isotope systematics and platinum group element fractionation during mantle melt extraction: a study of massif and xenolith peridotite suites. *Chemical Geology* **208**, 29-59.

Peressini G., Quick J. E., Sinigoi S., Hofmann A. W. and Fanning M. (2007) Duration of a large Mafic intrusion and heat transfer in the lower crust: A SHRIMP U-Pb zircon study in the Ivrea-Verbano Zone (Western Alps, Italy). *Journal of Petrology* **48**, 1185-1218.

Pertermann M. and Hirschmann M. M. (2003) Partial melting experiments on a MORB-like pyroxenite between 2 and 3 GPa: Constraints on the presence of pyroxenite in basalt source regions from solidus location and melting rate. *Journal of Geophysical Research-Solid Earth* **108**.

Peucker-Ehrenbrink B., Bach W., Hart S. R., Blusztajn J. S. and Abbruzzese T. (2003) Rhenium-osmium isotope systematics and platinum group element concentrations in oceanic crust from DSDP/ODP Sites 504 and 417/418. *Geochemistry, Geophysics, Geosystems* **4**, Doi 10.1029/2002gc000414.

Peucker-Ehrenbrink B., Hanghoj K., Atwood T. and Kelemen P. B. (2012) Rhenium-osmium isotope systematics and platinum group element concentrations in oceanic crust. *Geology*.

Piña R., Gervilla F., Barnes S.-J., Ortega L. and Lunar R. (2012) Distribution of platinum-group and chalcophile elements in the Aguablanca Ni–Cu sulfide deposit (SW Spain): Evidence from a LA-ICP-MS study. *Chemical Geology* **302–303**, 61-75.

Piccardo G. B., Zanetti A. and Muntener O. (2007a) Melt/peridotite interaction in the Southern Lanzo peridotite: Field, textural and geochemical evidence. *Lithos* **94**, 181-209.

Piccardo G. B., Zanetti A., Pruzzo A. and Padovano M. (2007b) The North Lanzo peridotite body (NW Italy): lithospheric mantle percolated by MORB and alkaline melts. *Periodico Di Mineralogia* **76**, 199-221.

Piccardo G. B. (2008) The Jurassic Ligurian Tethys, a fossil ultraslow - spreading ocean: the mantle perspective. *Geological Society, London, Special Publications* **293**, 11-34.

Plessen H.-G. and Erzinger J. (1998) Determination of the platinum-group elements and gold in twenty rock reference materials by inductively coupled plasma-mass spectrometry (ICP-MS) after pre-concentration by nickel sulfide fire assay. *Geostandards Newsletter* **22**, 187-194.

Puchtel I. S., Brandon A. D. and Humayun M. (2004a) Precise Pt-Re-Os isotope systematics of the mantle from 2.7-Ga komatiites. *Earth and Planetary Science Letters* **224**, 157-174.

Puchtel I. S., Humayun M., Campbell A. J., Sproule R. A. and Lesher C. M. (2004b) Platinum group element geochemistry of komatiites from the Alexo and Pyke Hill areas, Ontario, Canada. *Geochimica et Cosmochimica Acta* **68**, 1361-1383.

Puchtel I. S. and Humayun M. (2005) Highly siderophile element geochemistry of Os-187-enriched 2.8 ga kostomuksha komatiites, Baltic shield. *Geochimica et Cosmochimica Acta* **69**, 1607-1618.

Puchtel I. S., Humayun M. and Walker R. J. (2007) Os-Pb-Nd isotope and highly siderophile and lithophile trace element systematics of komatiitic rocks from the Volotsk suite, SE Baltic Shield. *Precambrian Research* **158**, 119-137.

Puchtel I. S., Walker R. J., James O. B. and Kring D. A. (2008) Osmium isotope and highly siderophile element systematics of lunar impact melt breccias: Implications for the late accretion history of the Moon and Earth. *Geochimica et Cosmochimica Acta* **72**, 3022-3042.

Puchtel I. S., Walker R. J., Brandon A. D. and Nisbet E. G. (2009) Pt-Re-Os and Sm-Nd isotope and HSE and REE systematics of the 2.7 Ga Belingwe and Abitibi komatiites. *Geochimica et Cosmochimica Acta* **73**, 6367-6389.

Quick J. E., Sinigoi S. and Mayer A. (1995) Emplacement of Mantle Peridotite in the Lower Continental-Crust, Ivrea-Verbano Zone, Northwest Italy. *Geology* **23**, 739-742.

Quick J. E., Sinigoi S., Peressini G., Demarchi G., Wooden J. L. and Sbisa A. (2009) Magmatic plumbing of a large Permian caldera exposed to a depth of 25 km. *Geology* **37**, 603-606.

Rampone E. and Borghini G. (2008) Melt migration and intrusion in the Erro-Tobbio peridotites (Ligurian Alps, Italy): Insights on magmatic processes in extending lithospheric mantle. *European Journal of Mineralogy* **20**, 573-585.

Rampone E. and Hofmann A. W. (2012) A global overview of isotopic heterogeneities in the oceanic mantle. *Lithos* **148**, 247-261.

Rehkämper M., Halliday A. N., Alt J., Fitton J. G., Zipfel J. and Takazawa E. (1999a) Non-chondritic platinum-group element ratios in oceanic mantle lithosphere: petrogenetic signature of melt percolation? *Earth and Planetary Science Letters* **172**, 65-81.

Rehkämper M., Halliday A. N., Fitton J. G., Lee D. C., Wieneke M. and Arndt N. T. (1999b) Ir, Ru, Pt, and Pd in basalts and komatiites: New constraints for the geochemical

behavior of the platinum-group elements in the mantle. *Geochimica et Cosmochimica Acta* **63**, 3915-3934.

Reisberg L. C., Allègre C. J. and Luck J.-M. (1991) The Re-Os systematics of the Ronda Ultramafic Complex of southern Spain. *Earth and Planetary Science Letters* **105**, 196-213.

Reisberg L., Zhi X., Lorand J.-P., Wagner C., Peng Z. and Zimmermann C. (2005) Re-Os and S systematics of spinel peridotite xenoliths from east central China: Evidence for contrasting effects of melt percolation. *Earth and Planetary Science Letters* **239**, 286-308.

Riches A. J. V. and Rogers N. W. (2011) Mineralogical and geochemical constraints on the shallow origin, ancient veining, and multi-stage modification of the Lherz peridotite. *Geochimica et Cosmochimica Acta* **75**, 6160-6182.

Righter K., Humayun M. and Danielson L. (2008) Partitioning of palladium at high pressures and temperatures during core formation. *Nature Geoscience* **1**, 321-323.

Rivalenti G., Mazzucchelli M., Vannucci R., Hofmann A. W., Ottolini L., Bottazzi P. and Obermiller W. (1995) The relationship between websterite and peridotite in the Balmuccia peridotite massif (NW Italy) as revealed by trace element variations in clinopyroxene. *Contributions to Mineralogy and Petrology* **121**, 275-288.

Rose-Weston L., Brenan J. M., Fei Y. W., Secco R. A. and Frost D. J. (2009) Effect of pressure, temperature, and oxygen fugacity on the metal-silicate partitioning of Te, Se, and S: Implications for earth differentiation. *Geochimica et Cosmochimica Acta* **73**, 4598-4615.

Rouxel O., Ludden J., Carignan J., Marin L. and Fouquet Y. (2002) Natural variations of Se isotopic composition determined by hydride generation multiple collector inductively coupled plasma mass spectrometry. *Geochimica et Cosmochimica Acta* **66**, 3191-3199.

Rubie D. C., Frost D. J., Mann U., Asahara Y., Nimmo F., Tsuno K., Kegler P., Holzheid A. and Palme H. (2011) Heterogeneous accretion, composition and core-mantle differentiation of the Earth. *Earth and Planetary Science Letters* **301**, 31-42.

Rudnick R. L. and Gao S., 2003. 3.1 The Composition of the Continental Crust. In: Turekian H. D. H. a. K. K. (Ed.), Treatise on Geochemistry. **3**, Oxford, pp. 1-64.

Rudnick R. L. and Walker R. J. (2009) Interpreting ages from Re-Os isotopes in peridotites. *Lithos* **112**, 1083-1095.

Saal A. E., Hauri E. H., Langmuir C. H. and Perfit M. R. (2002) Vapour undersaturation in primitive mid-ocean-ridge basalt and the volatile content of Earth's upper mantle. *Nature* **419**, 451-455.

Savard D., Bédard L. P. and Barnes S.-J. (2009) Selenium concentrations in twenty-six geological reference materials: New determinations and proposed values. *Geostandards and Geoanalytical Research* **33**, 249-259.

Savard D., Barnes S.-J. and Meisel T. (2010) Comparison between nickel-sulfur fire assay Te co-precipitation and isotope dilution with high-pressure asher acid digestion for the determination of platinum-group elements, rhenium and gold. *Geostandards and Geoanalytical Research* **34**, 281-291.

Schönbächler M., Carlson R. W., Horan M. F., Mock T. D. and Hauri E. H. (2010) Heterogeneous Accretion and the Moderately Volatile Element Budget of Earth. *Science* **328**, 884-887.

Schaefer L. and Fegley B. (2010) Volatile element chemistry during metamorphism of ordinary chondritic material and some of its implications for the composition of asteroids. *Icarus* **205**, 483-496.

Schmidt G., Palme H., Kratz K. L. and Kurat G. (2000) Are highly siderophile elements (PGE, Re and Au) fractionated in the upper mantle of the earth? New results on peridotites from Zabargad. *Chemical Geology* **163**, 167-188.

Schmidt G., Witt-Eickschen G., Palme H., Seck H., Spettel B. and Kratz K. L. (2003) Highly siderophile elements (PGE, Re and Au) in mantle xenoliths from the West Eifel volcanic field (Germany). *Chemical Geology* **196**, 77-105.

Sen I. S., Bizimis M., Sen G. and Huang S. (2011) A radiogenic Os component in the oceanic lithosphere? Constraints from Hawaiian pyroxenite xenoliths. *Geochimica et Cosmochimica Acta* **75**, 4899-4916.

Shervais J. W. (1979). Petrology and structure of the Alpine lherolite massif at Balmuccia, Italy. **PhD dissertation**, p. 429.

Shervais J. W. and Mukasa S. B. (1991) The Balmuccia Orogenic Lherzolite Massif, Italy. *Journal of Petrology* **Special Volume(2)**, 155-174.

Shirey S. B. and Walker R. J. (1998) The Re-Os isotope system in cosmochemistry and high-temperature geochemistry. *Annual Review of Earth and Planetary Sciences* **26**, 423-500.

Sinigoi S., Cominchiaramonti P. and Alberti A. A. (1980) Phase relations in the partial melting of the Baldissero spinel-lherzolite (Ivrea-Verbano zone, Western Alps, Italy). *Contributions To Mineralogy And Petrology* **75**, 111-121.

Sinigoi S., Cominchiaramonti P., Demarchi G. and Siena F. (1983) Differentiation of partial melts in the mantle: Evidence from the Balmuccia peridotite, Italy. *Contributions To Mineralogy And Petrology* **82**, 351-359.

Smith C. L., de Laeter J. R. and Rosman K. J. R. (1977) Mass spectrometric isotope dilution analyses of tellurium in meteorites and standard rocks. *Geochimica et Cosmochimica Acta* **41**, 676-681.

Sobolev A. V., Hofmann A. W., Sobolev S. V. and Nikogosian I. K. (2005) An olivine-free mantle source of Hawaiian shield basalts. *Nature* **434**, 590-597.

Sobolev A. V., Hofmann A. W., Kuzmin D. V., Yaxley G. M., Arndt N. T., Chung S. L., Danyushevsky L. V., Elliott T., Frey F. A., Garcia M. O., Gurenko A. A., Kamenetsky V. S., Kerr A. C., Krivolutskaya N. A., Matvienkov V. V., Nikogosian I. K., Rocholl A., Sigurdsson I. A., Sushchevskaya N. M. and Teklay M. (2007) The amount of recycled crust in sources of mantle-derived melts. *Science* **316**, 412-417.

Suen C. J. and Frey F. A. (1987) Origins of the mafic and ultramafic rocks in the Ronda peridotite. *Earth and Planetary Science Letters* **85**, 183-202.

Sutton S., Delaney J., Smith J. and Prinz M. (1986). PIXE Trace Element Analyses of Metal, Troilite and Schreibersite in Iron Meteorites. Lunar and Planetary Institute Science Conference Abstracts. **17**, pp. 853-854.

Sylvester P. J. and Eggins S. M. (1997) Analysis of Re, Au, Pd, Pt and Rh in NIST glass certified reference materials and natural basalt glasses by laser ablation ICP-MS. *Geostandards Newsletter* **21**, 215-229.

Terashima S. and Imai N. (2000) Determination of selenium in fifty two geochemical reference materials by hydride generation atomic absorption spectrometry. *Geostandards Newsletter* **24**, 83-86.

Terashima S. (2001) Determination of indium and tellurium in fifty nine geological reference materials by solvent extraction and graphite furnace atomic absorption spectrometry. *Geostandards Newsletter* **25**, 127-132.

Tribuzio R., Thirlwall M. F. and Vannucci R. (2004) Origin of the gabbro-peridotite association from the Northern Apennine ophiolites (Italy). *Journal of Petrology* **45**, 1109-1124.

van Acken D., Becker H. and Walker R. J. (2008) Refertilization of Jurassic oceanic peridotites from the Tethys Ocean - Implications for the Re-Os systematics of the upper mantle. *Earth and Planetary Science Letters* **268**, 171-181.

van Acken D., Becker H., Hammerschmidt K., Walker R. J. and Wombacher F. (2010a) Highly siderophile elements and Sr-Nd isotopes in refertilized mantle peridotites - A case study from the Totalp ultramafic body, Swiss Alps. *Chemical Geology* **276**, 257-268.

van Acken D., Becker H., Walker R. J., McDonough W. F., Wombacher F., Ash R. D. and Piccoli P. M. (2010b) Formation of pyroxenite layers in the Totalp ultramafic, massif (Swiss Alps) - Insights from highly siderophile elements and Os isotopes. *Geochimica et Cosmochimica Acta* **74**, 661-683.

Van Den Bleeken G., Müntener O. and Ulmer P. (2010) Reaction Processes between Tholeiitic Melt and Residual Peridotite in the Uppermost Mantle: an Experimental Study at 0·8 GPa. *Journal of Petrology* **51**, 153-183.

Voshage H., Sinigoi S., Mazzucchelli M., Demarchi G., Rivalenti G. and Hofmann A. W. (1988) Isotopic constraints on the origin of ultramafic and mafic dikes in the Balmuccia peridotite (Ivrea Zone). *Contributions to Mineralogy and Petrology* **100**, 261-267.

Voshage H., Hofmann A. W., Mazzucchelli M., Rivalenti G., Sinigoi S., Raczek I. and Demarchi G. (1990) Isotopic evidence from the Ivrea Zone for a hybrid lower crust formed by magmatic underplating. *Nature* **347**, 731-736.

Walker R. J., Carlson R. W., Shirey S. B. and Boyd F. R. (1989) Os, Sr, Nd, and Pb Isotope Systematics of Southern African Peridotite Xenoliths - Implications for the Chemical Evolution of Subcontinental Mantle. *Geochimica et Cosmochimica Acta* **53**, 1583-1595.

Walker R. J., Horan M. F., Morgan J. W., Becker H., Grossman J. N. and Rubin A. E. (2002) Comparative Re-187-Os-187 systematics of chondrites: Implications regarding early solar system processes. *Geochimica et Cosmochimica Acta* **66**, 4187-4201.

Walker R. J. (2009) Highly siderophile elements in the Earth, Moon and Mars: Update and implications for planetary accretion and differentiation. *Chemie Der Erde-Geochemistry* **69**, 101-125.

Walsh T. M. and Lipschutz M. E. (1982) Chemical studies of L chondrites—II. Shock-induced trace element mobilization. *Geochimica et Cosmochimica Acta* **46**, 2491-2500.

Walter M. J. (2003). Melt extraction and compositional variability in mantle lithosphere. In: Holland H. D. and Turekian K. K. (Eds.), *The Mantle and Core, Treatise on Geochemistry*. **2**, pp. 363-394.

Wang K. L., O'Reilly S. Y., Griffin W. L., Pearson N. J. and Zhang M. (2009) Sulfides in mantle peridotites from Penghu Islands, Taiwan: Melt percolation, PGE fractionation, and the lithospheric evolution of the South China block. *Geochimica et Cosmochimica Acta* **73**, 4531-4557.

Wang M. S., Wolf S. F. and Lipschutz M. E. (1999) Chemical studies of H chondrites-10: Contents of thermally labile trace elements are unaffected by late heating. *Meteoritics & Planetary Science* **34**, 713-716.

Wang M. S. and Lipschutz M. E. (2005) Thermal metamorphism of primitive meteorites - XII. The enstatite chondrites revisited. *Environmental Chemistry* **2**, 215-226.

Wang Z. and Becker H. (2013) Ratios of S, Se and Te in the silicate Earth require a volatile-rich late veneer. *Nature* **499**, 328-331.

Wang Z., Becker H. and Gawronski T. (2013) Partial re-equilibration of highly siderophile elements and the chalcogens in the mantle: A case study on the Baldissero and Balmuccia peridotite massifs (Ivrea Zone, Italian Alps). *Geochimica et Cosmochimica Acta* **108**, 21-44.

Wang Z. and Becker H. (In press) Abundances of sulphur, selenium, tellurium, rhenium and platinum group elements in eighteen reference materials by isotope dilution sector-field ICP-MS and negative TIMS. *Geostandards and Geoanalytical Research*, Doi: 10.1111/j.1751-1908X.2013.00258.x.

Wasson J. T. and Kallemeyn G. W. (1988) Compositions of Chondrites. *Philosophical Transactions of the Royal Society A: Mathematical, Physical and Engineering Sciences* **325**, 535-544.

Witt-Eickschen G., Palme H., O'Neill H. S. C. and Allen C. M. (2009) The geochemistry of the volatile trace elements As, Cd, Ga, In and Sn in the Earth's mantle: New evidence from in situ analyses of mantle xenoliths. *Geochimica et Cosmochimica Acta* **73**, 1755-1778.

Wolf S. F. and Lipschutz M. E. (1995a) Chemical Studies of H Chondrites .4. New Data and Comparison of Antarctic Suites. *Journal of Geophysical Research-Planets* **100**, 3297-3316.

Wolf S. F. and Lipschutz M. E. (1995b) Chemical Studies of H Chondrites .6. Antarctic Non-Antarctic Composition Differences Revisited. *Journal of Geophysical Research-Planets* **100**, 3335-3349.

Wolf S. F., Wang M. S., Dodd R. T. and Lipschutz M. E. (1997) Chemical studies of H chondrites .8. On contemporary meteoroid streams. *Journal of Geophysical Research-Planets* **102**, 9273-9288.

Wolf S. F. and Lipschutz M. E. (1998) Chemical studies of H chondrites 9: Volatile trace element composition and petrographic classification of equilibrated H chondrites. *Meteoritics & Planetary Science* **33**, 303-312.

Wolf S. F., Unger D. L. and Friedrich J. M. (2005) Determination of cosmochemically volatile trace elements in chondritic meteorites by inductively coupled plasma mass spectrometry. *Analytica Chimica Acta* **528**, 121-128.

Wood B. J., Walter M. J. and Wade J. (2006) Accretion of the Earth and segregation of its core. *Nature* **441**, 825-833.

Wood B. J. and Halliday A. N. (2010) The lead isotopic age of the Earth can be explained by core formation alone. *Nature* **465**, 767-U764.

Xiao X. and Lipschutz M. E. (1992) Labile trace elements in carbonaceous chondrites: A survey. *Journal of Geophysical Research-Planets* **97**, 10199-10211.

Yi W., Halliday A. N., Lee D.-C. and Rehkämper M. (1998) Precise determination of cadmium, indium and tellurium using multiple collector ICP-MS. *Geostandards Newsletter* **22**, 173-179.

Yi W., Halliday A. N., Alt J. C., Lee D. C., Rehkamper M., Garcia M. O. and Su Y. J. (2000) Cadmium, indium, tin, tellurium, and sulfur in oceanic basalts: Implications for chalcophile element fractionation in the Earth. *Journal of Geophysical Research-Solid Earth* **105**, 18927-18948.

Yu L. L., Fassett J. D. and Guthrie W. F. (2002) Detection limit of isotope dilution mass spectrometry. *Analytical Chemistry* **74**, 3887-3891.

Yu M. Q., Liu G. Q. and Jin Q. (1983) Determination of trace arsenic, antimony, selenium and tellurium in various oxidation-states in water by hydride generation and atomic-absorption spectrophotometry after enrichment and separation with thiol cotton. *Talanta* **30**, 265-270.

Zhang H. F., Ying J. F., Tang Y. J. and Zhang J. (2004) Transformation of lithospheric mantle from old refractory to young fertile through peridotite-melt interaction. *Geochimica et Cosmochimica Acta* **68**, A711-A711.

Zhou M. F., Robinson P. T., Malpas J., Edwards S. J. and Qi L. (2005) REE and PGE geochemical constraints on the formation of dunites in the Luobusa ophiolite, Southern Tibet. *Journal of Petrology* **46**, 615-639.

Zingg A., Handy M. R., Hunziker J. C. and Schmid S. M. (1990) Tectonometamorphic History of the Ivrea Zone and Its Relationship to the Crustal Evolution of the Southern Alps. *Tectonophysics* **182**, 169-192.

Curriculum Vitae

For reasons of data protection, the Curriculum vitae is not published in the online version.

Acknowledgements

Three years' PhD study in Berlin has shaped my solid knowledge about mantle geochemistry and planetary accretion and sharpened my laboratory skills from a total beginner. I am full of great gratitude for anyone who has contributed to my step-by-step progress. It is the right supervision, kind suggestions, invaluable supports and warm care in the past years that have made it possible for me to complete the excellent PhD work and to have wonderful life in Berlin. The joint program from Chinese Scholarship Council and Freie Universität Berlin has provided three years' scholarship and funds for the PhD research work.

I would like to appreciate Prof. Dr. Harry Becker, my PhD supervisor who has opened up my new research field from mineral deposits to mantle processes by state of the art projects and has given the hand-by-hand scientific supervision for every aspects. I have benefited from his strong scientific background and analytical skills. His kindness, patience and responsibility have encouraged me to overcome every arising difficulty in the work and life.

I am very thankful to Prof. Dr. Andreas Stracke at Westfälische Wilhelms Universität Münster for being the second reviewer of the thesis.

Great gratitude has to go to Mr. Konrad Hammerschmidt and Ms. Monika Feth who have taught me general laboratory skills and supported my laboratory work. Their patient explanation and assistance have greatly avoided my mistakes, facilitated me to master laboratory skills quickly and guaranteed my laboratory work to run efficiently.

I am very thankful to my colleagues Uwe Wiechert, Timo Gawronski, Marc Weynell, Christian Meyer, Simon Hohl, Wiebke Bäro, Yogita Kadlag and Philipp Gleißner for guidance and support in any analytical issues, intensive discussion about scientific questions and thoughtful help in the daily life. Timo gave me step-by-step guidance for my initial work, and Christian and Simon assisted to do sampling in Italy in 2011. Marc, Simon and Timo helped to translate English summary to German one.

Dr. Rudolf Naumann at the GFZ in Potsdam is thanked for analyses of major elements and some trace elements in peridotites and pyroxenites. Dr. Frank Wombacher and Claudia Funk at Köln Universität are acknowledged for discussion about chalcogen elements and providing some ICP-MS standard solutions. Some peridotite, meteorite and reference samples were provided by Shan Gao, Konrad Hammerschmidt, Jean-Pierre Lorand, Glenn MacPherson, Meenakshi Wadhwa and Thomas Meisel. Ms. Behr is thanked for preparing thin sections.

All members of the geochemistry group of Freie Universität Berlin are gratefully acknowledged for proving kind help, wonderful and delightful atmosphere. Thank you Ms. Feth, Ms. Schreiber, Mr. Hammerschmidt, Harry, Uwe, Bernd, Timo, Simon, Marc, Christian, Bi, Wiebke, Chunhui, Yogita, Philipp, Matthias, Sebastian and Frederike. It is my great honor to work and discuss with you.

Thank the mentors of Education section, Embassy of China in Berlin for long-term support and care. Thank all friends who have helped and encouraged me, irrespectively of, in Berlin or in other places, for study or for daily life. Thank my family for kind concern, support and understanding.